

**Extended D-E knob-hole interaction sites in fibrin  
polymerisation, clot formation and clot mechanics**

Nathan Lee Asquith

Submitted in accordance with the requirements for the degree of

Doctor of Philosophy

The University of Leeds

School of Medicine

2019

The candidate confirms that the work submitted is his/her own, except where work which has formed part of jointly-authored publications has been included. The contribution of the candidate and the other authors to this work has been explicitly indicated below. The candidate confirms that appropriate credit has been given within the thesis where reference has been made to the work of others.

This copy has been supplied on the understanding that it is copyright material and that no quotation from the thesis may be published without proper acknowledgement.

The right of Nathan Asquith to be identified as Author of this work has been asserted by him in accordance with the Copyright, Designs and Patents Act 1988.

© 2018 The University of Leeds and Nathan Lee Asquith

## Acknowledgements

This research has been carried out by myself (Nathan Asquith) with the support of the laboratory of Professor Robert Ariëns (Dr.Cédric Duval, Dr. Stephen Baker, Miss Helen McPherson, Mr Fraser MacRae and Professor Robert Ariëns) our collaborators Marco Manso Domingues (University of Lisbon) and Professor Valeri Barsegov (University of Massachusetts, Lowell). My own contributions, fully and explicitly indicated in the thesis, have been the preparation and analysis of all data unless otherwise stated in the text. The other members of the group and their contributions have been as follows:

Professor Robert Ariëns has contributed to the work by contributing to the design of the experimental methods, interpretation of the data and provided feedback on the thesis. I would like to personally thank him for accepting me as a PhD student into his laboratory and for securing a prestigious British Heart Foundation Scholarship on my behalf. I am very grateful for his support, the time he has invested into my training and his fantastic feedback on my thesis.

Dr. Simon Connell contributed to the design and troubleshooting of the Atomic Force Microscopy methods, the interpretation of the AFM and magnetic tweezer data. I would like to personally thank him for his excellent ideas and support and his assistance in the interpretation of the biophysical results (AFM, light scattering studies and magnetic tweezers).

Dr. Cédric Duval contributed to the work by aiding in the execution of the confocal and scanning electron imaging. He also contributed to the design of the experiments and interpretation of the data and provided intensive feedback and guidance on the thesis. Although Cédric rules with an iron fist (ha!), his continuous help and patience throughout the three years has definitely shaped me into a far better academic (and person!), which in my opinion, is reflected by the several oral and poster presentations this project has been selected for.

Dr. Stephen Baker has contributed greatly by optimising the AFM imaging method used in the Ariëns laboratory, he also contributed to the interpretation of the AFM data. I would like to thank him personally for his extreme patience (which is sorely needed in AFM imaging) with me when teaching the method but also for his emotional support in what I call “the dark art of AFM imaging”.

Miss Helen McPherson assisted in aspects of the production and purification of the recombinant variants. I would like to thank her personally for her amazing organisational skills in the very early stages of my Ph.D. that allowed for the timely and more importantly, successful production of four recombinant fibrinogen variants, without her help the project would not have run so smoothly.

I would also like to thank her for helping me conquer my fear and frustrations with the AKTA Avant during the purification phase of the recombinant fibrinogen variants. She has been a pleasure to sit next to in the office and I will miss our 'chats' when I move to the U.S.

Dr. Marco Manso Domingues contributed to the project by aiding in the interpretation of the micro-rheology, atomic force microscopy, and light scattering studies. I would like him especially for this as even though he no longer works at the University of Leeds he is always happy to make time available to respond to all my queries and is always happy to have lengthy skype chats to help me grasp the complicated biophysical procedures.

Dr. Martin Fuller of the Astbury center for structural molecular biology contributed to the critical point drying of the SEM preparations, for this I am extremely grateful for.

I would like to thank Dr. Julia Sandrin-Gauer and Samantha Heal for their discussions of the literature, help with the technical and formatting aspects of the thesis and in my opinion, it looks great because of it.

I would like to extend my thanks to those technicians, Masters and PhD students, past and present, at LICAMM, University of Leeds. The list is too long to name all of them here, however, it includes all of those in the Whatsapp group "Dumbledore's army". I think it is a great injustice to just say 'I would like to thank them for so much in and out of university life' but again, the memories would be too long to list here. I would like to thank them for a memorable three years but especially for flying all the way to Italy for my wedding, much appreciated.

I would like to thank my sister Natasha Asquith for her amazing support and kindness and for allowing my wife and I to live with her for a very reasonable price. Her accommodating nature and beautiful home has made the gruelling task of thesis writing bearable. I would like to thank the cats (Quill, Ivy and Pepper) for being playful friends during the respite periods of thesis writing.

Lastly, but certainly not the least, I would like to thank my wife Carla Asquith for everything. I have not met and I do not think I will meet a more kind person. I would like to thank her for her love and never ending support in everything I do. She is an avid listener whenever I display worry and I would not have made it to this stage without her.

I am very grateful to my sponsors including the British Heart Foundation who funded the PhD fellowship (FS/15/37/31513). I am also grateful to the University of Leeds and the British Society of Haemostasis and Thrombosis for funding visits to ISTH Berlin 2017 and a collaboration visit to the University of Massachusetts, Lowell, USA.

## Publications

The following peer-reviewed publications are in print and have been published during the PhD programme, however they are unrelated from the contents of the thesis and no data has been used from them.

### Research investigations

Macrae F.L., Duval C., Papareddy P., Baker S.R., Yuldasheva N., Kearney K.J., McPherson H.R., **Asquith N.**, Konings J., Casini A., Degen J.L., Connell S.D., Philippou H., Wolberg A.S., Herwald H., Ariëns R.A. A fibrin biofilm covers the blood clot and protects from microbial invasion. *J Clin Invest*; 2018 Aug 1;128(8):3356-3368 PMID: 29723163.

### Other peer-reviewed publications

Spronk HMH, Padro T, Siland JE, Prochaska JH, Winters J, van der Wal AC, Posthuma JJ, Lowe G, d'Alessandro E, Wenzel P, Coenen DM, Reitsma PH, Ruf W, van Gorp RH, Koenen RR, Vajen T, Alshaikh NA, Wolberg AS, Macrae FL, **Asquith N** (+44 co-authors). Atherothrombosis and Thromboembolism: Position Paper from the Second Maastricht Consensus Conference on Thrombosis. *Thromb Haemost*; 2018 118(2), pp.229-250 PMID: 29378352

## Conference Abstracts

### National Abstract Oral/Poster Presentations

Role of extended knob-hole interaction sites in fibrin polymerization and clot stability (Oral presentation).

British Society of Haemostasis and Thrombosis, Warwick, UK 2017.

**Asquith N.L.**, Duval C., Baker S., Domingues M.M., McPherson H.R., Macrae F.L., Connell S.D., Barsegov V., Ariëns R.A.S.

Role of extended knob-hole interaction sites in fibrin polymerization and clot stability (Poster Presentation).

5<sup>th</sup> British Heart Foundation Fellows Meeting, Cambridge, UK, 2017.

**Asquith N.L.**, Duval C., Baker S., Domingues M.M., McPherson H.R., Macrae F.L., Connell S.D., Barsegov V., Ariëns R.A.S.

### International Abstract Oral/Poster Presentations

Role of extended knob-hole interaction sites in fibrin polymerization and clot stability (Oral presentation).

International Society of Thrombosis and Haemostasis Congress, Berlin, Germany 2017.

**Asquith N.L.**, Duval C., Baker S., Domingues M.M., McPherson H.R., Macrae F.L., Connell S.D., Barsegov V., Ariëns R.A.S.

Role of extended knob-hole interaction sites in fibrin polymerization and clot stability (Oral Presentation)

International Fibrinogen Workshop, Winston Salem, North Carolina, USA 2018.

**Asquith N.L.**, Duval C., Baker S., Domingues M.M., McPherson H.R., Macrae F.L., Connell S.D., Barsegov V., Ariëns R.A.S.

## Honours and Prizes

International Fibrinogen Workshop, North Carolina, USA 2018.

Outstanding Abstract Award.

International Researcher Award, University of Leeds, UK 2018.

Awarded to collaborate with University of Massachusetts, Lowell, MA, USA, £2315.

British Society of Haemostasis and Thrombosis Travel Award.

Awarded to collaborate with University of Massachusetts, Lowell, MA, USA, £500.

XXVI ISTH congress and 63rd Annual SSC Meeting 2017.

International society of Haemostasis and Thrombosis, Berlin Germany.

Young Investigator Travel Award, €500.

British Society of Haemostasis and Thrombosis ISTH Travel Award.

Awarded for acceptance of oral presentation at ISTH, £750.

## Abstract

**Background:** Abnormal thrombus formation and occlusion of a vessel is one of the main events of cardiovascular disease. A main component of the thrombus is the protein fibrin, which is formed by proteolytic cleavage of its precursor fibrinogen by the serine protease thrombin. The cleavage of fibrinogen to fibrin releases fibrinopeptides from the E-region of the molecule which leads to the exposure of peptide sequences termed knobs A and B. The knobs A and B on one fibrin molecule are able to spontaneously interact to binding pockets (termed holes a and holes b) via hydrogen bonds forming half staggered protofibrils. These protofibrils laterally aggregate and form fibrin fibers, providing the clot its strength and stability. Recent molecular dynamic simulations have predicted that there are additional interactions involving amino acids  $\gamma$ Glu323 with  $\beta$ Lys58,  $\gamma$ Lys356 with  $\beta$ Asp61, and  $\gamma$ Asp297 with  $\beta$ His67, that surround the binding pocket and provide additional strength and stability to the 'classical' knob-hole contact. In this project I have termed these residues 'extended D-E knob-hole binding sites.'

**Aim:** The aim of this project was to probe the importance of these extended knob-hole interactions in the process of fibrin polymerisation, clot structure and clot mechanics, using recombinant fibrinogen variants with mutations that abolish these electrostatic interactions.

**Methods:** Four recombinant human fibrinogen variants and WT proteins were produced. The following variants with single point mutations in the  $\gamma$ -chain of extended knob-hole binding region were produced:  $\gamma$ D297N,  $\gamma$ E323Q and  $\gamma$ K356Q. A triple variant,  $\gamma$ DEK ( $\gamma$ D297N/ $\gamma$ E323Q/ $\gamma$ K356Q) with mutations in all residues involved was also produced. Each variant was tested for integrity by

circular dichroism and SDS-PAGE. Turbidity and atomic force microscopy were used to study polymerisation kinetics, laser scanning confocal microscopy and scanning electron microscopy were used to study clot structure. Light scattering methods were used to study intrafibrillar protein structure, and clot mechanics was studied using an in-house micro-rheometer.

**Results:** Longitudinal protofibril growth was disrupted for all variants except  $\gamma$ K356Q at early stages of polymerisation, but normalised at later time points.  $V_{max}$  was reduced for all variants.  $\gamma$ DEK and  $\gamma$ E323Q produced denser clots, whereas  $\gamma$ D297N and  $\gamma$ K356Q were similar to WT. All variant clots had significantly thinner fibers compared to WT. All variants were slower to lyse, with the exception of  $\gamma$ D297N. Clot visco-elastic analysis showed that  $\gamma$ DEK was more readily deformable (loss tangent,  $\tan\delta$ ), at low frequencies but single mutant variants were unchanged at all frequencies compared to WT.

**Conclusion:** I produced pure and intact recombinant human fibrinogens with mutations at the extended knob-hole binding sites. These data provide clear evidence for the role of extended D-E interactions in supporting the classical knob-hole binding during fibrin formation. Furthermore, the extended D-E interactions were shown to alter clot structure and clot mechanics. Additional studies with these variants in the presence of cells and other vascular components may further elucidate the importance of extended knob-hole interactions in haemostasis and thrombosis.

## Table of Contents

<b>Acknowledgements</b> .....	<b>I</b>
<b>Publications</b> .....	<b>III</b>
<b>Conference Abstracts</b> .....	<b>IV</b>
<b>Honours and Prizes</b> .....	<b>IV</b>
<b>Abstract</b> .....	<b>V</b>
<b>List of Tables</b> .....	<b>XII</b>
<b>List of Figures</b> .....	<b>XIII</b>
<b>List of Equations</b> .....	<b>XVI</b>
<b>List of abbreviations</b> .....	<b>XVII</b>
<b>Chapter 1 - Introduction</b> .....	<b>1</b>
1.1 Cardiovascular disease and coagulation .....	2
1.2 Fibrinogen .....	9
1.3 Fibrin polymerisation and clot formation .....	12
1.4 Factor XIII.....	16
1.4.1 Factor XIII structure and secretion .....	16
1.4.2 Factor XIII function .....	17
1.5 Prevention of clot formation and clot lysis .....	17
1.6 Fibrinolysis .....	19
1.7 Fibrin clot structure .....	22
1.8 Intra-fibrillar fibrin structure.....	26
1.9 Fibrin mechanics .....	28
1.10 Fibrinogen disorders.....	32
1.11 Knob-hole interactions.....	35
1.11.1 Concept of knob-hole interactions.....	35
1.11.2 Force rupture of A:a knob-hole interactions .....	36
1.11.3 Catch-slip bonds in fibrin.....	39
1.12 Extended knob-hole interactions .....	40
1.12.1 Concept of extended D-E knob-hole interactions.....	40
1.12.2 Known variants in the vicinity of the extended knob-hole region .....	43
1.12.2.1 $\gamma$ D297 .....	43
1.12.2.2 $\gamma$ E323 .....	43
1.12.2.3 $\gamma$ K356 .....	44

1.13 Aims .....	46
1.14 Objectives.....	46
<b>Chapter 2 - Materials and Methods.....</b>	<b>48</b>
2.1 Materials.....	49
2.1.1 Molecular biology .....	49
2.1.2 Cell culture .....	49
2.1.3 Precipitation and purification .....	50
2.1.4 Fibrinogen ELISA.....	51
2.1.5 SDS-PAGE and circular dichroism spectroscopy.....	52
2.1.6 Functional analysis of fibrin clots.....	52
2.2 Mutagenesis .....	53
2.2.1 Primer design and mutagenesis.....	53
2.2.2 Bacterial transformation .....	55
2.2.3 DNA extraction .....	56
2.2.4 Sequencing .....	57
2.3 Cell culture .....	57
2.3.1 Thawing cells .....	57
2.3.2 Routine splitting of cells .....	58
2.3.3 Transfection – calcium phosphate method.....	58
2.3.4 Colonies selection .....	59
2.3.5 Roller bottle expression and precipitation .....	60
2.4 ELISA .....	61
2.5 Precipitation and purification .....	62
2.5.1 Precipitation .....	62
2.5.2 Affinity chromatography and dialysis.....	63
2.6 Protein concentration and dialysis.....	63
2.6.1 Concentration of recombinant fibrinogen variants.....	63
2.7 SDS-PAGE.....	64
2.8 Circular dichroism.....	64
2.9 Turbidity.....	65
2.9.1 Cleavage with thrombin.....	66
2.9.2 Cleavage with reptilase .....	67
2.10 Micro-rheology using magnetic tweezers .....	67
2.10.1 Magnetic micro-rheometer equipment.....	67

2.10.2	Calibration.....	69
2.11	Force measurements.....	71
2.12	Laser scanning confocal microscopy.....	75
2.12.1	Alexa Fluor labelling of fibrinogen variants.....	75
2.12.2	Fibrin clot formation in hydrated conditions.....	75
2.12.3	Final clot structure Imaging.....	76
2.12.4	Clot lysis.....	77
2.13	Scanning electron microscopy.....	78
2.14	Atomic force microscopy.....	80
2.15	Protofibril packing.....	81
<b>Chapter 3</b>	<b>- The production of human recombinant fibrinogen variants in a CHO cell system.....</b>	<b>84</b>
3.1	Introduction.....	85
3.2	Methods.....	86
3.2.1	Site directed mutagenesis.....	86
3.2.2	Bacterial transformation and DNA extraction.....	87
3.2.3	Cell culture.....	87
3.2.4	Precipitation and purification.....	88
3.2.5	Characterisation.....	88
3.3	Results.....	89
3.3.1	Sequencing results of $\gamma$ D297N, $\gamma$ E323Q $\gamma$ K356Q & $\gamma$ DEK recombinant human fibrinogen variants.....	89
3.3.2	Protein purification and integrity checks.....	93
3.3.3	SDS PAGE.....	95
3.3.4	Circular dichroism (CD) spectroscopy.....	96
3.4	Discussion.....	100
<b>Chapter 4</b>	<b>Polymerisation kinetics of recombinant human fibrinogen variants using light scattering analysis and atomic force microscopy.....</b>	<b>103</b>
4.1	Introduction.....	104
4.2	Objectives.....	105
4.3	Methods.....	105
4.3.1	Turbidity.....	105
4.3.2	Atomic force microscopy.....	106
4.3.3	Statistics.....	106
4.4	Results.....	107

4.5 Discussion .....	120
<b>Chapter 5 - Effects of abolished extended D-E interactions on clot structure at different spatial scales .....</b>	<b>125</b>
5.1 Introduction.....	126
5.2 Methods.....	128
5.2.1 Scanning electron microscopy (SEM) .....	128
5.2.2 Laser scanning confocal microscopy .....	129
5.2.2.1 Protein labelling .....	129
5.2.2.2 Fibrin clot structure .....	129
5.2.2.3 Clot lysis .....	130
5.2.3 Protofibril packing.....	130
5.2.4 Statistics.....	131
5.3 Results .....	131
5.4 Discussion .....	138
<b>Chapter 6 - The role of extended D-E knob hole interactions in clot mechanics .....</b>	<b>144</b>
6.1 Introduction.....	145
6.2 Methods.....	147
6.2.1 Clot preparation.....	147
6.2.2 Micro-rheology .....	147
6.2.3 Statistics.....	147
6.2.4 Results .....	148
6.3 Discussion .....	155
<b>Chapter 7 - Discussion .....</b>	<b>159</b>
7.1 Summary of data .....	160
7.2 Discussion .....	162
7.2.1 $\gamma$ D297N .....	163
7.2.2 E323Q .....	165
7.2.3 K356Q.....	166
7.3 Limitations .....	171
7.3.1 CD spectroscopy .....	171
7.3.2 Cell culture .....	171
7.3.3 Micro-rheology .....	172
7.3.3.1 Factor XIII .....	172
7.3.4 Limitations of turbidity measurements.....	173

7.3.5	Limitations of confocal microscopy.....	173
7.3.6	Limitations of scanning electron microscopy.....	174
7.3.7	Limitations of atomic force microscopy .....	175
7.4	Future Work.....	175
7.4.1	Clot mechanics.....	175
7.4.2	AFM studies .....	176
7.4.3	Interactions with other blood components.....	177
7.4.3.1	$\alpha_{IIb}\beta_3$ .....	177
7.4.3.2	GPVI.....	177
7.4.3.3	Plasminogen, tPA and $\alpha_2$ -Antiplasmin .....	178
7.4.3.4	$\alpha_M\beta_2$ .....	178
7.4.4	Complement protein C3 .....	179
7.4.5	Role of calcium binding.....	179
7.4.6	Molecular dynamic simulations .....	180
7.5	Physiological importance and relevance .....	181
7.6	Conclusions.....	183
<b>Chapter 8 - References.....</b>		<b>185</b>
<b>Chapter 9 - Appendices.....</b>		<b>201</b>
9.1	- The DNA sequence of the pMLP- $\gamma$ A .....	202
9.2	- Sequence alignments of WT with recombinant variants.....	204
9.3	- Representative SEM Images at x2000 magnification.....	209
9.4	- Representative SEM images at x5000 magnification .....	210
9.5	- Representative SEM images at x10000 magnification .....	211
9.6	- Representative SEM images at x50000 magnification .....	212
9.7	- Abstracts .....	213

## List of Tables

Table 2-1 PT200 Dpn-1 digestion parameters.....	55
Table 2-2 Primers for DNA sequencing.....	57
Table 2-3 Transfection reaction mix.....	58
Table 2-4 LSCM settings for clot formation experiments.....	76
Table 3-1 Primers designed and used for site-directed mutagenesis...	86
Table 3-2 Cycling parameters used in site directed mutagenesis.....	86
Table 3-3 Conditions for CHO cell transfections.....	87
Table 3-4 Clustal Omega protein alignment of Wild Type (WT) $\gamma$ -chain fibrinogen and $\gamma$ D297N mutant.....	90
Table 3-5 Clustal Omega protein alignment of Wild Type (WT) $\gamma$ -chain fibrinogen and $\gamma$ E323Q mutant.....	91
Table 3-6 Clustal Omega protein alignment of Wild Type (WT) $\gamma$ -chain fibrinogen and $\gamma$ K356Q mutant.....	91
Table 3-7 Clustal Omega protein alignment of Wild Type (WT) $\gamma$ -chain fibrinogen and $\gamma$ D297N/E323Q/K356Q ( $\gamma$ DEK) mutant .....	92
Table 3-8 Yields of recombinant WT and variant human fibrinogen ...	101
Table 4-1 Average length (mean) of protofibrils during polymerisation .....	116
Table 4-2 Parameters implicated in affecting polymerisation kinetics and clot structure .....	122
Table 5-1 LSCM parameters for final clot structure .....	129
Table 5-2 LSCM parameters for clot lysis.....	130
Table 6-1 Storage modulus ( $G'$ ) of WT and $\gamma$ DEK variant.....	148
Table 6-2 Storage modulus ( $G'$ ) of WT and single variants.....	148
Table 6-3 Loss modulus ( $G''$ ) of WT and $\gamma$ DEK variant.....	149
Table 6-4 Loss modulus ( $G''$ ) of WT and single variants.....	149
Table 6-5 Overall deformability ( $\tan\delta$ ) of WT and $\gamma$ DEK variant .....	149
Table 6-6 Overall deformability ( $\tan\delta$ ) of WT and single variants.....	149
Table 7-1 Ranking of overall percentage difference of recombinant variants compared to WT.....	170

## List of Figures

Figure 1-1 Mechanisms of atherosclerosis.....	5
Figure 1-2 Vessel following platelet plug formation .....	6
Figure 1-3 Diagrammatic representation of coagulation.....	9
Figure 1-4 Molecular dynamic representation of human fibrinogen .....	12
Figure 1-5 Fibrin(ogen) Polymerisation .....	14
Figure 1-6 Scanning electron microscopy image of a purified fibrin clot .....	15
Figure 1-7 Atomic force image of a single fibrin monomer.....	16
Figure 1-8 Clot formation and fibrinolysis .....	21
Figure 1-9 Schematic of digestion of cross-linked fibrin by plasmin....	21
Figure 1-10 Rotary shadowed fibrinogen .....	22
Figure 1-11 Transmission electron micrograph of human fibrin .....	23
Figure 1-12 Scanning electron micrograph of a fibrin clot prepared from whole blood.....	24
Figure 1-13 Theoretical schematics of different packing possibilities for fibrin fibers .....	28
Figure 1-14 Schematic of rupture of A:a knob-hole bonds. ....	38
Figure 1-15 A computational reconstruction of the alignment of fibrin molecules .....	42
Figure 1-16 Molecular computation of $\gamma$ nodule in fibrinogen co- complexed with knobs A.....	47
Figure 2-1 Plasmid map of pMLP- $\gamma$ A.....	54
Figure 2-2 Diagram to demonstrate the principal of turbidity (light scattering). ....	65
Figure 2-3 Typical profile of a fibrin polymerisation curve .....	66
Figure 2-4 Micro-rheometer setup .....	69
Figure 2-5 Time dependent compliance.....	72
Figure 2-6 Frequency dependent moduli $G'$ and $G''$ .....	74
Figure 2-7 Measurement of the distance travelled over time by the lysis front.....	77
Figure 2-8 SEM clot formation in an Eppendorf lid.....	79
Figure 2-9 UV-Vis spectra in the fully formed fibrin clot .....	82
Figure 3-1 Affinity chromatography chromatogram of $\gamma$ D297N-E323Q- K356Q .....	94
Figure 3-2 Reduced SDS-PAGE gel of recombinant wild type and single mutant recombinant variants.....	95

Figure 3-3 Reduced SDS-PAGE gel of recombinant wild type and triple mutant recombinant variant $\gamma$ DEK. ....	96
Figure 3-4 Raw CD spectroscopy curves of recombinant wild type and recombinant variants .....	98
Figure 3-5 CD spectroscopy data. ....	99
Figure 4-1 Turbidity curve of fibrin clots. ....	109
Figure 4-2 Maximum optical density and lag phase of fibrin clots.....	110
Figure 4-3 Turbidity curve of fibrin clots. ....	111
Figure 4-4 Maximum optical density and lag phase of fibrin clots.....	112
Figure 4-5 Turbidity of fibrin clots with reptilase. ....	113
Figure 4-6 Maximum polymerisation rate of WT and $\gamma$ DEK fibrin clots .....	114
Figure 4-7 Maximum polymerisation rate of WT, $\gamma$ D297N $\gamma$ E323Q and $\gamma$ K356Q. ....	115
Figure 4-8 Atomic force micrographs .....	117
Figure 4-9 Distribution of protofibrils .....	118
Figure 4-10 Distribution comparison of protofibril length (nm) following 10 minutes clot formation .....	119
Figure 4-11 Distribution comparison of protofibril length (nm) following 20 minutes clot formation .....	119
Figure 4-12 Distribution comparison of protofibril length (nm) following 20 minutes clot formation .....	120
Figure 5-1 Scanning electron micrographs of purified WT and fibrin variants at x20000 magnification.....	133
Figure 5-2 Thickness of WT and variant fibrin fibers in dehydrated conditions using scanning electron microscopy. ....	134
Figure 5-3 Laser scanning confocal microscopy micrographs of WT fibrin clots .....	135
Figure 5-4 Fiber count per 200 $\mu$ m.....	136
Figure 5-5 Clot lysis ( $\mu$ m/s) .....	136
Figure 5-6 Fiber radius in hydrated conditions. ....	137
Figure 5-7 Number of protofibrils in hydrated conditions.....	137
Figure 5-8 Average distance between protofibrils .....	138
Figure 5-9 Scanning electron micrograph of WT fibrin at x50000 magnification .....	140
Figure 6-1 Complete G' and G'' curves for WT and $\gamma$ DEK.....	150
Figure 6-2 Complete G' and G'' curves for the single mutant variants WT , $\gamma$ D297N, $\gamma$ E323Q and $\gamma$ K356Q .....	151

<b>Figure 6-3 The storage modulus (<math>G'</math>) for all fibrin variants. ....</b>	<b>152</b>
<b>Figure 6-4 The loss modulus (<math>G''</math>) for all fibrin variants .....</b>	<b>153</b>
<b>Figure 6-5 The visco-elastic ratio of <math>G''/G'</math> (<math>\tan\delta</math>).....</b>	<b>154</b>
<b>Figure 7-1 Cartoon representation of lateral force AFM experiments.</b>	<b>176</b>

## List of Equations

Equation 2-1 Absorbance calculation .....	65
Equation 2-2 Stoke's Law .....	70
Equation 2-3 Force calibration fitting.....	70
Equation 2-4 Time dependent compliance is related to the time dependent particle displacement .....	72
Equation 2-5 Compliance fitting Equation 1 .....	73
Equation 2-6 Compliance fitting equation 2 .....	73
Equation 2-7 The equation that is used to generate all G' and G'' data points using Octave 4.2 software.....	73
Equation 2-8 The degree of labelling. ....	75
Equation 2-9 Wavelength dependent turbidity .....	82
Equation 2-10 Turbidity of a solution of randomly orientated fibers ...	82
Equation 2-11 Number of protofibrils.....	83
Equation 2-12 Average protein density.....	83
Equation 2-13 Distance between protofibrils. ....	83

## List of abbreviations

$\alpha$ C	$\alpha$ -chain
$\beta$ C	$\beta$ -chain
$\epsilon$ -ACA	Epsilon aminocaproic acid
$\gamma$ C	$\gamma$ -chain
ADP	Adenosine di-phosphate
ATP	Adenosine tri-phosphate
AFM	Atomic force microscopy
BSA	Bovine serum albumin
CD	Circular dichroism
CHO	Chinese hamster ovary
CVD	Cardiovascular disease
DD	D-dimer
DMEM	Dulbecco's modified eagle medium
dNTP	Deoxyribonucleotide triphosphate
EDTA	Ethylenediaminetetraacetic acid
ELISA	Enzyme linked Immunosorbent assay
FBS	Foetal bovine serum
FpA	Fibrinopeptide A
FpB	Fibrinopeptide B
FXIII	Factor XIII
GHRP	Gly-Pro-Arg-Pro
GPRP	Gly-Pro-His-Pro
GPVI	Glycoprotein VI
HEBS	HEPES buffered saline
HEPES	4-(2hydroxyethyl)-1-piperazineethane
HRP	Horseraddish peroxidase

ITS	Insulin, transferrin and sodium selenite
kDa	Kilo dalton
LB	Lysogeny broth
LDL	Low density lipoprotein
L-His	L-Histidinol
mAb	Monoclonal antibody
MES	2 ethanesulfonic acid
NDSK	N-terminal disulphide knot
OPD	O-phenylenediamine
PAI	Plasmin activator inhibitor
PBS	Phosphate buffered saline
PCR	Polymerase chain reaction
PMSF	Phenyl-1-methylsulfonyl fluoride
SDS-PAGE	Sodium dodecyl sulphate polyacrylamide gel electrophoresis
SEM	Scanning electron microscopy
SK	Streptokinase
SOC	Super optimal broth
tPA	Tissue plasminogen activator
uPA	urokinase plasminogen activator
VTE	venous thromboembolism
vWF	von Willebrand factor
WT	Wild Type

# **Chapter 1 - Introduction**

## 1.1 Cardiovascular disease and coagulation

Approximately 17.5 million people died of cardiovascular diseases (CVD) in 2012 globally (Mendis, 2017) with over 4 million deaths per year in the European Union (Townsend *et al.*, 2016). This emphasises that CVD is an important area for research to further understand the aetiology of the disease in order to develop new methodologies and technologies to improve patient outcomes. The literature suggests that the rate of cardiovascular disease progression is in decline and is attributed to increased options for one to partake in a healthier lifestyle (Roth *et al.*, 2015). One of the main contributors to cardiovascular disease is thrombosis (Previtali *et al.*, 2011), with half a million deaths per year in Europe associated with venous thrombosis alone (Rosendaal, 2016).

Thrombosis is the formation of abnormal blood clots within a vessel. Arterial thrombosis occurs in high pressure arteries, whereas venous thrombosis forms in the deep veins under low shear stress (Cilia La Corte *et al.*, 2011). Arterial thrombosis, responsible for myocardial infarction and ischemic stroke can occur from the formation, build-up and rupture of atherosclerotic plaques (Zaman *et al.*, 2000) detailed in Figure 1-1, or through the formation of a platelet plug when collagen fibers are exposed to flowing blood due to endothelium damage (Tomaiuolo *et al.*, 2017). Formation of the atherosclerotic plaque is initiated when low density lipoprotein (LDL) can no longer be transported normally from the blood in the lumen of a vessel via transcytosis by endothelial cells (Magalhaes *et al.*, 2016). The endothelial cells of the vessel become damaged, which can be caused by many factors such as hypertension (Dharmashankar and Widlansky, 2010; Puddu *et al.*, 2000), smoking (Messner and Bernhard, 2014; Johnson *et*

*al.*, 2010), high blood glucose levels (Esper *et al.*, 2008; Hadi and Suwaidi, 2007), and hypercholesterolemia (Landmesser *et al.*, 2000; Stapleton *et al.*, 2010).

The damage that is caused by these factors increases the permeability of the endothelial wall giving rise to an influx of LDL molecules to the surrounding vessel intima. Damaged endothelial cells also express receptors where monocytes can bind, allowing them to undergo morphological changes and migrate through the endothelial wall (Gerhardt and Ley, 2015). Free radicals excreted by the monocytes oxidise the LDL (Xing *et al.*, 1998). The presence of oxidised LDL and monocytes enables the recruitment of more monocytes to the tissue that in turn produces more free radicals, causes further oxidation of LDL molecules, leading to the accumulation of monocytes and oxidised LDL in the tissue. Monocytes differentiate into macrophages in the tissue and engulf the oxidised LDL (Seo *et al.*, 2015). They eventually become saturated, becoming foam cells, which then undergo apoptosis, the accumulation of cell debris and oxidised LDL forms a lipid core (Tabas, 2010). The atherosclerotic plaque can rupture under physical stresses, and can release tissue factor originally from the apoptosis of macrophages within the plaque (Tatsumi and Mackman, 2015). This initiates the coagulation cascade with the end product being a clot known as an occlusive thrombus (Hagedorn *et al.*, 2010). When an occlusive thrombus forms in the coronary arteries, downstream oxygen levels become dramatically reduced (Tremoli *et al.*, 1999) often leading to death of cardiomyocytes and ultimately heart failure (myocardial infarction) (Talman and Ruskoaho, 2016). Thrombi can also break off from the site of formation travelling to a vessel downstream blocking the flow of blood, this process is known as embolisation. In arterial thrombosis, the thrombi that form are termed 'white thrombi' as they

are rich in platelets and fibrin due to the flowing blood coming into contact with tissue factor on the surface of the atherosclerotic plaque (Jerjes-Sanchez, 2005). Physical damage to the endothelium can also cause a platelet plug to occur, Figure 1-2. The first step of this process is when the damage to the endothelium causes the sub endothelial tissue (containing collagen) to be exposed, leading to von Willebrand factor (vWF) from the bloodstream binding to collagen fibers (Peyvandi *et al.*, 2011). Platelets are able to bind to collagen through this immobilised vWF but also through receptors on the platelets such as  $\alpha 2\beta 1$  (Wang *et al.*, 2003) and GPVI (Jung *et al.*, 2008). Platelet adhesion to collagen triggers a cascade of events that activate the platelets causing a morphological change and platelet aggregation where extruding filopodia can be observed, this process is commonly known as 'platelet spreading' (Aslan *et al.*, 2012). Platelet spreading increases the surface area of the platelets. The accumulation and aggregation of platelets at the site is called a platelet plug. Following activation and spreading, platelets release contents of their  $\alpha$ -granules such as fibrinogen, factor V, vWF (Paul *et al.*, 1999) and ADP, ATP, serotonin, calcium and polyphosphate from dense granules (Woulfe *et al.*, 2001). The release of ADP serves as a positive feedback loop for more platelet aggregation to occur. Platelets are linked together by fibrinogen via the platelet receptor  $\alpha_{II}B\beta_3$  (Podolnikova *et al.*, 2014). One of the final events of haemostasis and coagulation is the conversion of fibrinogen to fibrin by serine protease thrombin (Rocco, 2008), giving rise to the fibrin network that stabilises the clot (van Kempen *et al.*, 2014).

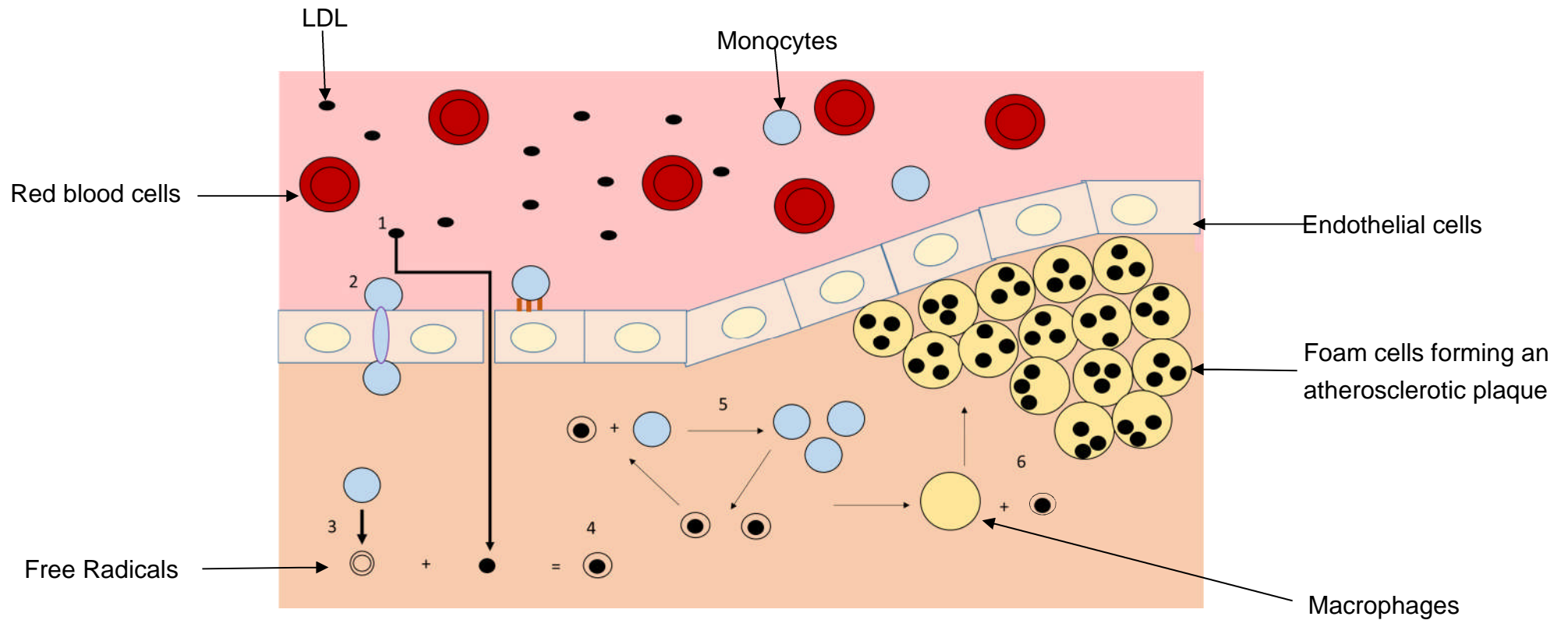


**Figure 1-1 Mechanisms of atherosclerosis** (1) Endothelial cells become compromised making the endothelial cell barrier more permeable and allowing influx of low density lipoprotein (LDL) to the surrounding tissue. (2) Upon damage, endothelial cells express receptors where monocytes bind and undergo morphological changes to migrate through the endothelial barrier. (3) Monocytes secrete free radicals. (4) The free radicals oxidise LDL molecules. (5) The presence of oxidised LDL and monocytes enables the recruitment of more monocytes which secrete more free radicals. Eventually, monocytes undergo morphological changes and become macrophages. (6) Macrophages engulf free oxidised LDL and are termed foam cells due to their foamy appearance, they undergo apoptosis and become incorporated into an atherosclerotic core/plaque which can rupture causing clot formation within the vessel.

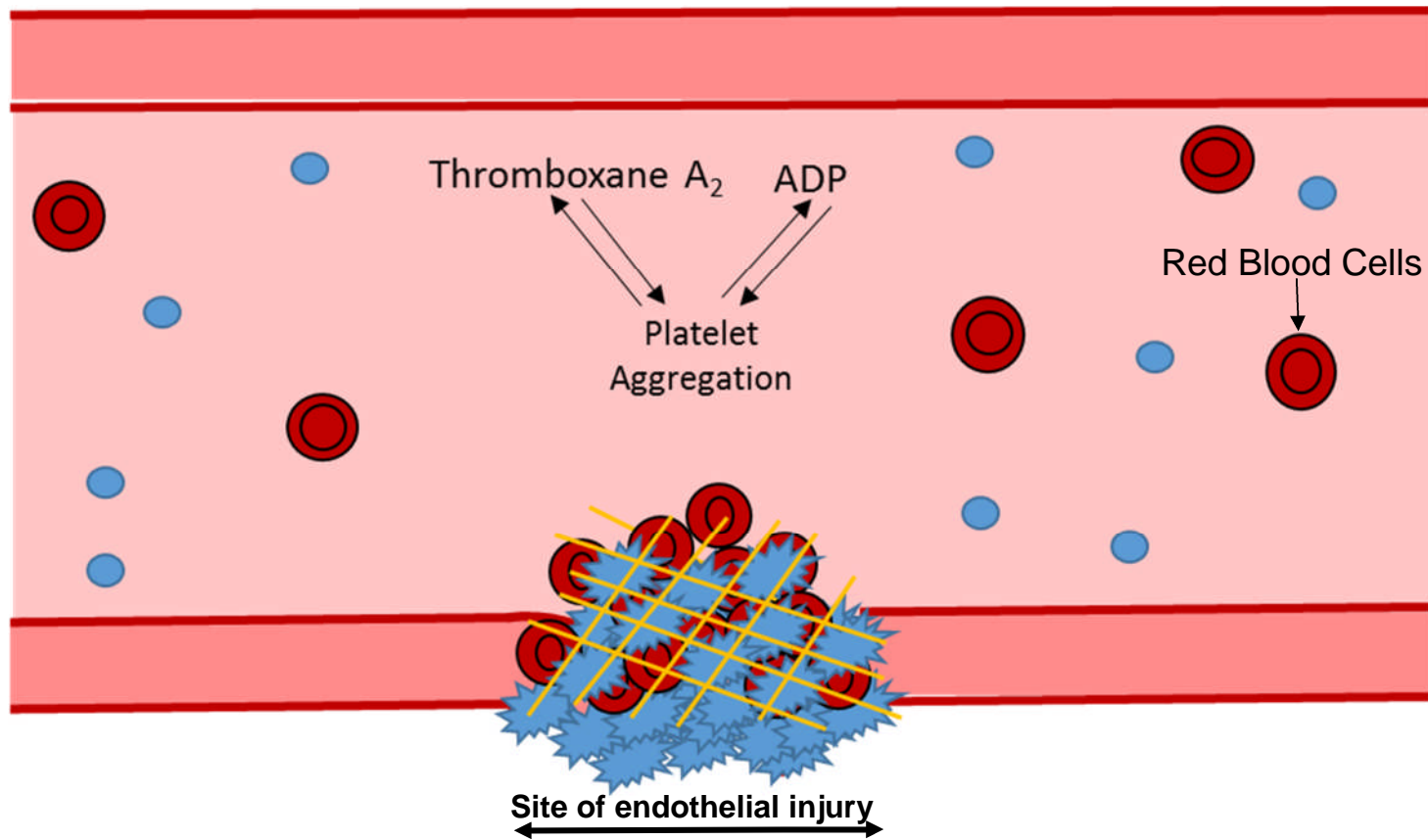


**Figure 1-2 Vessel following platelet plug formation** Damage to the endothelium causes the endothelial cells and collagen to be exposed. Platelets (blue) are able to bind, through immobilised vWF, (not shown), but also through receptors on the platelets such as  $\alpha 2\beta 1$  and GPVI, leading to activation of platelets (spiky blue cells). Activation triggers intracellular signalling events causing them to increase in surface area and spread. Platelets are linked together by fibrinogen via the platelet receptor  $\alpha IIB\beta 3$ . Fibrin (yellow strands) produced by the coagulation cascade forms a network around the platelet plug.

Venous thrombosis is caused by three factors that have been defined as the Virchow's triad (Esmon, 2009): stasis (or the disturbance of normal laminar flow of the blood), hypercoagulability and endothelial dysfunction. Stasis, the complete stopping or slowing down of the blood flow, can be caused by reduced mobility and increases one's risk due to the accumulation of coagulation factors (Wessler, 1962). Endothelial dysfunction can disrupt coagulant and anti-coagulant functions in addition to platelet adhesion and activation (Poredos and Jezovnik, 2017). The hypercoagulability of the blood can be caused by a number of factors such as pregnancy (James, 2009), surgery (Ulrych *et al.*, 2016), increased hormone levels (Tchaikovski and Rosing, 2010) and deficiencies in coagulation inhibitors (Esmon, 2009). The use of heparins has been the standard treatment of venous thromboembolism for many years as heparins are efficient at preventing further thrombus growth through the inhibition of factor Xa and thrombin by enhancing antithrombin (Ageno and Huisman, 2000).

Two pathways can initiate the coagulation cascade, the tissue factor pathway and the contact factor pathway, The contact and tissue factor pathway merge where factor Xa cleaves prothrombin to thrombin. Thrombin then converts fibrinogen to fibrin, but also activates factor XIII which cross-links fibrin monomers to create a cross-linked fibrin network. The tissue factor pathway is initiated by the exposure of tissue factor by damaged vessels (Mann *et al.*, 1998), whereas the contact factor pathway is initiated when factor XII is activated through contact with a negatively charged surface (Naudin *et al.*, 2017). In both pathways, clotting factors become activated by proteolytic cleavage by other clotting factors upstream in the cascade and both pathways consolidate to a common pathway. In this instance, factor Xa cleaves prothrombin to thrombin

(Cabral and Ansell, 2015), which in turn cleaves soluble fibrinogen that self-assembles into an insoluble fibrin polymer (Doolittle, 1984). Simultaneously thrombin also activates factor XIII, which forms  $\gamma$ -glutamyl lysine bonds that 'cross-link' the fibrin network, stabilising the clot network further (Ariëns *et al.*, 2002).

Coagulation occurs in two phases, initiation and propagation (Smith *et al.*, 2015). Coagulation is initiated when membrane bound tissue factor within the sub endothelial matrix is exposed and causes binding to factor VII in the blood forming activated FVII (FVIIa) (Mackman, 2009). The binding of these factors forms a protease complex that proteolytically activates factors FIX and FX, producing active forms FIXa and FXa. Factor Xa produces small amounts of thrombin through the cleavage of prothrombin. This small amount of thrombin that is generated is not enough to cleave fibrinogen to fibrin, however it is able to cleave FXI to FXIa which, in turn cleaves FIX to FIXa, which cleaves additional FX to FXa, producing even more thrombin. During the propagation phase the small amount of thrombin generated is able to activate factors FV and FVIII to their activated forms FVa and FVIIIa respectively which also cleave larger amounts FX to FXa by functioning as cofactors for FXa and FIXa respectively on the platelet surface (Yang and Walsh, 2005; Sinha *et al.*, 1983). Ultimately this leads to the generation of thrombin in large enough quantities to initiate fibrin polymerisation.

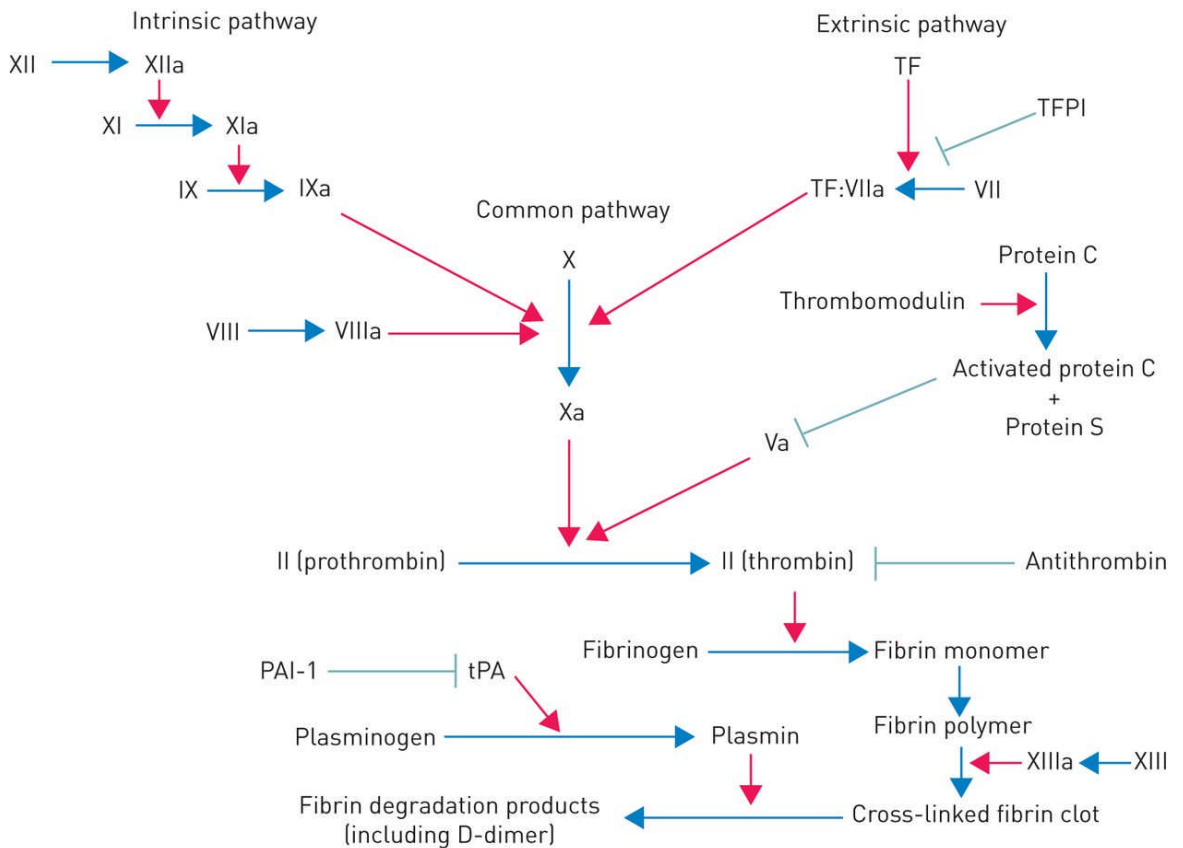


**Figure 1-3 Diagrammatic representation of coagulation** The contact and tissue factor pathway merge where factor Xa cleaves prothrombin to thrombin. Thrombin then converts fibrinogen to fibrin, but also activates factor XIII which cross-links fibrin monomers to create a cross-linked fibrin network. Image reused from (Crooks and Hart, 2015) with permission from *European Respiratory Review*.

## 1.2 Fibrinogen

Fibrinogen was originally known as factor I (Alami *et al.*, 1968) and its primary function is to provide the mechanical strength and stability to clots (Kim *et al.*, 2014; Glidden *et al.*, 2000; Zhmurov *et al.*, 2011). Other physiological roles include inflammation (Alexander *et al.*, 2011; Hennigs *et al.*, 2014; Davalos and Akassoglou, 2012), angiogenesis (Staton *et al.*, 2003; Sahni and Francis, 2000; Hadjipanayi *et al.*, 2015) and very recently it was found that fibrin is involved in wound protection through the production of a fibrin sheet (Macrae *et al.*, 2018).

In the blood of a healthy individual, fibrinogen circulates in the body at approximately 1.5g to 3.5g per litre (Takeda, 1966), this amount can increase rapidly during inflammation as fibrinogen is an acute phase response inflammatory protein (Jain *et al.*, 2011). Others have reported that fibrinogen levels can increase up to as much as 8g per litre in pathophysiological conditions (Machlus *et al.*, 2011).

A great deal of structural information has been gathered by crystallography efforts (Spraggon *et al.*, 1997; Everse *et al.*, 1998; Yee *et al.*, 1997). Fibrinogen is a large elongated trinodular glycoprotein (Fowler and Erickson, 1979) that is approximately 340kDa in size and is has three dimeric polypeptide chains  $(A\alpha B\beta\gamma)_2$  that organise into two identical halves (Doolittle, 1984), Figure 1-4A. The  $A\alpha$ -chain is 610 residues, whereas the  $B\beta$  and the most common splice variant of the  $\gamma$ -chain ( $\gamma A$ ) are 461 and 411 residues respectively (Henschen *et al.*, 1983). The  $\gamma'$  variant is created by an alternative splicing event that replaces  $\gamma A$  codons 408-411 with a negatively charged 20 amino acid sequence (Wolfenstein-Todel and Mosesson, 1981).  $\gamma'$  is an proportionally uncommon splice variant where the heterodimeric  $\gamma' \gamma A$  form contributes to approximately 15% of fibrinogen found in human plasma whereas the homodimeric  $\gamma' \gamma'$  form contributes less than 1% (Wolfenstein-Todel and Mosesson, 1980).

Each polypeptide chain of fibrinogen  $A\alpha$ ,  $B\beta$  and  $\gamma$  are encoded by their own gene, FGA, FGB and FGG respectively (Chung *et al.*, 1980) and are located on chromosome four, bands q23-q32 (Kant *et al.*, 1985). The polypeptide chains are all expressed in hepatocytes (Tennent *et al.*, 2007) where the  $B\beta$  and  $\gamma$  chains are glycosylated (Nickerson and Fuller, 1981). Firstly, the  $\gamma$ -chains form pre-complexes with the  $A\alpha$  and  $B\beta$  chains forming  $A\alpha$ - $\gamma$  and  $B\beta$ - $\gamma$  complexes, then

the missing chain (either B $\beta$  or A $\alpha$ ) combines to form A $\alpha$ B $\beta$  $\gamma$  half molecules. An in-depth discussion on fibrin assembly can be found in (Redman and Xia, 2001). The two half molecules then co-complex to form a complete hexameric fibrinogen monomer (A $\alpha$ B $\beta$  $\gamma$ )<sub>2</sub> before being secreted from the cell (Hirose *et al.*, 1988) (Yu *et al.*, 1984). Each of the fibrinogen chains has a signal peptide that is cleaved from the relative chain during the translocation process to the endoplasmic reticulum and the disulphide bonds are formed before secretion (Zhang and Redman, 1996). All sequence nomenclature discussed in the body of this work will be that of the mature product after removal of the signal peptide.

The N termini of the chains begin in the central globular central 'E' region where they extend outwards in a helical coiled coil fashion, and end in two distal 'D' regions, Figure 1-4A. The longer  $\alpha$ -chain, however, which is not resolved by X-ray crystallography, is thought to protrude from the D-region and fold back towards the E region. Fibrinogen has 58 cysteine residues, Figure 1-4B, the two pair of disulphide rings hold separate chains of the molecule together and at each end of the coiled coiled regions. There are five interchain disulphide bonds that hold the two halves of the molecule together (Huang *et al.*, 1993).

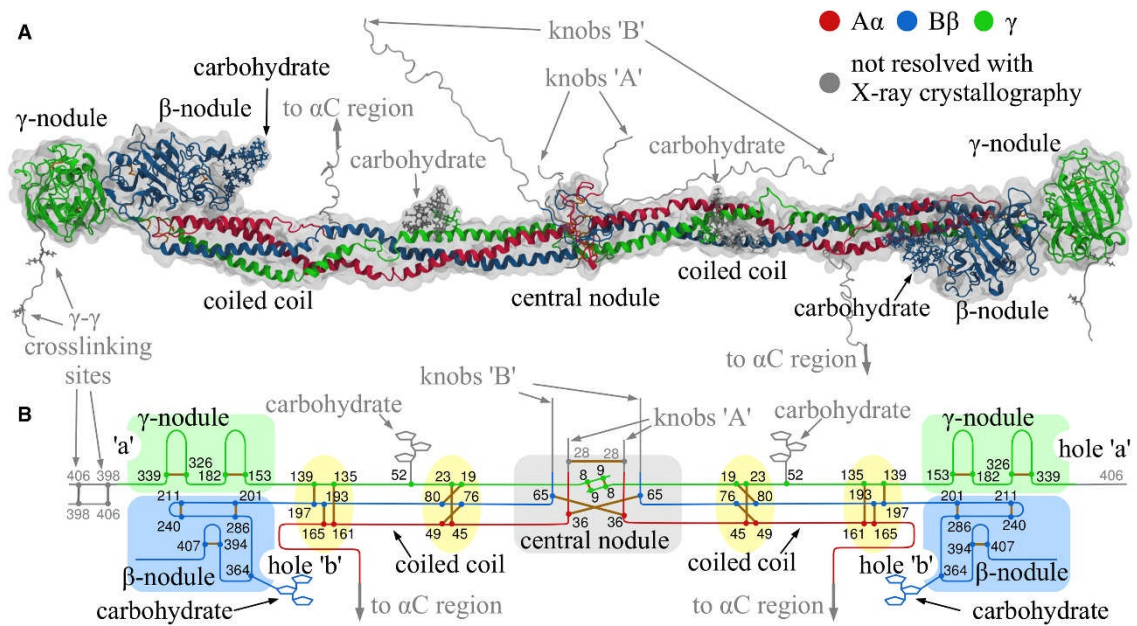


**Figure 1-4 Molecular dynamic representation of human fibrinogen (A)** Crystal structure PDB 3GHG was used to map structural elements of the fibrinogen molecule. Chains A $\alpha$  were highlighted in red,  $\beta$ b in blue and  $\gamma$ -chains in green. Items in grey such as knob A and knob B sequences and  $\alpha$ C sequences in (A) are modelled onto the crystal structure and represent portions of the molecule that were not resolved in the crystal structure. (B) Schematic of fibrinogen depicting disulphide bonds across all three polypeptide chains (shaded yellow). *Image reused with permission from the journal 'Structure' reference number 4445910717620. (Zhmurov et al., 2016)*

### 1.3 Fibrin polymerisation and clot formation

As highlighted in Figure 1-5 fibrinogen is converted to fibrin by the serine protease thrombin. Thrombin cleaves two fibrinopeptides, fibrinopeptide A (FpA) from the N-terminal region of the A $\alpha$  chain which is 16 residues in length and fibrinopeptide B from the N terminal region of the B $\beta$  chain which is 14 residues in length (Pechik et al., 2006). FpA is released faster than FpB due to higher affinity of FpA for thrombin (Mullin et al., 2000a), however during the polymerisation process the rate of FpB release increases, suggesting that the formation of protofibrils accelerates FpB release (Riedel et al., 2011). The removal of the fibrinopeptides has a crucial effect, the unmasking of knobs A (by

FpA removal) and knobs B (by FpB removal) which can then bind to permanently exposed holes on adjacent fibrin molecules (Averett *et al.*, 2008). Knobs A and B do not appear in the crystal structures as they are semi flexible. Synthetic peptides that replicate the N-terminal sequence of knobs A and B have been made. GPRP (binding to hole-a in the  $\gamma$ C pocket) and GHRP (binding to b-hole in  $\beta$ C pocket) have been crystallised into the D-regions, indicating the residues involved in the knob-hole interactions (Pratt *et al.*, 1997). Due to the dimeric properties of the molecule there are two A:a knob-hole and two B:b knob hole complexes that are able to form and do so in a half staggered fashion. The spontaneous polymerisation continues and forms structures called protofibrils which essentially are longer oligomers. Upon reaching a critical length (0.5 $\mu$ m) (Storm *et al.*, 2005), those protofibrils begin to laterally aggregate to form fibrin fibers which in turn form the fibrin matrix as seen in Figure 1-6.

The traditional view of polymerisation dynamics is that A:a interactions drive longitudinal growth forming oligomers and protofibrils whereas B:b knob-hole interactions are responsible for the lateral aggregation of protofibrils into fibrin fibers (Geer *et al.*, 2007). Evidence for this is that particular snake venom enzymes that cleave only FpA yield clots that have thinner fibers (Shen *et al.*, 1977). Dysfibrinogenaemia such as fibrinogen Metz demonstrates clots can be formed with only FpB cleavage, although the fibrin also yields clots that are have thinner fibers (Galanakis *et al.*, 1993).

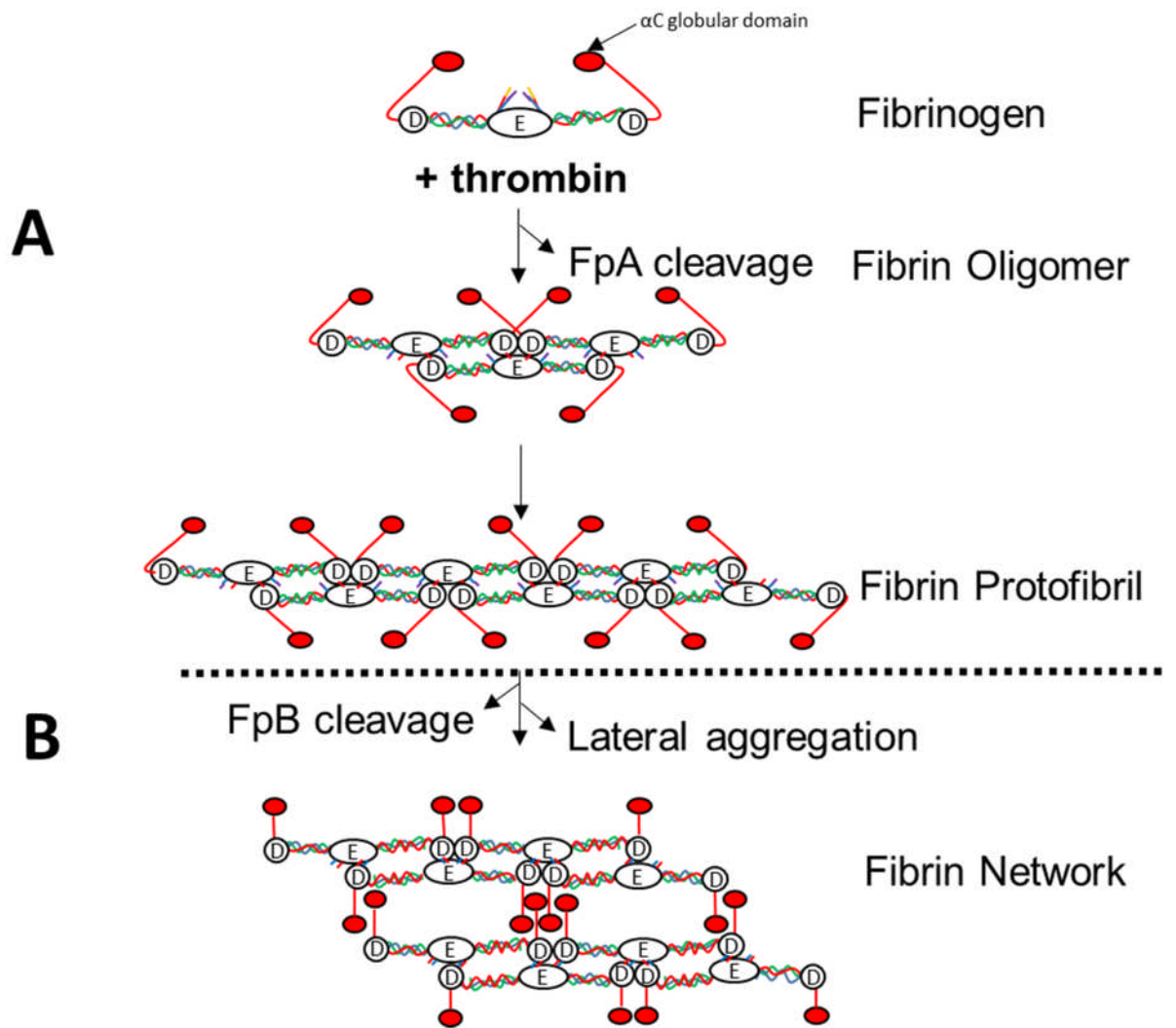


**Figure 1-5 Fibrin(ogen) Polymerisation (A)** Fibrinogen structure, A $\alpha$  chains (red) B $\beta$ -chains (blue) and  $\gamma$ -chains (green), fibrinopeptides, FpA and FpB (orange and purple respectively). Thrombin cleaves FpA situated in the E region and exposes knobs A which bind to permanently exposed holes-a located within E regions of other monomers forming fibrin oligomers, and at later time points fibrin protofibrils. **(B)** Fibrinopeptides B are cleaved by thrombin when the protofibrils reach a critical length exposing knobs B. Knobs B located on the E-region bind to permanently exposed holes-b located within the D-region. The binding of knobs B with holes-b in conjunction with release and interaction of  $\alpha$ C regions causes the protofibrils to laterally aggregate and form fibrin fibers.

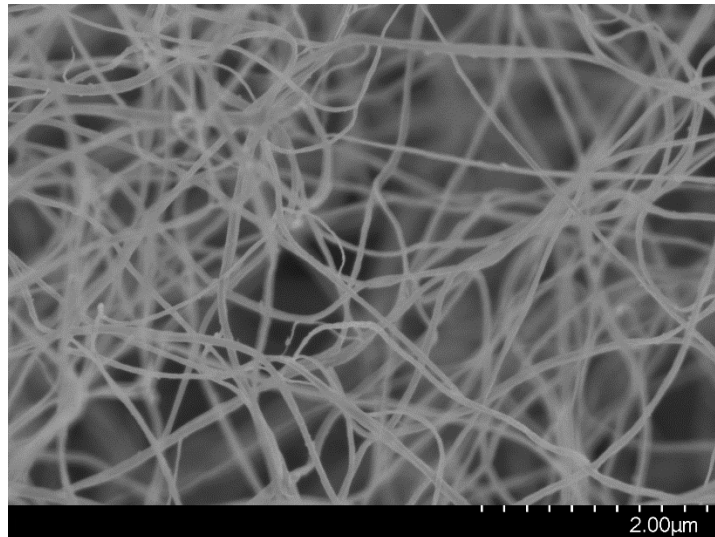


**Figure 1-6 Scanning electron microscopy image of a purified fibrin clot**  
Thrombin cleaves fibrinogen to form a fibrin clot and was imaged at 20,000x magnification. Image Nathan Asquith, University of Leeds.

Recent discoveries have shown that the  $\alpha$ C domains of fibrin(ogen) also play a role in polymerisation. The  $\alpha$ C domains cannot be resolved in the crystal structures because they are semi flexible regions. However, they have been recently imaged and characterised by AFM (Protopopova *et al.*, 2017; Protopopova *et al.*, 2015). The  $\alpha$ C domains have also been implicated in polymerisation (Weisel and Medved, 2001). It has been observed by AFM that the  $\alpha$ C domains usually interact with the central E domain when the molecule remains as fibrinogen. However, when converted to fibrin there is a large conformational change where the  $\alpha$ C dissociate from the E domain (Weisel and Medved, 2001), Figure 1-7.

The Ariëns laboratory has shown that recombinant variants missing the  $\alpha$ C connector have significantly different clotting times, clot structure (McPherson, unpublished), and when  $\gamma$ -chain cross-linking is inhibited clot stiffness still increases showing the importance of  $\alpha$ C regions and  $\alpha$ -chain crosslinking in the

mechanical properties of fibrin. (Duval *et al.*, 2014). Others have also shown remarkable differences using recombinant variant  $\alpha 251$  to investigate the role of the  $\alpha$ -chain in polymerisation (Collet *et al.*, 2005b). Here the authors showed that truncated recombinant  $\alpha 251$  variant (that is missing the  $\alpha$ -chain globular domain) impacted greatly on polymerisation through lateral aggregation, but this variant was similar to WT for longitudinal protofibril assembly as measured by turbidity. Additionally this variant produced clots that were 30% more deformable than WT control clots, even though the clot network was denser, suggesting that  $\alpha C$  domains in WT fibrinogen interact with each other to increase rigidity.

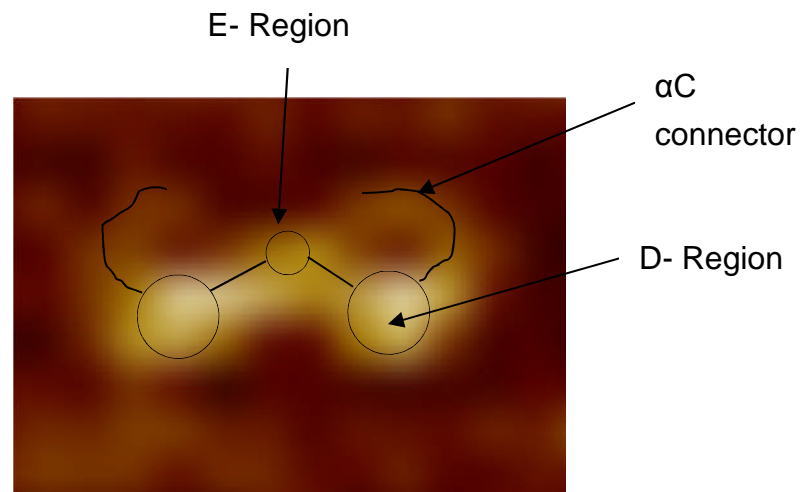


**Figure 1-7 Atomic force image of a single fibrin monomer.** Soft tapping mode in air was used to obtain the topology profile of a single fibrin monomer on a freshly cleaved mica surface. The high resolution capabilities of the AFM allowed the imaging of D and E globular regions in addition to the  $\alpha C$  connector. Image taken by Nathan Asquith.

## 1.4 Factor XIII

### 1.4.1 Factor XIII structure and secretion

FXIII is a tetramer composed of two A subunits, that provides the catalytic activity of the protein, and two B subunits (Nagy *et al.*, 1988). The molecular weight of the full protein structure (FXIII-A<sub>2</sub>B<sub>2</sub>) is 320kDa (Ashcroft *et al.*, 2000). Very little

information is known about the structure of the full molecule, however others have postulated that both the factor XIII B subunits protect the catalytic core A subunits (Ivaskevicius *et al.*, 2010). Patients that are deficient in either A- or B subunit demonstrate an increased bleeding phenotype. (Karimi *et al.*, 2009). Factor XIII A subunit is secreted by many cell types such as monocytes, macrophages and megakaryocytes (Cordell *et al.*, 2010), the B-subunit is secreted from hepatocytes in the liver (Ariëns *et al.*, 2002). More recent work has provided evidence that arterial macrophages provide the majority of plasma FXIII A (Beckers *et al.*, 2017).

#### **1.4.2 Factor XIII function**

As clot formation occurs, thrombin cleaves fibrinogen to fibrin, simultaneously thrombin also activates factor XIII (factor XIIIa) during clot formation, FXIIIa forms  $\gamma$ -glutamyl-lysine bonds between  $\gamma$ Gln398/399 of one fibrin monomer with  $\gamma$ 406 on an adjacent fibrin monomer. The  $\alpha$ -chains of fibrin are also crosslinked at sites 221, 237, 328, 366 (glutamine acceptor sites) with residues 508, 539, 556, 580 and 601 (lysine donor sites) (Ariëns *et al.*, 2002). The crosslinking process increases the stiffness of fibrin clots *in vitro* (Ryan *et al.*, 1999a) and it is hypothesised that this stiffness *in vivo* would lead to clots that are less prone to embolise (Weisel, 2004a). Factor XIIIa also crosslinks fibrinolytic inhibitors to fibrin such as  $\alpha_2$ -antiplasmin (Carpenter and Mathew, 2008).

### **1.5 Prevention of clot formation and clot lysis**

Naturally occurring anticoagulants are substances that can prevent coagulation and therefore reduce thrombus formation (Harter *et al.*, 2015). In a healthy vessel, endothelial cells and megakaryocytes secrete tissue factor pathway

inhibitor (TFPI) (Maroney and Mast, 2008). It has been identified that the K1 domain within TFPI binds to the active site of TF-FVIIa complex in the presence of calcium ions and co factor FXa (Mast Alan, 2016), whereas the K2 domain binds directly to FXa.

Thrombomodulin is expressed on the endothelial membrane which forms a complex with thrombin and reduces the conversion of fibrinogen to fibrin through the activation of protein C and subsequent inactivation of factor Va and factor VIIIa (Sadler, 1997). Antithrombin inhibits factor IXa, Xa and XIa, and also inhibits thrombin (factor IIa) in a more significant manner. Antithrombin does this by forming a covalent complex with these enzymes (Maaroufi *et al.*, 1997). Heparin, a therapeutic anticoagulant, enhances the efficiency of antithrombin via a conformational change and exposure of exosites enabling antithrombin to inactivate thrombin at a greater rate (Gray *et al.*, 2012).

*In vitro* peptides that mimic partial knob A and knob B sequences have been designed. GPRP competes with knob A for the hole-a; GHRP competes with the B knob for hole-b in fibrin monomers. Therefore knob-hole binding cannot take place and fibrin fibers do not form. These peptides have been used to aid in the determination of the crystal structure of fibrin monomers (Everse *et al.*, 1998).

*In vitro*, digestion of fibrinogen can be performed with cyanogen bromide, yielding DesAB-NDSK fragments (N-terminal Disulphide knot fibrinogen) which contains the E region and coiled coil connectors (Litvinov *et al.*, 2005). Trypsin has also been used to produce fragments of fibrinogen for X-ray crystallography analysis (Spraggon *et al.*, 1997). Fibrinogen can also be digested by plasmin (Slater *et al.*, 2018), which generates fragments X, Y, D and E in a time

dependent manner. Initially digestion will generate fragment X which is essentially fibrinogen but with truncated alpha chains, at later stages fragment Y is formed which is the further loss of one D region, upon further digestion of fragment Y, fragments D and E are obtained. Digestion of cross-linked fibrin removes  $\alpha$ -chain cross links to produce fragment X (240kDa) (Ferguson *et al.*, 1975) where further digestion leads to the production of fragments YD and D-dimer (Gaffney, 2001). D-dimer includes two cross-linked D regions non-covalently bonded to an E region by knob-hole bonds (Gaffney and Joe, 1979), Figure 1-9.

## **1.6 Fibrinolysis**

In blood, once the fibrin network has stemmed the loss of bleeding and is no longer required it is broken down into smaller fragments, this is known as the fibrinolytic process. The fibrinolytic process involves the degradation of fibrin fibers by serine protease plasmin. Plasmin is formed by the conversion of plasminogen to plasmin mainly by tissue plasminogen activator (tPA) (Didiasova *et al.*, 2014), urokinase plasminogen activator (uPA) (Lacroix *et al.*, 2007) or streptokinase (SK) (Sherry, 1954). The tPA circulating in the blood is derived from endothelial cells. The plasminogen and tPA bind to C-terminal lysines (via kringle domains) on the fibrin fibers where plasminogen becomes activated by tPA. As new C-terminal lysines become exposed they provide additional binding sites for plasminogen and tPA contributing to a positive feedback mechanism and enhancing the fibrinolytic process. Interestingly, fibrin also acts as a co-factor for tPA mediated plasminogen activation. It has been previously reported that the affinity for tPA for plasminogen increases 1000-fold when bound to fibrin

increasing the fibrinolytic activity 2 to 4-fold (Zamarron *et al.*, 1984). As mentioned in section 1.5 the digestion of fibrin by plasmin produces fibrin degradation products. The main difference between fibrinogen and fibrin degradation products being that the covalent crosslinks of factor XIIIa are present in fibrin leading to the formation of structures such as D-dimer. As D-dimer is a degradation product of fibrin, it has been widely used as a tool in the clinic to detect levels of intravascular fibrin deposition (Bates, 2012).

This fibrinolytic process can be inhibited by different mechanisms,  $\alpha_2$ -antiplasmin for example can decrease the digestion of fibrin by the formation of a complex with plasmin or by becoming crosslinked to the fibrin fibers via FXIIIa making the network more resistant to digestion (Sakata and Aoki, 1980). Lysis can also be prevented by plasmin activator inhibitor (PAI-1) through the binding of PAI-1 with either tPA or uPA (Gorlatova *et al.*, 2007). TAFI (thrombin activable fibrinolysis inhibitor) hinders fibrinolysis by the removal of C-terminal lysines from fibrin, which reduces tPA mediated plasminogen activation within the clot (Bouma and Mosnier, 2006). Mechanical and structural properties of the fibrin mesh can also influence the fibrinolytic properties. For example, density of the fibers, number of branch points and fiber thickness can all influence lysis rates. The accepted dogma is that denser networks with thinner fibers are slower to lyse and less dense networks with thicker fibers are faster to lyse (Weisel and Litvinov, 2017)

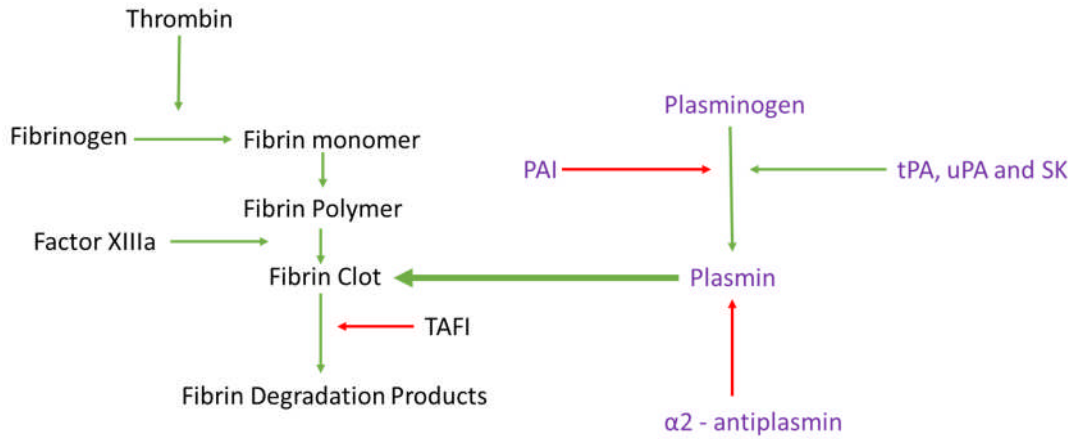


**Figure 1-8 Clot formation and fibrinolysis** Clot formation (left, green lines) and fibrinolysis (right) The fibrinolytic process can be inhibited by several molecules (red lines) including PAI (plasminogen activator inhibitor),  $\alpha_2$ -antiplasmin and TAFI (thrombin activatable fibrinolysis inhibitor).

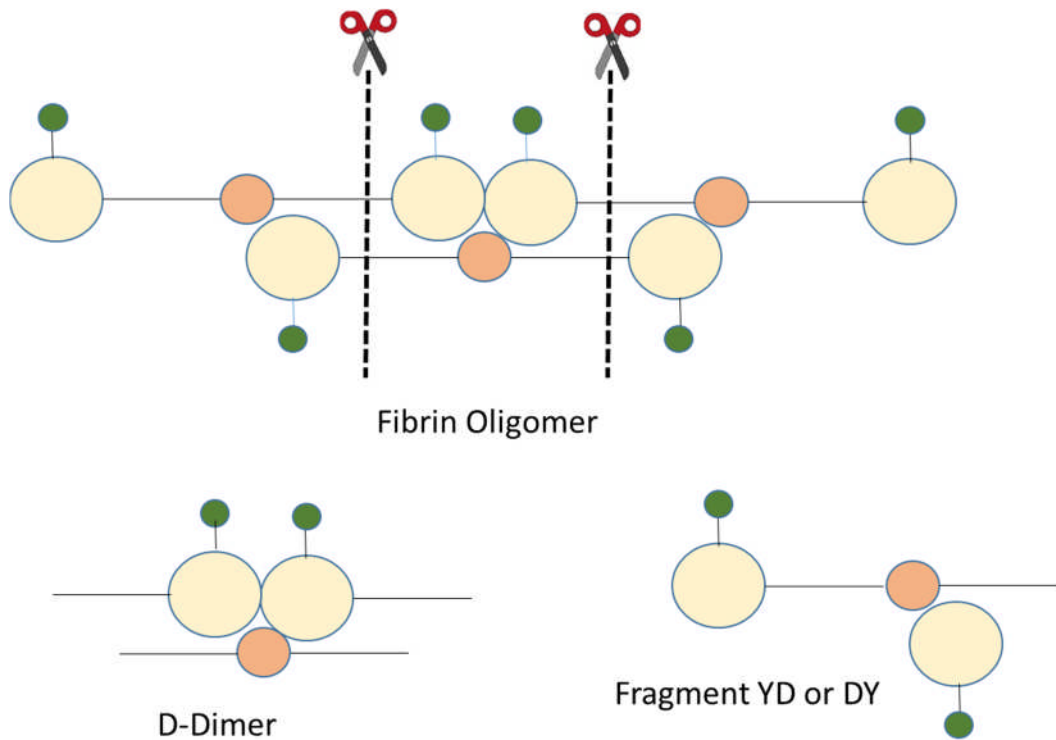


**Figure 1-9 Schematic of digestion of cross-linked fibrin by plasmin** Cleavage of a fibrin oligomer (yellow = D-region, orange = E-region and green =  $\alpha$ C domains) by plasmin initially removes cross-linked  $\alpha$ -chains and then cuts the coiled coils at the positions indicated with a dotted line. Fibrin degradation products are produced such as DD-E complex (d-dimer) and fragment YD.

## 1.7 Fibrin clot structure

Fibrin at the nanoscale has been imaged for at least the past 40 years as demonstrated the rotary shadow image of fibrinogen on a mica surface, Figure 1-10. In brief, Fowler was able to spray a glycerol/fibrinogen solution onto a mica surface and dried it using a vacuum evaporator, the samples were then sprayed with platinum and imaged using a scanning electron microscope, (Fowler and Erickson, 1979). Modern technology such as atomic force microscopy allows the imaging of  $\alpha$ C domains in fibrin (Protopopova *et al.*, 2017).

Fibrin monomers, Figure 1-10, undergo spontaneous polymerisation, and eventually lead to the formation of fibrin fibers, Figure 1-11. The fibers form branch points, become entangled with one another, and trap other blood components such as cells and other plasma proteins, Figure 1-12.

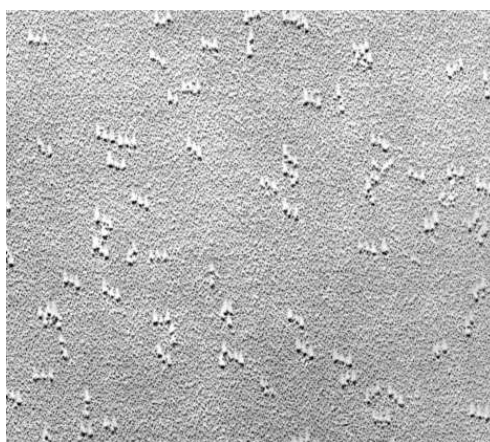


**Figure 1-10 Rotary shadowed fibrinogen** Fibrinogen prepared on freshly cleaved mica, and dried using a vacuum and observed using SEM at 100,000 magnification. The typical trinodular shape of fibrinogen can clearly be observed. (Fowler and Erickson, 1979)

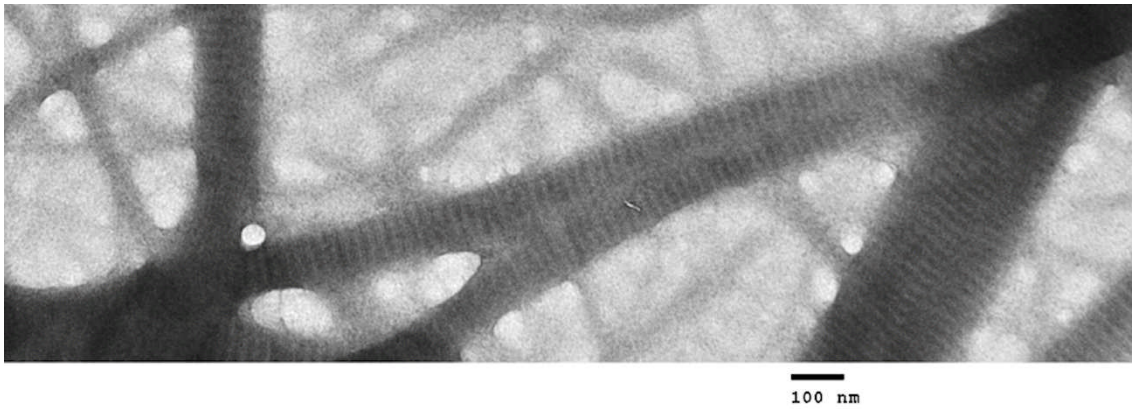


**Figure 1-11 Transmission electron micrograph of human fibrin** Human fibrinogen was cleaved with thrombin, fibers were negatively stained and imaged using an electron Microscope. The image from the authors clearly demonstrates the 22.5nm banding pattern of fibrin fibers. Image courtesy of Marco Domingues, University of Leeds.

The polymerisation that is initiated upon cleavage of fibrinogen monomers to fibrin monomers, allows fibrin to stack into half staggered protofibrils that was observed by Krakow *et al.*, using scanning electron microscopy (Krakow *et al.*, 1972). Another group has explored the use of negative staining techniques in an attempt to confirm that fibrin fibers are in fact made from half staggered protofibrils (Weisel, 1986). In this technique, areas that have lower protein density (coiled-coil regions) absorb stain and therefore appear dark, whereas the opposite is true for areas of high protein density (globular D and E regions) and therefore appear bright as demonstrated in a TEM image taken by Dr. Marco Domingues, University of Leeds, Figure 1-11.

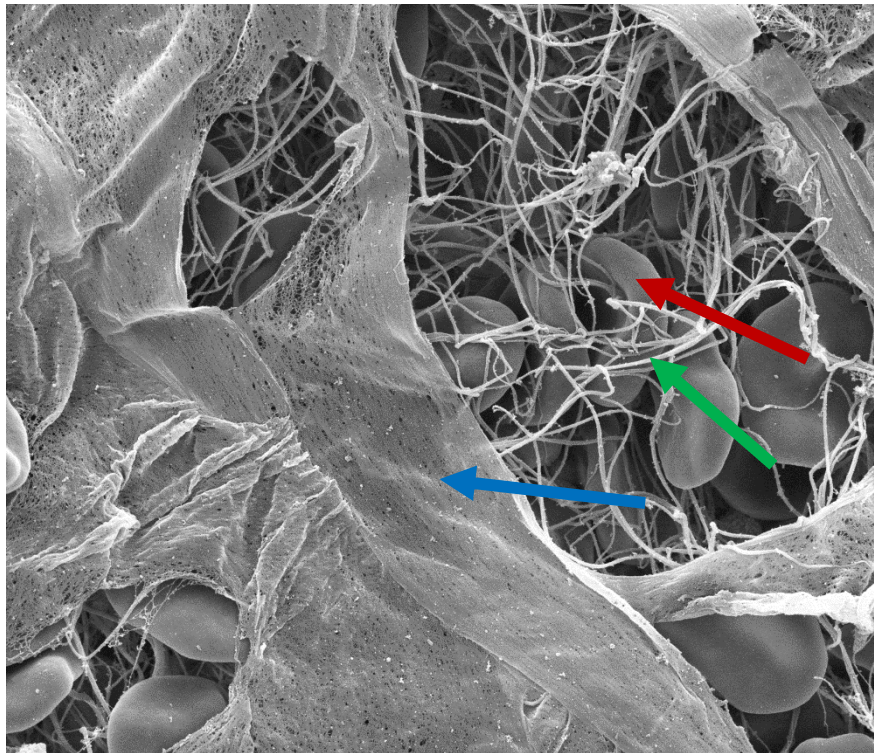


**Figure 1-12 Scanning electron micrograph of a fibrin clot prepared from whole blood.** Red arrow represents red blood cell, green arrow represents fibrin fibers and blue arrow indicates the presence of fibrin sheet covering the clot. Image courtesy of Fraser Macrae, University of Leeds.

Once the fibers are formed they intertwine and form a complex three dimensional network (Baradet *et al.*, 1995). In addition to the formation of a fibrin fibrillary network, a recent study by the Ariëns laboratory has shown that fibrin also produces a sheet covering the clot through Langmuir film formation at the air-liquid interface, Figure 1-12 . Each fibrin mesh within the clot can have varying characteristics such as different fiber thickness (Pretorius *et al.*, 2011), fibrin fiber density (Li *et al.*, 2017), pore sizes (Blombäck *et al.*, 1989), and mechanical properties. In physiological conditions, the fibrin network and the fibrin sheet prevent loss of red blood cells (Kim *et al.*, 2013).

In the literature many authors have investigated the role of differing substances and conditions on the clot network. An increase in pH or a decrease in

temperature of the fibrinogen solution (Nair *et al.*, 1986) was investigated by turbidity. It was found that the development of the clot was delayed. A reduction in temperature did not significantly reduce the mass length ratio of a fibrin fiber ( $\mu_0$ , proportional to fiber thickness) but this mass length ratio decreased with the increase in pH. In addition to turbidity, other techniques can be used to study fibrin polymer architecture. The Ariens group showed that light scattering can be used effectively to probe the average fiber radius within a fibrin clot (Domingues *et al.*, 2016). I showed that an increase in thrombin concentration decreased the radii of fibrin fibers as previously seen by others (Blombäck *et al.*, 1989). It has been reported that polyphosphates also play a role in regulating clot structure, in the presence of calcium. Clots that were formed with the inclusion of polyphosphate had a three-fold higher turbidity in addition to an increase in fiber thickness measured by SEM (Smith and Morrissey, 2008), however the Ariens laboratory demonstrated that fiber thickness was unchanged in the presence of polyphosphate but closely knit 'fibrin knots' were present in SEM micrographs (Mutch *et al.*, 2010). It was shown that increasing the concentrations of fibrinogen forms clots that are more dense (Ryan *et al.*, 1999b). The binding of calcium ions to fibrin protofibrils forms clots that are have thinner fibers than clots that are in the presence of Fluorine ions (Di Stasio *et al.*, 1998). The presence of calcium ions on clot structure were investigated using thrombin and reptilase. In the presence of calcium, with both enzymes the clots formed faster, the maximum optical density was increased, and larger fiber mass/length ratios were observed, indicating thicker fibers for clots (Carr *et al.*, 1986). Electron microscopy studies on the effect of cysteine show increased cardiovascular disease risk, clot structures were denser with many branch points (Lauricella *et al.*, 2006;

Mujumdar *et al.*, 2001). Even complex branched polysaccharides such as dextran can have an impact on clot structure, by increasing fiber thickness (Carr and Gabriel, 1980). More recently, clots that were formed *ex vivo* from blood samples taken from patients treated with dextran showed that these clots were subject to increased fibrinolysis (Jones *et al.*, 2008).

## **1.8 Intra-fibrillar fibrin structure**

Once protofibrils reach a critical length, they laterally aggregate to form fibrin fibers, (Weisel and Litvinov, 2017). However, the exact mechanism to how this occurs is not fully understood. The fibrin fiber diameter and consequently fibrin fiber packing arrangements have a direct effect on fiber stiffness and therefore could influence the formation of an embolus *in vivo* (Li *et al.*, 2016). Previous studies by other groups do not necessarily agree with each other on the packing arrangements of fibrin fibers, some groups have shown that protofibrils within a fiber are packed in a ordered fashion (Caracciolo *et al.*, 2003) whereas others have shown that fibers may not be homogeneous throughout (Guthold *et al.*, 2004). Light scattering is typically used to determine the amount of protofibrils, the distance between protofibrils and hence overall protein density of fibrin fibers (Carr and Hermans, 1978; Yeromonahos *et al.*, 2010). It is an indirect measure of fiber radius and the models are based on the assumption that all fibers are of equal thickness inside the clot, however the clot may be in fact heterogeneous. As discussed in section 1.3, fibrin polymerises in both the longitudinal space and lateral space. Using a combination of crystal structures and light scattering data a multi-bundle model of protofibril packing within fibrin fibers was proposed, hypothesising that protofibrils are packed homogenously within the fiber (Yang

*et al.*, 2000). This model was critiqued and a new model was proposed based on the relationship between stretch modulus of fibrin fibers and fibrin diameter (Li *et al.*, 2016) The authors argue that if a fibrin fiber really does have protofibrils that are packed homogenously then the stretch modulus ( $Y$ ) would be independent to fibrin diameter, Figure 1-13A. They propose a “bicycle wheel spokes” model Figure 1-13B where the stretch modulus decreases as fiber diameter increases. However, their experimental observations using lateral force pulling AFM show that stretch modulus decreases in an even more dramatic manner with increasing fibrin diameter than predicted by the “bicycle wheel spokes” model. They explained that this would lead to a model where fibrin fibers have a dense core leading to a less dense periphery (Figure 1-13C) as demonstrated in their later publication (Li *et al.*, 2017). The work by Li *et al.*, shows that protofibril packing may be more complex than the homogenous fiber density as proposed by (Carr and Hermans, 1978).

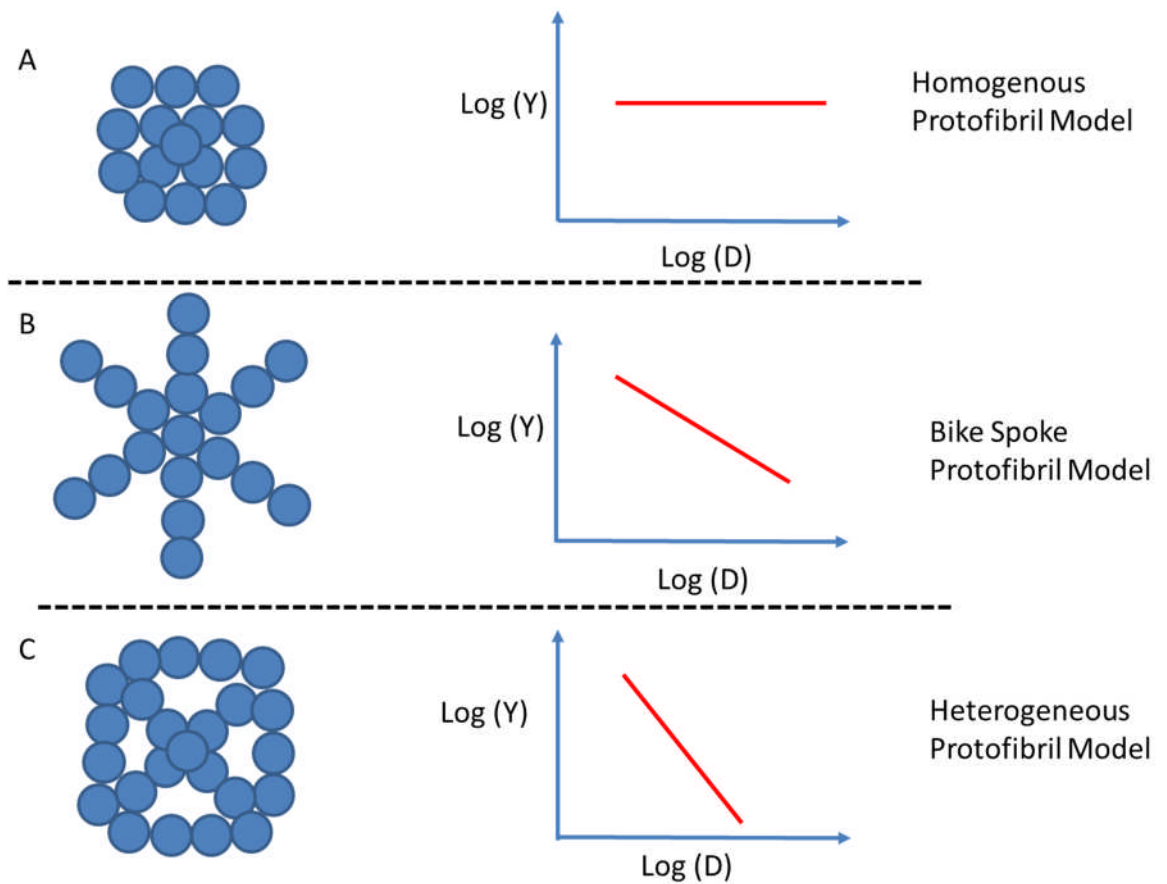


**Figure 1-13 Theoretical schematics of different packing possibilities for fibrin fibers** (Panel A) Homogenous protofibril model proposed by where stress modulus is independent of fibrin diameter. (Panel B) Bicycle wheel spokes protofibril model where the stretch modulus (Y) decreases as fiber diameter (D) increases. (Panel C) Heterogeneous protofibril model where stretch modulus decreases rapidly with increasing radius. Figure based on Figure 6 in (Li *et al.*, 2016)

## 1.9 Fibrin mechanics

Fibrin fibers are one of the strongest naturally occurring polymers in nature, which makes it a perfect candidate to stem a damaged vessel wall and to prevent the loss of blood, while the damage is repaired, despite the large shear forces present in the blood (Weisel, 2004a). Although, in normal physiological conditions it may seem like a good idea to have a strong polymer to prevent blood loss, in pathological conditions of thrombosis this may be detrimental. The

formation of pathological fibrin clots (thrombi) lead to conditions such as myocardial infarction (MI) (Delewi *et al.*, 2012), ischemic stroke (Stoll *et al.*, 2008) or VTE (venous thrombo embolism) (Phillippe, 2017). Therefore the visco-elastic properties of thrombi, with fibrin(ogen) as the key modulator, are key to preventing bleeding, and may contribute to the risk of thrombosis or embolization of thrombi.

Many previous studies have shown that clots formed *in vitro*, from the plasma taken from patients who had experienced myocardial infarction, are denser than those of control subjects (Fatah *et al.*, 1996). Others have also observed that *ex vivo* plasma from patients with premature coronary heart disease form denser fibrin networks that are more stiff (Collet *et al.*, 2006). The authors found an increase of storage modulus from 21.2 to 31.2 dynes/cm<sup>2</sup> (+47.2% ).

Micro-rheology studies of fibrin clots have been performed by many groups in the past (Nelb *et al.*, 1976; Ferry *et al.*, 1951; Shen and Lorand, 1983; Domingues *et al.*, 2016). Shear rate describes the flow of a liquid through a vessel, in the case of haemostasis and thrombosis this is the blood shear rate within arteries, veins and capillaries. The shear rate is influenced by the diameter of the vessel (Casa *et al.*, 2015) There is a direct relationship between the viscosity, wall shear rate and wall shear stress where; *Wall shear stress* = *viscosity* x *wall shear rate*. Build-up of athlerosclerotic plaques can narrow vessels, increasing the shear rate within the vessel and therefore the shear stress on the endothelium wall. Shear stress is important because it can influence biological processes such as platelet adhesion (Ruggeri *et al.*, 2006). Fibrin clots are exposed to shear rates that range from approximately 10s<sup>-1</sup> (in veins) to 2000s<sup>-1</sup> in (arteries) (Sakariassen *et al.*, 2015). In pathophysiological

conditions such as atherosclerosis, the shear rate in arteries can reach up to  $40,000\text{s}^{-1}$  (Sakariassen *et al.*, 2015). Molecular simulations of shear conditions have been performed previously by Kononova *et al.*, who calculated that knob-hole bonds must be exposed to tensile forces ranging from 150-400pN (Kononova *et al.*, 2013). Therefore clots must be able to withstand (patho)physiological stresses and not undergo permanent deformation. If the stresses are too great, the whole clot, or fragments, breaking off and traveling through the rest of the circulatory system, a process known as embolisation is possible. Thromboelastometry is used in the clinic for the prediction of need of a blood transfusion (Crochemore *et al.*, 2017), it measures the visco-elastic properties of a patient's whole blood sample and outputs parameters such as maximum clot firmness (Zaky, 2017). The basic principle involves the change in rotational torque of a pin during blood clotting. Weisel has discussed the difficulty of associating *ex vivo* tests like thromboelastometry to *in vitro* biophysical data obtained with rheometers or other biophysical methods to determine visco-elastic properties of clots. The *in vitro* biophysical methods generate visco-elastic moduli  $G'$  ( $G_{\text{prime}}$ ) and  $G''$  ( $G_{\text{double prime}}$ ), whereas it is not clear how the parameters obtained by thromboelastometry relate to these biophysical measures (Weisel, 2004a).

The  $G'$  (storage modulus), is defined as the amount of energy that is stored in a system. In work on fibrin clots, the  $G'$  is often used in the literature to describe clot or fiber stiffness (Konings *et al.*, 2011; Longstaff *et al.*, 2013; Piechocka *et al.*, 2010). The  $G''$  (loss modulus) is defined as the amount of energy that is dissipated from a clot, and is often used to represent the amount of permanent deformation or in other words viscosity (Schmitt *et al.*, 2011; Mason and Weitz,

1995). Fibrin clots are neither purely elastic or viscous, but they are visco-elastic, and therefore one must consider both moduli at the same timescale. Therefore the  $\tan\delta$  is calculated, which is the ratio of  $G''/G'$ , which indicates the amount of non-elastic deformation relative to the stiffness. A predominately viscous material would have a  $\tan\delta > 1$ , whereas a predominantly elastic material would have a  $\tan\delta < 1$  and a material where the  $\tan\delta = 1$  signifies that neither the storage or loss modulus is dominating, (Collet *et al.*, 2005b). Clots with a high  $G'$  and lower  $G''$  are stiffer and experience less permanent deformation, usually attributed to many branch points and increased fiber thickness. Clots with lower  $G'$  and high  $G''$  are more readily deformable due to fewer branch points and thinner fibers (Ryan *et al.*, 1999b). It has been shown that specific unfolding of molecular domains of the fibrinogen molecule such as the coiled coils (Lim *et al.*, 2008; Brown *et al.*, 2007) and D-domains (Guthold *et al.*, 2007) can impact on the mechanical properties of the fibrin clots. Interestingly, it has been observed that clot density (the number of fibers in a certain area of the clot) can impact on clot stiffness where an increase in clot density leads to an increase in  $G'$  (Ryan *et al.*, 1999b).

A magnetic micro-rheology apparatus was designed and created by Rob Harrand, University of Leeds (Harrand.R, 2007) and was further optimised to study the mechanical properties of fibrin clots by Peter Allan, University of Leeds (Allan.P, 2012). My studies utilise the same device and analysis procedure for the calculation of visco-elastic measurements of fibrin clots. The analysis is based on the theory of visco-elastic properties of semi-flexible polymer solutions suggested by groups who described three relaxation mechanisms of fibrin (Morse, 1998a; Morse, 1998b; Morse, 1999; MacKintosh *et al.*, 1995). Briefly,

moduli at the low frequency range are dictated by the alignment of fibers, intermediate frequencies are dictated by the twisting of fibers, and high frequencies are dictated by molecular deformation events. Following raw data collection, a mathematical procedure is then performed as previously described to calculate the  $G^*$ ,  $G'$  and  $G''$  from time dependent compliance (Evans *et al.*, 2009).

Mechanics at smaller scales, such as at the fibrin fiber level, and at the fibrin monomer level have also been investigated by others. At the fiber level, lateral force AFM has been used. Here, a single fibrin fiber has been pulled using a cantilever and has shown the great extensibility of fibrin fibers adding insight to the roles that particular protein domains play in fibrin deformation (Guthold *et al.*, 2007). The authors suggest that the load of small strains can be endured by fibrin monomers through knob-hole bonds, while at medium strains the  $\alpha$ -helical coiled coils unfold, and then at high strains they hypothesised that globular domains such as the  $\gamma$ C nodule unfold.

## **1.10 Fibrinogen disorders**

A large amount of research on fibrin and the disorders associated with it has been performed over the years (Neerman-Arbez *et al.*, 2016; Asselta *et al.*, 2007; Fish and Neerman-Arbez, 2012), this section will detail some variants that give rise to afibrinogenaemia and dysfibrinogenaemia.

Fibrinogen disorders are usually congenital and can either completely lack the presence of fibrinogen and are known as afibrinogenaemia. The lack of fibrinogen causes patients with afibrinogenaemia to commonly display excessive bleeding and to treat these episodes they can receive cryoprecipitate

(concentrated fibrinogen). Dysfibrinogenaemia patients do have the fibrinogen protein but contain one or more point mutations. The mutations are usually within the mature product often changing the function of the fibrinogen, impacting on polymerisation, clot structure and the patient's ability to clot normally. It has been reported that from all the known dysfibrinogenaemia 55% are asymptomatic, 25% are associated with bleeding tendency and the remaining 20% are associated with thrombosis (Hayes, 2002)

Interestingly, a dysfibrinogenaemia named Fibrinogen Miami ( $B\beta$  D61G) has been described in the literature. The variant described contained a mutation of the opposite interacting residue to  $\gamma$ K356 that is being investigated in my work. The current hypothesis is that  $\beta$ bD61 interacts with  $\gamma$ K356. The patient who had this dysfibrinogenaemia also showed tendency to bleed and delayed polymerisation kinetics, (Galanakis *et al.*, 1996) providing evidence that the K356 and  $B\beta$ D61 extended knob-hole interaction also plays an important role in clot formation in a physiological setting. The first dysfibrinogenaemia to be discovered was fibrinogen Detroit in 1969 (Mammen *et al.*, 1969), with mutation A $\alpha$ A19S changing a basic amino acid with a neutral amino acid in knob A that is exposed after thrombin cleavage of fibrinopeptide A. The patient's polymerisation rates were delayed and the literature describes the patient's thromboelastograms as 'grossly abnormal'. A database detailing other afibrinogenaemia and dysfibrinogenamias has been created in an effort to compile all the known fibrinogen variants and their relevant literature. The database can be found using the website <http://site.geht.org> (last accessed 15/10/18 for this work). As can be seen from the database, hundreds of fibrinogen variants have been discovered to date, but in this work I focus on

describing variants that surround the knob A cleavage site, variants that effect the hole-a binding pocket and variants that effect the D:D interface.

Other variants beside fibrinogen Detroit also play a role in influencing knob-hole interactions or FpA release. Heterozygous  $\text{A}\alpha\text{R16H}$  variant (fibrinogen Manchester) exhibits slower FpA than FpB release, which as expected gave rise to delayed polymerisation kinetics (Lane *et al.*, 1983). FpA release is completely prevented from  $\text{A}\alpha\text{R16C}$ , whilst FpB is still released, (Henschen *et al.*, 1984). There are a plethora of additional naturally occurring mutations affecting fibrinopeptide A release including,  $\text{A}\alpha\text{D7N}$  Fibrinogen Lille resulting in no FpA release (Denninger *et al.*, 1978). Fibrinogen Magdeburg I  $\text{A}\alpha\text{L9P}$  mutation that results in delayed FpA release (Meyer *et al.*, 2003b). Fibrinogen Mitaka II,  $\text{A}\alpha\text{E11G}$ , reduces fibrinogen binding with thrombin resulting in delayed FpA release (Niwa *et al.*, 1993). Fibrinogen Saint-Germain I,  $\text{A}\alpha\text{G12V}$ , displayed impaired release of FpA and FpB by thrombin (Mathonnet *et al.*, 2002).

Other residues have also been shown to be implicated in defects within the a hole pocket. Variants  $\gamma\text{D330V}$  fibrinogen Ales (Lounes *et al.*, 2000), fibrinogen Kyoto III  $\gamma\text{D330Y}$  (Terukina *et al.*, 1989) both disrupt extended ionic interactions involving  $\text{A}\alpha\text{R19}$ , resulting in impaired polymerisation.

Known mutations around the FpB cleavage site are rarer than mutations around the FpA cleavage site, so much so that only one variant at the FpB cleavage site has been discovered and characterised. The variant has a mutation at position 14 of the  $\beta$ -chain where an arginine is substituted for a cysteine. This variant has been described by more than one group and therefore has several names, Christchurch II, Christchurch III, Ijmuiden, and Seattle (Brennan *et al.*, 1997;

Branson *et al.*, 1983; Koopman *et al.*, 1992). The mutant fibrinogen displayed normal FpA release but abnormal FpB release resulting in altered polymerisation (Brennan *et al.*, 1997) and reduced maximum OD which indicates a difference in clot structure (Branson *et al.*, 1983).

## **1.11 Knob-hole interactions**

### **1.11.1 Concept of knob-hole interactions**

Although the cleavage of fibrinopeptides and the imaging of monomers and fibers had already been described (Lorand and Middlebrook, 1952) (Fowler and Erickson, 1979) (Van Zandt Hawn and Porter, 1947), it was still unknown where knobs A and B bound on adjacent fibrin molecules. The binding pockets were discovered somewhat 20 years ago through co-complexes that were formed between competitive inhibitors of knobs A and knobs B (Spraggon *et al.*, 1997). Further crystallography efforts using fragment D and GPRP peptide revealed that  $\gamma$ Gln329,  $\gamma$ His340,  $\gamma$ Asp364, and  $\gamma$ Arg375 are the residues responsible for the binding of the peptide (Kostelansky *et al.*, 2002). As these efforts were not using full fibrin molecules, it is expected that this interface will involve other residues that accommodate the binding pocket.

Since then there has been a strong interest in regards to the binding of knobs A and knobs B with holes a and b respectively. These key interactions in fibrin have been termed 'knob-hole interactions'. Particular interest has been attributed to distinguish their individual roles in fibrin polymerisation and ultimately how this results in altered clot structure and mechanics, (Bowley *et al.*, 2008) (Lord, 2011). It should be noted that these knob-hole bonds are not covalent and are mainly electrostatic in nature (Spraggon *et al.*, 1997). With the advances in recent

technologies such as optical tweezers and atomic force microscopy, it has been much easier to probe fibrin(ogen) at the nanoscale. Complementary to these two techniques, computational studies have also proven useful to determine interactions involving knob-hole bonds at the sub-molecular level, providing key insights into the regulation of knob-hole binding (Litvinov *et al.*, 2018).

The full hole-a (residues within and surrounding the binding pocket) is thought to span a 70 residue stretch of residues  $\gamma$ 295-365 as predicted by molecular dynamic simulations (Kononova *et al.*, 2013). It has been shown by others that mutations in hole-a can have significant effects on clot structure and polymerisation. The importance of the structural integrity of hole a can be seen where GPRP peptide prevented oligomer formation even though FpA was cleaved normally (Everse *et al.*, 1998). Residue  $\gamma$ D364 is one of the residues located in the binding pocket, and a variant  $\gamma$ D364A was made to investigate the importance of the binding (Bowley *et al.*, 2008). Surprisingly, a GPRP mimic that replicates knob A still bound to in the binding pocket even though ionic interactions between knobs A and hole a was disturbed. Additionally, turbidity and  $\gamma$ - $\gamma$  dimer formation analysis using  $\gamma$ D364A failed to measure any significant fibrin polymerisation.

### **1.11.2 Force rupture of A:a knob-hole interactions**

The force rupture of A:a knob-hole bonds were determined by Averett *et al.* The digestion of fibrin was performed using cyanogen bromide which yields a DesAB-NDSK fibrin fragment, containing the central E fragment of the molecule with both knobs A and B exposed. The authors focussed their attention on the force rupture of the A:a bonds as they are deemed the most important and influential on polymerisation of fibrin and the formation of the fibrin clot, (Averett *et al.*, 2009;

Averett *et al.*, 2008). Briefly, AFM cantilevers were functionalised with DesAB-NDSK fibrin fragment. Glass surfaces were prepared with recombinant fibrinogen and BSA. The functionalised tip (containing knobs A) was used to approach the functionalised fibrinogen surface (containing holes a) and the retraction of the tip allowed the force unbinding and unfolding mechanisms to be determined, Figure 1-14B. Using this technique, the authors describe four molecular deformation events that contribute to the complete dissociation of the A:a knob-hole bond. They measured the amount of force that was required to extend and dissociate the NDSK fragment and the fibrinogen molecule. In the first instance, the fibrinogen that is bound to the glass surface re-orientates. The second and third steps that they described were unfolding events that occur in the  $\gamma$ -nodule, potentially weakening the A:a interaction. The final deformation event described was the dissociation of knob A from hole a.

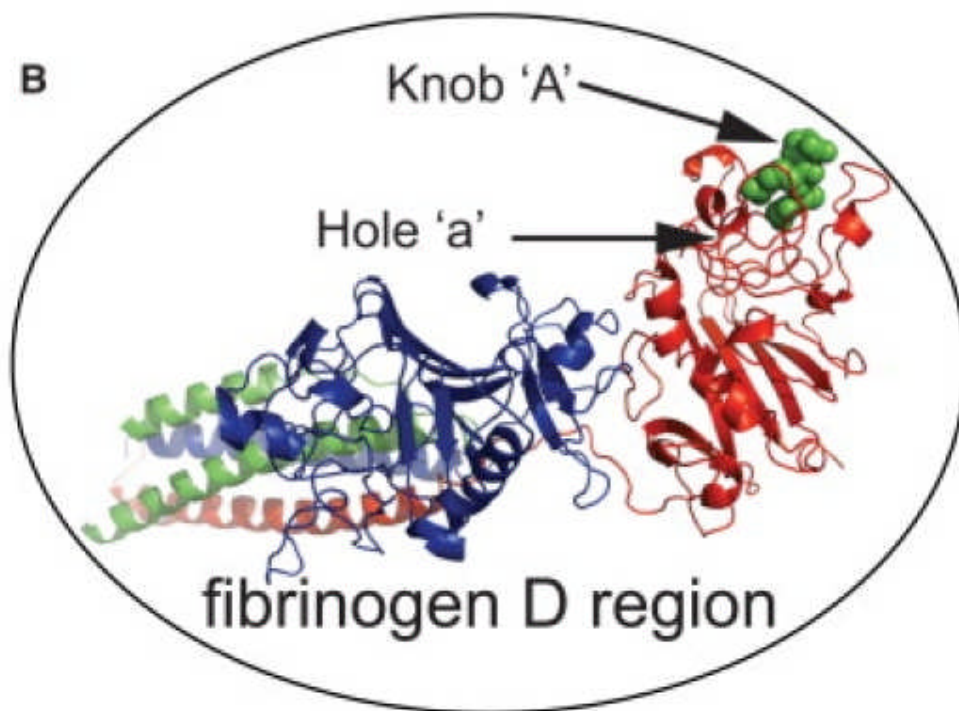
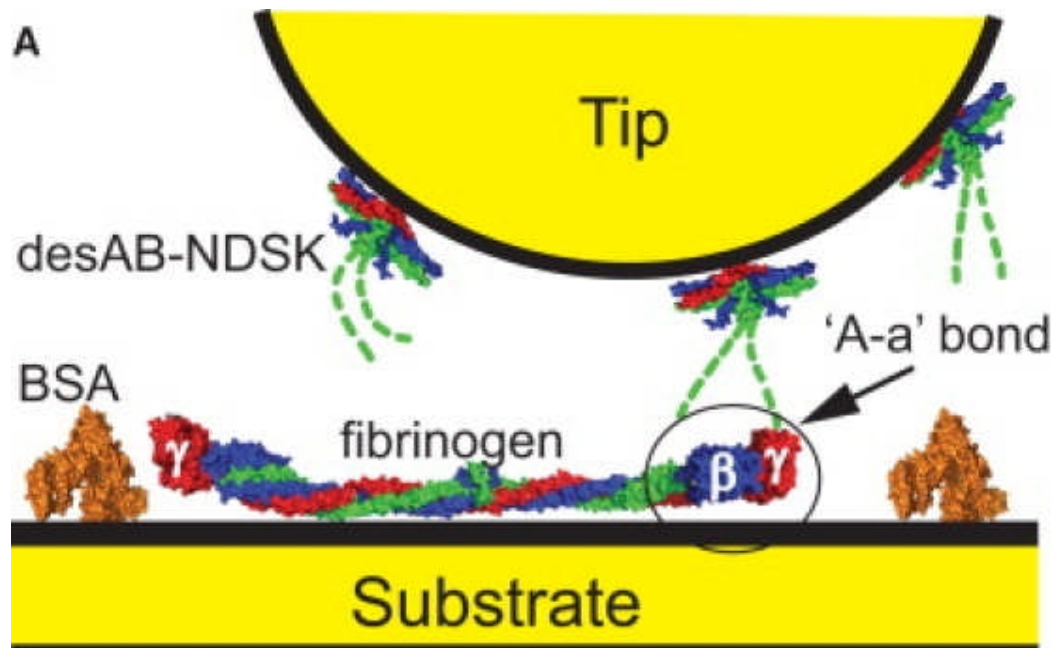


**Figure 1-14 Schematic of rupture of A:a knob-hole bonds.** Representation of the functionalised AFM tip with DesAB NDSK (N-terminal disulphide knot) fibrin fragment and functionalised surface with fibrinogen and BSA. (B) A molecular cartoon representation of the globular D region of the fibrinogen molecule. The  $\beta$ -nodule (blue) and  $\gamma$ -nodule (red). Knob A (green) binds to the polymerisation pocket and the AFM is utilised to calculate unfolding and unbinding kinetics. Image reused from (Averett *et al.*, 2009) with permission from the Biophysical Journal, reference number 4441860996422.

### 1.11.3 Catch-slip bonds in fibrin

Further simulations in combination with optical trap measurements have probed the importance of some of these residues in the role of calcium binding and how this regulates the atomic mechanics of knob-hole bonding (Litvinov *et al.*, 2018).

Fibrinogen has a total of four calcium binding sites, two of which are low affinity binding sites ( $\gamma 2$  and  $\beta 2$ ) and two of which are high affinity binding sites ( $\gamma 1$  and  $\beta 1$ ) (Marguerie *et al.*, 1977). The  $\gamma 1$  and  $\gamma 2$  sites are located on the  $\gamma$ -chain of fibrinogen, whereas sites  $\beta 1$  and  $\beta 2$  are located on the  $\beta$ -chain of the molecule. The  $\gamma 1$  binding site directly involves residues  $\gamma$ Asp318,  $\gamma$ Asp320,  $\gamma$ Phe322 and  $\gamma$ Gly324 (Yee *et al.*, 1997). The  $\gamma 2$  binding site has been shown to involve the residues  $\gamma 294$ ,  $\gamma 296$ ,  $\gamma 298$ , and  $\gamma 301$  (Everse *et al.*, 1999).

Optical trap pulling experiments of fibrin from fibrinogen showed that rather than decreasing with force as expected, the strength of A:a knob hole bonds increased as pulling force increased up to 30pN, and then the strength of the bond decreased hereafter. The binding of 3mM calcium reduced the A:a bond strength (Litvinov *et al.*, 2018).

The molecular simulation part of the article (Litvinov *et al.*, 2018) describes the importance of a movable flap motif that is adjacent to the  $\gamma 2$  binding site, and regulates the opening and closing of the hole-a. Some residues of the flap,  $\gamma 291$ ,  $\gamma 294$ ,  $\gamma 297$  and  $\gamma 301$  are normally positioned so that the hole-a is in a loose, open state that causes more frequent dissociation of knob A. In pulling experiments tension is applied to this region and the movable flap undergoes conformational change and causes interactions between  $\gamma 297$ - $\gamma 304$  in the flap and residues in knob A. Consequently, loop I (residues  $\gamma 315$ - $\gamma 330$ ) also undergo

conformational change leading to further electrostatic interactions between  $\gamma$ 321- $\gamma$ 323 and knob A, causing the hole-a to become more tightly bound to knob A (catch bond). In the optical trap experiments the authors showed that the catch bonds did not occur when 3mM CaCl<sub>2</sub> was present in the solution. They argue that the crystal structures show  $\gamma$ 297 and  $\gamma$ 301 interact with calcium and therefore the movable flap cannot undergo conformational change and form the catch bond. This provides evidence that knob-hole bonds could be regulated through calcium binding, altering the kinetics of the polymerisation of fibrin.

## **1.12 Extended knob-hole interactions**

### **1.12.1 Concept of extended D-E knob-hole interactions**

Weisel first postulated that additional binding contacts must occur in addition to the traditional A:a knob-hole interactions (Weisel, 2012). Using the cross-linked double D fragment, it has been reported that the GPRP mimic of knob A has a dissociation constant of K<sub>d</sub> 25 $\mu$ M with hole a. However, GHRP mimic and hole B has a K<sub>d</sub> of 140 $\mu$ M. (Everse *et al.*, 1998). Geer *et al.*, found that larger DesAB NDSK fibrin fragments dissociated with fibrinogen at a K<sub>d</sub> of 5.8 $\mu$ M There was no difference in dissociation between desAB fragments with fibrin and DesA fragments with fibrin suggesting that the binding was driven by residues involved in A:a interactions (Geer *et al.*, 2007). This shows that larger fibrin fragments dissociate less frequently than the knob A and hole a complex providing evidence that there are residues beyond the classical knob-hole interaction sites that mediate knob-hole binding. X-ray Crystallographic studies of fibrin(ogen) have provided a wealth of data in understanding not only the structure of fibrinogen but also the binding contacts made during polymerisation of the

molecule. However, these methods rely on the preparation of a crystal and imaging of the molecule when it is in a static state, and therefore provide limited information regarding the dynamic structure of proteins, particularly during the interactions between these proteins or peptides.

In 2013, computational molecular dynamic simulations provided evidence that extended knob-hole interactions may occur (Kononova *et al.*, 2013). The authors' goals were to provide computational evidence for the molecular transitions that occur at the sub-molecular level. In their study, in the first instance molecular pulling simulations of the co-complexed  $\gamma$ -nodule fragment of fibrin(ogen) and the peptide mimics GPRP and GHRP. They simulated the pulling of the knobs A and knobs B mimics away from the  $\gamma$ -nodule. They found that the average bond lifetimes A:a and B:b bonds was similar.

The authors performed another additional simulation but this time of a fibrin oligomer (consisting of double D interacting with E region of what would be another monomer), Figure 1-15. The advantage of performing this simulation was that the contacts between other residues and not only the immediate knob-hole interactions were also computed and analysed for binding. The authors found that the traditional A:a knob-hole binding pocket was enhanced by electrostatic interactions between the D region of one monomer and the E region of another monomer that flanked the traditional knob-hole interaction site. The three pairs of electrostatic interactions (as highlighted in Figure 1-15) were between  $\gamma$ Glu323 &  $\beta$ Lys58,  $\gamma$ Lys356 &  $\beta$ Asp61 and  $\gamma$ Asp297 &  $\beta$ His67. Their data showed that the binding interface may be more complicated than originally thought.

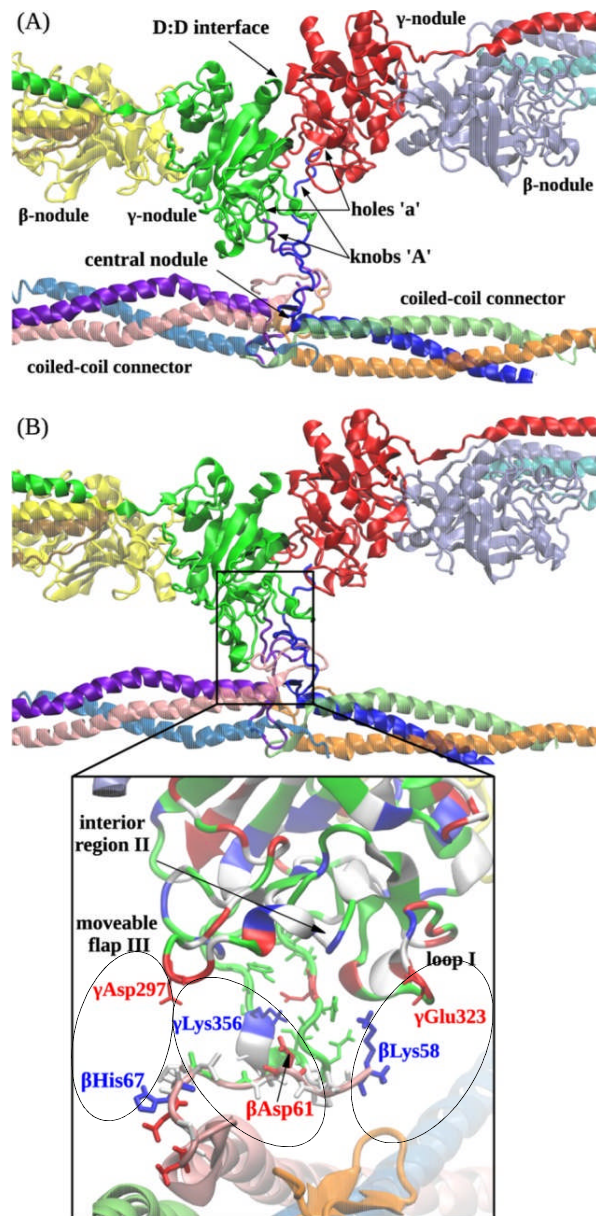


**Figure 1-15 A computational reconstruction of the alignment of fibrin molecules** (A) A cartoon representation shows the  $\beta$ - and  $\gamma$ -nodules of DD fragment alongside a fibrin monomer before equilibration of the simulation (B) Shows the same structures but after the 250ns simulation has taken place, the zoomed in window shows in detail the switch in conformation in  $\gamma$ -nodule binding pocket. Three pairs of electrostatic interactions beyond the classical knob-hole interactions occur between  $\gamma$ Asp297 -  $\beta$ His67,  $\gamma$ Lys356 -  $\beta$ Asp61 and  $\gamma$ Glu323 -  $\beta$ Lys58 (circled black). *This image was adapted from (Kononova et al., 2013) with permission from the Journal of Biological Chemistry.*

## **1.12.2 Known variants in the vicinity of the extended knob-hole region**

In this section I will be describing variants that are located in within proximity to the extended knob-hole interactions.

### **1.12.2.1 $\gamma$ D297**

Fibrinogen Baltimore I is sequentially the closest fibrinogen variant to  $\gamma$ D297 found within the clinic. Baltimore I incorporates a mutation at position  $\gamma$ 292 changing a glycine to a valine residue. It was one of the first congenital fibrinogens to be discovered and is known for its longer than normal clotting time that could be corrected by adding calcium chloride. Baltimore I shows a reduction in  $\gamma$ -chain synthesis which must lead to the observed delayed polymerisation possibly via reduced fibrinogen concentration (Bantia *et al.*, 1990).

Non clinical studies have also been performed by others researching residues very close to  $\gamma$ 297 in the sequence alignment.  $\gamma$ D298A-D301A recombinant variant was created to investigate the importance of the  $\gamma$ 2 calcium binding site that is located in moveable flap  $\gamma$ 294-301 (Kostelansky *et al.*, 2007). Their experimental investigations found that polymerisation was only effected very slightly with the D298A-D301A mutation, suggesting that the  $\gamma$ 2 binding site plays a minor role in polymerisation.

### **1.12.2.2 $\gamma$ E323**

No mutations were found in the literature for position 323 in the  $\gamma$ -chain. However, mutations have been reported for amino acids just a few residues up and downstream. Fibrinogen Beijing at  $\gamma$ 322 (Hua *et al.*, 2015) contains a mutation where phenylalanine is substituted for isoleucine, no phenotype was

determined by the authors. However, fibrin polymerisation was found to be delayed when cleaved by thrombin, the authors postulate that this was caused by the importance of residue 322 as its backbone has been reported to be involved in calcium binding at the  $\gamma$ 1 calcium binding site. D320A, fibrinogen Athens III which was asymptomatic (Galanakis *et al.*, 2014) and fibrinogen Krakow, N325I, resulted in delayed polymerisation, denser clot network and more resistant to lysis (Undas *et al.*, 2009).

The extended A:a binding pocket consists of residues  $\gamma$ 295-365 (Kononova *et al.*, 2013) which includes the  $\gamma$ 1 calcium binding site residues  $\gamma$ 311-336 (Varadi and Scheraga, 1986; Dang *et al.*, 1985; Yee *et al.*, 1997). Although not observed in the clinic, others have indicated that residue  $\gamma$ E323 could also play a role in the binding of calcium in the  $\gamma$ 1 binding site (Pratt *et al.*, 1997). They observed readjustment of the hole-a binding pocket when GPRP binds in the crystal structure. They notice a rearrangement of hydrogen bonds and salt links that stabilise the binding, and predicted that  $\gamma$ K338 and  $\gamma$ E323 form a salt link when GPRP is unbound, however when bound there is a slight shift resulting in the interaction of K338 with the peptide.

### **1.12.2.3 $\gamma$ K356**

No mutations were found in the literature for position 356 in the  $\gamma$ -chain either, although some mutations have been found within proximity to this residue of interest. Fibrinogen Homburg VII contains a mutation where tyrosine  $\gamma$ 354 is substituted for a cysteine residue (Meyer *et al.*, 2003a). The resulting polymerisation in plasma was delayed with clots displaying a much denser network and thinner fibers as compared to WT. The authors concluded that these effects could be attributed to abnormal packing of residues as this area has been

previously shown to have an importance in this mechanism (Yang *et al.*, 2000). Other dysfibrinogenaemia sequentially upstream of  $\gamma$ 356 have also been implicated in fibrin polymerisation and clot structure. Fibrinogen Milano VII where  $\gamma$ 358 serine was substituted to cysteine resulted in delayed polymerisation kinetics (Steinmann *et al.*, 1994). The authors also observed that when the fibrinogen was immunoblotted, albumin was found to be covalently bound to this variant via disulphide bonding. Also when bound albumin was removed using  $\beta$ 2-mercaptoethanol, the fibrinogen still produced abnormal polymerisation kinetics.

Additionally, packing analysis of DD fibrin fragments with bound ligands has shown the possibility of extra residues at play (Yang *et al.*, 2000). The authors created four D:D structures; DD-GP (DD with GPRP ligand bound to holes-a) DD-GH (DD with GHRP ligand bound to holes-b) DD-BOTH (DD with GPRP ligand bound to holes-a and GHRP bound to holes-b), and DD-NL (Both holes empty, no ligands). Structures that had one or both ligands occupying the holes displayed different lateral packing interactions when compared with crystals where holes were left empty. This suggests that the binding of knobs A and B induce a conformational change which could possibly lead to heightened polymerisation of the fibrin. The authors proposed that the two stretch of residues responsible were  $\gamma$ 350-360 and  $\gamma$ 370-380 (termed  $\gamma$ C- $\gamma$ C contacts), which contains the  $\gamma$ 356 residue.

### **1.13 Aims**

Molecular simulation studies have predicted that extended interactions underpinning and extending the classical knob-hole interactions during fibrin polymerisation involve electrostatic binding between three pairs of amino acid residues, i.e.  $\gamma$ Glu323 with  $\beta$ Lys58,  $\gamma$ Lys356 with  $\beta$ Asp61 and  $\gamma$ Asp297 with  $\beta$ His67. My aim was to probe the importance of these extended knob-hole interactions on fibrin polymerisation, clot structure and clot mechanics, using recombinant fibrinogen variants with mutations that abolish the electrostatic interactions.

### **1.14 Objectives**

My specific objectives were:

1. To generate fibrinogen variants of the extended knob-hole region using site directed mutagenesis, transfection of mammalian cells and purification by affinity chromatography. Variants of the  $\gamma$ -chain produced were:  $\gamma$ D297N,  $\gamma$ E323Q,  $\gamma$ K356Q and  $\gamma$ D297N/E323Q/K356Q ( $\gamma$ DEK triple mutant), Figure 1-16.
2. To validate the integrity of the recombinant fibrinogen preparations through CD spectroscopy and SDS-PAGE.
3. To determine the role of the extended knob-hole residues on fibrin clot formation. Turbidity was used to study lag time of clot formation, maximum polymerisation rate and maximum optical density. Atomic force microscopy was used to study the early polymerisation stages of clot formation.

4. To investigate the effects of the mutations within the recombinant variants on clot structure. Whole clot density was measured by Scanning Electron Microscopy (SEM) and LSCM (Laser Scanning Confocal Microscopy). Fiber thickness was also studied by SEM. Clot fibrinolytic properties were investigated using LSCM. Intrafibrillar fiber structure was analysed using light scattering approaches.
5. To examine the effect of the altered polymerisation and clot structure on the visco-elastic properties of the fibrin clots using an in-house micro-rheology device ('magnetic tweezers').
6. To collaborate with Professor Valeri Barsegov (University of Massachusetts, Lowell, USA) on the role of extended D-E interaction sites at the sub-molecular and atomic scales of fibrin polymerisation.

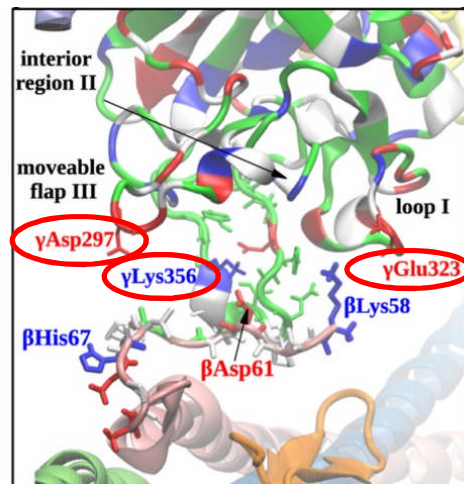


**Figure 1-16 Molecular computation of  $\gamma$  nodule in fibrinogen co-complexed with knobs A** Residues residing in the  $\gamma$ -chain were chosen for mutation based on their proposed function in extended knob-hole interactions (circled in red).  $\gamma$ Asp297,  $\gamma$ Lys356 and  $\gamma$ Glu323 were chosen to be mutated as previous experience from the Ariens laboratory with  $\gamma$ -chain mutants demonstrated good levels of expression. Mutations of the  $\beta$ -chain would have been performed in the event that the  $\gamma$ -chain mutants did not express.

# **Chapter 2 - Materials and Methods**

## **2.1 Materials**

### **2.1.1 Molecular biology**

The QuickChange site directed mutagenesis kit and XL-10 gold competent bacteria were purchased from Agilent Technologies (Stockport, UK). Mutagenesis primers and SOC medium were purchased from ThermoFisher-Scientific (Loughborough, UK). LB broth was made consisting of 10g/L tryptone LabM (Bury, UK), 5g/L Yeast extract (LabM) and 5g/L NaCl (Thermo-Fisher Scientific, Loughborough, UK) and Ultrapure water (resistivity of 18.2M $\Omega$  at 25°C, Millipore (Watford, UK)). LB agar was purchased from LabM. Ampicillin was purchased from Sigma-Aldrich (Dorset, UK) and reconstituted at 100 $\mu$ g/mL and stored in 1mL aliquots. 10cm culture dishes were purchased from Corning (HighWycombe, UK). 50mL Falcon tubes were purchased from Greiner Bio-One (Stonehouse, UK). Parafilm was purchased from Starlabs (Milton Keynes, UK).

### **2.1.2 Cell culture**

Growth medium consisted of DMEM F12 Ham (ThermoFisher-scientific), 5% foetal bovine Serum (Labtech; Heathfield, UK), 5% nu-serum (VWR International; Lutterworth, UK), 1x antibiotic-antimycotic (Sigma-Aldrich; Poole, UK). Serum free medium was made from DMEMF12 Ham and 1x Antibiotic-antimycotic. Selection medium was made from growth medium as detailed above with the addition of 800 $\mu$ M L-histidinol (Sigma-Aldrich). ITS medium consisted of DMEM F12 ham complemented with 1x antibiotic-antimycotic, 4 $\mu$ g/mL Aprotinin (Sigma Aldrich), ITS supplement (Insulin, 5 $\mu$ g/mL, transferrin, 5 $\mu$ g/mL, sodium selenite, 5ng/mL, Roche; Welwyn Garden City, UK). 2x HEBS solution was made using 150mM Na<sub>2</sub>HPO<sub>4</sub>, pH7.05 (Sigma- Aldrich), 2.5mM HEPES solution (Sigma-Aldrich) and 14mM NaCl (ThermoFisher-Scientific). Geneticin, Cell

culture grade glycerol, 10mL syringes and cryotubes were purchased from ThermoFisher Scientific. Dubecco's phosphate Buffered Saline (PBS), ethylenediaminetetraacetic acid (EDTA), 1x Trypsin-EDTA 0.25% solution, Calcium Chloride, sterile filtered water, phenylmethylsulphonyl fluoride (PMSF), cytodex microcarrier beads and dimethyl sulphoxide (DMSO) were all purchased from Sigma-Aldrich. 0.1M EDTA-PBS was made from 1xPBS supplemented with EDTA to a final concentration of 0.1M. Tissue culture treated 24 well plates, 10cm dishes, 6cm dishes, 75cm<sup>2</sup> flasks with vents and 850cm<sup>2</sup> roller bottles with vents were purchased from Corning. 0.2µm Filters were purchased from VWR International. Freezing mix was made consisting of 10% DMSO and 90% Foetal Bovine Serum.

### **2.1.3 Precipitation and purification**

Protease inhibitor cocktail (stored at 4°C) made from 5mM epsilon-aminocaproic acid ( $\epsilon$ -ACA), 5mM benzamidine, 1µM pepstatin, 1µM leupeptin, 100µM PMSF, and 20mM 2-ethanesulphonic acid (MES) buffer pH5.6 all purchased from Sigma-Aldrich. Saturated ammonium sulphate was made by dissolving 1.52kg ammonium sulphate (Sigma-Aldrich) in heated 2L ddH<sub>2</sub>O and stored at 4°C. Pellet resuspension mix pH 7.4 (stored at 4°C) consisted of 5mM  $\epsilon$ -ACA, 5mM benzamidine, 5µM pepstatin, 5µM leupeptin, 100µM PMSF, 10U/mL Soybean Trypsin Inhibitor (Sigma-Aldrich), 1mM EDTA, 300mM NaCl, 200mM Tris-Base pH 7.4 (ThermoFisher-Scientific).

IF-1 mAb 10mg was purchased from Kamiya Biomedical (Seattle, Washington, USA) and CnBr Activated Sepharose 4B 1.5mg was purchased from VWR (Lutterworth, UK) and packed into a XK16/20 column (GE Healthcare, Little Chalfont, UK) and was attached to the ÄKTA avant (GE healthcare). Purification

was initiated and the protocol was pre-programmed by Cédric Duval, University of Leeds.

The following buffers were made for use during affinity chromatography of recombinant fibrinogen variants:

Equilibration buffer pH 7.4 consisted of 20mM Tris-base, 300mM NaCl, 1mM CaCl<sub>2</sub>. Wash buffer I pH 7.4 consisted of 20mM Tris-base, 1M NaCl, and 1mM CaCl<sub>2</sub>. Wash Buffer II pH 6.0 was made from 300mM Na-acetate, 300mM NaCl and 1mM CaCl<sub>2</sub>. Elution buffer pH 7.4 consisted of 20mM Tris-base, 300mM NaCl and 5 mM EDTA. Dialysis buffer pH 7.4 was made from 50mM Tris-base and 100mM NaCl. All buffers were stored at 4°C.

#### **2.1.4 Fibrinogen ELISA**

Coating buffer pH 7.2 consisted of 2.5mM disodium phosphate (Sigma-Aldrich), 7.5mM sodium dihydrogen phosphate (Sigma-Aldrich), 145mM NaCl. Blocking buffer was made using 1x dilution buffer and 1% bovine serum albumin (ThermoFisher-Scientific). Dilution Buffer was made from 1x coating buffer, 0.2% Tween 20 (Sigma-Aldrich), 355mM NaCl. Citrate-phosphate buffer pH5.0 was made from 25mM citric acid (Sigma-Aldrich) 50mM Disodium phosphate (Sigma-Aldrich). Some 2mg o-phenylenediamine dihydrochloride tablets and hydrogen peroxide were purchased from Sigma-Aldrich. F96 maxiSorp nunc immuno plates were purchased from SLS (Nottingham, UK). Polyclonal Rabbit Anti-Human Fibrinogen antibody was purchased from Agilent Technologies. detecting sheep anti-human fibrinogen antibody was purchased from Enzyme Research Laboratories (Swansea, UK).

### **2.1.5 SDS-PAGE and circular dichroism spectroscopy**

SDS-PAGE samples were prepared using 2.5µg protein, 1x LDS running buffer and 1x sample reducing agent purchased from ThermoFisher-Scientific and tris buffered saline (50mM Tris-base, 100mM NaCl). MES running buffer was purchased from Sigma-Aldrich. Samples were loaded into NuPage 4-12% Bis-Tris Gels (ThermoFisher-Scientific) alongside precision plus protein standards (Bio-Rad, Hempstead, UK). Gels were inserted into Xcell sure lock gel tanks (Life Technologies) and 200V was applied across the gel for 90 mins using a Biorad power pack 300 (BioRad). Gels were stained with Gel Code<sup>®</sup> Blue Stain reagent (ThermoFisher-Scientific) and then de-stained using ddH<sub>2</sub>O. All reagents were stored at 4°C. The gel was imaged using Gbox imaging system (Syngene, Cambridge, UK).

Circular Dichroism (CD) spectra samples were prepared by diluting recombinant human fibrinogen variants to 0.2mg/mL in 200µL total volume and stored on ice for the duration of the experiment. The variants were placed in a cuvette with a 1 mm path length (Hellma Analytics, Southend on Sea, UK) and the near UV spectrum was measured using Chirascan instrument (Applied Photo Physics, Surrey, UK).

### **2.1.6 Functional analysis of fibrin clots**

Fibrin clots for turbidity measurements, magnetic tweezers and confocal microscopy experiments were performed using recombinant human fibrinogen generated in house, CaCl<sub>2</sub> (1M stock stored at room temperature), 0.1U/mL human thrombin (reconstituted to 250U/mL with ddH<sub>2</sub>O stored at -80°C (Merck-Millipore, Watford, UK) and tris-buffered saline (50mM Tris 100mM NaCl) stored at 4°C. Scanning electron microscopy clots were made using 0.5mg/mL, 10mM

CaCl<sub>2</sub> and 1U/mL thrombin. Clots used during AFM imaging were made using 0.02mg/mL Fibrinogen, 0.05 U/mL Thrombin and 2mM CaCl<sub>2</sub>.

Additional turbidity measurements were completed using 0.5BU/mL reptilase (Stago Diagnostics, Reading, UK) and 5mM CaCl<sub>2</sub>. Reptilase lyophilised powder was stored at 4°C and reconstituted by adding 2mL ddH<sub>2</sub>O to a final concentration of 10BU/mL prior to conducting experiments. Clots formed for magnetic tweezers had the addition of 1:250 v:v 4.5µm diameter paramagnetic beads (Thermo-Fisher Scientific), these were also stored at 4°C. Clots made for confocal microscopy had the addition of 5% Alexa 488-labelled recombinant fibrinogen by using the Alexa Fluor™ 488 labelling kit (Thermo-Fisher Scientific). Human Glu-plasminogen for confocal lysis experiments was purchased from Enzyme Research Laboratories, and was reconstituted in 1mL ddH<sub>2</sub>O following the manufacturer's instructions yielding a final concentration of 11µM, dispensed in 10µL aliquots and stored at -80°C. Tissue plasmin activator (tPA) was purchased from pathway diagnostics (Dorking, UK) diluted to 1380nM by diluting in 1mL ddH<sub>2</sub>O and stored at -80°C in 10µL aliquots.

## **2.2 Mutagenesis**

### **2.2.1 Primer design and mutagenesis**

The mutagenesis primers were designed using the Agilent primer design program (<https://www.genomics.agilent.com/primerDesignProgram.jsp>), and ordered from Thermo-Fisher Scientific at 200nmol and SDS-PAGE purified. The full primer sequences can be found in Table 3-1. The QuickChange site-directed mutagenesis kit (Thermo-Fisher Scientific) was used to mutate the human γA-chain cDNA contained within the expression vector (pMLP-γA, Figure 2-1) A mix

of 1x reaction buffer, 20ng pMLP-  $\gamma$ A expression vector, 125ng of forward and reverse primers, dNTP mix and 2.5U PfuUltra High Fidelity DNA polymerase in 50 $\mu$ L total volume was used in a thermal cycler (MJ Research, Waltham, MA, USA) set to the parameters shown in Table 3-2

Created with SnapGene®

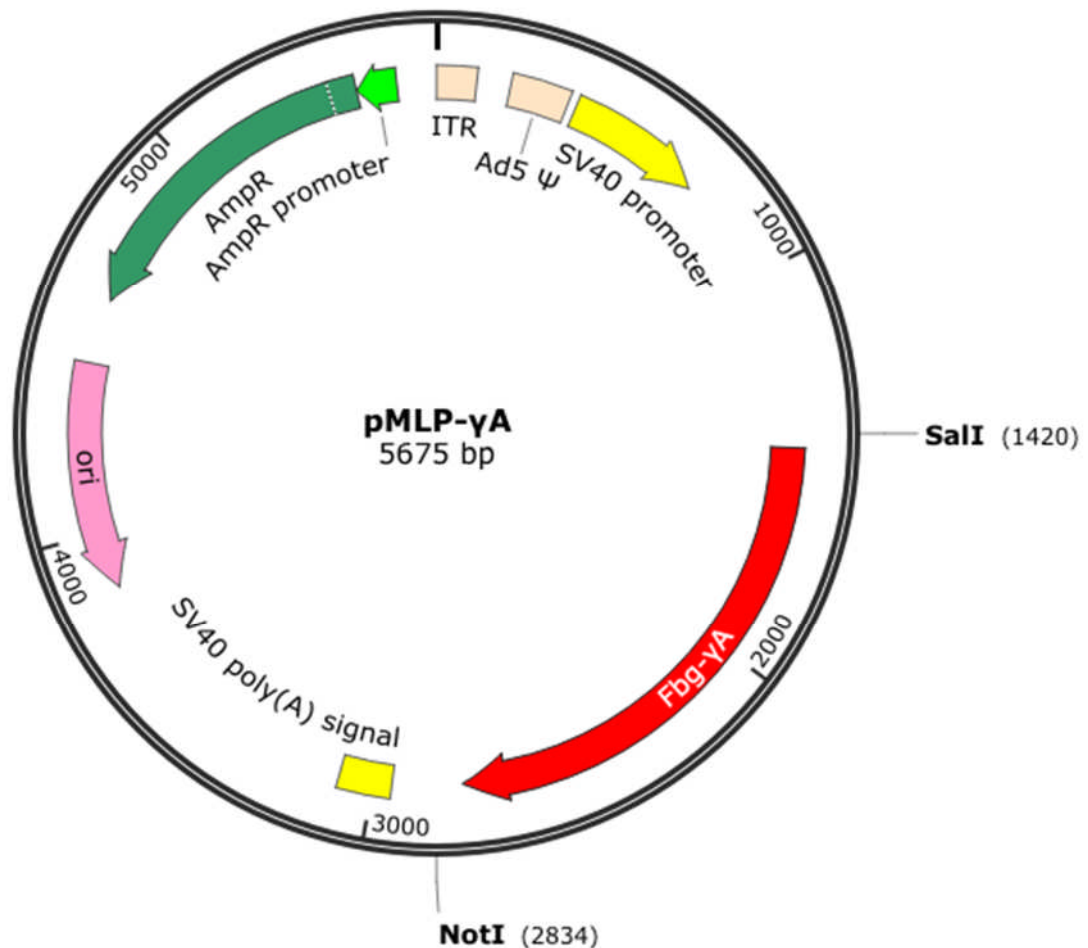


**Figure 2-1 Plasmid map of pMLP- $\gamma$ A** Plasmid map created using Snapgene Viewer (GSL Biotech; Chicago, USA). The map displays the SV40 promoter and SV40 poly(A) signal (yellow) the insertion of Fbg- $\gamma$ A (red) between restriction sites SalI (1420bp) and NotI (2834bp). This plasmid contains an ampicillin resistance promoter (light green) and the ampicillin resistance gene (dark green) and an origin of replication (pink).

When the PCR cycling had completed, non-mutated parental strands were digested by the addition of 10U Dpn-1 restriction enzyme and then incubated in the thermal cycler as described in 3.2.1

**Table 2-1 PT200 Dpn-1 digestion parameters**

Segment	Cycles	Temperature (°C)	Time (Minutes)
1	1	37°C	60
2	1	4°C	10

### **2.2.2 Bacterial transformation**

LB Agar was autoclaved and supplemented with 100µg/mL ampicillin to produce (LB-Agar<sup>Amp+</sup>), 15mL of LB-Agar<sup>Amp+</sup> were poured onto three 10cm dishes. XL10 gold bacteria were defrosted slowly on ice and a 50mL falcon tube was pre-chilled on ice, meanwhile SOC medium was defrosted and warmed to 42°C in a water bath. XL10 gold bacteria (50µL) and Dpn-1 treated DNA (1µL) from section 2.2.1 was transferred to the pre-chilled tube (now a transformation reaction). The transformation reaction was mixed gently and returned to the ice to incubate for 30 minutes, quickly transferred to 42°C and gently mixed for 45 seconds, then transferred to ice and incubated for a final two minutes. SOC medium (300µL) was then added to the transformation reaction and incubated at 37°C, while shaking (220rpm) for one hour. Three different volumes of transformed cells were plated at 37°C (50µL, 100µL and 150µL) onto LB-agar<sup>Amp+</sup> dishes which were wrapped in parafilm and incubated for 16 hours at 37°C. The following day, LB-agar<sup>Amp+</sup> dishes were checked for colony growth and stored at 4°C.

### **2.2.3 DNA extraction**

Six colonies from the transformation step 2.2.2 were picked using a wire loop (Starstedt, BrandErbisdorf, Germany) and individually inoculated into 10mL LB-broth (in a 50mL falcon tube, Starstedt) containing 100ug/mL ampicillin (LB-broth <sup>Amp+</sup>) and incubated overnight in a G25 shaking incubator (New Brunswick Scientific, NJ, USA) at 37°C, 220rpm. The following day, the cultures were centrifuged at 4600g for 10 minutes using a Rotana 460R (Hettich, Germany) and the supernatant was discarded. The QIAprep<sup>®</sup> Spin Miniprep Kit (Qiagen; Manchester, UK) was used for plasmid DNA extraction from the pellets produced and the manufacturer's instructions were followed with the exception that the DNA was eluted using DNase-free water (Thermo-Fisher Scientific) instead of buffer 'EB'. The concentration of the eluted DNA preparation was determined at A260nm using a Nanodrop ND 1000 (Fisher Scientific; Loughborough, UK) and the DNA was then stored at -20°C. This DNA was used for partial and then full sequencing of the fibrinogen  $\gamma$ -chain cDNA to check that the correct point mutation(s) had been performed. The vector containing the correct DNA mutation(s) confirmed by sequencing was used to perform a second transformation reaction. One colony was chosen, suspended in 5mL of LB-broth <sup>Amp+</sup> in a 50mL falcon and incubated for 4 hours at 37°C 220rpm. The cell mixture was then added to 200mL of LB-broth <sup>Amp+</sup> in a 1L conical flask and incubated overnight at 37°C, 220rpm. DNA extraction using the PureYield<sup>™</sup> Plasmid maxiprep system (Promega; Southampton, UK) was performed. All steps were performed using the manufacturer's instructions. The concentration of the DNA preparation was determined at A260nm using the Nanodrop ND 1000, the DNA

was stored at -20°C, and used for full fibrinogen  $\gamma$ -chain cDNA sequencing and transfection into mammalian cells.

## 2.2.4 Sequencing

In the first instance, the FbgGg-F1 primer was used to partially sequence the  $\gamma$ -chain DNA sequence within the area of the desired point mutations. Plasmids containing the desired point mutations had their entire  $\gamma$ -chain cDNA fully sequenced with the primers listed in Table 2-2. All sequencing was contracted to DNA Sequencing and Services, Dundee University (<https://www.dnaseq.co.uk>).

**Table 2-2 Primers for DNA sequencing**

Primer Name	Primer Sequence
pMLP-F1	5'-CCTTTCTCTCCACAGGTGTC-3'
FbgGg-F1	5'-TGCTACTTTGAAGTCCAGGAAAA-3'
FbgGg-F2	5'-GTACTGCAGACTATGCCATGTTC-3'
pMLP-R1	5'-GCTGCAATAAACAAGTTAACAACAA-3'

## 2.3 Cell culture

### 2.3.1 Thawing cells

Chinese Hamster Ovary (CHO) cells were previously transfected with fibrinogen  $\text{A}\alpha$ - and  $\text{B}\beta$ - chains by the Ariëns laboratory. The method was based on the works of (Lord *et al.*, 1993; Binnie *et al.*, 1993). The previously transfected cells were removed from liquid nitrogen storage. The cells were rapidly thawed in a water bath (Grant Instruments Cambridge, UK) set to 37°C, transferred to a 15mL falcon tube containing 9mL of Growth Medium, and centrifuged at 280g (Hettich, Tuttlingen, Germany) for 4 minutes. The supernatant was discarded and the cells were suspended in 10mL growth medium, 1mL of this suspension

was added to a T75cm<sup>2</sup> tissue culture flask containing 12mL growth medium, and incubated (Panasonic Biomedical, Loughborough, UK) at 37°C, 5% CO<sub>2</sub>.

### 2.3.2 Routine splitting of cells

Cell culture medium was discarded from 75cm<sup>2</sup> flasks containing CHO cells at 80% confluency, 10mL of 0.1M PBS-EDTA was used to wash the cell monolayer and was replaced by 1mL of Trypsin-EDTA. Following 2 minutes incubation at 37°C with the trypsin, the cells were checked for detachment using a light microscope (Olympus, Hamburg, Germany) and suspended in 10mL of growth media. This splitting of the flasks was performed every 2-3 days at a 1 in 10 dilution.

### 2.3.3 Transfection – calcium phosphate method

When 80% confluent, cells were split in a 1 in 10 dilution between three 10cm dishes (one dish for each of the two transfection reactions listed in Table 2-3 and one for a control). Geneticin (Thermo-Fisher Scientific) was added to the dishes at a final concentration of 400µg/mL and the dishes were incubated overnight at 37°C, 5% CO<sub>2</sub>.

The medium was replaced with fresh growth medium and incubated for 2 hours at 37°C, 5% CO<sub>2</sub>. Two transfection reactions were performed for the same mutation, where one contained 10µg and the other reaction contained 20µg of DNA as demonstrated in Table 2-3.

**Table 2-3 Transfection reaction mix**

Transfection 1	Transfection 2
10µg DNA	20µg DNA
1µg pMSV-his	2µg pMSV-his
2.5M CaCl <sub>2</sub>	2.5M CaCl <sub>2</sub>
Make up to 500µl with ddH <sub>2</sub> O	

The DNA mixture was added slowly, in a dropwise fashion to 500 $\mu$ L of bubbling 2x HEBS buffer. Following the addition of the DNA the mixture was allowed to stand for 30 minutes to enable the formation of a phosphate-DNA co-precipitate. The phosphate-DNA co-precipitate was then added evenly, dropwise across the dish and incubated for 4 hours at 37°C, 5% CO<sub>2</sub>. A glycerol shock step was then performed by discarding the growth medium, adding 2mL of 10% glycerol (VWR) that was previously sterile filtered using a 0.22 $\mu$ m filter (VWR) and incubating the cells for 3 minutes at room temperature. The cells were then washed three times with PBS and incubated in growth medium for 24 hours at 37°C and 5% CO<sub>2</sub>. The three dishes were then split into 10 dishes (5 dilutions in duplicate), the dilutions were 1 in 50, 1 in 100, 1 in 150, 1 in 200 and 1 in 400. The control dish was split 1:100 and 1:400. The following day the medium was removed and replaced with selection medium and incubated for 48 hours at 37°C, 5% CO<sub>2</sub>. Selection medium for all dishes were replenished every 2-3 days until single isolated cells appeared.

#### **2.3.4 Colonies selection**

Cells were selected for using L-histidinol for approximately two weeks. Single cell colonies had formed from the selection process and 24 colonies per transfection condition were selected (48 clones in total). The clones were trypsinised for 5 minutes, picked using a glass cloning cylinder, and transferred to a 24-well plate (one clone per well) containing 500 $\mu$ L of selection medium.

At 80% confluence, the supernatant from each well in the 24-well plates was removed and frozen at -80°C as separate aliquots, for the quantification of fibrinogen expression by ELISA. Each clone was split into two 5 cm dishes and incubated at 37°C, 5% CO<sub>2</sub> until confluent. At 80% confluence, one dish from

each pair was trypsinised by the addition of 0.5mL 0.25% Trypsin-EDTA, 9.5mL selection medium was added and the cell suspension was centrifuged (280g, 4 minutes). The supernatant was discarded and the pellet was suspended in 4mL freezing mix, aliquoted 1mL per cryotube and frozen at -80°C using a 'Mr Frosty' apparatus (Nalgene; Loughborough, UK), before being moved to liquid nitrogen storage the next day. The other dish was split 1 in 10 in selection medium. When 80% confluent, the medium was changed to serum-free medium and incubated for a period of 1 week at 37°C, 5% CO<sub>2</sub>, before the medium was harvested and stored at -80°C for ELISA.

### **2.3.5 Roller bottle expression and precipitation**

The top 50% highest fibrinogen expressing mutants in regular culture conditions were selected for expression for 1 week in 10cm dishes using serum free medium. The highest expression clone in these serum free conditions as determined by fibrinogen ELISA was selected for roller bottle expression. A cryovial of the highest expressing clone was removed from liquid nitrogen storage, thawed and re-suspended as described in section 2.3.1. The supernatant was removed and the cell pellet was suspended in 10mL of growth media and split equally into two 10cm dishes containing 10mL growth medium. Cells were routinely split to obtain 40 confluent 10cm dishes of the same passage.

When confluency had been reached two 10cm dishes were washed with 10mL of 0.1M EDTA-PBS followed by 1mL of Trypsin-EDTA. Following 2 minutes incubation at 37°C with the trypsin the supernatant was suspended in 20mL of growth media and added to a roller bottle supplemented with 180mL of growth, and incubated at 37°C until confluent. The growth medium was replaced every

2-3 days until confluence was reached. When the roller bottles had reached confluence, 20g of micro carrier beads were added to 1L of PBS and autoclaved. Supernatant PBS from sedimented autoclaved microcarrier beads was removed, replaced with 1L basal DMEM F-12 medium and the beads were allowed to sediment, this was repeated three times. 100mL of medium was removed from each roller bottle and replaced with 50mL of bead mixture and 50mL complete growth medium, and incubated for 2-3 days at 37°C, 5% CO<sub>2</sub>. After the 3 days had elapsed the medium from the roller bottles was removed and replaced with 100mL serum-free medium and incubated overnight at 37°C 5% CO<sub>2</sub>. The following day, the serum-free medium was removed and replaced with 200mL of ITS medium and incubated for 2-3 days at 37°C, 5% CO<sub>2</sub>. The supernatant was then collected for a period of 8 weeks by the removal of approximately 100mL ITS medium per roller bottle every 2-3 days and replaced with 100mL fresh ITS medium. The collected supernatant was filtered using filter paper (Whatmann, Little Chalfort, UK) and 150µL 100mM PMSF was added per 100mL harvested supernatant and 1mL harvested medium was aliquoted for fibrinogen ELISA. The remaining supernatant was then frozen at -40°C.

## **2.4 ELISA**

Anti-Fibrinogen antibody was diluted at 1:4000 in coating buffer and used to coat (100µL/well) a 96-well immuno-plate. The plate was covered and incubated overnight at 4°C. Following removal of the antibody, 150µL/well of blocking buffer was added and incubated at room temperature for 60 minutes on a shaker at 50rpm. Recombinant human fibrinogen was used to create a standard curve of 0.06-1000ng/mL in dilution buffer. The blocking buffer was removed and the

plate was washed 3x with 300 $\mu$ L/well of washing buffer. Standard or neat sample (100 $\mu$ L) were distributed, in duplicate, and incubated at room temperature for 120 minutes on a shaker set at 50rpm. The plate was washed 3x with 300 $\mu$ L/well washing buffer. The anti-fibrinogen/HRP antibody was diluted 1:16000 in dilution buffer, 100 $\mu$ L/well was added to each well, and the immuno-plate was incubated at room temperature for 60 minutes on a shaker. The plate was washed 3x with 300 $\mu$ L/well washing buffer and 5 $\mu$ L of 34% H<sub>2</sub>O<sub>2</sub> was added to an OPD and citrate buffer solution (8mg of 1,2-phenylenediamine dihydrochloride in 12mL citrate phosphate buffer), before being distributed 100 $\mu$ L/well and allowed to develop. The reaction was stopped with 100 $\mu$ L/well buffer 3M H<sub>2</sub>SO<sub>4</sub>. The plate was then read at 490nm using a Spectramax plate reader (Molecular Devices; California, USA). The log concentrations of the standards used in the ELISA were plotted against their corresponding ODs and a standard curve was constructed. A linear line of best fit was applied and the fitted equation was used to calculate the concentration of fibrinogen for each clone.

## **2.5 Precipitation and purification**

### **2.5.1 Precipitation**

Prior to precipitation, the frozen medium was thawed and 3L were added per 5L flask in conjunction with 90mL of protease inhibitor cocktail. Whilst stirring at 50rpm 2L of saturated ammonium sulphate was filtered into the medium, dropwise, and left overnight without stirring. The final concentration of ammonium sulphate was 40%. The precipitate (recombinant fibrinogen and other proteins) precipitate was collected by centrifugation at 14,500g, 45 minutes, 4°C using a Beckman High Speed Centrifuge (Beckman Coulter; California, US). The

excess ammonium sulphate was removed, pellets were dissolved in 9.6mL of pellet resuspension, incubated on ice for 30 minutes, then centrifuged for 30minutes at 43,000g, 4°C. The supernatant was collected and stored in 5mL aliquots at -80°C.

## **2.5.2 Affinity chromatography and dialysis**

The frozen supernatant 2.5.1 was defrosted and CaCl<sub>2</sub> was added to a 10mM final concentration. IF-1 immunoaffinity chromatography was performed as previously described (Takebe *et al.*, 1995), using an ÄKTA Avant 25 (GE Healthcare, Little Chalfort, UK). Following injection of the supernatant onto the column using equilibration buffer, non-specific binding was eliminated using wash I and wash II buffers, and the purified fibrinogen was recovered using elution buffer. Fibrinogen was then dialysed overnight using a D-tube™ dialyser mega 10mL (Millipore) against dialysis buffer made as described in 2.1.3. The purified fibrinogen was then concentrated by centrifugation at 4600g using Pierce 100,000 MWCO spin columns (Sigma-Aldrich) and the fibrinogen concentration was determined at A280nm (15.1 extinction coefficient) using the Nanodrop ND1000 before storage in 10 µL aliquots at -80°C.

## **2.6 Protein concentration and dialysis**

### **2.6.1 Concentration of recombinant fibrinogen variants**

The purified fibrinogens were concentrated using Pierce 100,000 MWCO spin columns and the fibrinogens were then dialysed overnight against dialysis buffer as mentioned in 2.5.2 and the fibrinogen concentration was determined at A280nm using the Nanodrop ND1000) before being stored at -80°C.

## **2.7 SDS-PAGE**

For SDS-PAGE (sodium dodecyl sulphate polyacrylamide gel electrophoresis) analysis samples were prepared using 2.5µg protein, 1x loading buffer, 1x sample reducing agent and TBS (50mM Tris, 100mM NaCl) to the final volume of 25µL. The samples were heated to 70°C for 10 minutes, incubated on ice for 2 minutes and then centrifuged at 14500rpm in a microfuge for 15 seconds. MES running buffer (500mL) was prepared and added to the gel tank and the samples were loaded (25µL) into a NuPage 4-12% Bis-Tris gel alongside 5µL of precision plus protein standards and 200V was applied for 1 hour. After completion the gel was washed with ddH<sub>2</sub>O and stained in Gel Code<sup>®</sup> Blue Stain reagent for 1 hour at room temperature. The gel was then washed with ddH<sub>2</sub>O for 1 hour and the water was replaced every 15 minutes, a final wash was performed overnight in ddH<sub>2</sub>O at 4°C. The gel was imaged the following morning using G:Box (Syngene, Cambridge, UK) in conjunction with Genesys computer software, (California, US).

## **2.8 Circular dichroism**

Circular Dichroism (CD) spectra samples were prepared by diluting recombinant human fibrinogen variants to 0.2mg/mL in 200 µL total volume and stored on ice for the duration of the experiment. The variants were placed in a cuvette with a 1 mm path length (Hellma Analytics, Southend on Sea, UK) and the near UV spectrum (190-270nm) was measured using Chirascan instrument (Applied Photo Physics). CDNN convolution software was used to calculate percentage folding for all variants.

## 2.9 Turbidity

Turbidity is a technique that is based on the changes of light scattering of a sample and in this particular case, fibrin matrices. During polymerisation, fibrinogen, a soluble transparent protein is converted to fibrin by thrombin resulting in a fibrin matrix which is insoluble and translucent/opaque. In brief, light is scattered and the amount of un-scattered light can be detected by the plate reader, Figure 2-2. In this work turbidity was measured over time by taking multiple light scattering readings of multiple samples at a time in a 384 well microtiter plate to generate a turbidity curve (opacity increase over time), Figure 2-3.

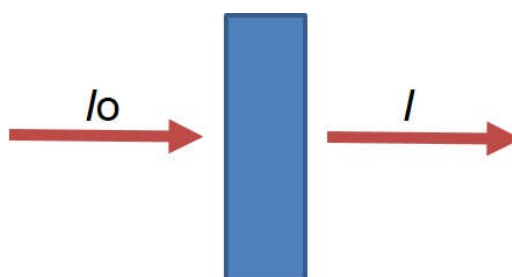


**Figure 2-2 Diagram to demonstrate the principal of turbidity (light scattering).** When light travels through a solution it scatters (known as the incidence point ( $I_0$ )). The detector is then able to measure the amount of transmitted light ( $I$ ) and determine the absorbance of the solution ( $A_\lambda$ ). This was adapted to a 384 well microtiter plate in the case of this work. Different patterns of light scattering by fibrin matrices reflect differences in clot structure.

The optical density can be calculated using the following equation;

$$A_\lambda = \log\left(\frac{I_0}{I}\right)$$

**Equation 2-1 Absorbance calculation** Where the absorbance ( $A_\lambda$ ) equals the log of the intensity of the incidence light ( $I_0$ ) divided by the intensity of the transmitted light ( $I$ ).

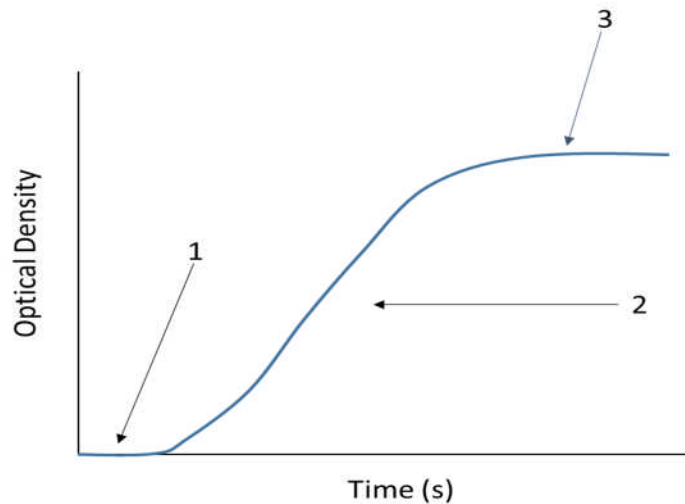


**Figure 2-3 Typical profile of a fibrin polymerisation curve** (1). Denotes the lag phase when FpA and FpB are being cleaved and formation of protofibrils, (2) represents fiber growth and (3) the plateau signifies the clot's maximum optical density and correlates with the average fibrin fiber diameter.

Figure 2-3 shows a typical fibrin polymerisation curve, in the early stages (1) a lag phase is typically observed where there is no increase in the optical density followed by a rapid increase (2) which then reaches a plateau (3). The lag phase corresponds to the cleavage of both FpA and FpB and the formation of protofibrils, the exponential rise in optical density results from lateral aggregation of protofibrils that form fibrin fibers. Previous studies have shown that the maximum OD (MaxOD) is directly related to the average cross sectional area of fibers (Carr and Hermans, 1978).

### 2.9.1 Cleavage with thrombin

All turbidity experiments were performed in 384 well plates using a Powerwave micro-plate reader (Bio-Tek; Swindon, UK). All fibrinogen variants, were diluted to 1mg/mL in TBS, pH 7.4 and 50 $\mu$ L were added in duplicate to a 384 well plate (Greiner). A reaction mix (50 $\mu$ L/well) comprising of 10mM CaCl<sub>2</sub> and 0.2U/mL

thrombin in TBS, pH 7.4 was added, to achieve a final concentration of 0.5mg/mL of fibrinogen 5mM CaCl<sub>2</sub> and 0.1U/mL thrombin in a total volume of 100µL and immediately transferred to the micro-plate reader. The absorbance of each well was measured at 340nm wavelength every 12 seconds for 2 hours at 37°C. Data analysis was performed using both Microsoft Excel, for the averaging of data, and GraphPad Prism for the statistical analysis and graphing of the data. Three outputs were analysed from the turbidity profiles of each fibrinogen variant; lag phase, maximum optical density (OD) and maximum polymerisation rate. The lag time was interpreted manually and chosen to be the last point before an exponential increase in optical density. The maximum OD was taken to be the highest absorbance value. The maximum polymerisation rate was calculated using a macro on excel designed by Fraser Macrae, University of Leeds. The macro analyses the most steep part of the turbidity curve which is equivalent to the Vmax. The results of lag phase and MaxOD were analysed for statistical significance with the use of a One-Way ANOVA test with multiple comparisons using WT as a control column

### **2.9.2 Cleavage with reptilase**

Cleavage of fibrinogen with reptilase was also performed as in 2.9.1 with the exception of 0.5U/mL (final concentration) reptilase was used instead of 0.1U/mL thrombin.

## **2.10 Micro-rheology using magnetic tweezers**

### **2.10.1 Magnetic micro-rheometer equipment**

The magnetic micro-rheometer was already built and designed by Robert Harrand, a past Ph.D student at the University of Leeds, (Harrand.R, 2007). In

brief, four magnetic poles (named up, down, left and right) are housed on a stage each connected to an individual BOP 20-5M amplifier (Kepco, Inc., NY, US) providing voltage to generate the magnetic field. Underneath the stage sits a Olympus IX-71 inverted microscope with CCD camera (Olympus, UK) equipped with a 40x ultra long working distance air objective. Images are recorded at 25Hz and processed by a PXI-8186 with particle tracking software (National Instruments; Texas, US) that the user can export as a .txt file of the X and Y displacement. All equipment, except for the amplifiers are housed on a vibration reduction optical table.

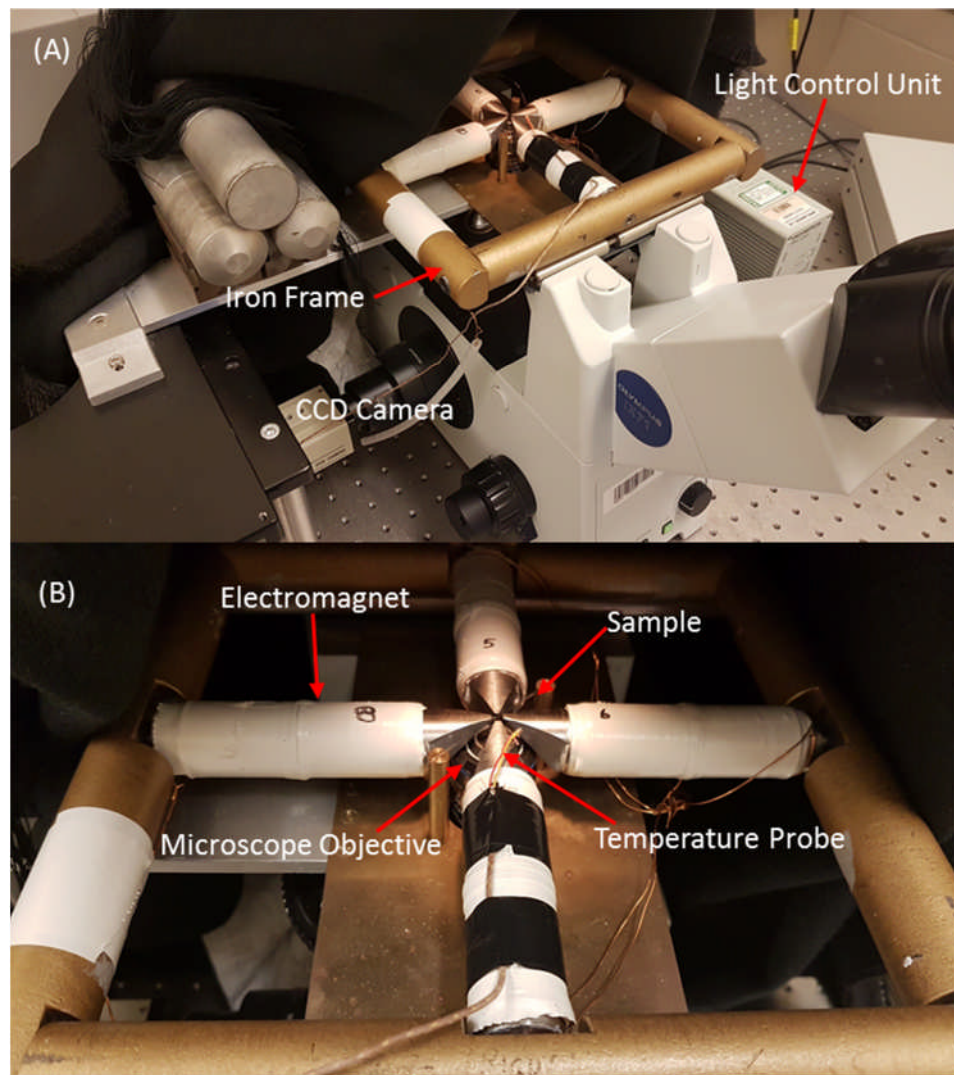


**Figure 2-4 Micro-rheometer setup** (A) Olympus IX-71 Microscope with 40x ultra long air objective and CCD camera attached. An iron frame housing electromagnets and the sample holder which are positioned above the objective. (B) The sample holder surrounded by four electromagnets that houses the capillary tube, paramagnetic beads are pulled and imaged using the microscope objective on the underside of the iron frame which is connected to the CCD camera.

### 2.10.2 Calibration

The magnetic tweezers micro-rheology setup is a very sensitive piece of equipment as the position of the electromagnets can have a great effect on the measurements taken, due to this the voltage applied from the amplifiers may not induce the correct force, therefore before every study the electromagnets are correctly positioned and the setup is calibrated.

To calibrate the magnetic tweezers apparatus a material that had a known viscosity was used as the medium with the addition of paramagnetic beads (4.5µm diameter) trapped in the solution. These were inserted into Hildenberg capillaries (Hildenberg GmbH, Germany) and the ends were blocked with Vaseline to prevent dehydration. In the case of this work, 99% glycerol (Sigma-Aldrich) was used at a dilution of 1:300 (V:V) beads to glycerol. The amount of force that the magnetic bead was subjected to can be then calculated using Equation 2-2 (Allan.P, 2012);

$$F = 6\pi\alpha\eta v$$

**Equation 2-2 Stoke's Law**  $F$  = the constant applied force,  $\eta$  = fluid viscosity and  $v$  = velocity of the particle.

The Labview 7.1 software was then used to locate a magnetic bead whose movements would not be influenced by the edges of the capillary tube or another magnetic bead. Voltages between 0 and 3 volts with 0.2V increments were applied to displace the magnetic bead followed by voltages of 3 to 5 volts with 0.5V increments for all electromagnets, for force calibration. Using the output data, the force calibration curves were plotted for all electromagnets and fitted with a curve determined by Equation 2-3 (Allan.P, 2012).

$$F = \frac{A_1 - A_2}{1 + \left(\frac{V}{V_0}\right)^p}$$

**Equation 2-3 Force calibration fitting**  $F$  = force,  $V$  = voltage and  $A_1$ ,  $A_2$ ,  $V_0$  and  $p$  are fitting parameters.

The equation was rearranged so that voltage became the subject and this was reprogrammed back to LabView7.1 to allow experiments to be performed using a particular force.

## **2.11 Force measurements**

To perform force measurements of WT and the four recombinant fibrinogen variants, clots were made of each type using 0.5mg/mL fibrinogen, 5mM CaCl<sub>2</sub> 1:250 (v:v) superparamagnetic beads and 0.1U/mL thrombin in a total volume of 25 $\mu$ L in an Eppendorf tube. Immediately following the addition of thrombin a VitroCom microcell (50mm length, 0.5mm diameter, VitroCom, New Jersey, US) was inserted and approximately 15 $\mu$ L of the forming clot was drawn into the capillary, the ends of the capillary were then blocked with vaseline to prevent dehydration. Each clot was manually rolled for 15 minutes to ensure the beads did not sediment onto one side of the capillary walls and the clot was allowed to fully form overnight at room temperature in a humidity chamber. Experiments showing the superparamagnetic beads do not have an effect on clot structure have been conducted previously (Allan.P, 2012).

The following day the capillary was housed on the sample stage and using the Labview7.1 software an appropriate superparamagnetic bead was located and a force of 40pN was applied using the 'right' electromagnet. The deformation of the fibrin clot was measured for a period of ten minutes, ten beads were measured per clot and three clots per recombinant variant were measured. There was a significant time difference between when triple mutant  $\gamma$ DEK variant was measured and when the single mutant variants were measured, requiring the magnetic tweezer apparatus to be re-calibrated before measurements were

taken. Therefore, WT clots were measured in both instances due to different calibration settings. The time dependent displacement (the 10 minute pulling) of the bead is related to time dependant compliance  $J(t)$  as can be seen in Equation 2-4 (Allan.P, 2012);

$$J(t) = \frac{6\pi a x(t)}{F}$$

**Equation 2-4 Time dependent compliance is related to the time dependent particle displacement**  $J(t)$  = time dependent compliance,  $a$  = radius of the paramagnetic bead and  $x(t)$  = time dependent particle displacement and  $F$  = Force.

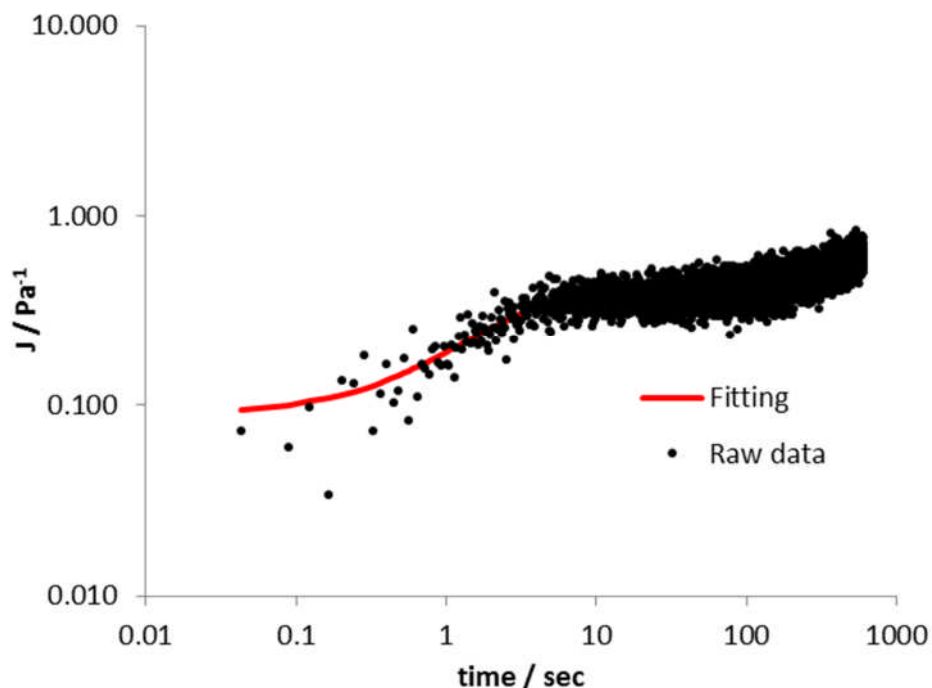


**Figure 2-5 Time dependent compliance** Each black dot represents a data point of the time dependent compliance  $J(t)$  of the super paramagnetic beads. The red line displays the compliance fitting applied as calculated by Equation 2-6.

The compliance fitting to the experimental data was attempted to be plotted by fitting Equation 2-5 in GraphPad Prism 7. However, using GraphPad 7 it is not possible to fit this equation therefore an approximation was used as in Equation 2-6, designed by Dr. Marco Domingues, University of Leeds.

$$J(t) = J_0 + \sum_1^n A_n e^{(-t/\tau_n)}$$

**Equation 2-5 Compliance fitting Equation 1**

The equation that is solved to obtain the fitting parameters of the time dependent compliance.

$$Y = \frac{1}{K_0} \left( 1 - \frac{K_1}{K_0 + K_1} \right) e^{-x/\tau} + \frac{x}{\text{viscosity}}$$

**Equation 2-6 Compliance fitting equation 2**

The equation that is inputted into GraphPad Prism 7 as an approximation of Equation 2-5.  $K_1$ ,  $K_0$ , viscosity and tau are fitting parameters.  $Y = J(t)$  from Equation 2-4 and  $x = \text{time}$ .

Peter Allan in his Ph.D thesis describes how to convert the time dependent compliance  $J(t)$  to frequency dependent moduli through the aforementioned equations and mathematical transformations developed by Professor Steve Evans, Molecular and Nanoscale Physics group, University of Leeds (Evans *et al.*, 2009). After these equations have been solved the  $G'$  and  $G''$  moduli using can be extracted from the data using Equation 2-7.

$$G^*(\omega) = G'(\omega) + iG''(\omega)$$

**Equation 2-7 The equation that is used to generate all  $G'$  and  $G''$  data points using Octave 4.2 software.**  $G^*$  is the complex modulus,  $G'$  is storage modulus and  $G''$  is the loss modulus

Equation 2-7 was executed using the mathematical software Octave 4.2 and generated curves for  $G'$  and  $G''$  as shown in Figure 2-6

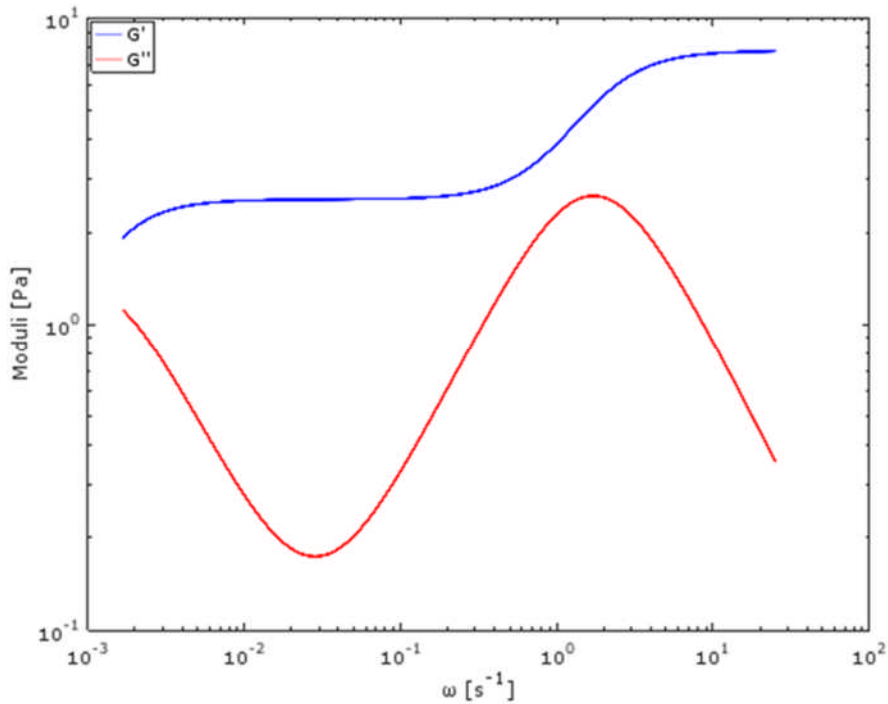


**Figure 2-6 Frequency dependent moduli  $G'$  and  $G''$**

The storage modulus  $G'$  (blue) and the loss modulus  $G''$  (red) plotted against frequency ( $\omega$ ) using values calculated from the equation in Equation 2-7

For all micro-rheology experiments 10 beads were measured per fibrin clot and were pulled with a force of 40pN, these results were averaged to generate a  $G'$  (storage modulus) and  $G''$  (loss modulus) value for each clot between 0 and 25Hz. The values for each clot type were averaged to obtain  $G'$  and  $G''$  as a function of frequency (between 0 and 25Hz) for all fibrinogen variants. Three frequencies of 0.1, 1 and 10Hz were chosen to make comparisons between each fibrinogen variant, these were chosen because they represent the timescales where deformation events occur when force is exerted on the fibrin clot.  $G'$  and  $G''$  values were analysed for statistical significance with the use of a One-Way ANOVA test with multiple comparisons using WT as a control column. The loss modulus (overall visco-elastic property of the fibrin clots) was then calculated by

dividing the G'' by G'. The tan delta ( $\delta$ ) were analysed for statistical significance with the use of a One-Way ANOVA test with multiple comparisons using WT as a control column.

## 2.12 Laser scanning confocal microscopy

### 2.12.1 Alexa Fluor labelling of fibrinogen variants

The Alexa Fluor 488 protein labelling kit was used to label approximately 100 $\mu$ g of each recombinant fibrinogen variant. Due to incompatibility of Tris buffers with the labelling kit each recombinant variant was dialysed against 1x PBS pH 7.4. The manufacturers' instructions were completed in full. Afterwards the degree of labelling was quantified using a Nanodrop ND-1000 using  $A_{280}$  for the detection of protein and  $A_{494}$  for the detection of bound label. The degree of labelling was then calculated using the absorbance from the Nanodrop using the following formula;

$$\frac{(A_{280} \times 10) - ((A_{494} \times 10) \times 0.11)}{1.51}$$

**Equation 2-8 The degree of labelling.** Where  $A_{280}$  is the value for the amount of absorbance detected at 280nm and  $A_{494}$  is the amount of absorbance detected at 494nm. 0.11 is the correction factor value of labelling provided by Thermofisher Scientific and 1.51 is the molar extinction coefficient of fibrinogen.

### 2.12.2 Fibrin clot formation in hydrated conditions

Fibrin polymerisation and clot formation was initiated in a total volume of 40 $\mu$ L in an Eppendorf tube. The tube was immediately mixed and 30 $\mu$ L of the volume was transferred to a channel in a VI flow, uncoated sterile  $\mu$ -slide (Thistle Scientific, Glasgow, UK), placed onto the piezo stage of the LSCM microscope

(Carl Zeiss, Cambridge, UK) and the clots were formed for a period of one hour with the first image being taken 1 minute after formation. For all confocal imaging an inverted Zeiss 880 LCSM with a 40x 1.4 DIC M27 oil immersion objective was used. Multiple scans of different focal planes (slices) were used to reconstruct a 3D image of each clot (z-stack), for clot formation experiments a z-stack was imaged every 30 seconds to create a series of images to visualise clot formation over time. For settings of the LCSM during clot formation experiments refer to Table 2-4.

**Table 2-4 LCSM settings for clot formation experiments**

Setting	Value
Laser Power	3%
Laser	488
Stack size	X = 212.13 $\mu$ m Y = 212.13 $\mu$ m Z = 15 $\mu$ m
Slices	21
Slice Depth	0.75 $\mu$ m
Series Time	30 seconds
Gain	762
Pinhole	34 $\mu$ m

The computer software ZEN was used to process the z-stacks, they were flattened into a 2D image and a 5fps avi. video file was created of clot formation over time.

### **2.12.3 Final clot structure Imaging**

Fibrin clots were formed as described in 2.12.2. Images of the final clot structure (1 hour after polymerisation initiation) were taken with a Zeiss 880 LCSM using the following parameters described in 5.2.2.3

The software package ZEN was used to process the z-stacks, they were flattened into a 2D image. Fiber density of the clots was determined by imaging three areas of each clot and a micrograph generated for each area. Three lines

spanning the entire length of the micrograph (212.13 $\mu$ m) were drawn horizontally and three lines vertically and the number of fibers that crossed these lines on were counted. The clot density between WT,  $\gamma$ DEK,  $\gamma$ D297N,  $\gamma$ E323Q and  $\gamma$ K356Q were compared with the use of a One-Way ANOVA test with multiple comparisons using WT as a control column.

#### 2.12.4 Clot lysis

Fibrin clots were formed as described in 2.12.2 and subsequently lysed by adding 20 $\mu$ L of 6nM tPA and 0.4 $\mu$ M Plasminogen.

The computer software ZEN was used to process the z-stacks, they were flattened into a 2D image and then converted into a 5fps avi. video file. The image window was calibrated to the known distance of the stack size which was 212.13 $\mu$ m using the computer image analysis software Fiji, ImageJ (Schindelin *et al.*, 2012). Now that the window had been calibrated, it was possible to calculate the rate of lysis by the distance of the window (measured by drawing a line between the lysis front in the first and last stacks) divided by the time elapsed for the complete disappearance of the lysis front.

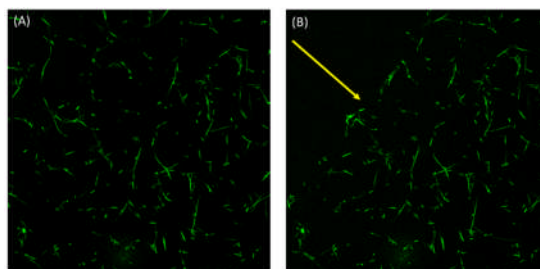


**Figure 2-7 Measurement of the distance travelled over time by the lysis front.** (A) The window is calibrated to 212.13 $\mu$ m length. (B) The clot is partially lysed at this particular frame with the direction of the lysis front indicated by the yellow. Ten seconds elapsed between the capture of each stack, so it was possible to calculate how much time had elapsed for the distance travelled. This information was used to calculate how fast the lysis front was travelling over time ( $\mu$ m/s).

The clot density between the recombinant variants were compared with the use of a One-Way ANOVA test with multiple comparisons using WT as a control column.

### **2.13 Scanning electron microscopy**

Scanning Electron Microscopy (SEM) is another imaging technique that can be used to study the structure of fibrin clots, it differs somewhat compared to LSCM as SEM is a surface imaging technique providing limited depth information, while LSCM provides full 3D visualisation through the reconstruction from z-stacks. In addition, SEM requires sample fixation, dehydration and critical point drying, while LSCM is performed on full hydrated samples. However, SEM delivers much greater imaging resolution and remarkable detail, resolving structures in the range of 1-10nm with the best microscopes, LSCM on the other hand provides no better resolution than light microscopy allows, for example 100-200nm being the limit of its resolving power. Some fibrin fibers are less than 100nm in diameter, and therefore SEM is an important addition to LSCM in the study of fibrin clot structures.

Fibrin Clots using all fibrinogen variants and WT were made to the final concentration of 0.5mg/mL fibrinogen, 5mM CaCl<sub>2</sub> and 1U/mL, thrombin in a total volume of 80µL. Eppendorf lids were pierced seven times with a needle and subsequently wrapped in parafilm in preparation to house the fibrin clot. The formation of the fibrin clot was initiated by the addition of thrombin, the mixture was gently vortexed and transferred to the Eppendorf lid reaction chamber Figure 2-8 and allowed to form in a humidity chamber for 2 hours.

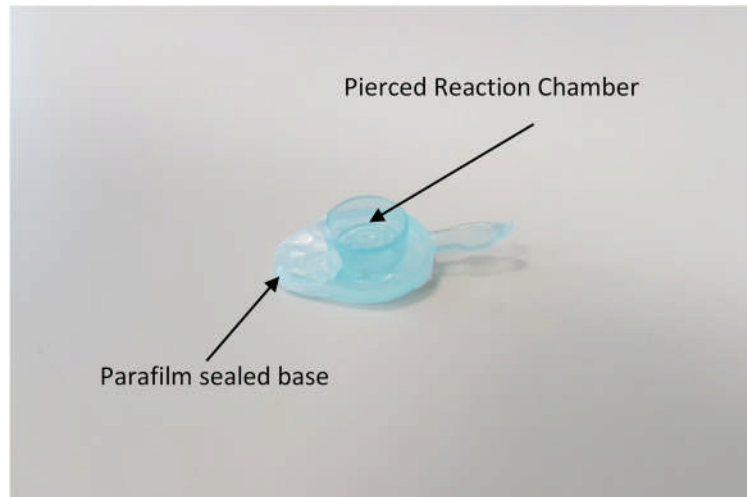


**Figure 2-8 SEM clot formation in an Eppendorf lid** The pierced reaction chamber is where the fibrin clot is formed. The parafilm seal is required to prevent leakage during clot formation, it can be removed at later stages when the clot has fully formed to expose the pierced side of the reaction chamber for the washing and fixing stages.

Following clot formation, the clots were washed in 50mM sodium cacodylate buffer (pH 7.4) for 20minutes three times (to remove excess salt). Clots were fixed with 2% Gluteraldehyde for a period of two hours and then washed another three times in 50mM sodium cacodylate buffer (pH 7.4) and dehydrated using an acetone dehydration series (30, 50, 60, 70, 80, 90, 95 and 100% acetone, 15 minutes per acetone concentration, 30 minutes for 100% acetone). The clots were transferred to fresh 100% acetone and left overnight. The following morning clots were critical point dried (performed by Martin Fuller of the Astbury Center, University of Leeds). In brief, the liquid acetone within the samples was replaced with liquid CO<sub>2</sub> under 800psi, the samples were heated to 35°C under 1200psi which allows the CO<sub>2</sub> to evaporate removing all excess liquid, samples were mounted onto 13mm diameter aluminium SEM imaging stubs and coated with 0.5nm thick layer of iridium using an Agar High resolution sputter coater (Agar Scientific, Stanstead, UK). Each clot type was made three times and each

individual clot was imaged at a minimum of two locations at x2000, x5000, x10000 x 20000 and x50000 magnifications using Hitachi SU8230 scanning electron microscope. Images at x20000 for all clot types were chosen to be used to calculate average fiber diameters. The images were imported into ImageJ software, a 9 x 6 line grid overlay was superimposed onto the image, creating 54 intersections across the image, the fibers that were closest to the intersections were measured for fiber thickness. The results were tabulated using GraphPad Prism 7 and the fiber thickness between WT, and the recombinant variants were compared with the use of a One-Way ANOVA test with multiple comparisons using WT as a control column.

## **2.14 Atomic force microscopy**

Atomic Force Microscopy (AFM) was used to study different stages of the polymerisation process and to investigate the effect of the abolition of the electrostatic extended D-E interactions on protofibril formation and assembly. A mica disc was cleaved and treated with 50 $\mu$ L 5mM NiCl<sub>2</sub> to positively charge the surface. Fibrin Clots of all fibrinogen variants and WT were made to the final concentration of 0.02mg/mL fibrinogen, 0.05U/mL Thrombin and 2mM CaCl<sub>2</sub> in a total volume of 45 $\mu$ L. All samples were mixed gently using a pipette and allowed to clot until either 10, 20, 30 minutes had elapsed, after the clotting time was reached the polymerisation reaction was stopped by the addition of 135 $\mu$ L of TBS buffer and 3 $\mu$ L was transferred to the treated mica disc. The surface was then washed with 150 $\mu$ L of ddH<sub>2</sub>O and dried using nitrogen gas, the sample was washed and dried in the same manner one more time. Samples were then imaged using a Nanoscope V MultiMode 8 (Bruker, Coventry, UK) in soft tapping

mode in air with Bruker Tespa-V2 tips. Images were then flattened by the third order, and streaks were removed during processing using Nanoscope Analysis v1.5 (Bruker). The modified file was then exported to ImageJ for further processing. Using ImageJ a macro "AFM Crop" was written to automatically crop and set the scale (4 $\mu$ m) to allow for accurate measurement of protofibrils. Protofibril length was measured using the measuring tool in the software, and the results were tabulated using GraphPad Prism 7. Histograms of protofibril formation were made using Origin Pro (Origin Lab, Northampton, MA USA).

## **2.15 Protofibril packing**

Fibrin clots (0.5mg/mL fibrinogen 5mM CaCl<sub>2</sub> and 0.1U/mL thrombin) of both WT and fibrinogen variants were made to a volume of 100 $\mu$ L in a polystyrene cuvette (Eppendorf) with 1cm path length and immediately closed with parafilm to prevent dehydration of the fibrin clot. The clots were formed for 24 hours at room temperature before measuring the light scattering properties. After complete clot formation the clots were scanned between 500 <  $\lambda$  < 780nm in a  $\lambda$  35 UV-Vis spectrophotometer (Perkin-Elmer, Cambridge, UK). The average fiber diameter of the fibrin fiber can be determined from the wavelength dependent turbidity of fibrin clots which has already been established by (Carr and Hermans, 1978) and more recently by (Yeromonahos *et al.*, 2010). Firstly the wavelength dependent absorbance was determined as demonstrated in Figure 2-9.

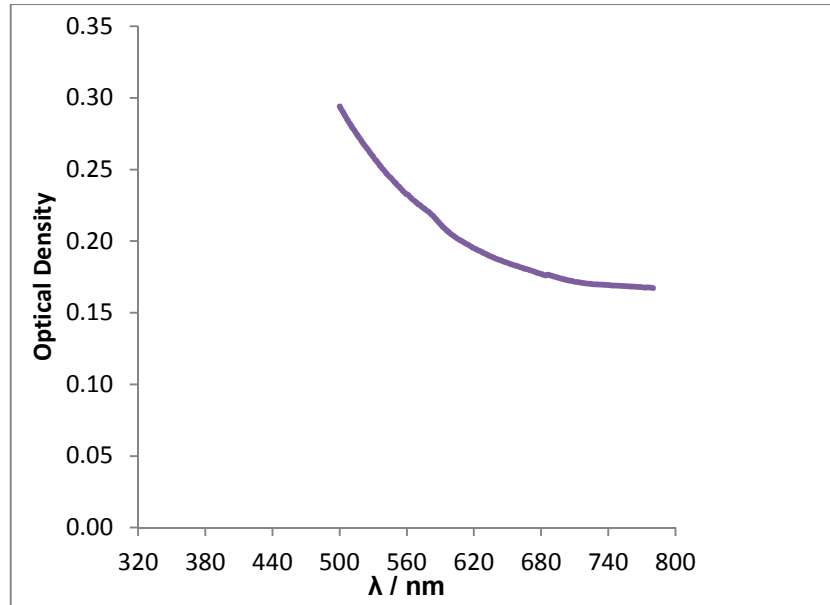


**Figure 2-9 UV-Vis spectra in the fully formed fibrin clot** Scan between 500 <  $\lambda$  <780nm) Example taken from K356Q fibrinogen variant.

The obtained optical density values were converted into turbidity values ‘ $\tau$ ’ using the following equation described in (Yeromonahos *et al.*, 2010).

$$\tau = 1 - e^{(-A.l.\ln(10))}$$

**Equation 2-9 Wavelength dependent turbidity** Wavelength dependent turbidity transformed into turbidity values where A= Absorbance and l= path length.

It has previously been estimated by both (Carr and Hermans, 1978) and (Yeromonahos *et al.*, 2010) that for a solution of randomly orientated fibers the turbidity is as described in Equation 2-10;

$$\tau\lambda^5 = \frac{2\pi^3 C n_s \mu}{N} \left(\frac{dn}{dc}\right)^2 \frac{44}{15} \left(\lambda^2 - \frac{184}{154} \pi^2 a^2 n_s^2\right)$$

**Equation 2-10 Turbidity of a solution of randomly orientated fibers** N = Avogadro’s number,  $\lambda$  = the incident wavelength (cm),  $\mu$  = the fiber protein mass/length ratio (Da.cm<sup>-1</sup>) and a = fiber radius (cm), C = initial fibrinogen mass concentration (g.mL<sup>-1</sup>)  $n_s = 1.33$  which is the solvent refractive index and  $dn/dc = 0.17594\text{cm}^3/\text{g}$  and is the solution refractive index change with protein concentration (Domingues *et al.*, 2016) (Perlmann and Longworth, 1948).

The average number of protofibrils that were contained in a fibrin fiber and the average radius of the fibers were calculated by plotting  $\tau\lambda^5$  as a function of  $\lambda^2$ . Fitting the linear Equation 2-10 to the experimental data makes it possible to calculate the mass length ratio ( $\mu$ ) as the mass length ratio is equivalent to the slope of the fitting (Yeromonahos *et al.*, 2010). The intercept of gradient allows the calculation of the square of the average radius by rearrangement of Equation 2-10. The average number of protofibrils per fiber was calculated using the mass/length ratio ( $\mu$ ) using Equation 2-11.

$$\text{Number of Protofibrils} = \frac{\mu}{\mu_0}$$

**Equation 2-11 Number of protofibrils**  $\mu_0 = 1.44 \times 10^{11}$  Da/cm = mass/length ratio of a single protofibril and  $\mu$  is the mass/length ratio of a fiber.

The average protein density can also be calculated using Equation 2-12.

$$\delta = \frac{\left(\frac{\mu}{(\pi a^2)}\right)}{N}$$

**Equation 2-12 Average protein density** Where  $\delta$  = average protein density,  $\mu$  = mass/length ratio of the fibrin fiber,  $a$  = radius of a single fibrin fiber,  $N$  = Avogadro's constant.

The distance between protofibrils can also be used as seen in Equation 2-13

$$z = \sqrt{\frac{\mu_0}{\delta}}$$

**Equation 2-13 Distance between protofibrils.**  $z$  = the average distance between protofibrils,  $\mu_0$  is the mass/length ratio of a single protofibril, and  $\delta$  is the average protein density.

# **Chapter 3 - The production of human recombinant fibrinogen variants in a CHO cell system**

### 3.1 Introduction

This chapter describes the molecular biology, cell culture and protein purification methods used to produce functional recombinant human fibrinogen variants with mutations in the extended knob-hole binding sites.

Recombinant human fibrinogen variants have been used to investigate clot polymerisation (Mullin *et al.*, 2000b), structure (Collet *et al.*, 2005b) and mechanics (Piechocka *et al.*, 2017) in the past. Today, recombinant techniques still remain a powerful tool to investigate the importance of individual residues or domains of the fibrinogen molecule. For example, the Ariëns laboratory has previously made variants to investigate the roles of  $\gamma$ - and  $\alpha$ -chain crosslinking in fibrin (Duval *et al.*, 2014). The work in this chapter will describe how the recombinant protein was produced, purified and characterised. This chapter has four sections;

1. Molecular Biology (Site-Directed Mutagenesis, Sequencing)
2. Mammalian Cell Culture Fibrinogen Production
3. Precipitation and Purification
4. Characterisation

Four recombinant human variants of fibrin have been produced using this method, these variants are; single point-mutation variants,  $\gamma$ D297N,  $\gamma$ E323Q and  $\gamma$ K356Q. A fourth variant ( $\gamma$ D297N/ $\gamma$ E323Q/ $\gamma$ K356Q) containing all three above mutations above was also created. These variants were developed to investigate the possible role of extended D-E electrostatic interactions between fibrin monomers, by changing the charged residues that facilitate the interaction in the

WT, to uncharged residues that disrupt the electrostatic interactions in each of the variants.

## 3.2 Methods

### 3.2.1 Site directed mutagenesis

The primers described in Table 3-1 were used in conjunction with cycling parameters described in Table 3-2 for mutagenesis of pMLP-γA expression vector (Figure 2-1) using the QuickChange mutagenesis kit to produce three constructs with a single point mutation and a fourth construct containing all three point mutations (refer to section 2.2.1 for further details).

**Table 3-1 Primers designed and used for site-directed mutagenesis**

Primer Name	Primer Sequence
FbgG-D297N-R	5'-aaaaactgtcactaggatcattgccaaaatcaaagccatcaaag-3'
FbgG-D297N-F	5'-ctttgatggctttgattttggcaatgatcctagtgacaagtttt-3'
FbgG-E323Q-R	5'-gcacagttgccttgaaacttatcattgtcattgtcca-3'
FbgG-E323Q-F	5'-tgggacaatgacaatgataagttcaaggcaactgtgc-3'
FbgG-K356Q-R	5'-cattaggagtagatgcttgtgagtaagtgccaccttg-3'
FbgG-K356Q-F	5'-caagggtggcacttactcacaagcatctactcctaag-3'

**Table 3-2 Cycling parameters used in site directed mutagenesis**

Segment	Cycles	Temperature (°C)	Time (s)	Cycling Stage
1	1	95	30	Initial Denaturation
2	16	95	30	Denaturation
		55	60	Annealing
		68	340	Extension

### 3.2.2 Bacterial transformation and DNA extraction

XL-10 gold bacteria were transformed as described in 2.2.2. using the mutated pMLP- $\gamma$ A expression vectors produced in 3.2.1. Bacterial colonies were selected using ampicillin resistance and DNA extraction was performed on these colonies as described in 2.2.3. The harvested mutated cDNA was sent for sequencing to Dundee University as described in 2.2.4 and 2.2.2.

### 3.2.3 Cell culture

Chinese Hamster Ovary (CHO) cells were used for expression of the wild type and all four recombinant human fibrinogen variants. Routine cell culture was performed as described in 2.3.2. CHO cells were then co-transfected with the sequenced cDNA produced in 3.2.2 and a plasmid containing the coding region of L-histidinol (selection marker) using a calcium phosphate transfection method described in 2.3.3. Two different transfection conditions, described in Table 3-3, were chosen in order to maximise the chances of cDNA successfully being incorporated into the cells.

**Table 3-3 Conditions for CHO cell transfections**

Transfection 1	Transfection 2
10 $\mu$ g DNA	20 $\mu$ g DNA
1 $\mu$ g pMSV-his	2 $\mu$ g pMSV-his
2.5M CaCl <sub>2</sub>	2.5M CaCl <sub>2</sub>

Cells were selected against L-histidinol resistance until the appearance of colonies, which were picked and cultured as described in 2.3.4. The supernatant was removed and frozen at -80°C as described in section 2.3.4 for determination of the rate of fibrinogen expression in serum-free conditions using fibrinogen

ELISA as described in section 2.4 The highest expressing clone was selected and grown for eight weeks in roller bottles.

### **3.2.4 Precipitation and purification**

Prior to precipitation, frozen medium from protein expression was thawed and mixed with a protease inhibitor cocktail as described in section 2.5.1. The resulting mix was then precipitated with ammonium sulphate and concentrated by centrifugation as described in 2.5.1. Precipitated protein was stored at -80°C until purification. The recombinant proteins were then purified by IF-1 immunoaffinity chromatography, dialysed, concentrated and the concentration of fibrinogen was determined by absorbance at A280nm using the Nanodrop ND1000 as described in sections 2.5.2 to 2.6.

### **3.2.5 Characterisation**

A reducing SDS-PAGE was performed to compare bands between recombinant WT fibrinogen and the fibrinogen variants as described in section 2.7. Circular Dichroism was performed to confirm expected secondary structure folding and convolutions were produced using CDNN software as described in section 2.8.

### **3.3 Results**

#### **3.3.1 Sequencing results of $\gamma$ D297N, $\gamma$ E323Q $\gamma$ K356Q & $\gamma$ DEK recombinant human fibrinogen variants**

To confirm that the correct cDNA sequences were obtained for each variant and that no undesired mutations were present, the cDNA for each construct was sent to Dundee University for sequencing. The results of the cDNA comparison of WT to the fibrin variants confirmed the desired point mutations in all mutants without any other unwanted random mutations. The genomic sequences converted to protein sequence for alignment of variant sequences using Clustal Omega (tables 3-4 to 3-7). In the alignments, the desired mutation is highlighted in yellow. In the case of the  $\gamma$ DEK mutant, sequential mutagenesis was performed and the cDNA was sent for sequencing to confirm no random mutations had occurred before the next mutation was introduced. The clustal omega alignments below depict the single point mutations being 26 residues longer in length than previously stated, this is because the alignment also includes a 26 residue long signal peptide that is cleaved during secretion, highlighted in blue.

**Table 3-4 Clustal Omega protein alignment of Wild Type (WT)  $\gamma$ -chain fibrinogen and  $\gamma$ D297N mutant**

WT	MSWSLHPRNLILYFYALLFLSSTCVA	YVATRDNCCILDERFGSYCPTTCGIADFLSTYQT	60
D297N	MSWSLHPRNLILYFYALLFLSSTCVA	YVATRDNCCILDERFGSYCPTTCGIADFLSTYQT	60
	*****	*****	
WT	KVDKDLQSLEDILHQVENKTSEVKQLIKAIQLTYNPDESSKPNMIDAATLKSrkMLEEIM		120
D297N	KVDKDLQSLEDILHQVENKTSEVKQLIKAIQLTYNPDESSKPNMIDAATLKSrkMLEEIM		120
	*****	*****	
WT	KYEASILTHDSSIRYLQEIYNSNNQKIVNLKEKVAQLEAQCQEPCKDTVQIHDITGKDCQ		180
D297N	KYEASILTHDSSIRYLQEIYNSNNQKIVNLKEKVAQLEAQCQEPCKDTVQIHDITGKDCQ		180
	*****	*****	
WT	DIANKGAKQSGLYFIKPLKANQQFLVYCEIDGSGNGWTVFQKRLDGSVDFKKNWIQYKEG		240
D297N	DIANKGAKQSGLYFIKPLKANQQFLVYCEIDGSGNGWTVFQKRLDGSVDFKKNWIQYKEG		240
	*****	*****	
WT	FGHLSPTGTTEFWLGNKIHLLISTQSAIPYALRVELEDWNGRTSTADYAMFKVGP EADKY		300
D297N	FGHLSPTGTTEFWLGNKIHLLISTQSAIPYALRVELEDWNGRTSTADYAMFKVGP EADKY		300
	*****	*****	
WT	RLTYAYFAGGDAGDAFDGDFGDDPSDKFFTSHNGMQFSTWDNDNDKFEgNCAEQDGSgW		360
D297N	RLTYAYFAGGDAGDAFDGDFGNDPSDKFFTSHNGMQFSTWDNDNDKFEgNCAEQDGSgW		360
	*****	*****	
WT	WMNKCHAGHLNGVYYQGGTYSKASTPNGYDNGIIWATWkTRWYSMKkTTMKIIPFNRLTI		420
D297N	WMNKCHAGHLNGVYYQGGTYSKASTPNGYDNGIIWATWkTRWYSMKkTTMKIIPFNRLTI		420
	*****	*****	
WT	GEGQQHHLGGAKQAGDV*	437	
D297N	GEGQQHHLGGAKQAGDV*	437	
	*****		

**Table 3-5 Clustal Omega protein alignment of Wild Type (WT)  $\gamma$ -chain fibrinogen and  $\gamma$ E323Q mutant**

WT	MSWSLHPRNLILYFYALLFLSSTCVA	YVATRDNCCILDERFGSYCPTTCGIADFLSTYQT	60
E323Q	MSWSLHPRNLILYFYALLFLSSTCVA	YVATRDNCCILDERFGSYCPTTCGIADFLSTYQT	60
WT	KVDKDLQSLLEDILHQVENKTSEVKQLIKAIQLTYNPDESSKPNMIDAATLKRKMLEEIM	120	
E323Q	KVDKDLQSLLEDILHQVENKTSEVKQLIKAIQLTYNPDESSKPNMIDAATLKRKMLEEIM	120	
WT	KYEASILTHDSSIRYLQEIYNSNNQKIVNLKEKVAQLEAQCQEPCKDTVQIHDITGKDCQ	180	
E323Q	KYEASILTHDSSIRYLQEIYNSNNQKIVNLKEKVAQLEAQCQEPCKDTVQIHDITGKDCQ	180	
WT	DIANKGAKQSGLYFIKPLKANQQFLVYCEIDGSGNGWTVFQKRLDGSVDFKKNWIQYKEG	240	
E323Q	DIANKGAKQSGLYFIKPLKANQQFLVYCEIDGSGNGWTVFQKRLDGSVDFKKNWIQYKEG	240	
WT	FGHLSPTGTTEFWLGNEKIHLISTQSAIPYALRVELEDWNGRTSTADYAMFKVGP EADKY	300	
E323Q	FGHLSPTGTTEFWLGNEKIHLISTQSAIPYALRVELEDWNGRTSTADYAMFKVGP EADKY	300	
WT	RLTYAYFAGGDAGDAFDGDFDGDPSDKFFTSHNGMQFSTWDNDNDKFE	360	
E323Q	RLTYAYFAGGDAGDAFDGDFDGDPSDKFFTSHNGMQFSTWDNDNDKFE	360	
WT	WMNKCHAGHLNGVYYQGGTYSKASTPNGYDNGIIWATWKTRWYSMKKTTMKIIPFNRLTI	420	
E323Q	WMNKCHAGHLNGVYYQGGTYSKASTPNGYDNGIIWATWKTRWYSMKKTTMKIIPFNRLTI	420	
WT	GEGQQHHLGGAKQAGDV*	437	
E323Q	GEGQQHHLGGAKQAGDV*	437	

**Table 3-6 Clustal Omega protein alignment of Wild Type (WT)  $\gamma$ -chain fibrinogen and  $\gamma$ K356Q mutant**

WT	MSWSLHPRNLILYFYALLFLSSTCVA	YVATRDNCCILDERFGSYCPTTCGIADFLSTYQT	60
K356Q	MSWSLHPRNLILYFYALLFLSSTCVA	YVATRDNCCILDERFGSYCPTTCGIADFLSTYQT	60
WT	KVDKDLQSLLEDILHQVENKTSEVKQLIKAIQLTYNPDESSKPNMIDAATLKRKMLEEIM	120	
K356Q	KVDKDLQSLLEDILHQVENKTSEVKQLIKAIQLTYNPDESSKPNMIDAATLKRKMLEEIM	120	
WT	KYEASILTHDSSIRYLQEIYNSNNQKIVNLKEKVAQLEAQCQEPCKDTVQIHDITGKDCQ	180	
K356Q	KYEASILTHDSSIRYLQEIYNSNNQKIVNLKEKVAQLEAQCQEPCKDTVQIHDITGKDCQ	180	
WT	DIANKGAKQSGLYFIKPLKANQQFLVYCEIDGSGNGWTVFQKRLDGSVDFKKNWIQYKEG	240	
K356Q	DIANKGAKQSGLYFIKPLKANQQFLVYCEIDGSGNGWTVFQKRLDGSVDFKKNWIQYKEG	240	
WT	FGHLSPTGTTEFWLGNEKIHLISTQSAIPYALRVELEDWNGRTSTADYAMFKVGP EADKY	300	
K356Q	FGHLSPTGTTEFWLGNEKIHLISTQSAIPYALRVELEDWNGRTSTADYAMFKVGP EADKY	300	
WT	RLTYAYFAGGDAGDAFDGDFDGDPSDKFFTSHNGMQFSTWDNDNDKFE	360	
K356Q	RLTYAYFAGGDAGDAFDGDFDGDPSDKFFTSHNGMQFSTWDNDNDKFE	360	
WT	WMNKCHAGHLNGVYYQGGTYSKASTPNGYDNGIIWATWKTRWYSMKKTTMKIIPFNRLTI	420	
K356Q	WMNKCHAGHLNGVYYQGGTYSKASTPNGYDNGIIWATWKTRWYSMKKTTMKIIPFNRLTI	420	
WT	GEGQQHHLGGAKQAGDV*	437	
K356Q	GEGQQHHLGGAKQAGDV*	437	

**Table 3-7 Clustal Omega protein alignment of Wild Type (WT)  $\gamma$ -chain fibrinogen and  $\gamma$ D297N/E323Q/K356Q ( $\gamma$ DEK) mutant**

WT	MSWSLHPRNLILYFYALLFLSSTCVA	YVATRDNCCILDERFGSYCPTTCGIADFLSTYQT 60
D297N-E323Q-K356Q	MSWSLHPRNLILYFYALLFLSSTCVA	YVATRDNCCILDERFGSYCPTTCGIADFLSTYQT 60
	*****	
WT	KVDKDLQSLIEDILHQVENKTSEVKQLIKAIQLTYNPDESSKPNMIDAATLKSARKMLEEIM	120
D297N-E323Q-K356Q	KVDKDLQSLIEDILHQVENKTSEVKQLIKAIQLTYNPDESSKPNMIDAATLKSARKMLEEIM	120
	*****	
WT	KYEASILTHDSSIRYLQEIYNSNNQKIVNLKEKVAQLEAQCQEPCKDTVQIHDITGKDCQ	180
D297N-E323Q-K356Q	KYEASILTHDSSIRYLQEIYNSNNQKIVNLKEKVAQLEAQCQEPCKDTVQIHDITGKDCQ	180
	*****	
WT	DIANKGAKQSGLYFIKPLKANQQFLVYCEIDGSGNGWTVFQKRLDGSVDFKKNWIQYKEG	240
D297N-E323Q-K356Q	DIANKGAKQSGLYFIKPLKANQQFLVYCEIDGSGNGWTVFQKRLDGSVDFKKNWIQYKEG	240
	*****	
WT	FGHLSPTGTTEFWLGNKIHLLISTQSAIPYALRVELEDWNGRTSTADYAMFKVGP EADKY	300
D297N-E323Q-K356Q	FGHLSPTGTTEFWLGNKIHLLISTQSAIPYALRVELEDWNGRTSTADYAMFKVGP EADKY	300
	*****	
WT	RLTYAYFAGGDAGDAFDGDFGDDPSDKFFTSHNGMQFSTWDNDNDFEGNCAEQDGS	360
D297N-E323Q-K356Q	RLTYAYFAGGDAGDAFDGDFGDDPSDKFFTSHNGMQFSTWDNDNDFEGNCAEQDGS	360
	*****	
WT	WMNKCHAGHLNGVYYQGGTYSKASTPNGYDNGIIWATWKTRWYSMKKTTMKIIPFNRLTI	420
D297N-E323Q-K356Q	WMNKCHAGHLNGVYYQGGTYSKASTPNGYDNGIIWATWKTRWYSMKKTTMKIIPFNRLTI	420
	*****	
WT	GEGQQHHLGGAKQAGDV*	437
D297N-E323Q-K356Q	GEGQQHHLGGAKQAGDV*	437
	*****	

### **3.3.2 Protein purification and integrity checks**

Following the collection of the CHO cell supernatant the medium was frozen at -80°C until required for protein concentration and purification. Precipitation and concentration of the medium was performed as described in section 2.5, whereas the purification of the medium was described in section 2.6. The purification of the recombinant variants was successful using the affinity chromatography technique in conjunction with the IF1 antibody. A representative chromatogram from the purification process using the AKTA Avant can be found below, Figure 3-1. This chromatogram is of triple point variant  $\gamma$ DEK. The chromatogram displays an inset (A) of all steps in the cycle of the purification process including; injection, wash I, wash II, elution and equilibration steps, whereas (B) is a zoomed in version of the same chromatogram detailing the elution of the fibrinogen molecules and the resulting absorbance peak. In this case fractions A2 to B8 contained fibrinogen therefore they were pooled, concentrated and dialysed as described in section 2.6

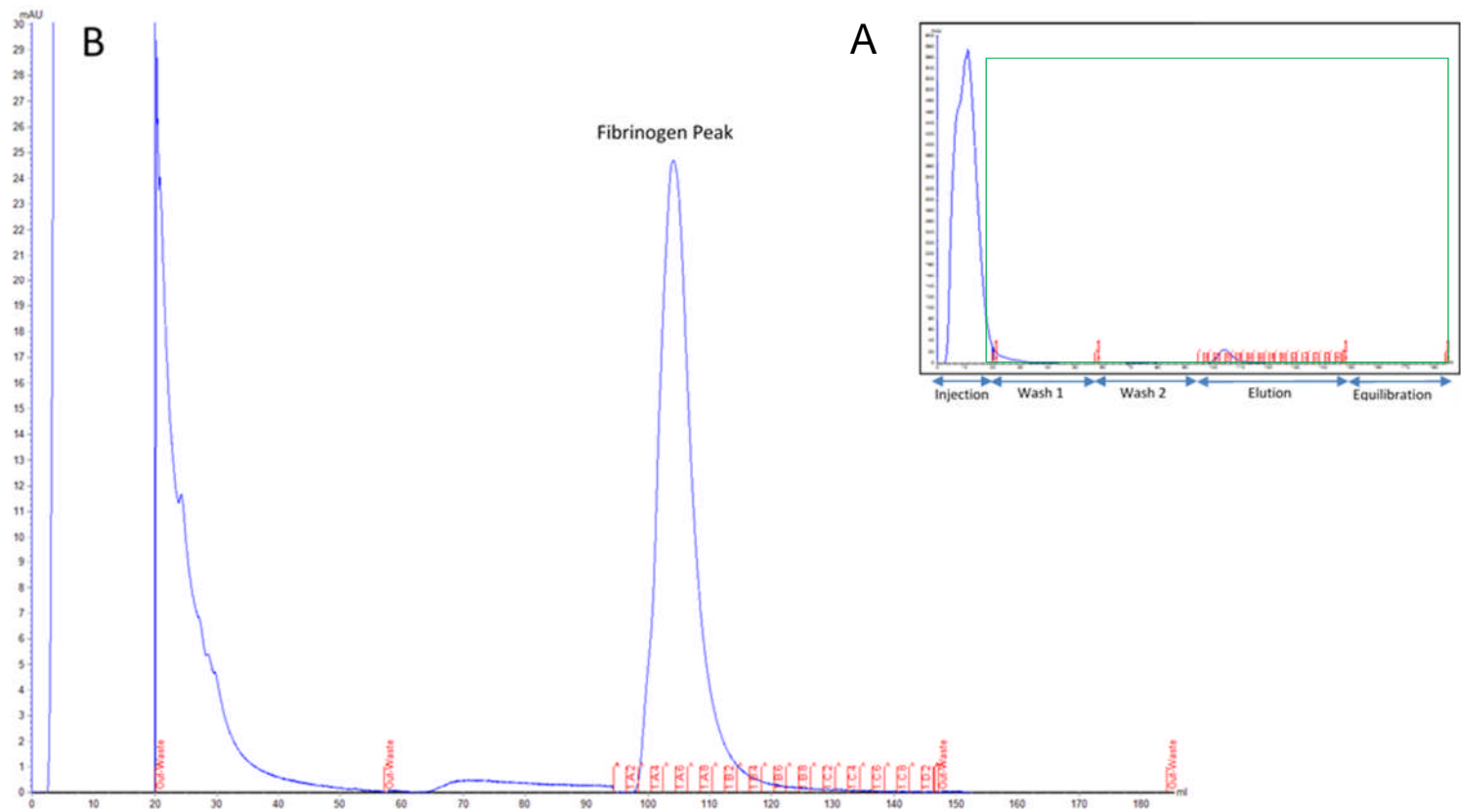


**Figure 3-1 Affinity chromatography chromatogram of  $\gamma$ D297N-E323Q-K356Q** (A) Inset of the complete purification process that contains all steps of the cycle (injection, wash I, wash II, elution and equilibration). The green box indicates the area chosen for zoomed in chromatogram (B). 'Fibrinogen peak' that arises from the elution of the recombinant fibrinogen molecules.

### 3.3.3 SDS PAGE

Following production and purification, the integrity of the fibrinogen expressed was determined by loading the fibrinogen variants onto a reducing SDS-PAGE gel, as described in section 2.7. Figure 3-2 shows reducing gel for each of the single point-mutation variants whereas Figure 3-3 shows the reducing gel for the  $\gamma$ DEK triple variant. The reduction of the fibrinogen molecules on the gel allowed clear visualisation of all three fibrinogen chains with separation of the  $\alpha$ -,  $\beta$ - and  $\gamma$ -chains. The gels also showed that there was no degradation amongst any of the fibrinogen variants. Furthermore, as expected each corresponding polypeptide band was of the same molecular weight when compared to WT.

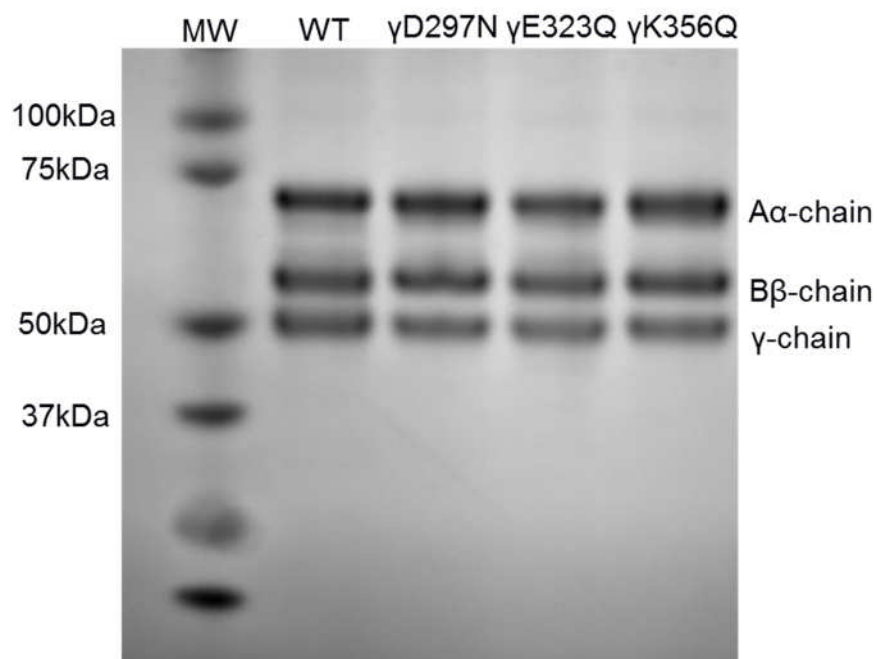


**Figure 3-2 Reduced SDS-PAGE gel of recombinant wild type and single mutant recombinant variants** Molecular weight Marker (MW), ranging from 37-100kDa. Bands were stained with Gel Code<sup>®</sup> Blue Stain reagent. No difference in the variants' molecular weight to WT was observed, and all bands for all variants were intact with no signs of degradation.

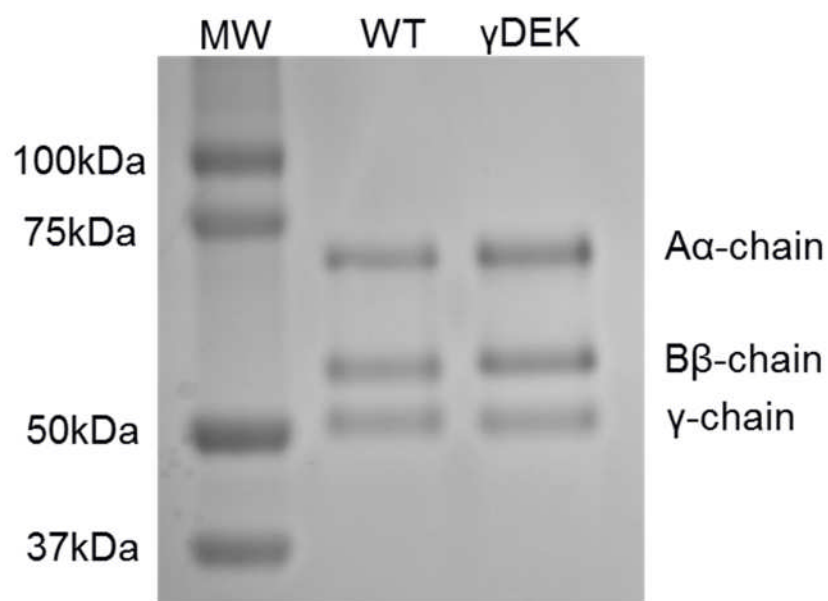


**Figure 3-3 Reduced SDS-PAGE gel of recombinant wild type and triple mutant recombinant variant  $\gamma$ DEK.** Molecular weight marker (MW), ranging from 37-100kDa. Bands were stained with Gel Code<sup>®</sup> Blue Stain reagent. No difference in molecular weight from any of the chains was observed compared to the WT, and all bands for  $\gamma$ DEK were intact with no signs of degradation.

### 3.3.4 Circular dichroism (CD) spectroscopy

Far-UV CD spectroscopy measures the amount of circularly polarised light absorbed by proteins. In this thesis, Far-UV CD was specifically performed at the 180-270nm range, here the peptide bonds of the protein are the chromophore which generate a different CD signal when they are either located in an  $\alpha$ -helix,  $\beta$ -turn or random coil structure (Johnson, 1990). Due to large amounts of noise at the extremities of the range provided, the CD spectra were truncated and only measurements from 190-250nm were analysed. To investigate whether there were any local changes in the folding of secondary structures, CD spectroscopy was performed and spectra were produced using CDNN software. When the spectra were calculated using CDNN software differences were observed for all variants, Figure 3-5. CDNN convolution software showed that for  $\gamma$ DEK there

was a 5% decrease in helical content, 3 % increase in antiparallel, 1% increase in parallel, 0.4% increase in  $\beta$  turn content and 1% increase in random coil content. For  $\gamma$ D297N, there was a 1.1% increase in helical content, 1.1% increase in antiparallel content, 0.2% in parallel content, 0.4% increase in  $\beta$  turn content and a 0.5% decrease in random coil content. For  $\gamma$ E323Q there was a 0.6% increase in helical content, 0.1% increase in antiparallel, 0.1% increase in parallel, 0.3% increase in beta turn and 1% decrease in random coil content. For  $\gamma$ K356Q there was a 2.8% increase in helical content, 0.9% increase in antiparallel, 0.3% increase in parallel, 0.3% increase in beta turn and 0.2% increase in random coil. Therefore SDS-PAGE and CD spectroscopy indicated that the fibrinogen variants produced had intact chains and overall had correctly folded secondary structure, since the observed differences in secondary structure were minimal.

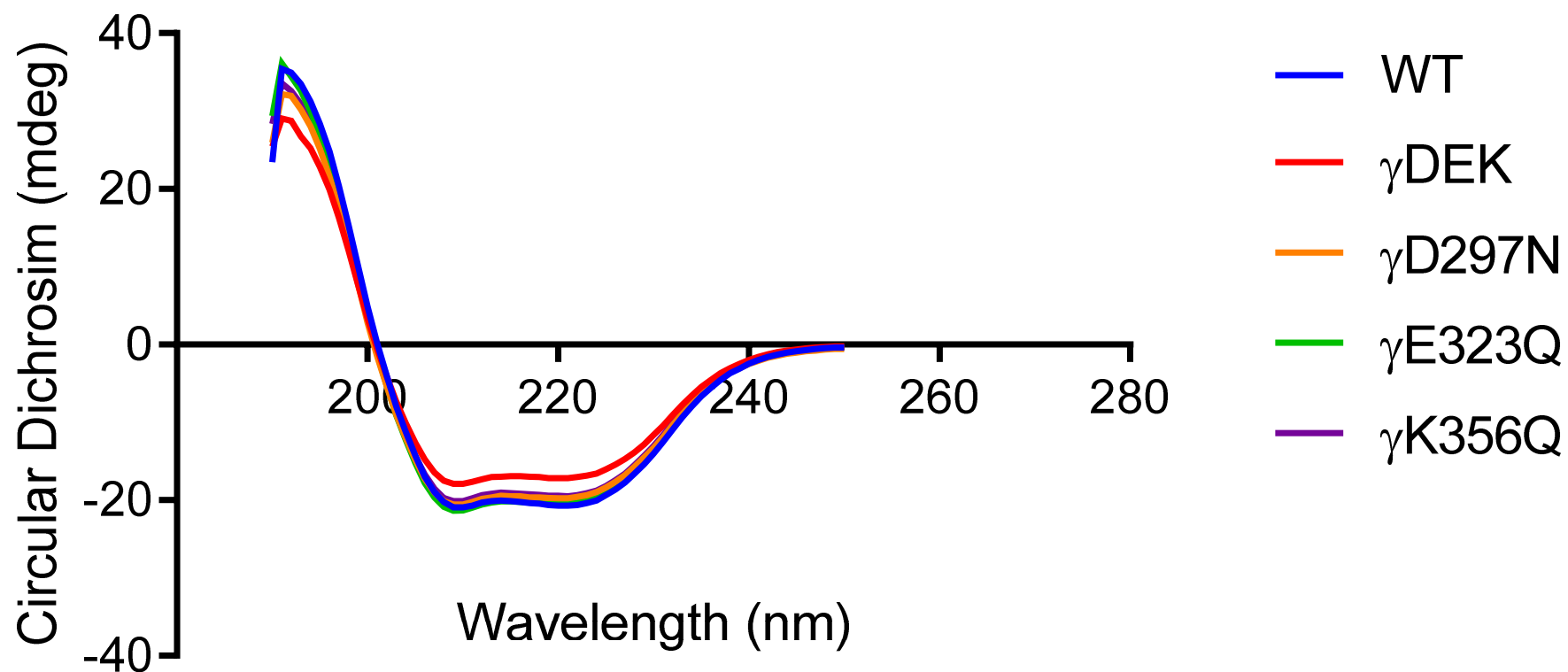


**Figure 3-4 Raw CD spectroscopy curves of recombinant wild type and recombinant variants** Spectra (190-250nm) measured in millidegrees (mdeg). WT (blue N=5)  $\gamma$ DEK (red N=4)  $\gamma$ D297N (orange N=3)  $\gamma$ E323Q (green N=3)  $\gamma$ K356Q (Purple N=3). There were changes between WT and mutant curves.

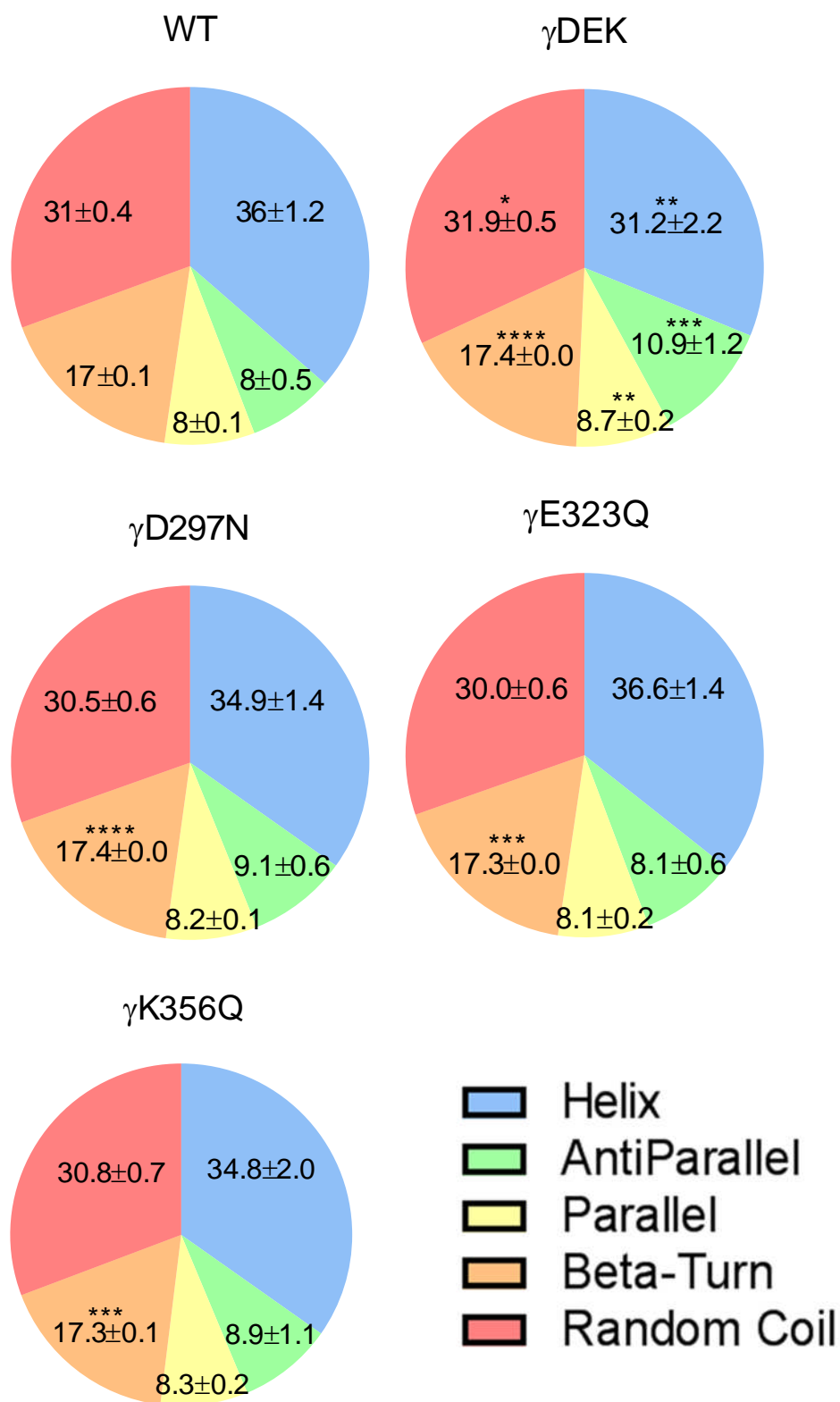


**Figure 3-5 CD spectroscopy data.** Calculated using CDNN software. Secondary structure composition ranged from helix (31-36%), antiparallel (8-11%), parallel (8-9%), β turn (17%) and random coil (30-32%) percentage content.

### 3.4 Discussion

Mammalian cells, e.g. CHO cells, are an important tool that can be used to express recombinant human proteins. Due to the importance of cardiovascular disease and the role of haemostasis and thrombosis in this devastating disease, several clotting factors have previously been expressed using a recombinant system to enable investigations into mutant variants. Factor VIII cDNA was cloned in 1984 which led to the production of recombinant factor VIII in 1992 as the product Recombinate<sup>®</sup> (Kingdon and Lundblad, 2002). Similarly, recombinant factor IX has been produced through recombinant CHO cell culturing with the first drug being licensed in 1997 (Swiech *et al.*, 2017).

The first functional recombinant fibrinogen was expressed in baby hamster kidney (BHK cells) in 1989 (Farrell, 1989). The system used in this work is based on a CHO cell system (Lord *et al.*, 1993), and this work demonstrates that it is possible to make several variants in a relatively short amount of time. The system by Lord's group has been characterised extremely well, recombinants have been developed to give insight of the traditional knob-hole regions (Okumura *et al.*, 1997), fibrinogen-platelet interactions binding sites (Rooney *et al.*, 1998), role of  $\alpha$ C domains in fibrinogen (Gorkun *et al.*, 1998) and calcium binding (Hogan *et al.*, 2000). Site directed mutagenesis was used on an expression vector already containing the coding sequence for the human  $\gamma$ -chain fibrinogen, these plasmids were duplicated on a large scale using XL 10 gold bacterium and when harvested they were sent for sequencing to Dundee University. The data in this chapter shows that the expected cDNA sequence was obtained, successful transfection was performed, using a calcium phosphate based method, that produced clones that expressed good yields of recombinant fibrinogen measured

directly from the supernatant using an ELISA method. The highest expressing clone was successfully used to produce fibrinogen in roller bottles.

The following amount of protein was produced per fibrinogen, in the case of WT this was produced by Helen McPherson, University of Leeds.  $\gamma$ K356Q was grown for a shorter period of time with fewer roller bottles due to the fact that maximum capacity had already been reached in the incubator by other projects.

**Table 3-8 Yields of recombinant WT and variant human fibrinogen**

<b>Variant</b>	<b>Total Supernatant (L)</b>	<b>Total Yield (mg)</b>
<b>WT</b>	72	122.4
<b><math>\gamma</math>DEK</b>	48	1.5
<b><math>\gamma</math>D297N</b>	48	15.2
<b><math>\gamma</math>E323Q</b>	48	5.0
<b><math>\gamma</math>K356Q</b>	9	4.5

SDS-PAGE and circular dichroism spectroscopy were both performed as integrity checks of the expressed variants. SDS-PAGE confirmed that the fibrinogen produced, for all variants, was made from all three intact  $\alpha$ -  $\beta$ - and  $\gamma$ -chains with no signs of degradation. SDS-PAGE does not give any information on the quality of the secondary structures of the protein, and therefore far-UV CD spectroscopy was used to investigate the percentage of  $\alpha$  helix, antiparallel, parallel  $\beta$ -turn and random coil structures for each variant. Secondary structure was shown to be similar across all recombinant variants with minor differences when compared to WT. Considering that fibrinogen variants have been produced

for some thirty years it is somewhat surprising that there is no indication from the literature of what the percentage fold of fibrinogen should be, making it difficult to judge if there would be any impact on fibrinogen function. Following consultation with the CD spectra laboratory manager, Dr. Nasir Khan at the University of Leeds and Professor Valeri Barsegov, University of Massachusetts, Lowell, it was suggested that these were small changes in local secondary structure and that there would be no impact on the functions of the fibrinogens, but the changes in function and structure of the fibrinogens as a consequence of 2D structural arrangement cannot be discounted. Further study could be performed by producing other variants that lead to similar changes in CD spectra but are not located in the knob-hole binding pocket and testing the functionality. This was not done in this thesis because it would have been impractical from both a time and cost perspective.

**Chapter 4 Polymerisation  
kinetics of recombinant  
human fibrinogen variants  
using light scattering  
analysis and atomic force  
microscopy**

## 4.1 Introduction

This chapter compares the polymerisation profiles and early polymerisation stages of the recombinant human WT fibrin(ogen) with those of recombinant variants,  $\gamma$ DEK ( $\gamma$ D297N/ $\gamma$ E323Q/ $\gamma$ K356Q),  $\gamma$ D297N,  $\gamma$ E323Q and  $\gamma$ K356Q, using light scattering and atomic force microscopy (AFM) methods. Parameters such as lag phase (when only protofibril formation is occurring) and the maximum optical density (corresponds to the cross sectional area of a fibrin fiber) were compared between the four variants.

Light scattering techniques to study fibrin polymerisation and clot structure have been used for several decades and are used commonly by laboratories within the field for the same purpose (Domingues *et al.*, 2016; Magatti *et al.*, 2013). The technique remains popular because of the easy preparation of a clot and the amount of information that can be gathered. Conveniently, the technique can be used for either purified fibrinogen samples or plasma samples from patients. Light scattering techniques are not sensitive enough at the earlier stages of clot formation (when protofibrils are growing longitudinally), therefore high resolution imaging techniques such as Atomic Force Microscopy (AFM) are used. Others have used Atomic Force Microscopy (AFM) to visualise protofibril formation and polymerisation at these earlier stages (Protopopova *et al.*, 2015). The Ariens laboratory has also used AFM to study polymerisation for  $\gamma$ A and  $\gamma'$  fibrin(ogen) (Allan *et al.*, 2012). Therefore it was decided that it was appropriate to use AFM to also study and visualise polymerisation at the early stages.

In this thesis the potential presence of extended knob-hole interaction sites beyond the classical binding pocket were investigated. As I am mutating amino acid residues that are thought to support knob-hole binding then it would be

reasonable to expect a delay in polymerisation at the early stages that would be detectable using AFM and may result in protofibril packing differences that result in changes in fiber growth, through destabilisation of these bonds. Therefore soft tapping mode AFM was used to visualise early protofibril formation and turbidity techniques were used to study polymerisation rate and fiber growth of these recombinant variants. Using AFM, differences in the early kinetics were observed where the longitudinal protofibril growth was delayed, turbidity showed larger, significant differences where there was a decrease in the  $V_{max}$  and all variants had a decreased maximum optical density which indicates a difference in fiber thickness and clot structure.

## **4.2 Objectives**

To investigate whether the abolition of extended knob-hole interactions alter the polymerisation kinetics.

## **4.3 Methods**

### **4.3.1 Turbidity**

Fibrin clots were prepared with 0.5mg/mL fibrinogen, 5mM  $CaCl_2$  and 0.1U/mL Thrombin (final concentrations) and the polymerisation of the fibrin was measured at 340nm for a period of 60 minutes, as described in 2.9.1. From the resulting turbidity curves, the lag phase was measured by calculating the time difference between the start of the reaction (the combination of fibrinogen and thrombin) and when an increase in OD was detected. The maximum optical density was calculated from the highest OD value. For comparisons of OD and lag phase between WT and  $\gamma$ DEK, a paired two-tailed t-test was performed at a significance level of  $p < 0.05$ . For the single fibrin variants a comparison was made

to WT using a One-way ANOVA at a significance level of  $p < 0.05$ . When the variants were compared at different time points for AFM experiments, a one-way ANOVA was used with multiple comparisons to the WT at a significance level of  $p < 0.05$ .

#### **4.3.2 Atomic force microscopy**

Atomic Force microscopy was performed as described in section 2.14 on clots (0.02mg/mL fibrinogen, 0.05U/mL Thrombin and 2mM CaCl<sub>2</sub> formed at 10, 20 and 30 minutes after the initiation of clotting. Micrographs were taken using a Nanoscope AFM in air in soft tapping mode. Briefly, individual images were flattened using Nanoscope analysis software v9.2 and converted to a tiff file using a macro designed by Dr. Stephen Baker (University of Leeds) to allow accurate measurement of the length of individual protofibrils 'by hand' using ImageJ software. Histograms were created using GraphPad Prism 7 to study length of protofibrils and comparisons were made between WT and the fibrinogen variants at a significance level of  $p < 0.05$ .

#### **4.3.3 Statistics**

Data analysis was performed using GraphPad Prism statistical software package. A two-tailed t-test was used for comparisons between one variant and the WT, when more than one variant was compared a one-way ANOVA was used with multiple comparisons with the WT as a control column. Results are shown as mean  $\pm$  SD, and were considered significant when  $p < 0.05$ .

## 4.4 Results

Turbidity measurements were performed to investigate the differences in kinetics of the recombinant variants. In the first instance, turbidity was performed using the serine protease thrombin to cleave the fibrinogen for all variants. Additionally, turbidity was also performed with reptilase a snake venom that cleaves fibrinogen differently to thrombin by only cleaving FpA and exposing knob-A, FpB remains uncleaved.

The analysis of the turbidity data in Figure 4-1 and Figure 4-2 demonstrates that there are striking and significant differences in the polymerisation kinetics. The maximum OD was significantly reduced for  $\gamma$ DEK ( $0.23 \pm 0.03$  Abs, -41%) compared to WT ( $0.39 \pm 0.01$  Abs)  $p=0.0162$ . The lag phase was significantly increased for  $\gamma$ DEK ( $132 \pm 12$  seconds, +43.5%) compared to WT ( $92 \pm 14$  seconds)  $p=0.0194$ . Due to the differences seen here from the triple mutant ( $\gamma$ DEK), turbidity measurements were also performed on the fibrinogen variants that only consisted of single point mutations in order to identify whether the changes are driven by just one or more of the changes that were introduced.

The analysis of the turbidity data for the single mutants in Figure 4-3 and Figure 4-4 further demonstrate significant differences in the polymerisation kinetics. The percentage change from the WT ( $0.48 \pm 0.02$  Abs) to the variants was calculated. The maximum OD was significantly reduced for variants  $\gamma$ D297N ( $0.39 \pm 0.03$  Abs, -19%  $p=0.001$ ),  $\gamma$ E323Q ( $0.33 \pm 0.02$  Abs, -31%  $p=0.001$ ),  $\gamma$ K356Q ( $0.39 \pm 0.03$  Abs, -19%  $p=0.001$ ) However, there were no significant changes to lag phase for any of the single mutants.

Polymerisation kinetics using reptilase were also performed for all single recombinant variants, as shown in Figure 4-5. N=1 was performed due to limitations in material quantity. Turbidity with reptilase was not performed for the triple mutant due to limitations in material quantity. A similar turbidity trend as seen with previous measurements with thrombin was observed. WT (0.60Abs) had the highest maximum OD followed by the three single mutants  $\gamma$ D297N (0.43Abs, -28%),  $\gamma$ K356Q (0.43Abs, -28%), and  $\gamma$ E323Q (0.39Abs, -35%). There were changes for the lag phase with  $\gamma$ E323Q (108seconds, +12.5%), being extended compared to the WT (96seconds),  $\gamma$ D297N (84 seconds, -12.5%) was accelerated, and there was no difference for  $\gamma$ K356Q (96 seconds).

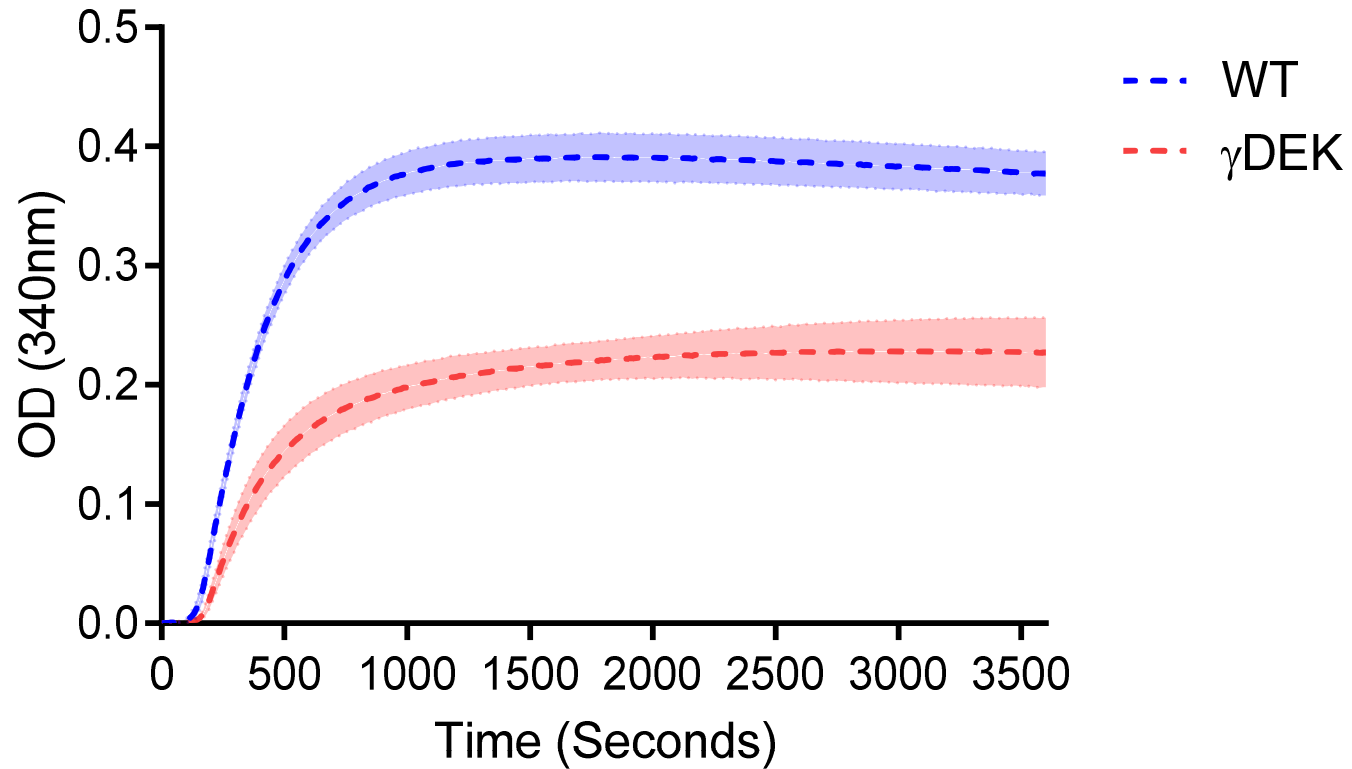


**Figure 4-1 Turbidity curve of fibrin clots.** WT (blue)  $\gamma$ DEK (red) Fibrin polymerisation over a period of one hour.  $\gamma$ DEK fibrinogen has an extended lag phase, slower polymerisation rate and reduced maximum optical density (OD). N=3. Dotted line represents the mean of three experiments, shaded areas depict standard deviation between repeats.

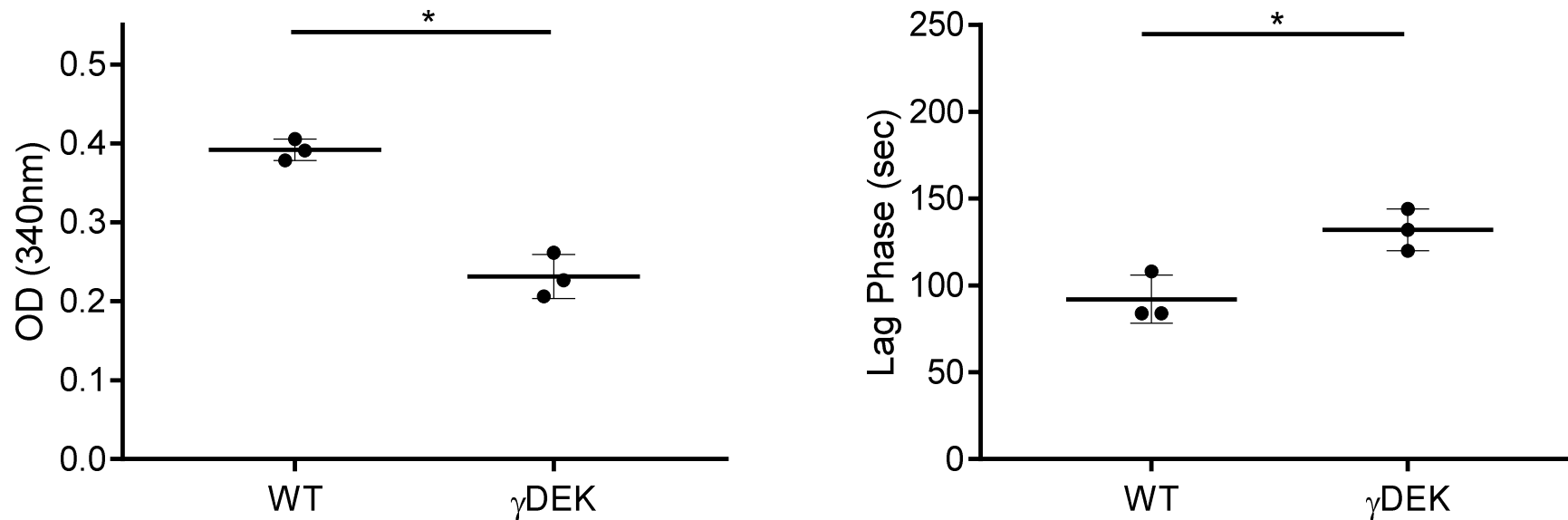


**Figure 4-2 Maximum optical density and lag phase of fibrin clots.** Altered polymerisation was seen for  $\gamma$ DEK. A significantly reduced max OD was observed for  $\gamma$ DEK when compared to WT,  $p=0.0162$ . Lag Phase was determined using Microsoft Excel to be the last point before exponential growth of the polymerisation curve. A significantly extended lag phase was observed for  $\gamma$ DEK when compared to the WT,  $p=0.0194$ . For both graphs max OD and lag phase were compared using a paired t-test with a significance level of  $p<0.05$ . Error bars represent standard deviation.

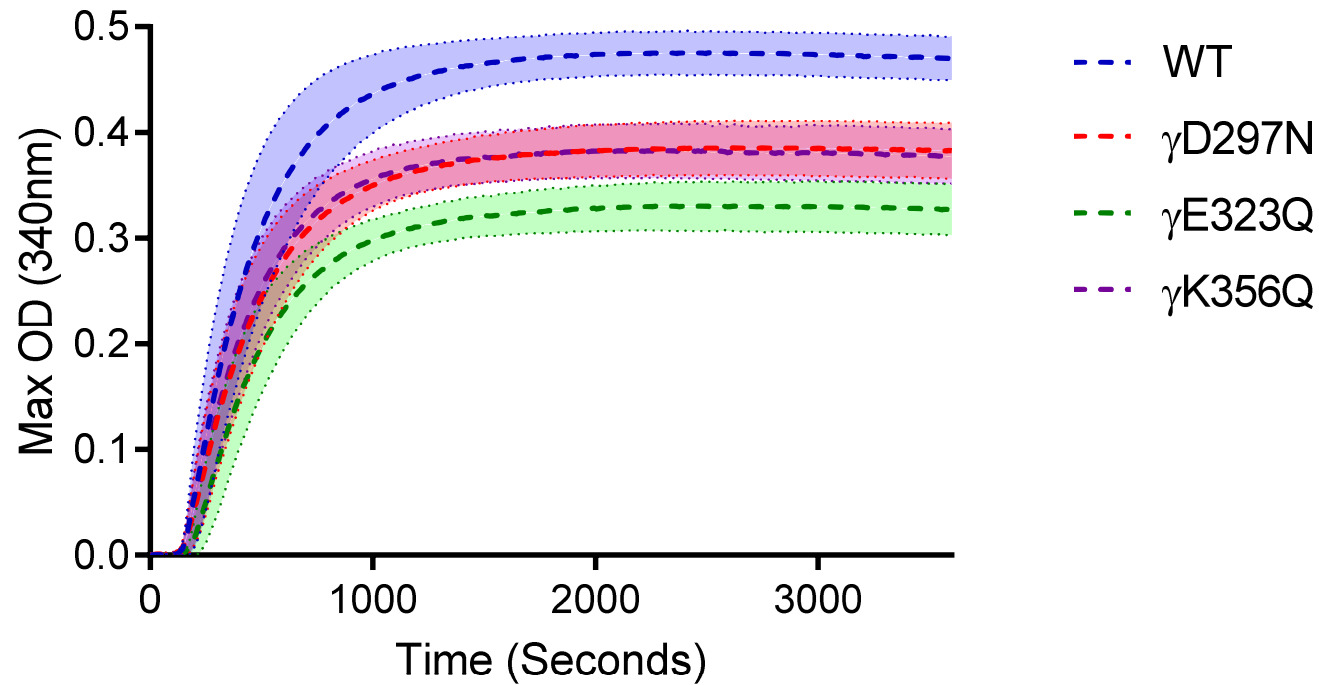


**Figure 4-3 Turbidity curve of fibrin clots.** WT (blue),  $\gamma$ D297N (red),  $\gamma$ E323Q (green),  $\gamma$ K356Q (purple). Altered polymerisation was also observed for the single fibrin variants when over a period of 1 hour of polymerisation. Lag Phase was determined using Microsoft Excel to be the last point before exponential growth of the polymerisation curve. There were no changes in lag phase, but maximum optical density of all the single variants were significantly different. N=3, dotted line represents the mean of three experiments, shaded areas depict standard deviation between repeats.

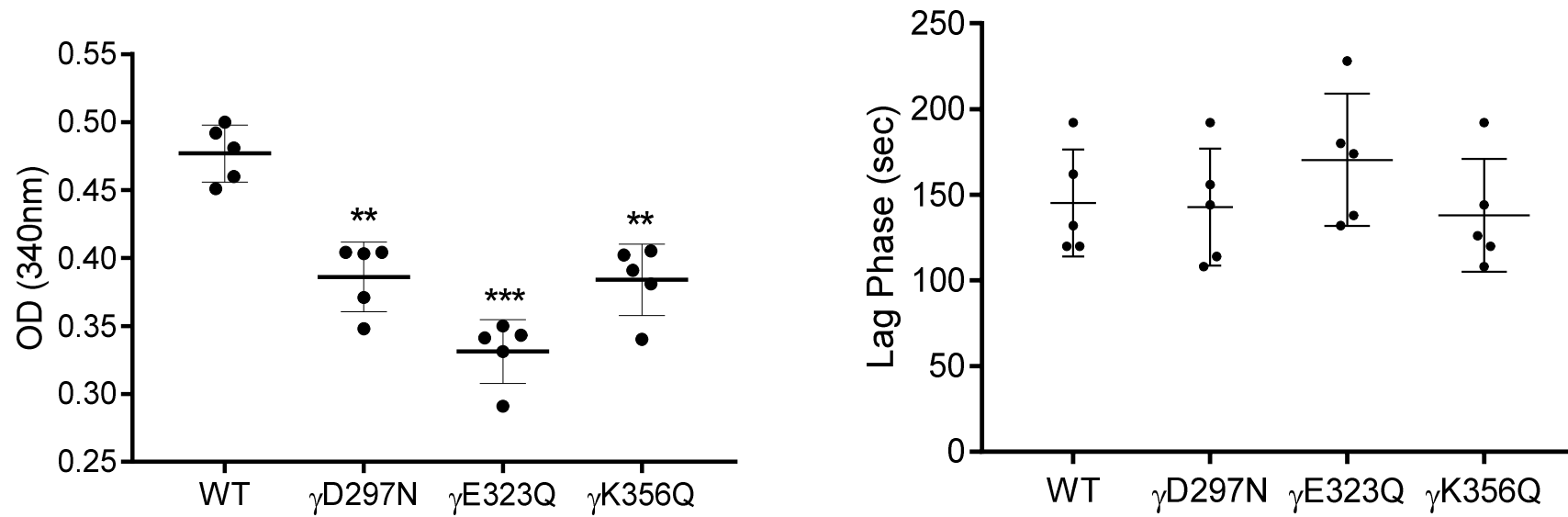


**Figure 4-4 Maximum optical density and lag phase of fibrin clots.** Maximum OD was significantly reduced for all single mutant variants when compared to the WT. Lag Phase was determined using Microsoft Excel to be the last point before exponential growth of the polymerisation curve. No significant differences in lag phase were observed. For both graphs max OD and lag phase were compared using an one way ANOVA with a significance level of  $p < 0.05$ . Error bars represent standard deviation.

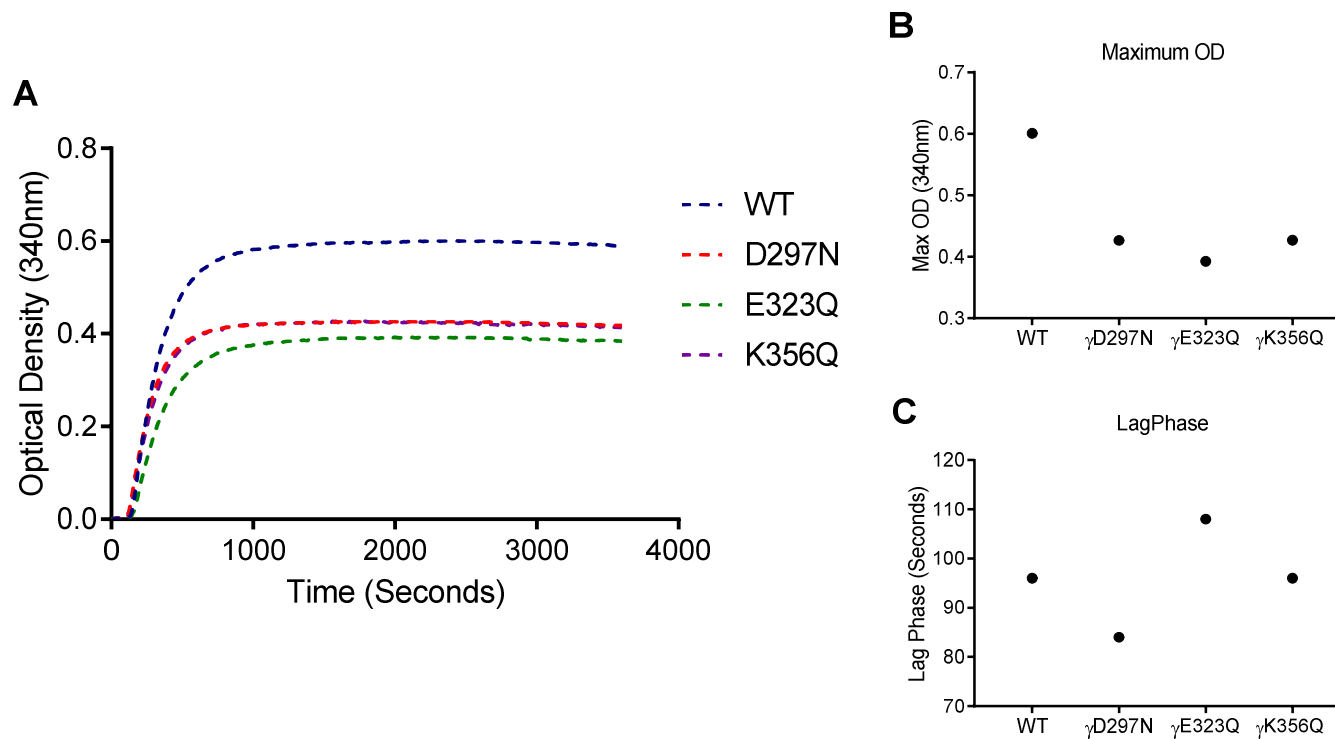


**Figure 4-5 Turbidity of fibrin clots with reptilase.** WT (blue),  $\gamma$ D297N (red),  $\gamma$ E323Q (green),  $\gamma$ K356Q (purple). The overall turbidity profile of clot formation over 1 hour. (A) Shows different kinetics for the single mutant variants vs WT. (B) Maximum OD was reduced for all single mutant variants when compared to the WT. Lag Phase was determined using Microsoft Excel to be the last point before exponential growth of the polymerisation curve. Lag phase was varied for the single mutants with  $\gamma$ D297N being accelerated compared to WT,  $\gamma$ E323Q was extended compared to WT and  $\gamma$ K356Q remained unchanged compared to WT.

The Vmax ( $\Delta$ Abs/min) was measured to study the rate of polymerisation of the recombinant variants. Due to abolition of the electrostatic interactions, the knob-hole bonds should be less stable causing higher dissociation, slower polymerisation rate and slower protofibril/fiber formation.  $\gamma$ DEK polymerisation rate, Figure 4-6, was significantly impaired ( $0.0375 \pm 0.005$  Abs/min, -46.1%) compared to WT ( $0.070 \pm 0.001$  Abs/min)  $p=0.004$ . Polymerisation rate for  $\gamma$ D297N ( $0.065 \pm 0.014$  Abs/min, -35.6%)  $\gamma$ E323Q ( $0.057 \pm 0.013$ , -43.6%) and  $\gamma$ K356Q ( $0.072 \pm 0.017$ , -28.1%) variants were significantly lower compared to the WT ( $0.100 \pm 0.023$  Abs/min), Figure 4-7.

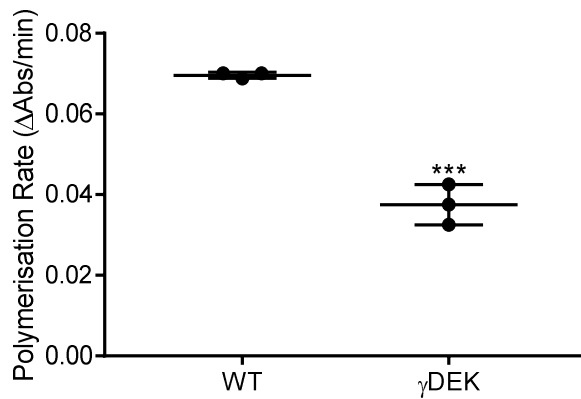


**Figure 4-6 Maximum polymerisation rate of WT and  $\gamma$ DEK fibrin clots**  
Polymerisation rate was decreased for  $\gamma$ DEK when compared to WT, error bars depict standard deviation at  $P < 0.05$  using two tailed t-test analysis.

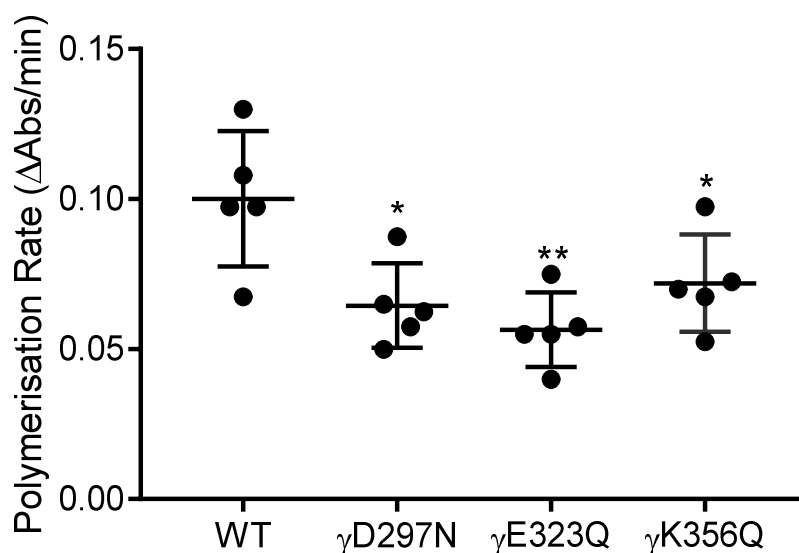


**Figure 4-7 Maximum polymerisation rate of WT, γD297N γE323Q and γK356Q.** Polymerisation rate was significantly decreased for all single mutants, error bars depict standard deviation at P<0.05 using one-way ANOVA analysis.

Based on the altered polymerisation kinetics as analysed by the turbidity experiments, Atomic Force Microscopy was used to visualise protofibril formation at the very early stages following clotting initiation by thrombin. Clots for the WT and all variants were allowed to form for either 10, 20 or 30 minutes, and then added to freshly cleaved mica for AFM imaging. Figure 4-8 shows the progressive longitudinal polymerisation of protofibrils over time for WT and each recombinant variant. At the 10 minute timepoint delayed polymerisation was observed for the recombinant variants except γK356Q, while at longer time points 20 and 30 minutes most variants were longer in length Table 4-1. However, it was decided that analysis of only average protofibril length was insufficient as the amount of protofibrils within each sample may also change, therefore distribution curves of protofibril length for each variant were made as seen in Figures 4-9 to 4-12.

**Table 4-1 Average length (mean) of protofibrils during polymerisation**  
Significance at  $p < 0.05$  is represented by an asterisk (\*) when variants are compared to their matching WT time point.

Recombinant Variant	Time point		
	10 Minute	20 Minute	30 Minute
WT	183.3 ± 43.5 nm	244.7 ± 31.3nm	238.0 ± 19.4nm
γDEK	163.1 ± 0.7nm	213.1 ± 40.3nm	268.5 ± 46.7nm
γD297N	149.0 ± 8.1nm	287.0 ± 14.8nm	276.6 ± 31.0nm
γE323Q	176.5 ± 26.9nm	258.2 ± 45.3nm	302.7 ± 33.8nm
γK356Q	225.4 ± 24.8nm	282.4 ± 42.1nm	346.4 ± 22.5nm *

Following image processing, protofibrils were measured by hand using Image J software. Origin Pro Software (OriginLab Corporation, Northampton, MA, USA) was used to plot the distribution of protofibrils over time for the WT and each variant as demonstrated in Figure 4-9 to Figure 4-12. For WT and all fibrin variants there was an increase in the number of larger species at later 20 minute and 30 minute time points although the larger differences of protofibril length were seen between 10 and 20 minutes time points. However for a more direct comparison between variants, each variant was plotted on the same histogram for the same time point, 10minutes (Figure 4-10), 20 minutes (Figure 4-11) and 30 minutes (Figure 4-12). All fibrin variants median length increased between the 10 minute and 20 minute time points, γDEK (163.1→193.4nm), γD297N (149.0→291.3nm), γE323Q (172.3→235.2nm), γK356Q (211.7→302.3nm). Between 20 and 30 minutes WT (251.6→232.9nm) and γD297N (291.3→261.1nm) median length plateaued, however median protofibril length increased for γDEK (193.4→250.9nm), γE323Q (235.2→295.5nm) and γK356Q (302.3→337.6nm) between these time points.

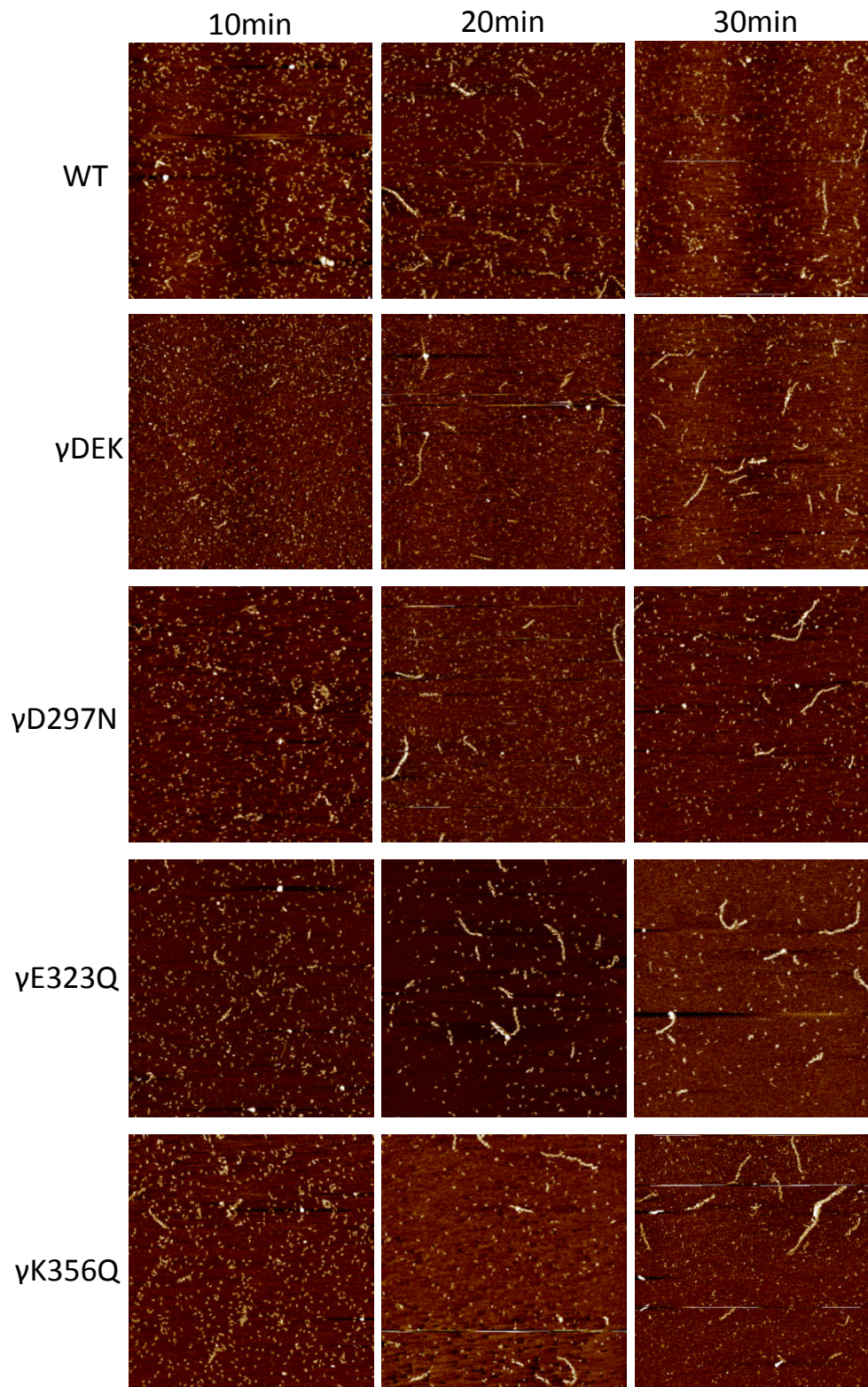


**Figure 4-8 Atomic force micrographs** Protofibril formation of WT and recombinant variants. Clotting was stopped at 10, 20 and 30 minutes after initiation of polymerisation, added dropwise to a cleaved mica surface and imaged in a  $4\mu\text{m} \times 4\mu\text{m}$  area. Images taken in dried conditions during soft tapping mode in air.

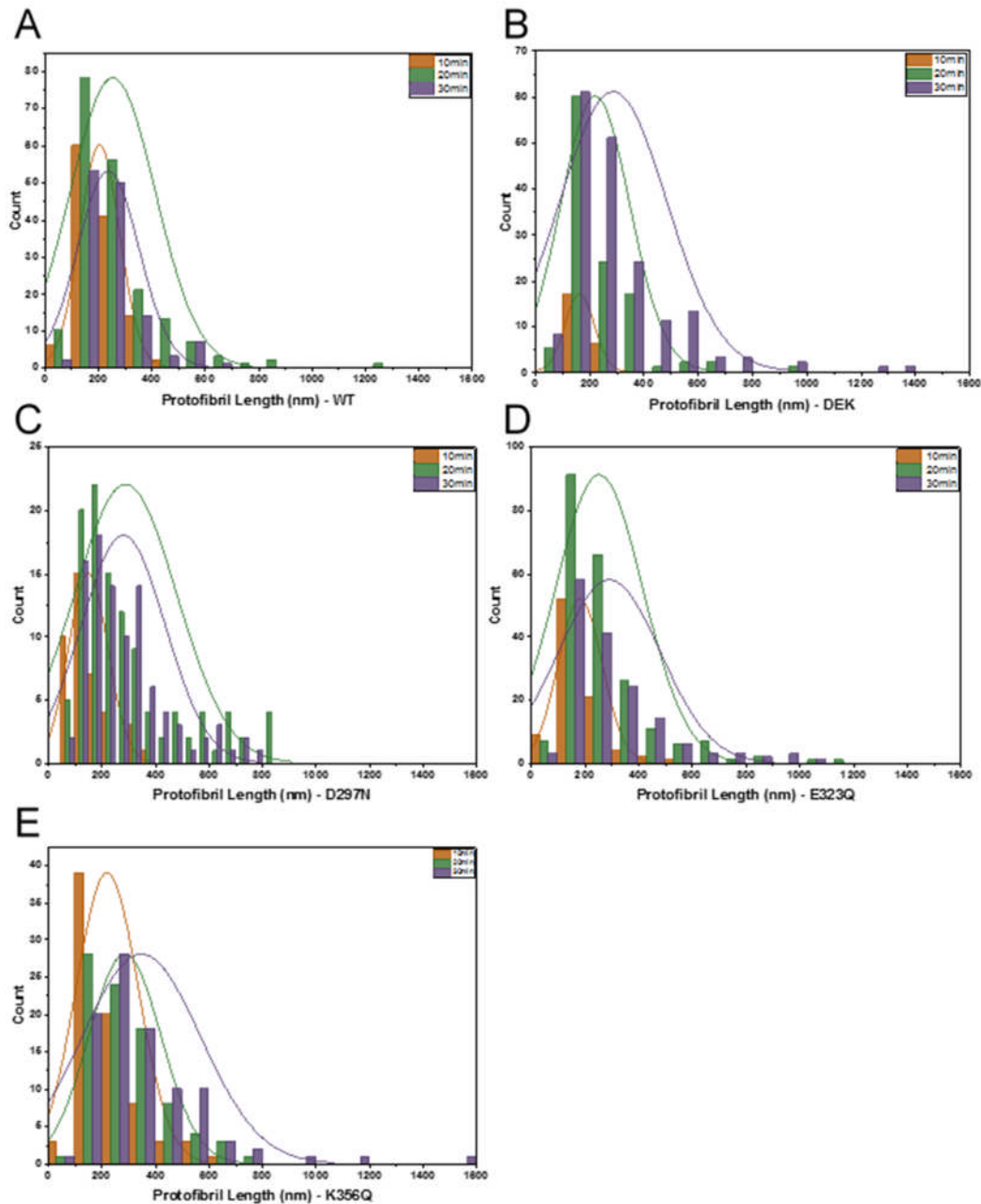


**Figure 4-9 Distribution of protofibrils** WT (A)  $\gamma$ DEK (B)  $\gamma$ D297N (C)  $\gamma$ E323Q (D)  $\gamma$ K356Q (E) 10minute time point (orange), 20 minute time point (green) and 30 minute time point (purple). For WT protofibrils formed at 10 minutes were shorter than 20 and 30 minutes, average protofibril length at 20 minutes was similar to 30 minutes time point. For  $\gamma$ DEK protofibrils were shorter and less abundant at 10 minutes compared to 20 and 30 minute time points. For  $\gamma$ D297N 10 minutes had the shortest and least abundant amount of protofibrils whereas 20 and 30 minutes were similar.  $\gamma$ E323Q had an increasing amount of and an increased length of protofibrils as time points progressed.  $\gamma$ K356Q had many short fibers at 10 minutes but fewer and longer protofibrils at 20 and 30 minutes. Normal distribution curves were plotted on each graph where bin size was limited to 50 per group.

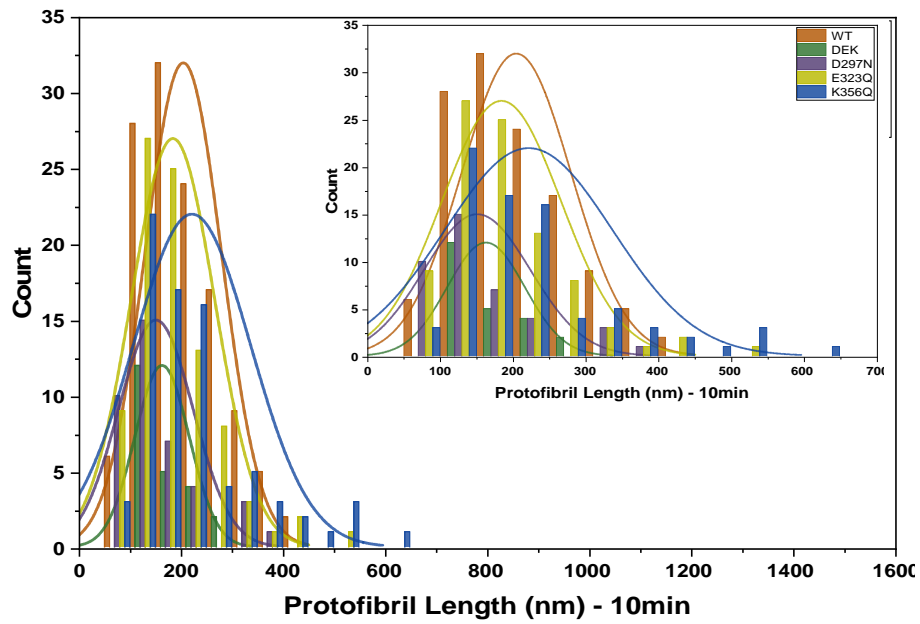


**Figure 4-10 Distribution comparison of protofibril length (nm) following 10 minutes clot formation** WT (Orange),  $\gamma$ DEK (green),  $\gamma$ D297N (purple),  $\gamma$ E323Q (yellow), and  $\gamma$ K356Q (blue). Inlet represents the same data but with a shorter x axis. All fibrin variants, except from  $\gamma$ K356Q had fewer and shorter protofibrils than the WT. The triple mutant ( $\gamma$ DEK appeared to have the shortest protofibrils followed by  $\gamma$ D297N,  $\gamma$ E323Q). Normal distribution curves were plotted on each graph where bin size was limited to 50 per group.

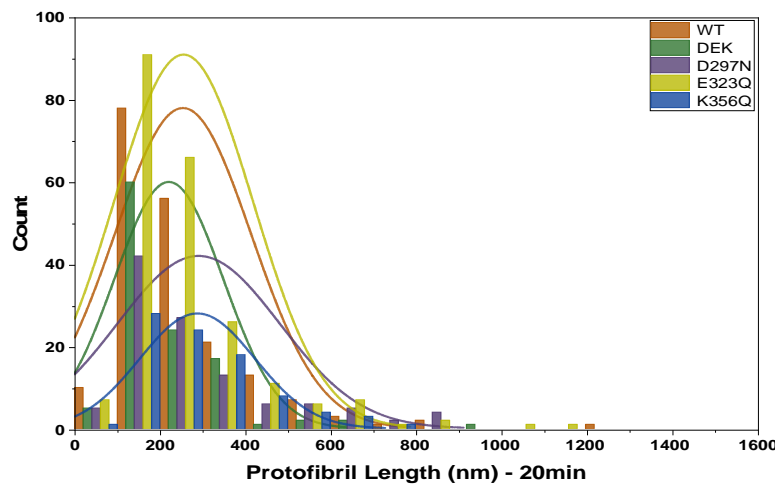


**Figure 4-11 Distribution comparison of protofibril length (nm) following 20 minutes clot formation** WT (Orange),  $\gamma$ DEK (green),  $\gamma$ D297N (purple),  $\gamma$ E323Q (yellow), and  $\gamma$ K356Q (blue). At the 20 minute time point  $\gamma$ DEK still had the shortest protofibrils followed by WT,  $\gamma$ E323Q,  $\gamma$ K356Q,  $\gamma$ D297N. Normal distribution curves were plotted on each graph where bin size was limited to 50 per group.

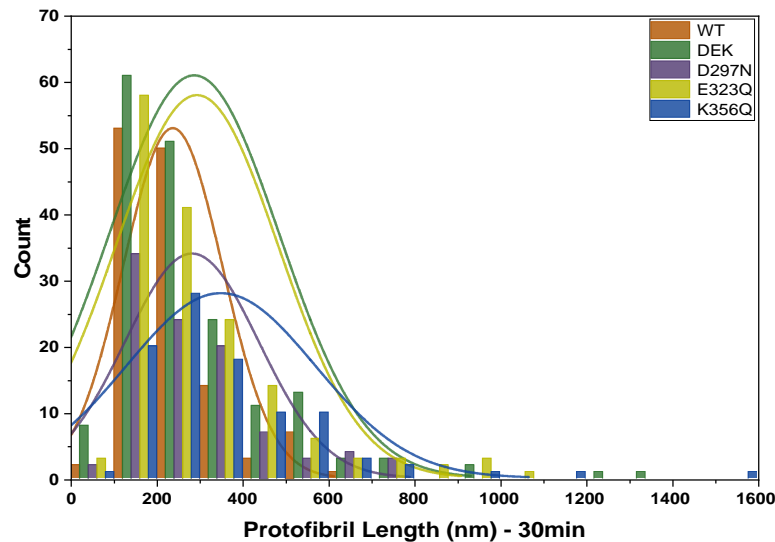


**Figure 4-12 Distribution comparison of protofibril length (nm) following 20 minutes clot formation** WT (Orange),  $\gamma$ DEK (green),  $\gamma$ D297N (purple),  $\gamma$ E323Q (yellow), and  $\gamma$ K356Q (blue). All variants have a longer average protofibril length compared to the WT. From the variants  $\gamma$ DEK, still has the average shortest protofibrils followed by  $\gamma$ D297N,  $\gamma$ E323Q and  $\gamma$ K356Q) Normal distribution curves were plotted on each graph where bin size was limited to 50 per group.

## 4.5 Discussion

In this chapter, the polymerisation kinetics were studied by light scattering and atomic force microscopy methods. The main focus in the light scattering studies was to study the difference in maximum optical density and lag phase, whereas for the AFM experiments protofibril growth was the main focus. Turbidity as a function of time has commonly been used to assess the kinetics of clot formation (Reganon *et al.*, 1984; Duval *et al.*, 2016). The typical shape of the turbidity curve as discussed in section 2.9 is somewhat distorted for the recombinant variants, as they all have a significantly reduced maximum optical density and in the case of the triple mutant a significantly extended lag phase. The following percentage reductions of optical density by the variants were observed;  $\gamma$ DEK -41%,  $\gamma$ D297N -19%,  $\gamma$ E323Q -31% and  $\gamma$ K356Q -20%. It has previously been published that

maximum optical density values have a direct correlation with the radial cross section of a fibrin fiber with higher amounts of scattering representative of thicker fibers and lower amounts of scattering representing thinner fibers (Carr and Hermans, 1978). Therefore, based on this knowledge and other reports (Weisel and Litvinov, 2013) I hypothesise that in the clot structure experiments the recombinant variants should produce clots that are more dense with many more fibers, that are thinner, more branch points and have smaller pore sizes compared to the WT. It is worth noting that the  $\gamma$ DEK variant has the largest reduction in maximum OD, followed by the three single variants perhaps suggesting that each point mutation has a somewhat additive effect on the reduction of the maximum optical density.

For the triple mutant ( $\gamma$ DEK) it is interesting that the early kinetics (lag phase) was significantly different from that of the WT suggesting that the abolition of the extended D-E electrostatic interactions play a key role in polymerisation of the fibrin fibers or during protofibril formation. On the contrary, the single mutants were not different from the WT, indicating that all three single point mutations are required to observe an effect on lag phase, as when mutated individually no changes were observed. Therefore, the effect of the mutations do not appear to be cumulative or additive, rather the combination of the mutations triggers an effect, perhaps by local conformational changes of the binding pocket.

Although it is reasonable to assume that each mutation contributes a change in the overall polymerisation profile, one must consider the possibility that even though the polymerisation curves for the single mutant variants are very similar to each other, especially  $\gamma$ D297N and  $\gamma$ K356Q, they still may be different at the protofibril and intrafibril level. The varying parameters (FpA cleavage, protofibril

initiation, protofibril growth, fiber initiation, fiber growth, fiber aggregation and fibrin concentration) that regulate the kinetics of protofibril formation have extensively been investigated (Weisel and Nagaswami, 1992). These authors used computer modelling, light scattering methods and scanning electron micrographs to describe the effects of each of these parameters and their influence on maximum fiber size, maximum rate of assembly, lag period, and number of fibers. Table 4-2 is based on Table 1 found in Weisel's paper. If the polymerisation profiles of the mutant variants are to be compared to Table 4-2 then one can see that an decrease in the parameter 'fiber growth' ( $k_{fg}$ ) gives rise to a similar turbidity profile that is observed in the variants (decrease in maximum fiber size, a decrease in maximum rate of assembly, an increase in the number of fibers). Therefore it is likely that the point mutations that abolish the extended D-E electrostatic interactions limit fiber growth.

**Table 4-2 Parameters implicated in affecting polymerisation kinetics and clot structure** An increase in the rate constant results in an increase or decrease in maximum fiber size, polymerisation rate, lag period and number of fibers. This table is based on Table 1 found in (Weisel and Nagaswami, 1992).

Increase in the rate constant	Maximum Fiber Size	Polymerisation Rate	Lag Period	Number of Fibers
$k_A$ - FPA cleavage	↓	↑	↓	↑
$k_{pi}$ - protofibril initiation	↓	↑	↓	↑
$k_{pg}$ - protofibril growth	0	0	0	0
$k_{fi}$ - fiber initiation	↓	↓	0	↑
$k_{fg}$ - fiber growth	↑	↑	↓	↓
$k_{fa}$ - fiber aggregation	↑	0	0	↑
$k_{fc}$ - fiber concentration	↑	↑	↓	↓

Polymerisation of the recombinant variants was further investigated using reptilase, a snake venom enzyme which cleaves fibrinopeptide A only, (unlike thrombin). This was performed to confirm that the differences in turbidity were not just due to change in affinity of the recombinant variants with thrombin. There

was not enough material of  $\gamma$ DEK remaining for this experiment to be performed. These data demonstrated that the altered polymerisation kinetics that are observed for the recombinant variants are independent of their binding affinity to thrombin and these mutated residues are likely to affect polymerisation directly. This data is also supported by the significant reduction in maximum polymerisation rate that is observed for all recombinant variants.

The early stages of protofibril formation and fibril initiation were investigated using Atomic Force Microscopy (AFM studies). In these experiments, high resolution images are captured at the nanoscale range of protofibril formation. Three time points were used to assess protofibril formation and fibril initiation over time; 10 minutes, 20 minutes and 30 minutes. Clotting usually occurs within a few minutes, however to truly observe the early polymerisation kinetics the clotting conditions for AFM measurements must be slowed down by reducing the fibrinogen and thrombin concentrations. This allows the imaging of protofibril formation where very little information can be gathered from turbidity measurements.

When studying the early stages of protofibril formation using atomic force microscopy there was already a difference in polymerisation between the WT and the recombinant variants at the 10 minute time point, where all variants, except for  $\gamma$ K356Q, have a reduced average length. For  $\gamma$ DEK,  $\gamma$ D297N,  $\gamma$ E323Q this is expected because the extended knob-hole interactions have been disrupted therefore the polymerisation process should be less stable leading to fewer and/or shorter protofibrils. However it is quite surprising that  $\gamma$ K356Q variant forms longer protofibrils than the WT, it may be possible that although the extended electrostatic interaction has been abolished, the  $\gamma$ K356Q variant is able

to form new contacts counter intuitively to enable it to form longer protofibrils. It is interesting to note that a publication from the laboratory of Professor Doolittle (Yang *et al.*, 2000) focuses on a model of fibrin formation and through the use of crystal structures and molecular simulations postulates that regions  $\gamma$ 350-360 and  $\gamma$ 370-380 are the 'driving force' of  $\gamma$ C domain lateral interactions that give rise to protofibril association. Maybe it is possible that  $\gamma$ K356Q forms  $\gamma$ C-  $\gamma$ C contacts that are more favourable and cause faster longitudinal growth.

At 20 and 30 minute time points there is no significant difference between the average length of the variant protofibrils compared to the WT. At these later time points it appears that the variants have 'recovered' from their initial disruption to longitudinal protofibril formation. It was not possible to check whether protofibrils had accelerated polymerisation beyond 30 minutes because the mixture had become fully clotted.

Additionally, when analysing the distribution of protofibrils, it is interesting that the 'normal distribution' curve that was fitted is slightly shifted to the right for all variants at all time points. This is because extremely large species of fibers are influencing the overall distribution.

In summary, the turbidity profiles for all fibrin variants were very different, Max OD was significantly reduced for all variants and lag phase was significantly extended for  $\gamma$ DEK, longitudinal protofibril formation was also disrupted albeit it recovered at later time points. This suggests that the fibrin variants have an effect on longitudinal protofibril formation, which could influence the packing mechanisms involved, reducing lateral aggregation and greatly impacting on fiber growth.

# **Chapter 5 - Effects of abolished extended D-E interactions on clot structure at different spatial scales**

## 5.1 Introduction

Following spontaneous longitudinal self-assembly, protofibrils finally reach a so called critical length and begin to laterally aggregate forming fibrin fibers which give rise to the 3D fibrin network (Hantgan *et al.*, 1980).

What causes the lateral aggregation of protofibrils to form fibrin fibers is still unclear and the fact that protofibrils are required to reach a critical length before they begin to aggregate suggests that the interactions between the protofibrils themselves are weak and increase with longer protofibrils.

Although the exact mechanism is not known, the most accepted hypothesis is that the binding of Knobs B and holes 'b' following thrombin cleavage are responsible for lateral aggregation (Litvinov *et al.*, 2007), in addition to the interactions exhibited by the  $\alpha$ C domains where they untether from the E region during FpA and FpB cleavage by thrombin (Tsurupa *et al.*, 2011).

The literature suggests that it is likely that extended knob-hole interactions should exist. It was demonstrated that a GPRP mimetic of knob A has a binding affinity of  $K_d = 25\mu\text{M}$  (Everse *et al.*, 1998) with hole a. While NDSK (N-terminal disulphide knot) fibrin fragment binding with fibrinogen has a reported  $K_d$  of  $5.8\mu\text{M}$  (Geer *et al.*, 2007), suggesting that extra interactions besides the conventional knob and hole complex must be at play. Recent molecular simulations (Kononova *et al.*, 2013; Zhmurov *et al.*, 2016) further support this hypothesis. Work by Kononova modelled a DD-fragment and aligned it with a fibrin monomer, the knobs were mapped manually as these do not appear in the crystal structure and it was proposed that the electrostatic interactions studied in this work play a key role in supporting the A:a knob-hole bond.

In the previous chapter the effect of the abolition of the extended knob hole interactions on polymerisation was studied, and it was found that the disruption of extended D-E interactions impacted mainly on fiber growth. There was a significant difference in maximum OD between the WT and recombinant variants. As discussed previously, it has been shown by others that results such as Max OD generated from light scattering methods have a direct relationship with the cross sectional area of a fibrin fiber (Hantgan and Hermans, 1979; Yeromonahos *et al.*, 2010). Therefore, this change in maximum optical density during turbidity measurements is a sign that there may be differences in protofibril packing resulting in thicker or thinner fibers. It is also likely that these packing differences then lead to differences in the final clot structure.

Previous reports by others have already demonstrated how final fibrin clot structure can be influenced;

- pH, temperature and ionic strength (Nair *et al.*, 1986)
- the concentration of Ca<sup>2+</sup> ion (Carr *et al.*, 1986)
- the concentration of thrombin (Blombäck *et al.*, 1989)

The effect of thrombin appears to have the most striking effect on clot structure, lower concentrations give rise to clots that have thicker fibers, whereas higher concentrations give rise to thinner fibers (Domingues *et al.*, 2016).

Work from the Ariëns laboratory has shown that thrombin concentration is also very important during fibril assembly and protofibril packing of fibrin fibers (Domingues *et al.*, 2016). In both hydrated (light scattering) and dehydrated (Transmission Electron Microscopy, TEM) conditions an increase in thrombin concentration leads to a decrease in fiber radius.

Myself and others have shown that it is possible to produce recombinant human variants of fibrinogen to study the importance of single residues on clot structure (McPherson, PhD thesis; Sabban, PhD thesis, (Duval *et al.*, 2014)). The work in this chapter will compare the differences in clot structure between the WT and recombinant variants that impair extended D-E interactions. To do this, clot density, hydrated conditions were studied using laser scanning confocal microscopy. Fiber thickness was compared in hydrated conditions (using light scattering) and dehydrated conditions (using SEM). Protofibril packing arrangements of single fibrin fibers were studied using light scattering, and clot lysis was also compared using confocal microscopy.

## **5.2 Methods**

### **5.2.1 Scanning electron microscopy (SEM)**

Detailed methods can be found in section 2.13. In brief, fibrin clots were made to the final concentration of 0.5mg/mL fibrinogen, 5mM CaCl<sub>2</sub> and 1U/mL of Thrombin in a pierced Eppendorf lid and excess salt was removed from the clots by washing with 50mM sodium cacodylate buffer (pH 7.4) and later fixed with 2% Gluteraldehyde. The clots were then subjected to another 50mM sodium cacodylate wash followed by dehydration of the clots in a 30-100% acetone dehydration series and left overnight in 100% acetone. Martin Fuller, Astbury Center - University of Leeds, critically dried and mounted the subsequently prepared clots onto aluminium SEM imaging stubs which were then coated with a 0.5nm thick layer of iridium. Each clot was imaged at x2000, x5000, x10000, x20000 and x50000 magnification. Images taken at x20000 were used to calculate fiber thickness.

## 5.2.2 Laser scanning confocal microscopy

### 5.2.2.1 Protein labelling

Prior to labelling, 100µg of WT and each recombinant variant was dialysed against 1x PBS pH 7.4 and consequently labelled using Alexa Fluor 488 Protein Labelling kit™ as described in 2.12.1.

### 5.2.2.2 Fibrin clot structure

Fibrin polymerisation and clot formation was initiated by the addition of a reaction mix containing 5mM CaCl<sub>2</sub> and 0.1U/mL thrombin to 0.5mg/mL fibrinogen variant and 5% Alexa Fluor 488 labelled fibrinogen variant (final concentrations) to a total volume of 40µL in an Eppendorf tube. 30µL was transferred to a channel in a VI flow, uncoated sterile µ-slide), placed into a dark humidity chamber and allowed to clot for 1 hour. After formation, the clots were housed onto the piezo stage of the LSCM microscope and z stack was imaged using parameters as described in Table 5-1.

**Table 5-1 LSCM parameters for final clot structure**

Setting	Value
Laser Power	3%
Laser	488
Stack size	X = 212.13µm Y = 212.13µm Z = 15µm
Slices	21
Slice Depth	0.75µm
Gain	762
Pinhole	44µm

The computer software ZEN™ was used to process the images and fiber density of the clots was determined as described in 2.12.3. The clot densities between WT, γDEK, γD297N, γE323Q and γK356Q were compared.

### 5.2.2.3 Clot lysis

Fibrin clots were formed in a  $\mu$ -slide as described above in 5.2.2.2. After formation, 20 $\mu$ L of 6nM tPA and 0.4 $\mu$ M Plasminogen was added to the fully formed clot and allowed to permeate the network for two minutes with the slide tilted at 45°C followed by 5 minutes with the slide flat. The slide was mounted on the microscope and a lysis front was located and clot lysis was imaged using the following parameters as described in Table 5-2.

**Table 5-2 LSCM parameters for clot lysis**

Setting	Value
Laser Power	3%
Laser	488
Stack size	X = 212.13 $\mu$ m Y = 212.13 $\mu$ m Z = 2 $\mu$ m
Slices	5
Slice Depth	0.5 $\mu$ m
Series Time	10 seconds
Gain	762
Pinhole	34 $\mu$ m

The images were processed as described in 2.12.4 and clot lysis was measured by the rate of travel of the lysis front.

### 5.2.3 Protofibril packing

Fibrin clots 0.5mg/mL fibrinogen 5mM CaCl<sub>2</sub> and 0.1U/mL thrombin of WT and fibrinogen variants were made to a volume of 100 $\mu$ L and the average fibrin fiber diameter was determined from the wavelength dependent turbidity using a Perkin-Elmer spectrophotometer. The average fiber radius, the number of protofibrils, and distance between protofibrils was calculated as discussed in 2.15.

#### 5.2.4 Statistics

Data analysis was performed using GraphPad Prism statistical software package. A one-way ANOVA was used with multiple comparisons with the WT as a control column. Results are shown as mean  $\pm$  SD, and were considered significant when  $p < 0.05$ .

### 5.3 Results

Clot structure was first compared between WT and the fibrinogen variants using Scanning Electron Microscopy, although clots were imaged at 5 different magnifications, and x20000 micrographs were chosen for clot analysis as they were the most suitable for comparison. The fiber network density of the mutants were visually compared to WT (Figure 5-1) and it is very clear that the variants were denser, with the  $\gamma$ DEK being the most dense followed by the single mutants and then the WT. Fibers also looked visually different in thickness so this was investigated using Image J. As demonstrated in Figure 5-2, there is a significant difference in fiber thickness for all variants compared to the WT ( $65.0 \pm 7.2 \text{ nm}$ ), with  $\gamma$ DEK being the thinnest ( $43.2 \pm 5.6 \text{ nm}$ )  $p = 0.0004$ , followed by  $\gamma$ E323Q ( $48.1 \pm 2.3 \text{ nm}$ )  $p = 0.0014$ ,  $\gamma$ K356Q ( $50.6 \pm 4.2 \text{ nm}$ )  $p = 0.0078$  and  $\gamma$ D297N ( $53.1 \pm 3.3 \text{ nm}$ )  $p = 0.0425$ .

To confirm the differences in fiber density, laser scanning confocal microscopy experiments were also performed, Figure 5-3 is an illustrative image of each variant and shows a difference in clot structure. The fiber count per  $200 \mu\text{m}$  (Figure 5-4) was quantified,  $\gamma$ K356Q was the least dense ( $25 \pm 4$  fibers), followed by WT ( $29 \pm 1$  fibers),  $\gamma$ D297N ( $29 \pm 3$  fibers),  $\gamma$ E323Q ( $34 \pm 3$  fibers) and  $\gamma$ DEK was the most dense ( $40 \pm 2$  fibers). To gather insight whether the difference in

density gave rise to changes in clot breakdown, lysis rates were measured (Figure 5-5), however none of the mutants were significantly different to the WT. The average lysis speeds (fastest to slowest) are as follows;  $\gamma$ D297N ( $0.64 \pm 0.11 \mu\text{m/s}$ ), WT ( $0.45 \pm 0.07 \mu\text{m/s}$ ),  $\gamma$ E323Q ( $0.36 \pm 0.09 \mu\text{m/s}$ ),  $\gamma$ K356Q ( $0.33 \pm 0.13 \mu\text{m/s}$ ) and  $\gamma$ DEK ( $0.28 \pm 0.08 \mu\text{m/s}$ ).

Protofibril packing analysis was then conducted in fully hydrated conditions to study the intrafibrillar structure of fibrin fibers, there were no significant differences in fiber radius in hydrated conditions (Figure 5-6) when comparing WT ( $104 \pm 1 \text{nm}$ ) to  $\gamma$ D297N ( $98 \pm 6 \text{nm}$ ),  $\gamma$ E323Q ( $102 \pm 3 \text{nm}$ ) and  $\gamma$ K356Q ( $102 \pm 1 \text{nm}$ ). It was not possible to measure  $\gamma$ DEK due to limitations in material quantity. There was a large but not significant decrease in protofibril number (Figure 5-7); for  $\gamma$ D297N ( $206 \pm 82$ ),  $\gamma$ E323Q ( $270 \pm 82$ ) and  $\gamma$ K356Q ( $253 \pm 25$ ) compared to WT ( $375 \pm 92$ ). This reduction led to the hypothesis that if the radii of the fibers are the same but a large reduction in the total number of protofibrils then the packing between protofibrils for the variants must be different. The average distance between protofibrils (Figure 5-8) was then calculated as described in 2.15. The WT was the most densely packed with  $9.7 \pm 1.0 \text{nm}$  spacing between each protofibril followed by  $\gamma$ E323Q ( $11.2 \pm 1.4 \text{nm}$ )  $\gamma$ K356Q ( $11.4 \pm 0.0 \text{nm}$ ) and  $\gamma$ D297N ( $12.6 \pm 2.2 \text{nm}$ ) being the least densely packed.

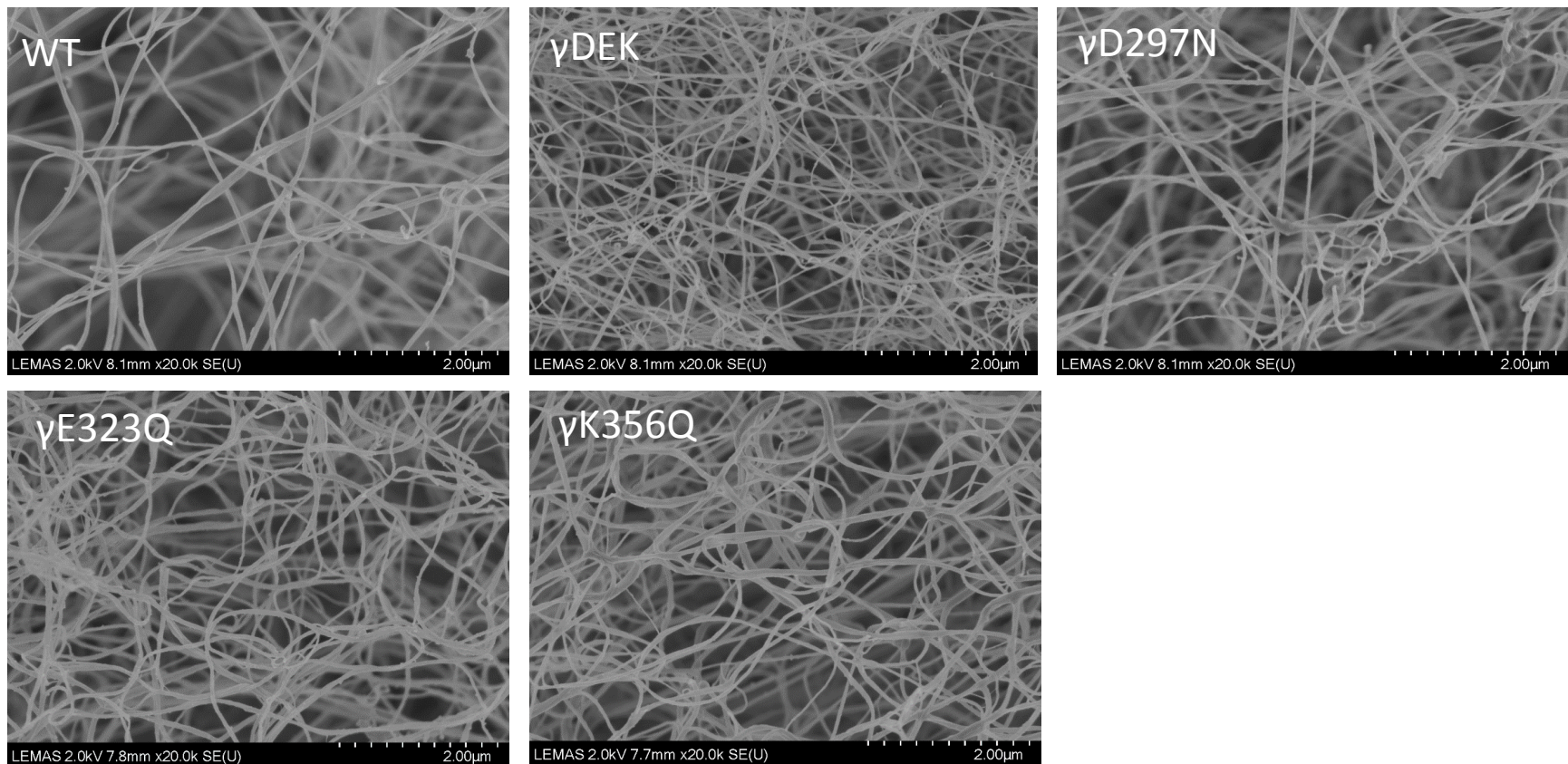


**Figure 5-1 Scanning electron micrographs of purified WT and fibrin variants at x20000 magnification.** WT clots were visually the least dense followed by the extended knob-hole single variants with the triple variant being the most dense. Fibers were thinner for the variants with  $\gamma$ DEK being the thinnest.

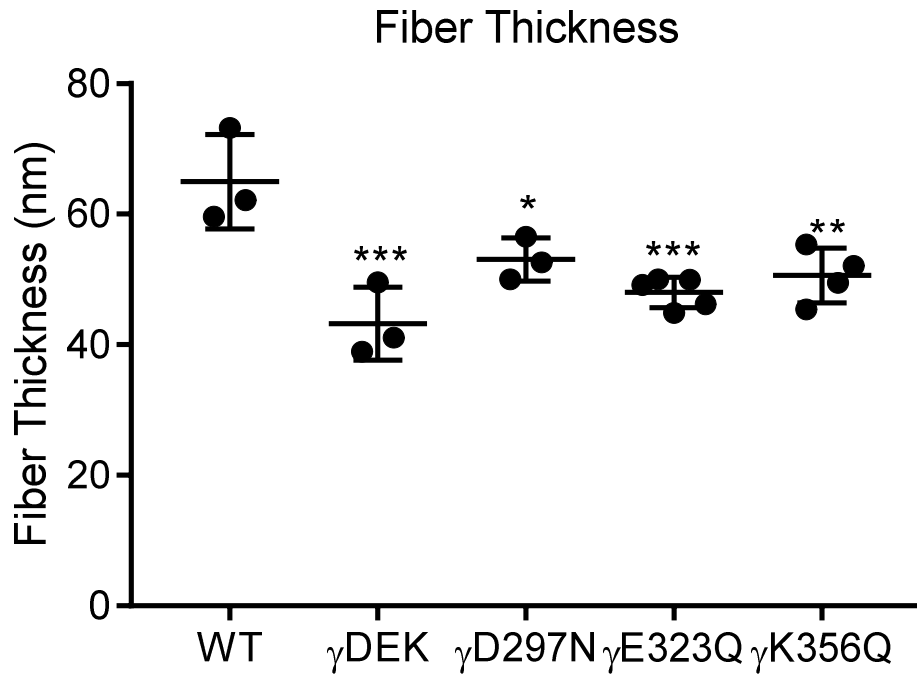


**Figure 5-2 Thickness of WT and variant fibrin fibers in dehydrated conditions using scanning electron microscopy.** Fiber thickness was quantified using ImageJ analysis software and a significant reduction was observed for all fibrin variants.

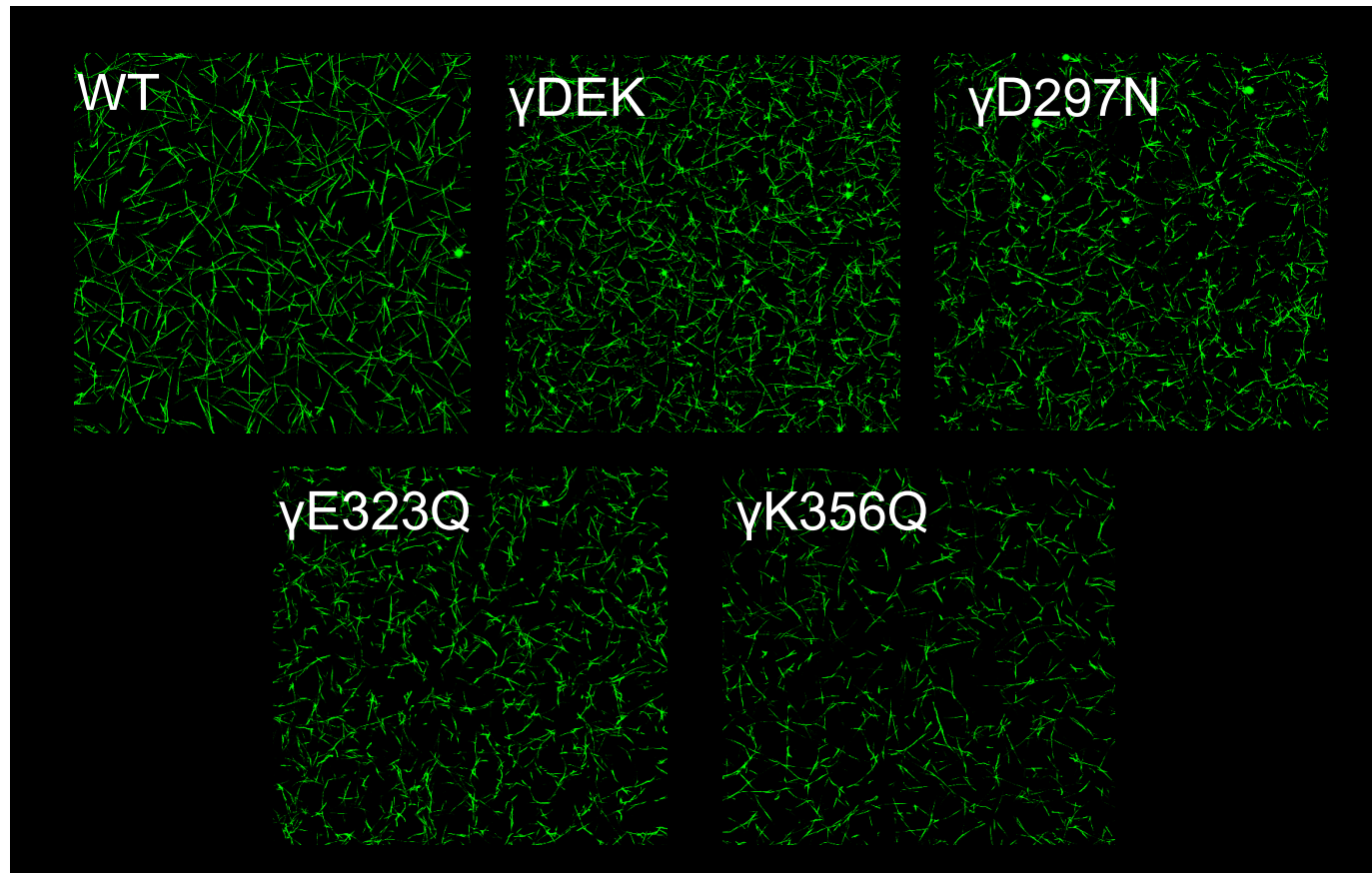


**Figure 5-3 Laser scanning confocal microscopy micrographs of WT fibrin clots** Alexa 488 labelled fibrin was incorporated into the clots to allow for visualisation of clot structure in hydrated conditions.  $\gamma$ DEK clots appeared to be the most dense followed by  $\gamma$ E323Q  $\gamma$ D297N WT and  $\gamma$ K356Q.

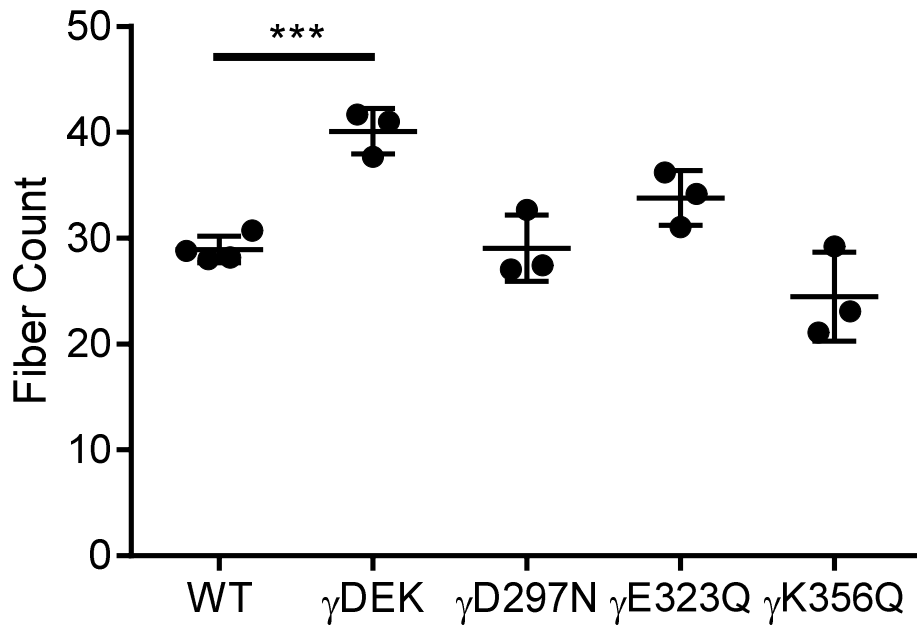


**Figure 5-4 Fiber count per 200µm** Grids were overlaid on LSCM micrographs using ImageJ analysis software, and fibers that intersected with grid lines were counted as an indication of clot density.

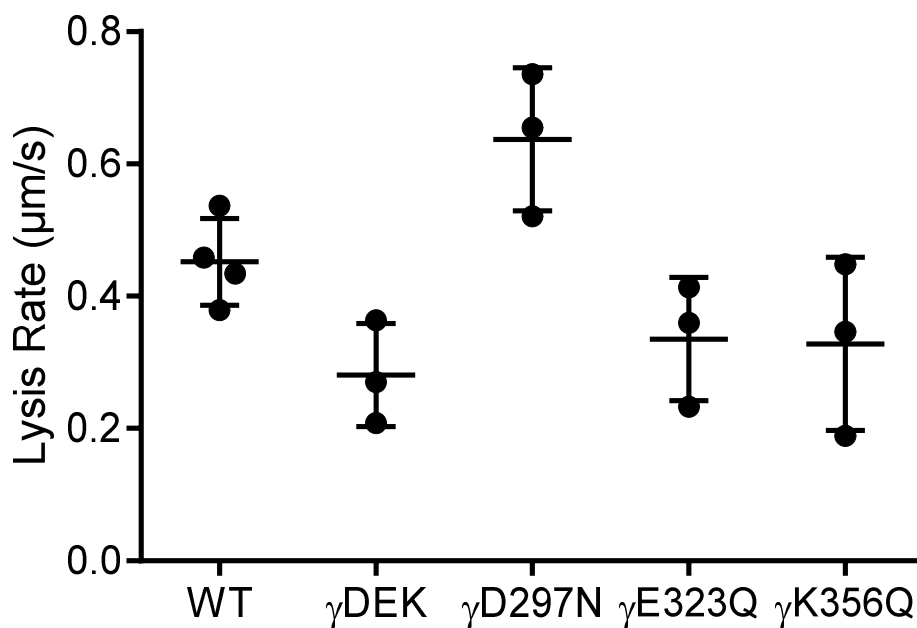


**Figure 5-5 Clot lysis (µm/s)** After one hour of clot formation clots were lysed and the rate of movement by the lytic front was measured using ImageJ analysis software, γDEK, γE323Q and γK356Q were all slower to lyse, whereas γD297N was faster to lyse.

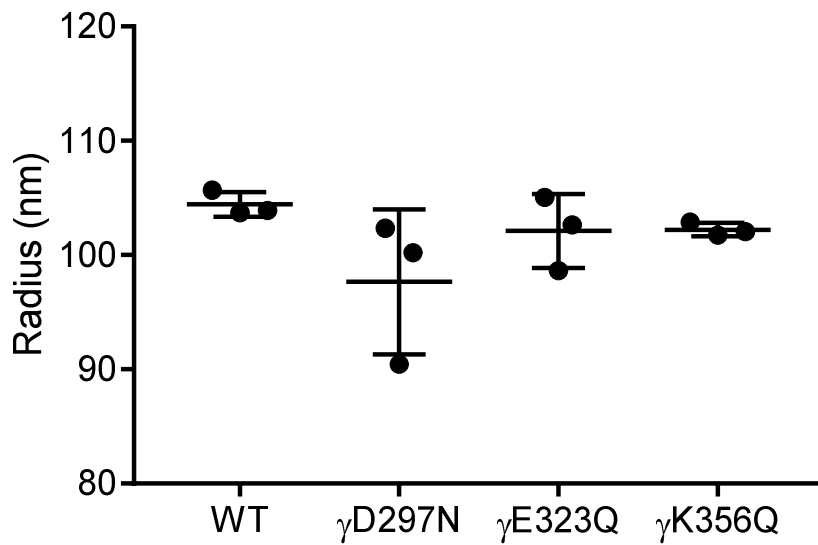


**Figure 5-6 Fiber radius in hydrated conditions.** Fiber radius was calculated by the proportion of light scattering by the variant fibrin networks. None of the clots were significantly different compared to WT.

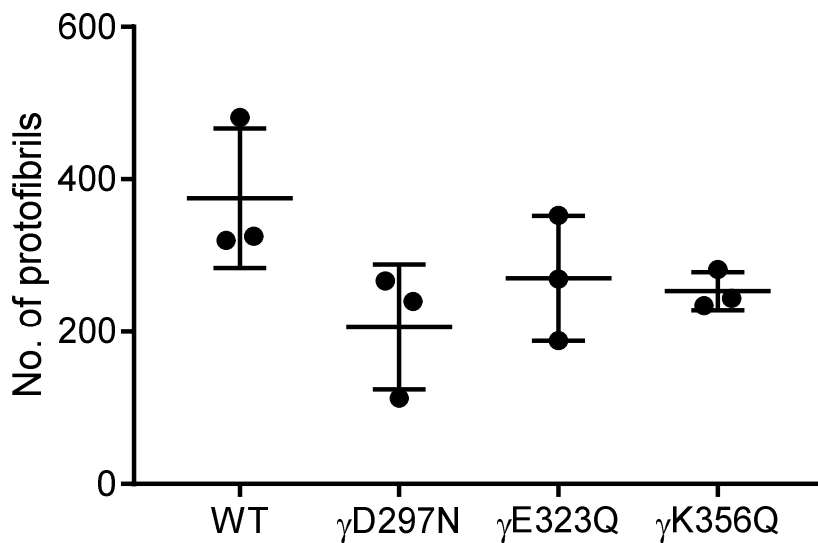


**Figure 5-7 Number of protofibrils in hydrated conditions** The proportion of light scattering for each variant was also used to calculate the total number of protofibrils contained within a fiber for each fibrin variant. None of the mutants were significantly different to the wild-type, however the average number of protofibrils per fiber appeared borderline reduced for the variants.

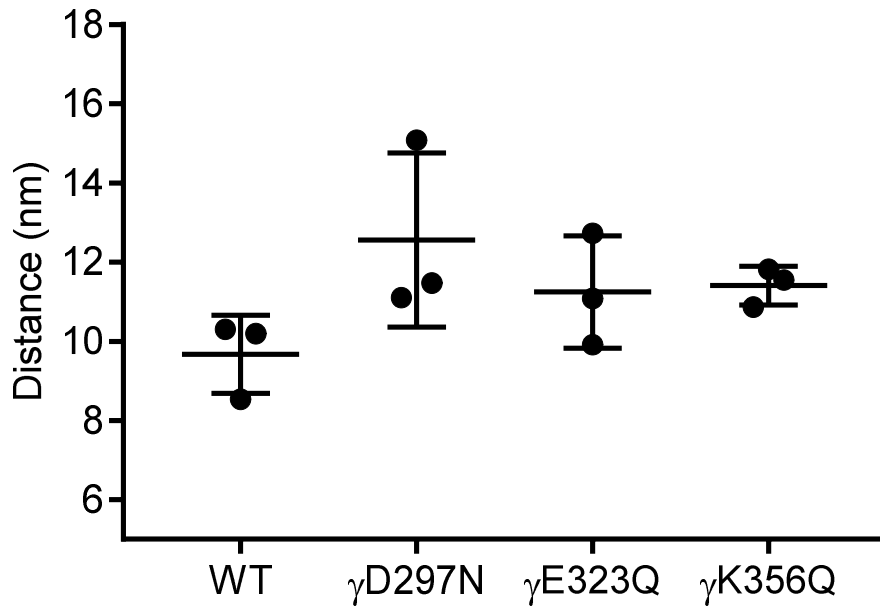


**Figure 5-8 Average distance between protofibrils** A non-significant increase in the distance between protofibrils were observed for all variants which indicated fibers that were less densely packed.

## 5.4 Discussion

In this chapter, final clot structure in hydrated and dehydrated conditions, clot lysis and the intrafibrillar structure was studied using SEM, LSCM and light scattering methods.

Upon visual inspection of the SEM micrographs it is obvious that the recombinant variants give rise to an altered clot structure being denser and comprising of thinner fibers. It is probably worth noting that the triple mutant (γDEK) gives rise to the most different clot structure compared to WT followed by γE323Q then γD297N and γK356Q (which are similar to each other). The order of which the variants that are most different to the WT are in agreement with the turbidity profiles as discussed in the previous chapter. This data supports the notion that the disruption of electrostatic extended D-E interactions is a combination effect

with  $\gamma$ E323Q being more potent than  $\gamma$ D297N and  $\gamma$ K356Q but when all mutations are combined in  $\gamma$ DEK they have a more profound and significant effect.

Hydrated conditions using LSCM however do not match this pattern so clearly.  $\gamma$ DEK formed the densest clots followed by single variant  $\gamma$ E323Q agreeing with the SEM data, but  $\gamma$ K356Q was less dense than the WT, albeit by a small margin, whilst  $\gamma$ D297N appears to be the same as the WT. The main difference between these two sets of data is the environment in which the fibrin fibers form, in scanning electron microscopy clots are formed, washed, fixed, dehydrated and critically dried all before imaging is performed, whereas in confocal microscopy clots are allowed to form and imaged 1 hour after formation without any additional sample preparation required. One could argue that the dehydration process in scanning electron microscopy may influence the final results, especially fiber thickness, making confocal microscopy the more reliable data set. However one must also be mindful of the interpretation of the confocal data because it is not known for certain that all the variants will behave in a similar manner when bound with Alexa Fluor label. On the other hand, experiments performed in the Ariëns laboratory (unpublished) have shown that there is no difference for polymerisation kinetics by turbidity when comparing WT with bound label and WT without label. Regardless, when both experimental methods are taken into consideration, the triple mutant clearly displayed a different phenotype and was the densest overall, with the single mutants density range in-between  $\gamma$ DEK and WT. These changes in clot structure further supports the hypothesis that extended D-E knob-hole interactions play a role in thrombus formation. What is causing this striking difference in the clot structure? Two factors could play such a role, the

longitudinal kinetics of oligomer formation through knob-hole interactions, and aggregation and branching. The previous chapter demonstrates that in the early stages of protofibril formation there is a delay in polymerisation at earlier timepoints (10minutes), but the variants at later timepoints (30 minutes) appear to 'catch up' and no difference in the length of protofibrils between WT and variants is observed, therefore lateral aggregation and branching in these variants could be altered. As can be seen from both the SEM (Figure 5-1) and confocal micrographs (Figure 5-3), variant clots typically have many more branch points (where protofibrils that form fibrin fibers diverge from each other, Figure 5-9).

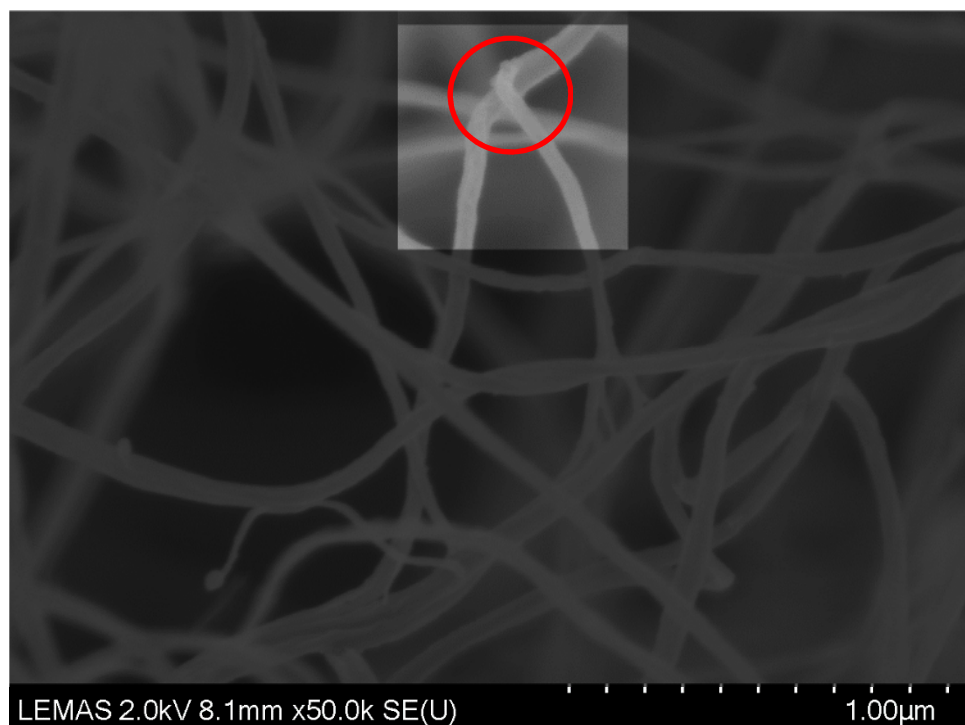


**Figure 5-9 Scanning electron micrograph of WT fibrin at x50000 magnification** Box highlighted in grey shows fibrin fiber branching. The red circle shows the intersection where the branching takes place.

Therefore there might be some influence on the formation of branch points in the fibrin variants, as kinetics that favour lateral aggregation form clots that have

thicker fibers with fewer branch points, while kinetics that are less favourable to lateral aggregation give rise to clots that have thinner fibers with many branch points (Weisel and Litvinov, 2017). This hypothesis is supported by the finding that the variants have significantly thinner fibers compared to the WT.

Fibrin clots are degraded by the fibrinolytic system after they have performed their function. In brief, plasminogen is converted to plasmin by either urokinase-type plasminogen (uPA) activator or tissue-type plasminogen activator (tPA), the plasmin then cuts the fibrin network into degradation products (Longstaff and Kolev, 2015).

Clot lysis is a very important function in haemostasis as increased lysis can cause increased bleeding (Szczepaniak *et al.*, 2015) Clot structure can have a large impact on the rate of lysis as shown by Collett *et al.*, who demonstrated that fibrinogen Dusart (a congenital dysfibrinogenemia), associated with abnormal polymerisation and thrombotic embolism, had a tight clot network configuration and slower lysis rates (Collet *et al.*, 1993). Additionally Carr and Alving directly studied the effect of fibrin structure on lysis and found lysis was faster for clots composed of thicker fibers (Carr and Alving, 1995). These two pieces of work show similar results to my studies where dense fibrin networks take a longer amount of time to lyse.

Clot lysis (Figure 5-5) was investigated using a LSCM to visualise the progress of a lysis front over time, tPA in combination with plasminogen were added to a fully formed clot network. None of the single mutants were significantly different to the WT, however most of the recombinant variants were slower to lyse than the WT, which is to be expected because they all have a denser network.

Surprisingly,  $\gamma$ D297N variant is actually faster to lyse than the WT, this is somewhat unexpected because  $\gamma$ D297N has a similar clot density to the WT and therefore one would expect lysis rates to be also similar.

In a recent article (Bannish *et al.*, 2017), the author highlighted that the fibrin fibers are approximated only 20% protein and the rest contains water, meaning there is space for small molecules such as tPA to diffuse within the fibers themselves. Perhaps  $\gamma$ D297N clots contains fibers that are less densely packed which leads to unexpectedly quicker lysis. Perhaps more repeats for this data would help come to a clearer conclusion as the current data only stands at  $n=3$ .

Protofibril packing analysis was then conducted to study the intrafibrillar structure of fibrin fibers. Recently, others have already investigated the role of thrombin concentration and the concentration of  $\gamma'$  variant on protofibril packing (Domingues *et al.*, 2016). In this thesis, the effects of extended knob-hole interactions on protofibril packing were investigated. In contrast with previous scanning electron microscopy data described above the fiber radii for the variants were not different. However, there was a large but not significant decrease in protofibril number. This is interesting because if the radii remains unchanged between the WT and the variants but there is a large decrease in protofibril number the packing must be different. The average distance between protofibrils was increased by 2-3nm. It was hypothesised earlier that perhaps this increased distance between protofibrils would account for why  $\gamma$ D297N would be quicker to lyse, however this explanation is not entirely consistent with the data because both  $\gamma$ E323Q and  $\gamma$ K356Q have increased distances between protofibrils yet their lysis times were slower.

To summarise,  $\gamma$ DEK variant produces the most dense clots as observed by SEM and LSCM, with two out of three single mutant variants being denser and the final single variant being similar to the wild type, suggesting that to observe differences in clot structure all extended D-E interactions need to be abolished. In the lysis experiments, most variants were overall slower to lyse as discussed earlier in this chapter, which is to be expected as they have denser structures, however variant  $\gamma$ D297N was faster to lyse. Fiber thickness was significantly reduced for all variants and light scattering studies showed that these fibers were reduced in packing density showing that the abolition of the extended D-E interactions translates to a difference in fiber thickness and clot structure.

# **Chapter 6 - The role of extended D-E knob hole interactions in clot mechanics**

## 6.1 Introduction

In the body, thrombi can be exposed to a range of tensile forces (150-400pN) as predicted by molecular simulations of shear conditions in the blood (Kononova *et al.*, 2013). Fibrin provides the mechanical strength for the thrombi by forming an interconnecting network of fibrin fibers (Collet *et al.*, 2005a). Because of this central role in thrombi formation and prevention of bleeding, fibrin clot mechanics have been extensively studied by others for many years (Ma *et al.*, 2017; Ryan *et al.*, 1999b; Ferry and Morrison, 1944). The multiscale mechanics of fibrin fibers have now been predicted by the Ariëns laboratory and others (Allan.P, 2012; Brown *et al.*, 2009) identifying key strain related deformation events in fibrin. A study has investigated the microstructural arrangement and clot mechanics through the use of fractal dimensions in conjunction with other diseases such as lung cancer (Davies *et al.*, 2015). Single fiber mechanics have been studied to elucidate the molecular mechanism(s) of fibrin fiber extension (Guthold *et al.*, 2007). These authors suggest that an adjustment in the alignment of the fibrin monomers can bear the load of small strains, whilst at medium strains the  $\alpha$ -helical coiled coils become unravelled acting as springs and at high strains a deformation of the  $\gamma$ C domains is thought to occur. Clinically, an indication of clot mechanics can be made by thromboelastometry. Here a rotating pin (connected to an optical detector system) is inserted into a cup of blood and continuously rotated, when the blood is clotting the rotational torque of the pin is slowed and this can indicate the 'clot firmness' (Zaky, 2017). The output parameters such as clot firmness that are generated in thromboelastometry (Kelly *et al.*, 2018) are not directly comparable to studies investigating visco-elastic properties of fibrin clots at the nanoscale where frequency dependent moduli  $G'$  and  $G''$  (Ma *et al.*,

2017; Duval *et al.*, 2014) are calculated, increasing the difficulty of associating *in vitro* and *ex vivo* work (Weisel, 2004b).

Chapter 5 demonstrated that the variants inhibiting extended D-E interactions significantly changed the clot structure, suggesting that it is possible that the extended interactions will also influence mechanical properties.

The methodology in this thesis was based on work conducted previously in the Ariëns laboratory. Here, a piece of micro-rheology apparatus (named 'magnetic tweezers') was created by Robert Harrand and optimised for the study of the mechanical properties of fibrin clots by Peter Allan, University of Leeds. Using this apparatus, non-crosslinked fibrinogen purified from plasma fibrinogen  $\gamma A/\gamma'$  splice variant fibrinogen was approximately 2.7 times less stiff than homozygous  $\gamma A/\gamma A$  fibrin (Allan *et al.*, 2012). A key difference with this new, novel method is that visco-elastic properties could be determined using active particle tracking and mathematical transformation (Evans *et al.*, 2009). Two moduli can be 'extracted', the storage modulus ( $G'$ ) which is the amount of energy that is stored in a system (also known as clot stiffness) and the loss modulus ( $G''$ ) which is the amount of energy that is lost from the system (also known as clot viscosity) (Mason and Weitz, 1995). However fibrin clots are not only purely elastic nor purely viscous, therefore the tan delta (a ratio of  $G''/G'$ ) will be calculated to give the overall visco-elastic properties of the fibrin clots.

## **6.2 Methods**

### **6.2.1 Clot preparation**

Fibrin clots were prepared with 0.5mg/mL fibrinogen, 5mM CaCl<sub>2</sub>, 1:250 (v:v) paramagnetic beads and 0.1U/mL Thrombin (final concentration) in an Eppendorf tube. Immediately following clot initiation, the clotting mixture and drawn up in a capillary tube by capillary action, the ends of the tube were sealed with Vaseline to prevent dehydration and the clots were rotated very slowly by hand for 10 minutes to prevent the sedimentation of paramagnetic beads on the capillary wall. The clots were then stored in a humidity chamber at room temperature overnight prior to force measurements the following day.

### **6.2.2 Micro-rheology**

The clots were placed on an in-house built micro-rheometer and the creep response was measured for a period of 10 minutes. A minimum of ten beads per clot were measured as described in 2.11. Time-dependant compliance was calculated from the time dependant displacement of the bead and a best fit of the data was plotted using Equation 2-6. The compliance was then converted into frequency dependent moduli using the mathematical procedure of Evans (Evans *et al.*, 2009) as described in 2.11. The storage modulus (G'), loss modulus (G'') was then used to compare the mechanical properties of the recombinant variants.

### **6.2.3 Statistics**

Data analysis were performed using GraphPad Prism statistical software package. A one-way ANOVA was used with multiple comparisons with the WT as a control column. Results are shown as mean  $\pm$  SD, and were considered significant when  $p < 0.05$

## 6.2.4 Results

The mechanical properties of the fibrin clots were measured by the entrapment of paramagnetic beads into the fibrin network, three parameters were ultimately measured, the  $G'$ ,  $G''$  and  $\tan\delta$  ( $G''/G'$ ). These parameters were measured from very short frequencies (0.004Hz) to long frequencies (25Hz). The  $G'$  and  $G''$  response from the entire frequency range can be observed in Figure 6-1 for  $\gamma$ DEK triple mutant, and in Figure 6-2 for the single fibrin variants. Three frequencies were selected (0.1Hz, 1Hz and 10Hz) to make comparisons and perform statistical analysis between the variants as these frequencies span a frequency range where key deformation events in fibrin networks occur. All comparisons below are to the WT control samples.

**Table 6-1 Storage modulus ( $G'$ ) of WT and  $\gamma$ DEK variant**

$G'$	Frequency	WT	$\gamma$ DEK
	0.1 Hz	0.44±0.01 Pa	0.38±0.10 Pa
1 Hz	0.71±0.05 Pa	1.01± 0.15 Pa *	
10 Hz	1.10±0.23 Pa	1.69±0.45 Pa	

**Table 6-2 Storage modulus ( $G'$ ) of WT and single variants**

$G'$	Frequency	WT	$\gamma$ D297N	$\gamma$ E323Q	$\gamma$ K356Q
	0.1 Hz	0.64±0.09 Pa	0.86 ±0.14 Pa	0.98 ±0.40 Pa	1.56 ±0.24 Pa **
1 Hz	0.98±0.07 Pa	1.68 ±0.34 Pa	1.71 ±0.61 Pa	2.23 ±0.50 Pa *	
10 Hz	3.0±0.69 Pa	3.57±0.12 Pa	4.05±0.50 Pa	5.42 ±0.83 Pa **	

As shown in Table 6-1 significant differences of storage modulus ( $G'$ ) were observed for  $\gamma$ DEK at 1Hz level in addition to significant differences across all frequencies for  $\gamma$ K356Q single variant as demonstrated in Table 6-2.

**Table 6-3 Loss modulus (G'') of WT and  $\gamma$ DEK variant**

G''	Frequency	WT	$\gamma$ DEK
	0.1 Hz	0.08±0.01 Pa	0.14 ±0.01 Pa **
1 Hz	0.27±0.09 Pa	0.57 ±0.14 Pa *	
10 Hz	0.13±0.09 Pa	0.17 ±0.09 Pa	

**Table 6-4 Loss modulus (G'') of WT and single variants**

G''	Frequency	WT	$\gamma$ D297N	$\gamma$ E323Q	$\gamma$ K356Q
	0.1 Hz	0.10±0.01 Pa	0.19±0.03 Pa	0.19±0.04 Pa	0.19±0.07 Pa
1 Hz	0.78±0.16 Pa	1.15 ±0.07 Pa	1.22 ±0.15 Pa	1.30±0.39 Pa	
10 Hz	0.78±0.28 Pa	0.52 ±0.15 Pa	0.68 ±0.23 Pa	1.38±0.51 Pa	

As shown in Table 6-3 significant differences were observed for  $\gamma$ DEK at 0.1 Hz and 1Hz, no significant differences were observed for the single mutant variants, Table 6-4.

As fibrin clots are neither solely elastic or solely viscous, but visco-elastic polymers, the  $\tan\delta$  parameter (ratio of G''/G') was calculated, Table 6-5 and Table 6-6. Although not statically significant, these  $\tan\delta$  values show that when the overall visco-elastic properties are considered there is only noticeable changes at 0.1Hz in  $\gamma$ DEK. Indicating that each residue appears to be contributing to an additive overall effect.

**Table 6-5 Overall deformability ( $\tan\delta$ ) of WT and  $\gamma$ DEK variant**

Tan $\delta$	Frequency	WT	$\gamma$ DEK
	0.1 Hz	0.19±0.04 Pa	0.40±0.11 Pa *
1 Hz	0.38±0.11 Pa	0.56±0.05 Pa	
10 Hz	0.11±0.06 Pa	0.10±0.04 Pa	

**Table 6-6 Overall deformability ( $\tan\delta$ ) of WT and single variants**

Tan $\delta$	Frequency	WT	$\gamma$ D297N	$\gamma$ E323Q	$\gamma$ K356Q
	0.1 Hz	0.16±0.04 Pa	0.22±0.01 Pa	0.21±0.07 Pa	0.12±0.03 Pa
1 Hz	0.81±0.21 Pa	0.70±0.09 Pa	0.75±0.16 Pa	0.58±0.09 Pa	
10 Hz	0.26±0.12 Pa	0.15±0.04 Pa	0.17±0.06 Pa	0.26±0.12 Pa	

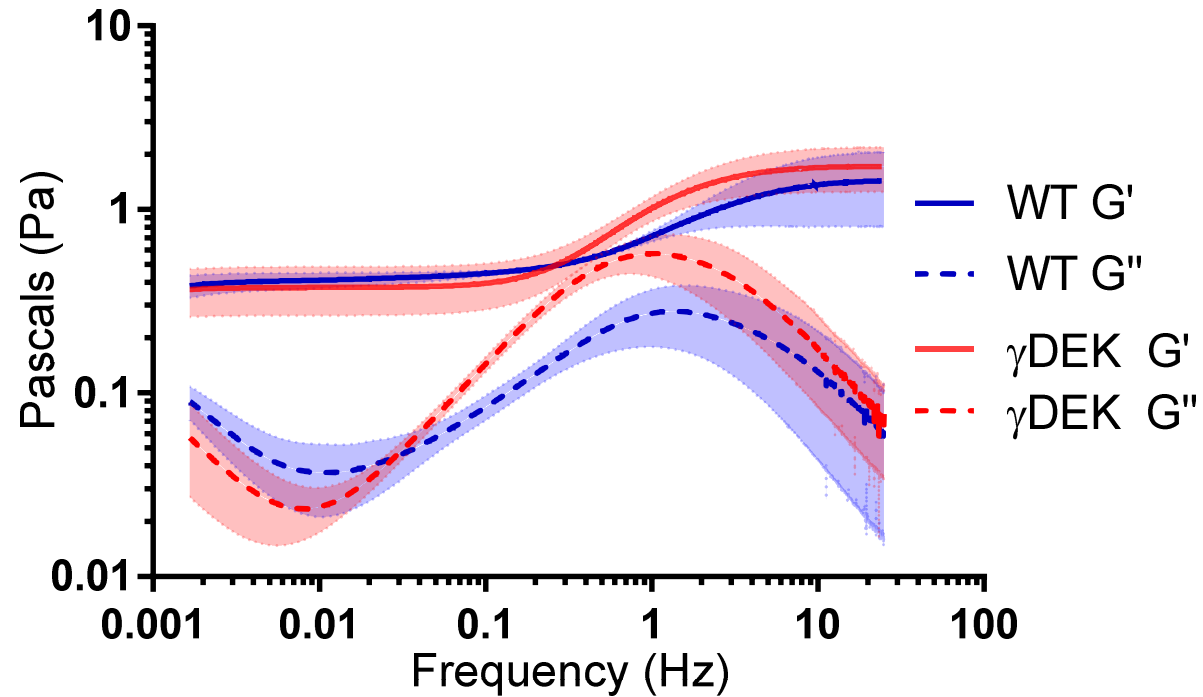


**Figure 6-1 Complete G' and G'' curves for WT and  $\gamma$ DEK** G' is represented by a solid line and G'' is represented by a dotted line. WT in blue and  $\gamma$ DEK in red, very short frequencies 0.01Hz-1Hz represent deformation events occurring at branch points and along fibrin fibers no change is observed for G' but a significant increase is found for G''. Frequencies at 1Hz represent deformation events at the fiber level such as twisting and stretching, and high frequencies an increase for  $\gamma$ DEK is seen here for both G' and G''. <10 Hz represents deformation events occurring at the molecular level there are no significant differences at this frequency for  $\gamma$ DEK.

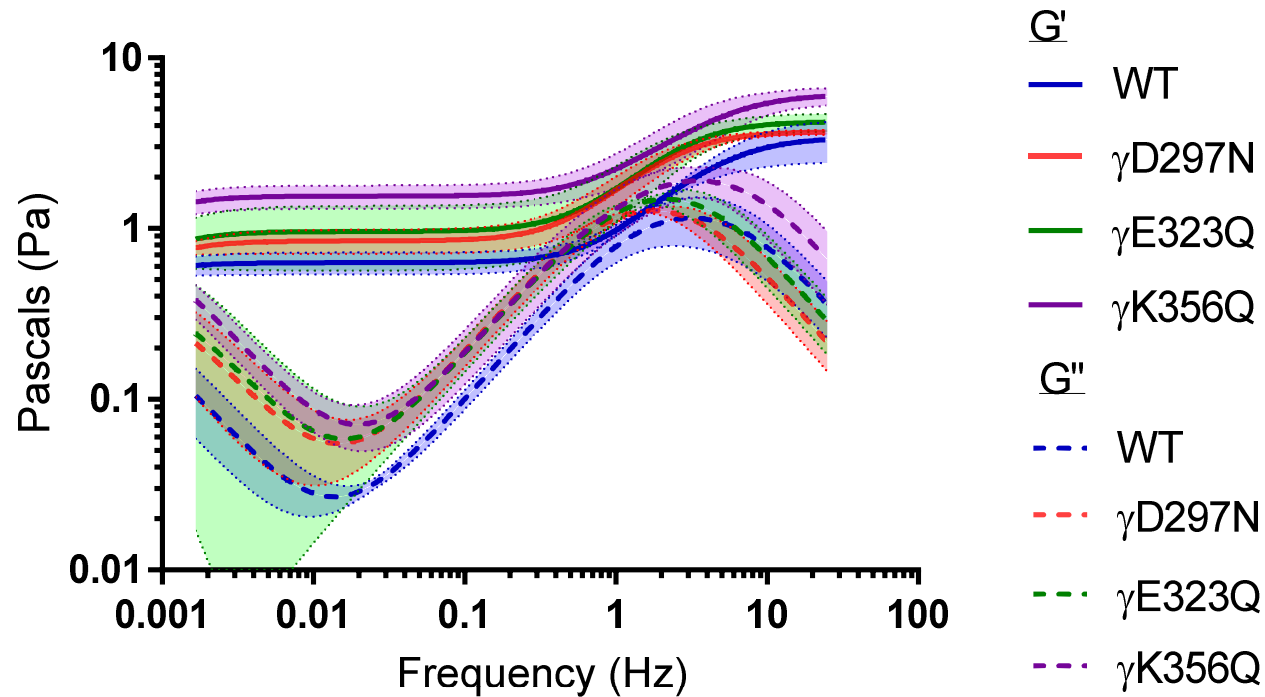


**Figure 6-2 Complete  $G'$  and  $G''$  curves for the single mutant variants WT ,  $\gamma$ D297N,  $\gamma$ E323Q and  $\gamma$ K356Q**  $G'$  is represented by a solid line and  $G''$  is represented by a dotted line. WT in blue and  $\gamma$ D297N in red,  $\gamma$ E323Q in green and  $\gamma$ K356Q in purple. Very short frequencies 0.01Hz-1Hz represent deformation events occurring at branch points and along fibrin fibers  $\gamma$ K356Q is significantly increased for  $G'$  but no change is observed for  $G''$ . Frequencies at 1Hz represent deformation events at the fiber level such as twisting and stretching  $\gamma$ K356Q is significantly increased for  $G'$  but no change is observed for  $G''$ . <10 Hz represents deformation events occurring at the molecular level  $\gamma$ K356Q is significantly increased for  $G'$  but no change is observed for  $G''$ .

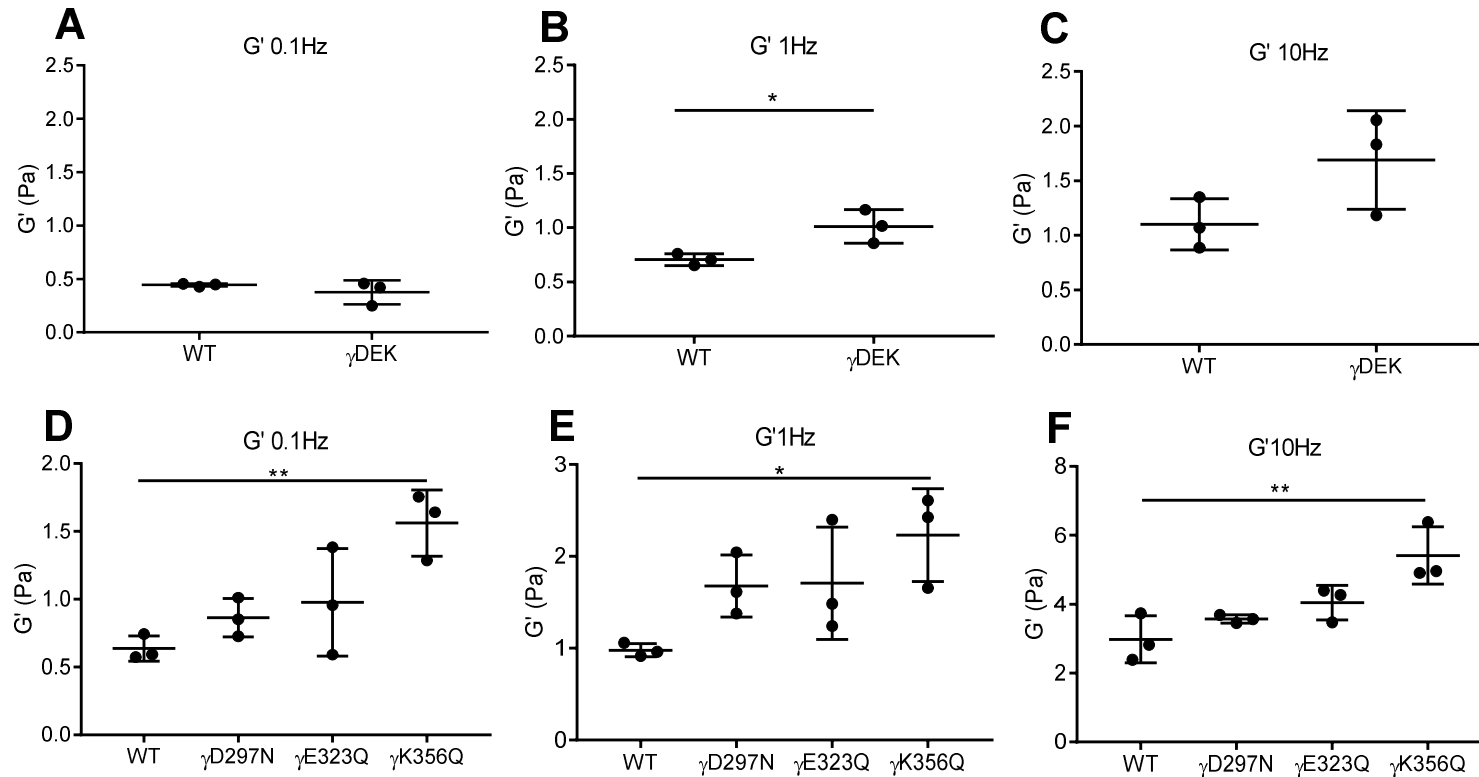


**Figure 6-3 The storage modulus (G')** for all fibrin variants. For  $\gamma$ DEK, there was no difference in G' at 0.1Hz (A), there was a significant increase in G' at 1Hz (B) and a non-significant increase of G' at 10Hz (C) when compared to WT. For the single fibrin variants there was a trend of an increased G' at 0.1Hz (D) that was significantly different for  $\gamma$ K356Q,  $p < 0.05$ . Measurements conducted at 1Hz (E) also showed an increase of G' for all single variants with a significant difference for  $\gamma$ K356Q  $p < 0.05$ . Single mutant variants were also increased at 10Hz (F), significantly for  $\gamma$ K356Q.

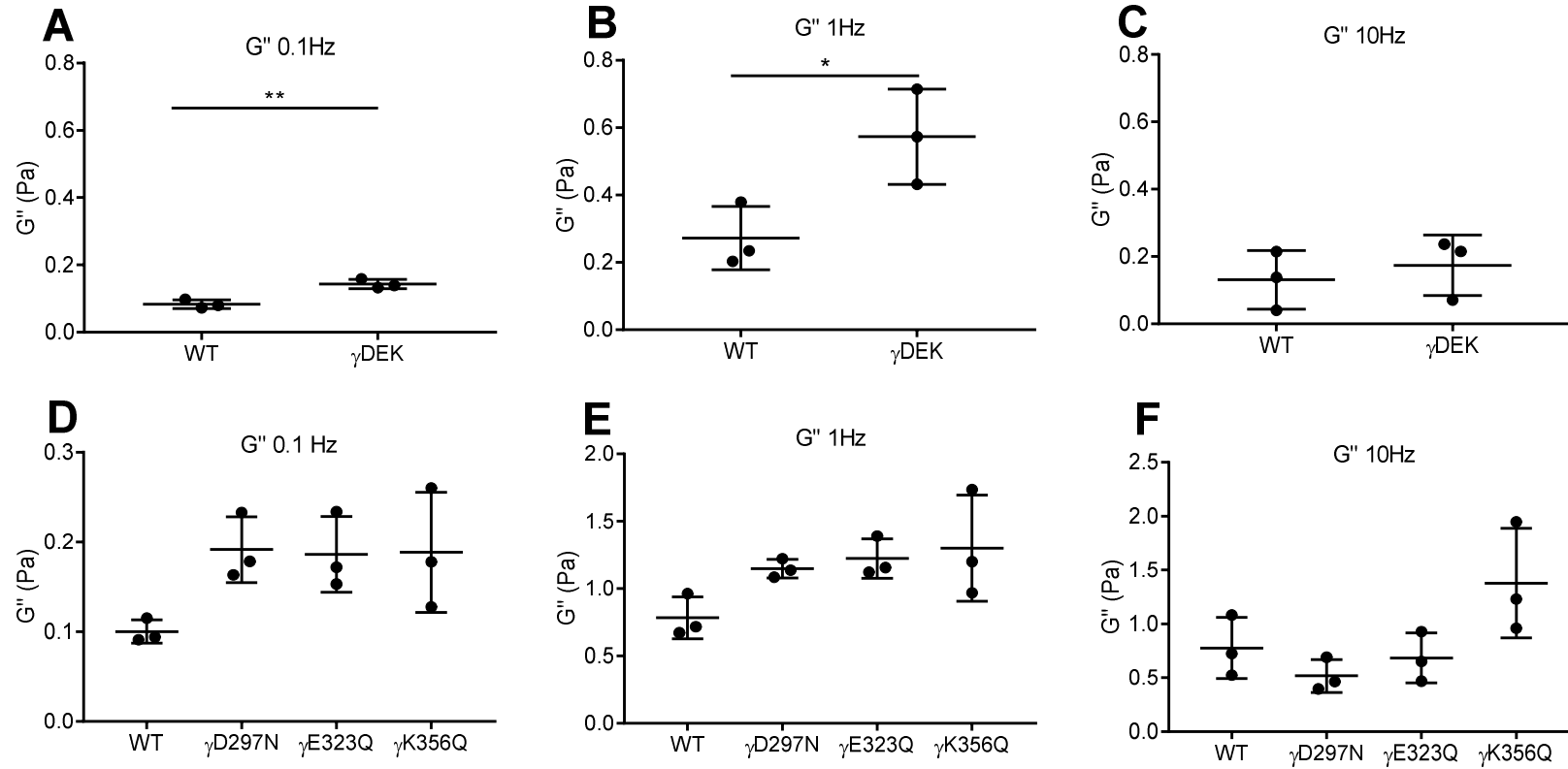


**Figure 6-4 The loss modulus ( $G''$ ) for all fibrin variants** For  $\gamma$ DEK  $G''$  was increased across all frequencies (A-C) but only significantly at 0.1Hz and 1Hz,  $p < 0.05$ . At 0.1Hz (D) and 1Hz (E) all single mutants had a non-significant increase in  $G''$ , however at 10Hz (F)  $\gamma$ D297N and  $\gamma$ E323Q had a non-significant reduction in  $G''$  whereas  $\gamma$ K356Q had a non-significant increase in  $G''$ .

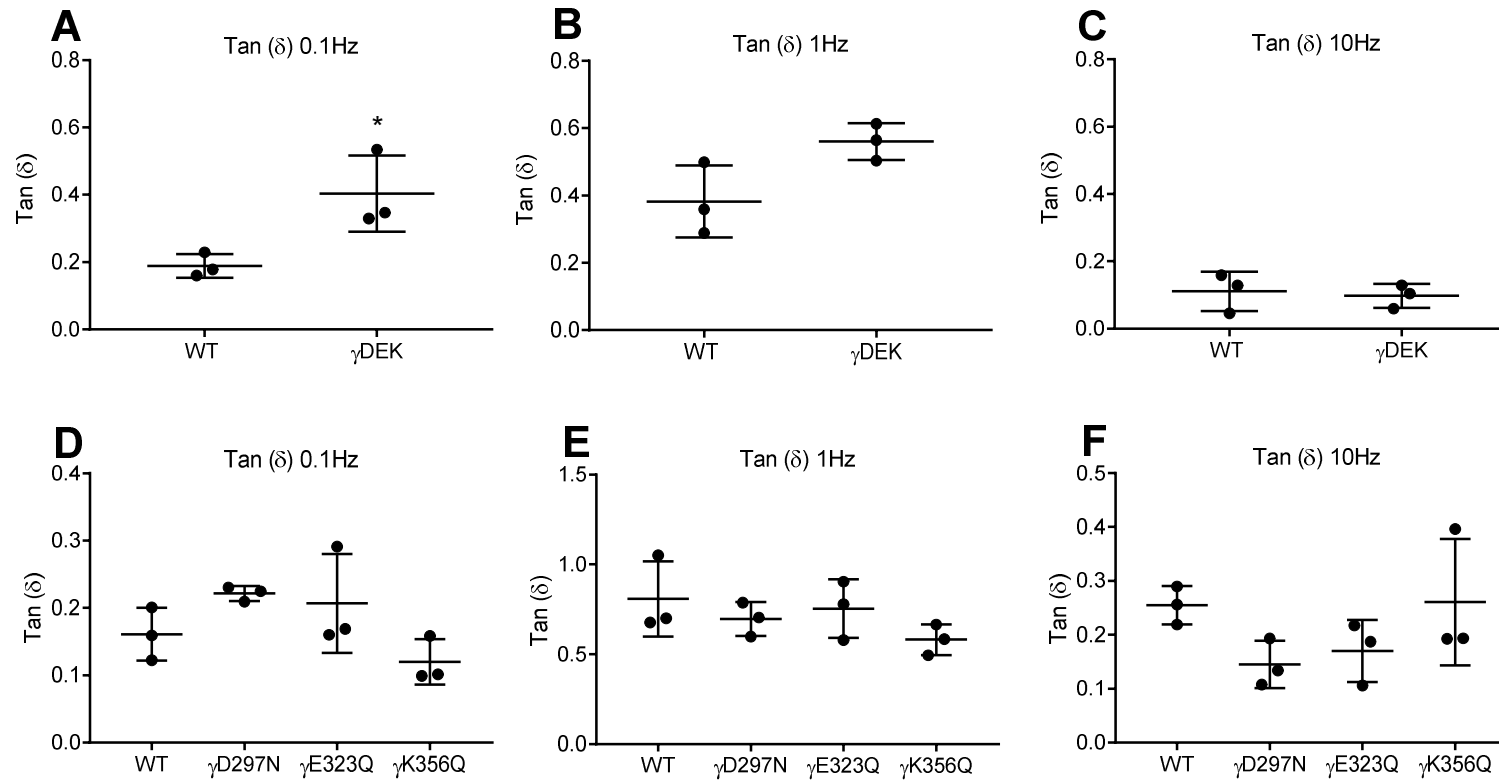


**Figure 6-5 The visco-elastic ratio of  $G''/G'$  ( $\tan\delta$ ).** For  $\gamma$ DEK, at 0.1Hz and 10Hz there was a non-significant increase in the  $\tan\delta$ , however at 10Hz no change was observed. For the single variants, at 0.1Hz there was an insignificant increase for  $\gamma$ D297N and  $\gamma$ E323Q whereas there was a non-significant decrease for  $\gamma$ K356Q. At 1Hz there was a slight reduction in  $\tan\delta$  for  $\gamma$ D297N and  $\gamma$ E323Q followed by a greater decrease in  $\tan\delta$  by  $\gamma$ K356Q. At 10Hz both  $\gamma$ D297N and  $\gamma$ E323Q were non significantly reduced whereas  $\gamma$ K356Q was similar to the WT.

### 6.3 Discussion

In this chapter, the effects of the extended D-E interactions on clot mechanics were investigated using an in-house magnetic tweezers apparatus. Due to material limitations at the time, two sets of experiments have been conducted, the first set is a comparison of the triple mutant variant  $\gamma$ DEK to the WT. A second set of experiments comparing mechanics between single fibrin variants and the WT was performed later within the project. The same batch of WT was used to perform the experiments for both data sets, however the magnetic rheology equipment was calibrated before both data sets were collected. The frequencies selected (0.1Hz, 1Hz and 10Hz) are representative of deformation events happening within the clot, 0.1Hz observes deformation at whole clot scale where large scale motions of the fibers and branches align, fibers bending and twisting occur at 1Hz, whilst at 10Hz molecular deformation events occur such as stretching of the molecular domains. This was shown by the Ariëns group (Allan.P, 2012) based on a previous model of rheology of semi flexible fibers (Morse, 1998b).

When WT is compared to  $\gamma$ DEK one can see an increase in  $G'$  for  $\gamma$ DEK at 1Hz (significant) and 10Hz (insignificant). This is unexpected as one would think that the  $\gamma$ DEK fibrinogen would lead to clots that are less stiff and more deformable due to weaker electrostatic interactions and less stable A:a knob-hole bonds. However as demonstrated in the Ariëns laboratory (Allan.P, 2012) the deformation events that occur at these intermediate and short frequencies are in the order of fibrin fibers, therefore it is possible that due to the nature of the  $\gamma$ DEK's denser clot network the fibers are less able to rotate and the clot is more

stiff overall. This hypothesis does agree with the literature as clots that are denser have previously reported to be more stiff, (Ryan *et al.*, 1999b; Weisel, 2004a). It is difficult to postulate why this difference is not seen at 0.1Hz but it could be that 0.1Hz is at the early stages of this unfolding event therefore not all of the deformation from the pulling experiments has taken place. This hypothesis also fits for the single fibrin variants as they are different density to the WT but also have significantly thinner fibers. Interestingly  $\gamma$ K356Q is the least dense mutant however, it is the most significantly different for G' compared to the WT. Perhaps this residue is more influential on packing arrangements within the fiber. Furthermore, when introduced to the triple mutant this residue may contribute to an increase in clot stiffness more than  $\gamma$ D297N and  $\gamma$ E323Q.

As for the loss modulus (G'') the  $\gamma$ DEK triple mutant is significantly increased at 0.1Hz and 1Hz suggesting that more deformation is occurring. The single mutant variants have an increased (G'') at these frequencies however they are not significantly different to the WT. This suggests that the abolition of just one electrostatic bond introduced by the single variants is not enough to cause a significant change in the loss modulus, but all three amino acid changes are required for there to be an effect. At 10Hz there is a small increase in G'' between the WT and  $\gamma$ DEK which is also reflected in the single variant experiments, as there is a small decrease for  $\gamma$ D297N and  $\gamma$ E323Q and a non-significant increase with  $\gamma$ K356Q, so there is no change overall. The higher deformation observed for the variants at 0.1Hz and 1Hz could be attributed to thinner fibers that are less densely packed. Chapter 5 demonstrates that all variant clots are made of significantly thinner fibers, that have an approximate 30-50% reduction

in the number of protofibrils. This would indicate that when pulled there are fewer protofibrils to bear the stress applied.

$\tan\delta$ , a ratio of  $G''/G'$ , was calculated as fibrin clots do not have the mechanical properties of purely elastic or purely viscous materials, fibrin clots are visco-elastic. When a material has a  $\tan\delta = 1$  the elastic and viscous components are acting by the same magnitude, when the  $\tan\delta$  is  $<1$  then the elastic component is dominating and when  $\tan\delta >1$  the viscous component is dominating. The experiments in this thesis observed that all of the  $\tan\delta$  values are  $<1$ , which is to be expected because pulling was conducted at 40pN. Pulling at 40pN allows multiple beads to be measured without permanent deformation of the clot. At 0.1Hz  $\gamma$ DEK had a large 2 fold (although not significant) increase compared to WT in the  $\tan\delta$ , however there were only small changes for the single mutant variants, suggesting again that all three single mutations are required for an effect. A similar observation was also made for 1Hz as there was a moderate increase in  $\tan\delta$  for  $\gamma$ DEK but when comparing the single fibrin variants there was little change. At 10Hz there is no significant change for any of the variants albeit there is a decrease in  $\tan\delta$  for  $\gamma$ D297N and  $\gamma$ E323Q suggesting that there is less deformation for these two variants. The data is very difficult to interpret within this range because, at frequencies of 10-25Hz limitations of the micro-rheometer are being reached, more specifically the CCD camera. A replacement of the current camera with one that could measure higher rates up to 100Hz would give more insight to if/and how many deformation events are occurring in fibrin networks at the molecular domain level.

The technique utilises an in-house micro-rheometer and therefore there is currently very little data for a comparison to be made to other studies, however

there have been two publications from the Ariëns group. It was demonstrated that protofibril packing had an effect on clot mechanics (Domingues *et al.*, 2016). Here the authors observed that plasma depleted affinity purified fibrin clots increased in decreased in rigidity when made with higher thrombin concentrations at 1Hz (only this frequency was measured using the micro-rheology device by the authors). A non-significant decrease in protofibril number did not have an effect on the overall visco-elastic properties of the clot. Unfortunately due to limitations in material,  $\gamma$ DEK was not measured for protofibril packing therefore I can only postulate that  $\gamma$ DEK would have even fewer protofibrils than the single variants which gives rise to the increase in  $\tan\delta$ .

Another work (Duval *et al.*, 2014) showed that the microrheological properties of fibrin is regulated by fibrin  $\alpha$ -chain crosslinking. The values for WT(-FXIII)  $G'$ ,  $G''$  and  $\tan\delta$  are in the same order of magnitude between the studies showing that the method is somewhat consistent.

To summarise, the clot stiffness ( $G'$ ) is increased for all variants for the majority of frequencies, the increase in  $G'$  is due to the increase in clot density that is observed in the previous chapter. The clot viscosity ( $G''$ ) is increased at 0.1Hz and 1Hz but not at 10Hz, this signifies that more deformation events are occurring at the fiber level and is attributed this to a decrease in protofibril number which leads to thinner fibers as described in the previous chapter. When both  $G'$  and  $G''$  are taken into consideration in the form of  $\tan\delta$ , there is no significant difference in the micro-rheological properties of the fibrin clots.

# **Chapter 7 - Discussion**

## 7.1 Summary of data

The work presented in this thesis has used a wide range of biochemical and biophysical experimental methods to study fibrin polymerisation, clot structure and clot mechanics. A large proportion of this work focused on the successful expression and purification of recombinant human fibrinogen with chosen mutation(s) in the  $\gamma$ -chain,  $\gamma$ DEK,  $\gamma$ D297N,  $\gamma$ E323Q and  $\gamma$ K356Q. These fibrinogen variants were studied using turbidity for polymerisation kinetic analysis. Confocal microscopy and scanning electron microscopy were used to probe the structure of the fibrin clots, and a light scattering method was used to investigate internal fiber structure. Atomic force microscopy was used to study early polymerisation methods and clot mechanics were investigated using an in-house micro-rheology device.

CHO cells were used to successfully produce recombinant proteins. Following purification by affinity chromatography, SDS-PAGE analysis showed no signs of degradation of the three fibrinogen chains ( $A\alpha\beta\gamma$ ) with no unexpected contaminating bands. When investigating the local confirmation in the far-UV range using CD spectroscopy small differences between the variants and the WT were observed.

Early polymerisation kinetics by AFM showed that at the earliest time point measured (10minutes) all variants except  $\gamma$ K356Q had shorter protofibrils indicating that the alteration of the extended D-E interactions hinders the polymerisation process. While indeed protofibrils were shorter after 10 minutes for the  $\gamma$ D297N,  $\gamma$ E323Q and  $\gamma$ DEK variants, no difference in protofibril length distribution was seen at the 20 and 30 minute time points between the variants and the WT, suggesting that the rate of longitudinal growth 'catches up' with the

WT. Turbidity was used to measure progressively later stages of polymerisation (lateral aggregation of the protofibrils). A significant reduction in  $V_{max}$  for the variants along with a large reduction in maximum OD was observed. The maximum OD was the most different for  $\gamma$ DEK followed by the single point mutation variants. Overall, it therefore appears that the extended D-E interactions have some effect during the initiation of longitudinal protofibril growth at the early stages of polymerisation. Shorter protofibrils at 10 minute timepoints in AFM studies were observed for the majority of variants, and an effect of the mutations resulting in an extended lag phase as seen in turbidity for  $\gamma$ DEK. The disruption in longitudinal growth later impacts on lateral fiber growth as can be seen from the reduction in  $V_{max}$  and  $MaxOD$  in the turbidity assay, which is an indication of altered fiber thickness.

This large reduction in the ability to laterally aggregate effectively as shown by the  $Max\ OD$  results indicated that the overall clot structures could be different. To investigate this further, clot micrographs using both laser scanning confocal microscopy (LSCM) and scanning electron microscopy (SEM) were produced. Visual inspection of SEM micrographs and quantitative analysis of confocal micrographs showed that the  $\gamma$ DEK clot is significantly denser and the single mutants were more dense than WT, but not to the same extent as  $\gamma$ DEK, this confirmed the pattern seen in maximum optical density results. In confocal lysis experiments all variants were slower to lyse compared to WT, with the exception of  $\gamma$ D297N.

Next, it was investigated whether the abnormal structures had an impact on clot mechanics, as the structures were denser and the fibers were thinner, as seen by SEM, and therefore it remained to be seen whether these clots would behave

in a more elastic or a more viscous behaviour. The results from the micro-rheometer studies showed that there were increases in storage modulus for  $\gamma$ DEK at the fiber level.  $\gamma$ K356Q was the only single variant with an increase in storage modulus (all frequencies), perhaps suggesting that the interaction mediated by  $\gamma$ K356Q is required during polymerisation somewhat more so in order to produce fibers of the correct elasticity. For the loss modulus,  $\gamma$ DEK was the only variant to significantly dissipate energy, both at the whole clot (0.1Hz) and fiber level (1Hz). This indicates that alterations of all three extended D-E residues are required for permanent deformation to take place. When taking both the elastic and viscous properties of the clot into consideration, the  $\tan\delta$  is increased for  $\gamma$ DEK at 0.1Hz and 1Hz but remains similar across all frequencies for the single mutants. This could be due to the reduction in D-E binding in  $\gamma$ DEK variant resulting in less stable knob-hole bonds resulting in protofibrils that are more easily deformable.

To conclude, the data summarised shows that the fibrinogen variants produced in this thesis lead to slower forming, denser clots that are harder to lyse (with the exception of  $\gamma$ D297N) and  $\gamma$ DEK is more readily deformable at lower frequencies.

## **7.2 Discussion**

The results as summarised in section 7.1 show that there were altered polymerisation kinetics, structures and clot mechanics, even for the single fibrin variants, this suggests that each of the extended D-E interactions has an effect and culminate into a larger effect in triple mutant  $\gamma$ DEK. Unfortunately due to time and material limitations I was unable to probe further to the sub-molecular

mechanistic reasoning as to why these variants have an effect on polymerisation, however residues and stretches of residues containing the mutations have previously been investigated in the literature.

### 7.2.1 $\gamma$ D297N

Fibrinogen has a total of four calcium binding sites, two of which are low affinity binding sites ( $\gamma$ 2 and  $\beta$ 2) and two of which are high affinity binding sites ( $\gamma$ 1 and  $\beta$ 1) (Marguerie *et al.*, 1977). The  $\gamma$ 1 and  $\gamma$ 2 sites are located on the  $\gamma$ -chain of fibrinogen, whereas sites  $\beta$ 1 and  $\beta$ 2 are located on the  $\beta$ -chain of the molecule.

It was previously unclear whether the  $\gamma$ 2 calcium binding site was present or not in fibrinogen solution or if it was a result of molecular packing interactions (Kostelansky *et al.*, 2004b; Kostelansky *et al.*, 2004a). Studies with  $\gamma$ D298A/D301A recombinant variant (which is adjacent to  $\gamma$ D297 residue of interest) was made to probe and confirm the presence of the  $\gamma$ 2 calcium binding site (Kostelansky *et al.*, 2007). It was observed that the binding site is located within a loop spanning residues  $\gamma$ 294-301. The authors found that polymerisation differed slightly with the D298A/D301A variant meaning that the  $\gamma$ 2 calcium binding site has a small role in fibrin polymerisation but attributed their observed differences to “subtle structural changes in the hole-a polymerisation site”. Their data and other work (Varadi and Scheraga, 1986) also indicated that it is the  $\gamma$ 1 site (331-336) which has greater affinity for calcium, and therefore a more crucial for A:a knob-hole interactions. Due to its’ proximity, the  $\gamma$ D297N mutant could affect the  $\gamma$ 2 calcium binding site and therefore it would be difficult to interpret whether the observed effects would be because of altered calcium binding or the abolishment of D-E interactions. However, considering that the study discussed above mutated the  $\gamma$ 2 calcium binding site and observed a small change in

polymerisation, I cannot rule out that the altered polymerisation profile, clot structure and thinner fibers for  $\gamma$ D297N that are observed are due to the abolition of the extended D-E electrostatic interactions, and not from a potentially affected calcium binding site. Unfortunately, there was not enough material available to perform experiments with and without calcium ions for this variant.

Interestingly very recent advances in molecular dynamic simulations and optical trap methodologies have implicated residue  $\gamma$ D297 in catch-slip bond regulation in fibrin(ogen) (Litvinov *et al.*, 2018). Catch-slip bonds are bonds that strengthen under acute tension (catch) but then dissociate at higher forces (slip). Catch-slip bonds have also been discovered in other biological systems, for example between the adhesion molecules P-Selectin and PSLG-1 in rolling cells such as leukocytes (McEver and Zhu, 2010; Marshall *et al.*, 2003).

In this publication the authors have used optical trap microscopy in combination with molecular dynamic simulations to investigate the rupture forces of knob-hole bonds. A:a bonds are non-covalent and can rupture by force pulling experiments. In brief, beads functionalised with either fibrinogen or fragment D (contains holes-a) were flowed into a compartment where 'pedestals' were functionalised with fibrin. The beads are trapped using a laser and the immobilised single molecules on the pedestal are put into proximity with the beads and the two fibrin fragments interact. Pulling experiments are then performed by increasing the distance of the pedestal from the bead. In their pulling experiments the authors discovered that the knob-hole bonds behave differently to most non covalent bonds, they noticed that initially the average bond lifetime increases with force, then decreases with force displaying a catch-slip mechanism. They further investigate this interesting finding using molecular dynamic simulations of the  $\gamma$

nodule of human fibrin(ogen). In their model they postulate that a moveable flap containing residues  $\gamma$ 295 to  $\gamma$ 305 regulates the  $\gamma$ 2 calcium binding site, when calcium is bound,  $\gamma$ D297 along with  $\gamma$ D301 undergo spatial reorientation and interact with the calcium ion therefore hindering catch-slip bonds, when calcium is unbound they are able to interact with knob A and mediate the catch-slip bond mechanism.

### 7.2.2 E323Q

For the  $\gamma$ E323Q variant, one study (Pratt *et al.*, 1997), in addition to the molecular simulations previously mentioned (Kononova *et al.*, 2013) did elucidate a potential role for  $\gamma$ E323 in polymerisation. They show through the use of crystal structures that several amino acid residues in the hole-a polymerisation pocket re-adjust to accommodate the binding of the GPRP peptide, resulting in the rearrangement of hydrogen bonds and salt links that stabilise the A:a interactions. They predicted that  $\gamma$ K338 and  $\gamma$ E323 form a salt link when GPRP is unbound. When bound there is a slight shift resulting in the interaction of K338 with the peptide.  $\gamma$ E323Q could have a local effect by the disruption of extended D-E electrostatic interactions and therefore could lead to changes to other residues that interact directly with knob-A leading to the delayed polymerisation, thinner fibrin fibers, and denser clot network observed in the results. Interestingly studies have shown that the  $\gamma$ 1 calcium binding site consists of residues  $\gamma$ 311-336 (Varadi and Scheraga, 1986; Dang *et al.*, 1985; Yee *et al.*, 1997), which is immediately next to the A:a binding pocket, residues  $\gamma$ 337-379 (Shimizu *et al.*, 1992). This suggests that the stretch of residues encompassing both this calcium binding site and the polymerisation site are extremely important, which is supported in the literature where three residues (318-320) are deleted leading to

delayed polymerisation and reduced calcium binding (Koopman *et al.*, 1991). The  $\gamma$ E323Q mutant could additionally play a role in the binding and unbinding of the  $\gamma$ 2 binding site but more work would need to be performed to confirm this.

### **7.2.3 K356Q**

As observed in the literature, the variant K356Q has also been implicated in packing interactions. It was originally thought that cleavage of FpA and formation of A:a interactions drive the longitudinal protofibril formation, whereas FpB is responsible for lateral aggregation, and ultimately packing of the fibrin fiber along with the  $\alpha$ C domains. However, work utilising different snake enzymes have been used instead of thrombin to cleave fibrinopeptide A only (Blomback *et al.*, 1958) and showed that fibrin networks are still able to form. It is known that B:b interactions still do occur physiologically due to the existence of dysfibrinogenaemia Metz where only FpB can be cleaved from the patient's fibrinogen (Galanakis *et al.*, 1993). Ultimately, even though only FpB is cleaved from these clots the monomers are still able to form fibers (Mosesson *et al.*, 1987). More recent work was performed by Professor Doolittle's laboratory, who is a pioneer in analysis of fibrin crystals and relating them to polymerisation and protofibril packing (Yang *et al.*, 2000), here they investigated whether or not there were extra residues/domains facilitating in the lateral aggregation of fibrin protofibrils. In this selected paper the authors created four D:D structures; DD-GP (DD with GPRP ligand bound to hole-a) DD-GH (DD with GHRP ligand bound to b-holes) DD-BOTH (DD with GPRP ligand bound to hole-a and GHRP bound to b-holes), and DD-NL (Both holes empty, no ligands). Through the creation of these four crystal variants the authors found that structures that had ligand(s) occupying the holes 'a' and/or 'b' had very different lateral packing interactions

to crystals where holes were left empty. Two stretches of residues were proposed by the authors to be responsible for lateral packing interactions, these were  $\gamma$ 350-360 and  $\gamma$ 370-380 (termed  $\gamma$ C- $\gamma$ C contacts), which also contains the  $\gamma$ K356Q variant. With this in mind, it is difficult to say without further work whether the results such as slower kinetics, reduced fiber thickness, reduced network density and increased  $G'$  (stiffness) are the result of abolition of extended D-E interaction or a disruption of lateral packing mechanisms proposed by Doolittle *et al.*, or perhaps a combination of both.

Congenital dysfibrinogenaemia, fibrinogen Detroit, contains a substitution at Arginine 19 on the  $A\alpha$ -chain to a serine residue, changing the knob A sequence, and causing interference with the binding with hole-a. When the patient's plasma was added to 'normal' purified fibrinogen a delay in polymerisation was observed resulting in an delay in polymerisation initiation, indicating that the fibrinogen molecules were defective (Blomback *et al.*, 1968). A new fibrin variant R19S/R17S recently produced in the Ariëns laboratory, which mutates the  $\alpha$ - and  $\beta$ -chain knob sequences yields fibrinogen that does not polymerise at all upon cleavage by thrombin (Duval, unpublished). Interestingly, a dysfibrinogenaemia named Fibrinogen Miami ( $B\beta$  D61G) has been described, this variant contains a mutation in the opposite interacting residue to  $\gamma$ K356 that is being investigated. This dysfibrinogenaemia also showed delayed polymerisation kinetics, (Galanakis *et al.*, 1996) suggesting that the K356 and  $B\beta$ D61 ion pair interaction may be more important than originally thought for the polymerisation of fibrin.

To summarise, the data shows abnormal polymerisation kinetics, clot structures and some differences in clot stiffness for  $\gamma$ DEK and  $\gamma$ K356Q. Due to the additional potential functions of residues  $\gamma$ D297N,  $\gamma$ E323 and  $\gamma$ K356 it is difficult to say with confidence if the aberrant results are due to the fact that extended D-E interactions are negated, or if other mechanisms are involved. For example, D297 could play a role in catch slip bonds,  $\gamma$ E323 could destabilise salt links to other residues in the binding pocket and  $\gamma$ K356 may be involved in the alteration of  $\gamma$ C- $\gamma$ C contacts. As each of these single variants may contribute differently to the overall effect of the triple mutant  $\gamma$ DEK, I have tried to simplify the contributions of each single variant into a ranking system in Table 7-1. This table ranks the percentage change of all mutants (positive or negative) with regards to the WT. Only experimental data where all variants were compared were included, therefore discounting protofibril packing and turbidity with reptilase as there was not enough material for these assays. The clot mechanic data at 0.1Hz, 1Hz and 10Hz were compared for  $\tan\delta$  only as clots are visco-elastic materials as I would like to compare the overall deformability of the variant clots. At earlier stages of polymerisation single mutants  $\gamma$ D297N and  $\gamma$ K356Q, are more different compared with the WT than  $\gamma$ DEK. It is expected that  $\gamma$ DEK is the most different because it has altered residues in all positions, so this was somewhat surprising. Later stages of polymerisation (lateral aggregation) is measured by rate of lateral aggregation. The abolition of the extended D-E interactions has an effect on lateral aggregation  $\gamma$ DEK is the most reduced followed by  $\gamma$ E323Q then the two other single mutants  $\gamma$ D297N and  $\gamma$ K356Q. Maximum optical density is mathematically relatable to fiber thickness and to some extent clot density (Carr and Hermans, 1978), therefore it is no surprise

that  $\gamma$ DEK is the most dense and has the thinnest fibers to WT, again this seems to be followed by  $\gamma$ E323Q,  $\gamma$ D297N and  $\gamma$ K356Q. As seen in Table 7-1 clot mechanics are most different for  $\gamma$ DEK at 0.1Hz and 1Hz. Clot density for  $\gamma$ DEK is significantly higher than WT, therefore clot density is likely having an effect on the  $\tan\delta$ , +111% at 0.1Hz. These lower frequencies detect changes in mechanics at a whole clot level. At 10Hz however (molecular deformation events), the pattern is completely changed,  $\gamma$ DEK has a smaller  $\tan\delta$  than that of  $\gamma$ D297N and  $\gamma$ E323Q. This is unusual because I would expect that when all three residues are altered in  $\gamma$ DEK, fewer interactions are able to occur between monomers and therefore easier to deform molecular domains. Lastly,  $\gamma$ D297N appears to be fastest to lyse (even faster than WT) in the lysis experiments, although initially I would not expect this to be the case. It maybe that perhaps protofibril packing could be responsible for this, as larger spacing between protofibrils could allow faster diffusing of lytic proteins.  $\gamma$ D297N has the largest reduction in protofibril number (-45%) which would fit with this hypothesis, but other single variants  $\gamma$ E323Q and  $\gamma$ K356Q also had similar reduction in protofibril number (-28% and -32.5%, respectively). As the latter were slower to lyse, this does not concur with this hypothesis and hence further investigations need to be done to explain why D297N is the fastest to lyse.

**Table 7-1 Ranking of overall percentage difference of recombinant variants compared to WT.**  $\gamma$ DEK in orange,  $\gamma$ D297N in green,  $\gamma$ E323Q in blue and  $\gamma$ K356Q in yellow. Percentage differences most different from the WT were ranked (1) whereas the variants with the lowest percentage differences were ranked (4). Red boxes indicate a significantly different result.

		(Most different) <b>Ranking</b> (Least different)			
		1	2	3	4
Polymerisation Early Stages	Protofibril Length 10min	$\gamma$ K356Q (+)	$\gamma$ D297N (-)	$\gamma$ DEK (-)	$\gamma$ E323Q (-)
	Protofibril Length 20min	$\gamma$ D297N (+)	$\gamma$ K356Q (+)	$\gamma$ DEK (-)	$\gamma$ E323Q (+)
	Protofibril Length 30min	$\gamma$ K356Q (+)	$\gamma$ E323Q (+)	$\gamma$ D297N (+)	$\gamma$ DEK (+)
Polymerisation Later Stages	Maximum OD	$\gamma$ DEK (-)	$\gamma$ E323Q (-)	$\gamma$ K356Q (-)	$\gamma$ D297N (-)
	Lag Phase	$\gamma$ DEK (+)	$\gamma$ E323Q (+)	$\gamma$ K356Q (-)	$\gamma$ D297N (-)
	Max polymerisation Rate	$\gamma$ DEK (-)	$\gamma$ E323Q (-)	$\gamma$ D297N (-)	$\gamma$ K356Q (-)
Structure	Fiber Thickness	$\gamma$ DEK (-)	$\gamma$ E323Q (-)	$\gamma$ K356Q (-)	$\gamma$ D297N (-)
	Density	$\gamma$ DEK (+)	$\gamma$ E323Q (+)	$\gamma$ K356Q (-)	$\gamma$ D297N (+)
	Lysis	$\gamma$ D297N (+)	$\gamma$ DEK (-)	$\gamma$ K356Q (-)	$\gamma$ E323Q (-)
Mechanics	Tan $\delta$ 0.1Hz	$\gamma$ DEK (+)	$\gamma$ D297N (+)	$\gamma$ E323Q (+)	$\gamma$ K356Q (-)
	Tan $\delta$ 1Hz	$\gamma$ DEK (+)	$\gamma$ K356Q (-)	$\gamma$ D297N (-)	$\gamma$ E323Q (-)
	Tan $\delta$ 10Hz	$\gamma$ D297N (-)	$\gamma$ E323Q (-)	$\gamma$ DEK (-)	$\gamma$ K356Q (+)

## **7.3 Limitations**

### **7.3.1 CD spectroscopy**

As previously discussed in section 3.3.4 it is surprising there is a small amount of data available for CD spectroscopy of fibrinogen, making it more difficult to confirm the result. Additionally CD requires strict cross calibration and validation of reference CD spectra of proteins that have been fully or almost fully crystallised, fibrinogen has many disordered regions and therefore this must be taken into consideration when interpreting the CD result. The data shows that across all types of secondary structures that  $\gamma$ DEK is different to the WT. It is worth noting that the protein concentration has a significant effect on the output spectra and therefore even though all precautionary measures and practices were performed one cannot negate the possibility that in fact protein aggregates were present or the protein concentration slightly varied for  $\gamma$ DEK compared to WT. Due to the high sensitivity of the equipment, the small concentration change perturbed the CD output slightly. This is a possibility as when the raw CD curves of WT and  $\gamma$ DEK are analysed all peaks are shifted to the same degree, which is a reflection upon a difference in concentration rather than a change in the secondary structure.

### **7.3.2 Cell culture**

In this work, the yield for some of the variants was limiting the amount of work that could be performed. Yields ranged from 1.5mg total protein ( $\gamma$ DEK) to 15mg total protein ( $\gamma$ D297N). To improve on this a greater number of clones could be selected for, increasing the number of clones from 48 to 100, therefore it would be more likely to select for a highly expressing clone. However, this obviously would impact on the cost and the time required for clone selection.

### **7.3.3 Micro-rheology**

At present, the magnetic tweezers set up does not completely measure intramolecular deformation events due to the limitations of the frequency of the CCD camera. To gather more data using the current micro-rheology setup I could replace the current camera with a camera that performs at a higher frequency (e.g. 100Hz). Collecting data at higher frequencies would enable me to completely measure the  $G'$ ,  $G''$  and  $\tan\delta$  of molecular unfolding events. Optical trap methods could also be used to support the data. Pulling of individual fibrin monomers from fibrinogen could be performed to investigate the magnitude of molecular unfolding events in the variants compared with WT.

#### **7.3.3.1 Factor XIII**

The crosslinking of fibrin chains with FXIII influences overall clot density (Hethershaw *et al.*, 2014), but more importantly FXIII changes the mechanical properties of the blood clot by increasing the elastic modulus (Dorgalaleh and Rashidpanah, 2016) (Shen and Lorand, 1983). Lateral force single fiber pulling experiments have shown that the storage modulus is significantly increased by factor XIII crosslinked fibrin (Liu *et al.*, 2010), suggesting that the crosslinks form at early stages during protofibril and fiber formation rather than FXIII permeating through pores in the network following clot formation.

Unfortunately, due to material and time constraints, factor XIII experiments were not performed. Factor XIII  $\gamma$ -chain crosslinking sites are localised to residues 398/399 and K406 therefore, it is unlikely that the variants would disrupt the crosslinking process. The fibrin variants are denser than the WT with more fibers, albeit thinner. It would be interesting to know what impact FXIII has on the mechanics of the mutants, due to material limitations I did not prioritise FXIIIa

experiments as I do not expect factor XIIIa to introduce a significant effect to the variants compared to the WT. I suspect that each mutant will be cross-linked to a similar extent by factor XIIIa leading to a similar increase in  $G'$  and  $G''$ , however further experimentation would be needed to test this.

#### **7.3.4 Limitations of turbidity measurements**

Turbidity, a light scattering method, can be performed to investigate the kinetics of fibrin polymerisation. However, turbidity profiles do not represent the full extent of the kinetics as early stages of polymerisation such as longitudinal protofibril growth. This is because the turbidity technique is not sensitive enough to measure these small changes in protofibril formation, however the method is particularly useful for measuring fiber growth (lateral aggregation). To complement the turbidity method atomic force microscopy was used to image early stages of protofibril formation.

#### **7.3.5 Limitations of confocal microscopy**

Confocal microscopy was used in this work to quantify the density and lysis rates of fibrin clots. Confocal microscopy is particularly useful because it allows the formation of a fibrin clot in hydrated conditions. However, confocal microscopy does not have the resolving power of a scanning electron microscope and therefore one cannot image beyond the detail of fibrin fibers, nor can one accurately determine fibre diameter using confocal microscopy. In this work, clot structure experiments were supported with scanning electron microscopy to obtain greater detail of the fibrin fibers. Images taken at x20,000

Another limitation of the confocal experiments is that the addition of the Alexa 488 fluorophore could affect the fibrin polymerisation and clot formation. The label reacts with primary amines and forms stable dye-protein conjugates. I must

consider that the labelling of fibrinogen had an effect on the clot structure observed in the confocal experiments because the degree of labelling (moles per dye per moles of protein) between the WT and the variants varied between the WT (18.66) and the variants  $\gamma$ DEK (24.07)  $\gamma$ D297N (20.24),  $\gamma$ E323Q (21.47)  $\gamma$ K356Q (20.3). Although the recommended degree of labelling using the Alexa Fluor Labelling kit is in the range of 4-9 moles of dye per moles of protein, meaning that the protein is over labelled, I did not observe aggregation of protein conjugates. Due to material limitations it was not possible to relabel the proteins. However, previous turbidity experiments have been conducted in the Ariëns laboratory (data not shown) where labelled recombinant WT fibrinogen has been incorporated and the formation of a clot has been observed. No differences were seen between clots formed with labelled fibrinogen compared to those made without. If enough material was available turbidity profile experiments should also have been be conducted on the variants in the presence of labelled fibrinogen. The effect of labelled fibrinogen on longitudinal protofibril formation using atomic force microscopy could also be performed, to support the turbidity result.

### **7.3.6 Limitations of scanning electron microscopy**

Scanning electron microscopy has been used to highlight in detail the fiber composition of the variant clots. However, scanning electron microscopy does have its limitations, the most crucial being that clots for SEM are dehydrated to allow for imaging. Dehydration of the clots could lead to inaccurate measuring of fibrin fiber diameters. Additionally, due to the multiple processing and handling procedures, fibrin clots have to be made with a higher concentration of thrombin (1U/mL compared to 0.1U/mL used for turbidity) to create a meshwork that is sufficiently stable and does not collapse during clot processing.

### **7.3.7 Limitations of atomic force microscopy**

Although AFM experiments have been particularly insightful with regards to early protofibril formation, the method does have its limitations. One has to be careful when interpreting the AFM data, as one cannot know for certain whether all protofibrils that form during the polymerisation process and transferred to the mica surface, remain at the surface during the washing and drying process (see section 4.3.2). An assumption was made that the WT and all the variants were absorbed to the mica surface in equal amounts. To investigate this further one could study whether changing the surface to another substrate or using chemical modifiers to change the mica surface has an impact on number of protofibrils attaching. Further work as described in 7.4.2 could also be performed to increase the robustness of the method.

## **7.4 Future Work**

### **7.4.1 Clot mechanics**

It is known that altered clot structures have an impact on the mechanical measurements taken, especially clot stiffness (Weisel, 2004a). This makes rheology data difficult to interpret when comparing the variants to WT because differences observed may be ultrastructure related. To provide additional insight single fiber lateral force AFM could be performed and this would allow me to further assess whether there is any mechanical differences at the single fiber level without clot density influencing the outcome. In the future, I would like to perform lateral force single fiber pulling experiments to test the hypothesis that the thinner variant fibers are mechanically weaker than WT fibers. Detailed explanations of experimental equipment used and experimental procedures for lateral force AFM can be found in the literature (Carlisle *et al.*, 2009). In brief,

fibrin fibers are formed and are suspended between two ridges, as demonstrated in Figure 7-1, it is then possible to pull the suspended fibers with an AFM cantilever tip. When the AFM cantilever pulls on the fibrin fiber it is possible to calculate strain-stress curves. Additionally, SEM and light scattering studies would need to be performed to measure fiber thickness and protofibril packing as these may impact on the single fiber mechanics.



**Figure 7-1 Cartoon representation of lateral force AFM experiments.** Fibrin fibers (solid red line) are suspended between grooves (blue), the fiber can be pulled with an AFM cantilever tip (represented by a green circle). During pulling the fibers stretch and eventually rupture.

#### 7.4.2 AFM studies

AFM experiments were previously conducted with 0.5mg/mL Fibrinogen, 2.5mM CaCl<sub>2</sub> and 0.1U/mL thrombin, and imaged a 5µm x 5µm window size. However the resolution of the protofibrils was poor because it was apparent that there was too much material to distinguish between monomers and protofibrils. The current setup using 0.02mg/mL fibrinogen and 0.05U/mL thrombin as described in section 2.14 was optimised by Stephen Baker, University of Leeds and based on the method published by Protopopova *et al.* (Protopopova *et al.*, 2015). As an improvement I would like to optimise and develop a new method using a FAST-SCAN AFM this will allow me to image much larger window sizes 50µmx50µm

to 100µmx100µm encapsulating more protofibrils in an image and making the overall count more robust.

### **7.4.3 Interactions with other blood components**

#### **7.4.3.1 $\alpha_{IIb}\beta_3$**

In this thesis, all of the studies into polymerisation, clot structure and clot mechanics were in a purified *in vitro* system. In physiology however there is an abundance of plasma proteins, not to mention other cell types such as platelets and red blood cells. Fibrinogen has other functions such as aiding platelet aggregation through the platelet  $\alpha_{IIb}\beta_3$  receptor (Bennett, 2005), therefore would the mutants still perform other functions such as fibrin platelet interactions? In the case of  $\alpha_{IIb}\beta_3$  it is likely that normal fibrin function would be intact as  $\alpha_{IIb}\beta_3$  interactions with fibrin are localised to residues  $\alpha 95-97$  and  $\gamma 400-411$ , far away from the residues of interest. To test this in the future platelet aggregometry could be performed similar to as described in (Farrell *et al.*, 1992), in the presence of variant and WT fibrinogen.

#### **7.4.3.2 GPVI**

Glycoprotein VI (GPVI) is a platelet receptor and typically binds to collagen at a gly-pro-hydroxypro (GPO) sequence, this subsequently activates the platelet through the dimerisation of GPVI (Nieswandt and Watson, 2003). It has recently been shown that GPVI can also bind fibrinogen (Mangin *et al.*, 2018).

GPVI binds to fibrin and also fibrin degradation product D-dimer, and this induces platelet activation (Induruwa *et al.*, 2018). The exact binding interface of GPVI and fibrin has not yet been described, so it is difficult to say whether the recombinant variants would have an effect of the intensity of platelet binding and platelet aggregation. With the production of additional recombinant fibrinogen I

could perform surface plasmon resonance (SPR) and isothermal titration calorimetry (ITC) to investigate the binding intensities of the fibrinogen variants with GPVI.

#### **7.4.3.3 Plasminogen, tPA and $\alpha$ 2-Antiplasmin**

The results demonstrate that the rate of lysis is mainly influenced by the final architecture of the clot, with the fiber density and fiber thickness being the most prevalent of factors. Plasminogen and tPA both bind via kringle domains and bind to exposed lysine residues, (Mutch *et al.*, 2010). Other fibrin interaction sites (not fibrin) have also been identified. Firstly a stretch of residues in the  $\alpha$ -chain spanning from  $\alpha$ 148-160 binds both tPA and plasminogen to low affinity (Schielen *et al.*, 1990), but it is unlikely that the recombinant variants will impact on this interaction as the residues are located away from this region on the  $\gamma$ -chain. Another additional plasminogen binding site includes residues  $\gamma$ 311-336 and  $\gamma$ 337-379 (Yonekawa *et al.*, 1992). These regions do encompass the residues where two of the variants are,  $\gamma$ E323Q and  $\gamma$ K356Q. Further work such as binding assays would need to be conducted to investigate whether the mutations enhance or reduce plasminogen binding.

The enzyme  $\alpha$ 2-Antiplasmin plays a key role in the fibrinolytic process by inhibiting plasmin. FXIII crosslinks  $\alpha$ 2-Antiplasmin to the fibrin clot at residue  $\alpha$ 303K (Rijken and Uitte de Willige, 2017). As the point mutations in the variants are not in proximity to this region it is unlikely that the variants will have an impact on  $\alpha$ 2-Antiplasmin binding.

#### **7.4.3.4 $\alpha_M\beta_2$**

Fibrinogen also binds to the leukocyte receptor  $\alpha_M\beta_2$  (Forsyth *et al.*, 2001), which has implicated fibrinogen in leukocyte adhesion and the overall inflammatory

response. Fibrinogen binds  $\alpha_M\beta_2$  receptor via residues  $\gamma$ 190-202 and  $\gamma$ 377-395 (Ugarova *et al.*, 1998). The  $\gamma$ E323Q and  $\gamma$ K356Q mutated residues in these variants are somewhat closely located to the  $\alpha_M\beta_2$  site. It is therefore possible that the variants would have abnormal leukocyte adhesion functionality, however further study would be required to confirm this.

#### **7.4.4 Complement protein C3**

Complement protein 3 (C3) is an important protein in the initiation of innate immunity and is involved in inflammatory response (Sahu and Lambris, 2001). In addition to these roles, it has been shown that complement C3 can effect turbidity and clot structure (Howes *et al.*, 2012). The data shows that a difference in clot structure can influence clot mechanics and therefore the presence of C3 could also influence clot mechanics. Howes *et al.* also showed that C3 can bind to immobilised fibrinogen using SPR. The recombinant variants could affect the amount of C3 that is able to integrate into fibrin clots, however further work would need to be completed because these articles do not describe where C3 specifically binds to fibrin.

#### **7.4.5 Role of calcium binding**

As discussed in section 7.2, fibrinogen has a total of four calcium binding sites, two of which are low affinity binding sites ( $\gamma$ 2 and  $\beta$ 2) and two of which are high affinity binding sites ( $\gamma$ 1 and  $\beta$ 1).

Variant  $\gamma$ D297N interestingly resides within the low affinity  $\gamma$ 2 calcium binding site, whereas the variant  $\gamma$ E323Q resides within the high affinity  $\gamma$ 1 binding site. In the case of the  $\gamma$ 2 binding site recombinant variant Kostelansky *et al.*, developed recombinant variant  $\gamma$ D298A/D301A to investigate the role of calcium binding on polymerisation (Kostelansky *et al.*, 2007). The authors found that

polymerisation differed slightly with the D298A/D301A variant meaning that the  $\gamma$ 2 calcium binding site has a small role in fibrin polymerisation. I observe much larger changes in the  $\gamma$ D297N variant which is closely related to the calcium binding site.

Therefore to confirm that my results are from the lack of catch bonds and not through the loss of calcium binding, it would be necessary to test the variants, with and without calcium throughout all of the biophysical *in vitro* assays. Interestingly a recent publication has proposed that in fact the catch-slip bonds are regulated by the presence of calcium (Litvinov *et al.*, 2018), this makes it very difficult to predict on what are observed changes are from as catch-slip may actually be dependent on calcium binding. An additional caveat is that the  $\beta$ 2 calcium binding sites also play a role polymerisation and clot formation, mainly lateral aggregation of protofibrils (Kostelansky *et al.*, 2004b), making it even more difficult to assess the effects of each individual calcium binding on polymerisation and clot formation.

#### **7.4.6 Molecular dynamic simulations**

In the past, X-ray crystallography studies of fibrin(ogen) have provided a tremendous amount of information in regards to the structure of fibrinogen, some groups have co-crystallised the synthetic knob (GPRP) with the D-region in order to produce fibrin crystals (Yang *et al.*, 2000)

On my behalf, my collaborators at University of Massachusetts, (Lowell) are currently performing molecular dynamic simulations using available fibrin crystal structure 3GHG in the protein data bank (Kollman *et al.*, 2009).

I am interested in discovering the dynamic binding contacts formed in and near A:a binding pocket during fibrin polymerisation that lead to the striking differences observed in this work. Molecular pulling simulations (Kononova *et al.*, 2013) of GPRP peptide from  $\gamma$ C nodule will map the binding and unbinding transitions for the variants, allowing the assessment of the importance of individual residues and their dissociation kinetics. The simulations will identify the role of the variants in three distinct regions of the  $\gamma$ C nodule,  $\gamma$ D297N in the moveable flap,  $\gamma$ E323Q in loop I and  $\gamma$ K356Q in the interior region. The force required to rupture the A:a bond as a function of time for each variant will be simulated. The number of residues that are actively participating in the extended knob-hole binding pocket will also be analysed, WT fibrinogen will also be simulated.

## **7.5 Physiological importance and relevance**

Interestingly, a dysfibrinogenaemia named Fibrinogen Miami ( $B\beta$  D61G) has been described in the literature. The variant described contained a mutation of the opposite interacting residue to  $\gamma$ K356 that is being investigated in my work. The current hypothesis is that  $\beta\beta$ D61 interacts with  $\gamma$ K356. The patient who had this dysfibrinogenaemia also showed tendency to bleed and delayed polymerisation kinetics, (Galanakis *et al.*, 1996) providing evidence that the K356 and  $B\beta$ D61 extended knob-hole interaction also plays an important role in clot formation in a physiological setting and may be extremely important in the clinic. Based on the literature I predict that small changes within the side chains of these key extended knob-hole residues will influence catch-slip bonds and reduce the unbinding force of knob A from hole-a, which later amplifies into significant

changes in polymerisation kinetics and overall clot structure. In physiological circumstances this could be extremely important during development of thrombosis as the catch mechanism allows the bonds to counterintuitively strengthen under shear stresses such as blood flow, possibly preventing embolization, providing more evidence of the importance of this extended knob-hole interactions.

The work in this thesis is somewhat limited in terms of scope as it only explores the role of these residues in fibrin polymerisation and clot formation *in vitro* and *in silico* (data still processing). The next stage to take this research further would be to explore the role of these variants in fibrinogen deficient plasma to determine whether the effects of denser clots and thinner fibers observed in the *in vitro* studies are still evident when other blood components are involved. FXIIIa crosslinking, platelet contraction and red blood cell retention are all mechanisms that are influenced by the final clot structure and mechanics.

Additionally, it was also initially planned that I would investigate the role of these extended knob-hole interactions on clot formation and stability *in vivo*. To do this, an *in vivo* murine model of thrombosis was proposed. Briefly, in fibrinogen knockout mice (Fib<sup>-/-</sup>) a carotid artery would be cannulated to allow for administration of anaesthetic and injection of recombinant fibrinogen mutants labelled with Alexa Fluor 488, for 5 minutes prior to exposure of the femoral vein and application of 10% FeCl<sub>3</sub> filter paper for 3 minutes to induce thrombosis. Real time observation of the clots would have been made using an intra-vital microscope where clot formation and final clot size would have been measured. However, due to limitations with the yield of the recombinant variants it was not possible to conduct such experiments. Power calculations were performed by

Marco Domingues of the Ariëns laboratory on my behalf and predicted that 5-6 mice would be required to perform a *in vivo* murine model of thrombosis and therefore to complete these type of experiments 20-30mg total protein would be required. Although this would be possible with further protein expression of the extended knob-hole variants. Therefore, without further studies in *ex vivo* (plasma) and *in vivo* (mouse model) data it is difficult to correlate the effects of extended knob-hole interactions to DVT risk in patients. However, the results observed especially in regards to mechanics does show that clots become more readily deformable when these interactions are abolished, showing that the mechanical properties of clots could potentially be regulated through extended knob-hole interactions in additional to traditional mechanisms such as factor XIIIa crosslinking.

## **7.6 Conclusions**

To conclude, I have used well characterised CHO cell expression and purification systems to produce pure, and intact recombinant human fibrinogen with mutations at the extended knob-hole binding sites. I have explored the functional consequence of these mutations during polymerisation using biophysical light scattering and atomic force microscopy imaging methods where I observed delayed polymerisation kinetics. I further probed the role of these variants on fibrin clot structure using light scattering, laser scanning confocal microscopy and scanning electron microscopy and observed variant clots that were denser with thinner fibers. The effects on clot mechanics were also investigated where I observed that  $\tan\delta$  was mainly increased at 0.1Hz and 1Hz indicating that all point mutations are required to have a mechanical effect on the clots. This work

has exclusively been completed using *in vitro* biochemical and biophysical *in vitro* assays, I recommend that further work should be completed in the future to test the effects of the variants in the presence of cells and other blood components.

Although the experiments performed in this thesis are not directly clinically relevant, the additional understanding of the mechanisms that regulate extended D-E interactions in fibrin polymerisation, clot formation and clot mechanics may have future implications for the understanding and prevention of thromboembolic diseases.

# **Chapter 8 - References**

- Ageno, W. and Huisman, M.V. 2000. Low-molecular-weight heparins in the treatment of venous thromboembolism. *Current Controlled Trials in Cardiovascular Medicine*. **1**(2), pp.102-105.
- Alami, S.Y. et al. 1968. The Relationship of Plasma Fibrinogen (Factor I) Level to Fibrin Stabilizing Factor (Factor XIII) Activity. *Blood*. **31**(1), p93.
- Alexander, K.S. et al. 2011. Association between gamma' fibrinogen levels and inflammation. *Thromb Haemost.* **105**(4), pp.605-9.
- Allan, P. et al. 2012. Evidence that fibrinogen gamma' directly interferes with protofibril growth: implications for fibrin structure and clot stiffness. *J Thromb Haemost.* **10**(6), pp.1072-80.
- Allan.P. 2012. *Microrheology of fibrin clots*. thesis, University of Leeds.
- Ariëns, R.A.S. et al. 2002. Role of factor XIII in fibrin clot formation and effects of genetic polymorphisms. *Blood*. **100**(3), p743.
- Ashcroft, A.E. et al. 2000. A study of human coagulation factor XIII A-subunit by electrospray ionisation mass spectrometry. *Rapid Communications in Mass Spectrometry*. **14**(17), pp.1607-1611.
- Aslan, J.E. et al. 2012. Platelet shape change and spreading. *Methods Mol Biol.* **788**, pp.91-100.
- Averett, L.E. et al. 2008. Complexity of "A-a" knob-hole fibrin interaction revealed by atomic force spectroscopy. *Langmuir*. **24**(9), pp.4979-88.
- Averett, L.E. et al. 2009. Kinetics of the Multistep Rupture of Fibrin 'A-a' Polymerization Interactions Measured Using Atomic Force Microscopy. *Biophysical Journal*. **97**(10), pp.2820-2828.
- Bannish, B.E. et al. 2017. Molecular and Physical Mechanisms of Fibrinolysis and Thrombolysis from Mathematical Modeling and Experiments. *Scientific Reports*. **7**, p6914.
- Bantia, S. et al. 1990. Fibrinogen Baltimore I: polymerization defect associated with a gamma 292Gly---Val (GGC---GTC) mutation. *Blood*. **76**(11), p2279.
- Baradet, T.C. et al. 1995. Three-dimensional reconstruction of fibrin clot networks from stereoscopic intermediate voltage electron microscope images and analysis of branching. *Biophysical Journal*. **68**(4), pp.1551-1560.
- Bates, S.M. 2012. D-dimer assays in diagnosis and management of thrombotic and bleeding disorders. *Semin Thromb Hemost.* **38**(7), pp.673-82.
- Beckers, C.M.L. et al. 2017. Cre/lox Studies Identify Resident Macrophages as the Major Source of Circulating Coagulation Factor XIII-A. *Arteriosclerosis, Thrombosis, and Vascular Biology*. **37**(8), pp.1494-1502.
- Bennett, J.S. 2005. Structure and function of the platelet integrin  $\alpha$ (IIb) $\beta$ (3). *Journal of Clinical Investigation*. **115**(12), pp.3363-3369.
- Binnie, C.G. et al. 1993. Characterization of purified recombinant fibrinogen: partial phosphorylation of fibrinopeptide A. *Biochemistry*. **32**(1), pp.107-13.
- Blomback, B. et al. 1958. Coagulation studies on reptilase, an extract of the venom from *Bothrops jararaca*. *Thromb Diath Haemorrh.* **1**(1), pp.76-86.
- Blombäck, B. et al. 1989. Native fibrin gel networks observed by 3D microscopy, permeation and turbidity. *Biochimica et Biophysica Acta (BBA) - Protein Structure and Molecular Enzymology*. **997**(1), pp.96-110.
- Blomback, M. et al. 1968. Fibrinogen Detroit—a Molecular Defect in the N-terminal Disulphide Knot of Human Fibrinogen? *Nature*. **218**, p134.

- Bouma, B.N. and Mosnier, L.O. 2006. Thrombin activatable fibrinolysis inhibitor (TAFI)--how does thrombin regulate fibrinolysis? *Ann Med.* **38**(6), pp.378-88.
- Bowley, S.R. et al. 2008. Polymerization-defective fibrinogen variant gammaD364A binds knob "A" peptide mimic. *Biochemistry.* **47**(33), pp.8607-13.
- Branson, H.E. et al. 1983. Fibrinogen Seattle Releases Half the Normal Amount of Fibrinopeptide B. *Acta Haematologica.* **70**(4), pp.257-263.
- Brennan, S.O. et al. 1997. Electrospray ionisation mass spectrometry facilitates detection of fibrinogen (Bbeta 14 Arg --> Cys) mutation in a family with thrombosis. *Thromb Haemost.* **78**(6), pp.1484-7.
- Brown, A.E. et al. 2007. Forced unfolding of coiled-coils in fibrinogen by single-molecule AFM. *Biophys J.* **92**(5), pp.L39-41.
- Brown, A.E.X. et al. 2009. Multiscale Mechanics of Fibrin Polymer: Gel Stretching with Protein Unfolding and Loss of Water. *Science.* **325**(5941), p741.
- Cabral, K.P. and Ansell, J.E. 2015. The role of factor Xa inhibitors in venous thromboembolism treatment. *Vascular Health and Risk Management.* **11**, pp.117-123.
- Caracciolo, G. et al. 2003. Protofibrils within fibrin fibres are packed together in a regular array. *Thromb Haemost.* **89**(04), pp.632-636.
- Carpenter, S.L. and Mathew, P. 2008.  $\alpha$ 2-Antiplasmin and its deficiency: fibrinolysis out of balance. *Haemophilia.* **14**(6), pp.1250-1254.
- Carr, M.E. and Gabriel, D.A. 1980. Dextran-Induced Changes in Fibrin Fiber Size and Density Based on Wavelength Dependence of Gel Turbidity. *Macromolecules.* **13**(6), pp.1473-1477.
- Carr, M.E. et al. 1986. Influence of Ca<sup>2+</sup> on the structure of reptilase-derived and thrombin-derived fibrin gels. *Biochemical Journal.* **239**(3), pp.513-516.
- Carr, M.E., Jr. and Alving, B.M. 1995. Effect of fibrin structure on plasmin-mediated dissolution of plasma clots. *Blood Coagul Fibrinolysis.* **6**(6), pp.567-73.
- Carr, M.E., Jr. and Hermans, J. 1978. Size and density of fibrin fibers from turbidity. *Macromolecules.* **11**(1), pp.46-50.
- Casa, L.D.C. et al. 2015. Role of high shear rate in thrombosis. *Journal of Vascular Surgery.* **61**(4), pp.1068-1080.
- Chung, D.W. et al. 1980. The biosynthesis of bovine fibrinogen, prothrombin, and albumin in a cell-free system. *Ann N Y Acad Sci.* **343**, pp.210-7.
- Cilia La Corte, A.L. et al. 2011. Role of fibrin structure in thrombosis and vascular disease. *Adv Protein Chem Struct Biol.* **83**, pp.75-127.
- Collet, J.-P. et al. 2005a. The elasticity of an individual fibrin fiber in a clot. *Proceedings of the National Academy of Sciences of the United States of America.* **102**(26), p9133.
- Collet, J. et al. 1993. Dusart syndrome: a new concept of the relationship between fibrin clot architecture and fibrin clot degradability: hypofibrinolysis related to an abnormal clot structure. *Blood.* **82**(8), pp.2462-2469.
- Collet, J.P. et al. 2006. Altered fibrin architecture is associated with hypofibrinolysis and premature coronary atherothrombosis. *Arterioscler Thromb Vasc Biol.* **26**(11), pp.2567-73.

- Collet, J.P. et al. 2005b. The alphaC domains of fibrinogen affect the structure of the fibrin clot, its physical properties, and its susceptibility to fibrinolysis. *Blood*. **106**(12), pp.3824-30.
- Cordell, P.A. et al. 2010. Association of coagulation factor XIII-A with Golgi proteins within monocyte-macrophages: implications for subcellular trafficking and secretion. *Blood*. **115**(13), pp.2674-81.
- Crochemore, T. et al. 2017. A new era of thromboelastometry. *Einstein*. **15**(3), pp.380-385.
- Crooks, M.G. and Hart, S.P. 2015. Coagulation and anticoagulation in idiopathic pulmonary fibrosis. *European Respiratory Review*. **24**(137), pp.392-399.
- Dang, C.V. et al. 1985. Localization of a fibrinogen calcium binding site between gamma-subunit positions 311 and 336 by terbium fluorescence. *J Biol Chem*. **260**(17), pp.9713-9.
- Davalos, D. and Akassoglou, K. 2012. Fibrinogen as a key regulator of inflammation in disease. *Semin Immunopathol*. **34**(1), pp.43-62.
- Davies, N.A. et al. 2015. Fractal dimension (df) as a new structural biomarker of clot microstructure in different stages of lung cancer. *Thromb Haemost*. **114**(6), pp.1251-9.
- Delewi, R. et al. 2012. Left ventricular thrombus formation after acute myocardial infarction. *Heart*. **98**(23), p1743.
- Denninger, M.H. et al. 1978. Congenital dysfibrinogenemia: fibrinogen Lille. *Thromb Res*. **13**(3), pp.453-66.
- Dharmashankar, K. and Widlansky, M.E. 2010. Vascular Endothelial Function and Hypertension: Insights and Directions. *Current hypertension reports*. **12**(6), pp.448-455.
- Di Stasio, E. et al. 1998. Cl<sup>-</sup> regulates the structure of the fibrin clot. *Biophys J*. **75**(4), pp.1973-9.
- Didiasova, M. et al. 2014. From Plasminogen to Plasmin: Role of Plasminogen Receptors in Human Cancer. *International Journal of Molecular Sciences*. **15**(11), pp.21229-21252.
- Domingues, M.M. et al. 2016. Thrombin and fibrinogen gamma' impact clot structure by marked effects on intrafibrillar structure and protofibril packing. *Blood*. **127**(4), pp.487-95.
- Doolittle, R.F. 1984. Fibrinogen and fibrin. *Annu Rev Biochem*. **53**, pp.195-229.
- Dorgalaleh, A. and Rashidpanah, J. 2016. Blood coagulation factor XIII and factor XIII deficiency. *Blood Reviews*. **30**(6), pp.461-475.
- Duval, C. et al. 2016. Factor XIII A-Subunit V34L Variant Affects Thrombus Cross-Linking in a Murine Model of Thrombosis. *Arterioscler Thromb Vasc Biol*. **36**(2), pp.308-16.
- Duval, C. et al. 2014. Roles of fibrin alpha- and gamma-chain specific cross-linking by FXIIIa in fibrin structure and function. *Thromb Haemost*. **111**(5), pp.842-50.
- Esmon, C.T. 2009. Basic Mechanisms and Pathogenesis of Venous Thrombosis. *Blood reviews*. **23**(5), pp.225-229.
- Esper, R.J. et al. 2008. Endothelial dysfunction in normal and abnormal glucose metabolism. *Adv Cardiol*. **45**, pp.17-43.
- Evans, R.M. et al. 2009. Direct conversion of rheological compliance measurements into storage and loss moduli. *Phys Rev E Stat Nonlin Soft Matter Phys*. **80**(1 Pt 1), p012501.

- Everse, S.J. et al. 1999. Conformational changes in fragments D and double-D from human fibrin(ogen) upon binding the peptide ligand Gly-His-Arg-Pro-amide. *Biochemistry*. **38**(10), pp.2941-6.
- Everse, S.J. et al. 1998. Crystal structure of fragment double-D from human fibrin with two different bound ligands. *Biochemistry*. **37**(24), pp.8637-42.
- Farrell, D.H., Mulvihill, E. R., Chung, D. W., & Davie, E.W. . 1989. *Blood*. **74**(55 a. ).
- Farrell, D.H. et al. 1992. Role of fibrinogen alpha and gamma chain sites in platelet aggregation. *Proceedings of the National Academy of Sciences of the United States of America*. **89**(22), pp.10729-10732.
- Fatah, K. et al. 1996. Proneness to formation of tight and rigid fibrin gel structures in men with myocardial infarction at a young age. *Thromb Haemost*. **76**(4), pp.535-40.
- Ferguson, E.W. et al. 1975. A re-examination of the cleavage of fibrinogen and fibrin by plasmin. *Journal of Biological Chemistry*. **250**(18), pp.7210-7218.
- Ferry, J.D. et al. 1951. The conversion of fibrinogen to fibrin. VII. Rigidity and stress relaxation of fibrin clots, eff. of calcium. *Arch Biochem Biophys*. **34**(2), pp.424-36.
- Ferry, J.D. and Morrison, P.R. 1944. CHEMICAL, CLINICAL, AND IMMUNOLOGICAL STUDIES ON THE PRODUCTS OF HUMAN PLASMA FRACTIONATION. XVI. FIBRIN CLOTS, FIBRIN FILMS, AND FIBRINOGEN PLASTICS. *Journal of Clinical Investigation*. **23**(4), pp.566-572.
- Forsyth, C.B. et al. 2001. Integrin alpha(M)beta(2)-mediated cell migration to fibrinogen and its recognition peptides. *J Exp Med*. **193**(10), pp.1123-33.
- Fowler, W.E. and Erickson, H.P. 1979. Trinodular structure of fibrinogen: Confirmation by both shadowing and negative stain electron microscopy. *Journal of Molecular Biology*. **134**(2), pp.241-249.
- Gaffney, P.J. 2001. Fibrin degradation products. A review of structures found in vitro and in vivo. *Ann N Y Acad Sci*. **936**, pp.594-610.
- Gaffney, P.J. and Joe, F. 1979. The lysis of crosslinked human fibrin by plasmin yields initially a single molecular complex, D dimer-E. *Thrombosis Research*. **15**(5), pp.673-687.
- Galanakis, D. et al. 1993. Unusual A alpha 16Arg-->Cys dysfibrinogenaemic family: absence of normal A alpha-chains in fibrinogen from two of four heterozygous siblings. *Blood Coagul Fibrinolysis*. **4**(1), pp.67-71.
- Galanakis, D.K. et al. 2014. Thromboelastographic phenotypes of fibrinogen and its variants: Clinical and non-clinical implications. *Thrombosis Research*. **133**(6), pp.1115-1123.
- Galanakis, D.K. et al. 1996. 17. Fibrinogen Miami: a Bb61 Asp rGly substitution associated with impaired fibrin polymerization. *Fibrinolysis*. **10**, p7.
- Geer, C.B. et al. 2007. Role of 'B-b' knob-hole interactions in fibrin binding to adsorbed fibrinogen. *Journal of Thrombosis and Haemostasis*. **5**(12), pp.2344-2351.
- Gerhardt, T. and Ley, K. 2015. Monocyte trafficking across the vessel wall. *Cardiovascular Research*. **107**(3), pp.321-330.
- Glidden, P.F. et al. 2000. Thromboelastograph assay for measuring the mechanical strength of fibrin sealant clots. *Clin Appl Thromb Hemost*. **6**(4), pp.226-33.

- Gorkun, O.V. et al. 1998. Analysis of A alpha 251 fibrinogen: the alpha C domain has a role in polymerization, albeit more subtle than anticipated from the analogous proteolytic fragment X. *Biochemistry*. **37**(44), pp.15434-41.
- Gorlatova, N.V. et al. 2007. Mechanism of Inactivation of Plasminogen Activator Inhibitor-1 by a Small Molecule Inhibitor. *Journal of Biological Chemistry*. **282**(12), pp.9288-9296.
- Gray, E. et al. 2012. The anticoagulant and antithrombotic mechanisms of heparin. *Handb Exp Pharmacol*. (207), pp.43-61.
- Guthold, M. et al. 2007. A comparison of the mechanical and structural properties of fibrin fibers with other protein fibers. *Cell Biochem Biophys*. **49**(3), pp.165-81.
- Guthold, M. et al. 2004. Visualization and Mechanical Manipulations of Individual Fibrin Fibers Suggest that Fiber Cross Section Has Fractal Dimension 1.3. *Biophysical Journal*. **87**(6), pp.4226-4236.
- Hadi, H.A.R. and Suwaidi, J.A. 2007. Endothelial dysfunction in diabetes mellitus. *Vascular Health and Risk Management*. **3**(6), pp.853-876.
- Hadjipanayi, E. et al. 2015. The Fibrin Matrix Regulates Angiogenic Responses within the Hemostatic Microenvironment through Biochemical Control. *PLOS ONE*. **10**(8), pe0135618.
- Hagedorn, I. et al. 2010. Arterial thrombus formation. Novel mechanisms and targets. *Hamostaseologie*. **30**(3), pp.127-35.
- Hantgan, R. et al. 1980. Fibrin assembly: a comparison of electron microscopic and light scattering results. *Thromb Haemost*. **44**(3), pp.119-24.
- Hantgan, R.R. and Hermans, J. 1979. Assembly of fibrin. A light scattering study. *J Biol Chem*. **254**(22), pp.11272-81.
- Harrand.R. 2007. *The viscoelastic properties of fibrin clots studied using magnetic tweezers*. thesis, University of Leeds.
- Harter, K. et al. 2015. Anticoagulation Drug Therapy: A Review. *Western Journal of Emergency Medicine*. **16**(1), pp.11-17.
- Hayes, T. 2002. Dysfibrinogenemia and Thrombosis. *Archives of Pathology & Laboratory Medicine*. **126**(11), pp.1387-1390.
- Hennigs, J.K. et al. 2014. Fibrinogen plasma concentration is an independent marker of haemodynamic impairment in chronic thromboembolic pulmonary hypertension. *Scientific Reports*. **4**, p4808.
- Henschen, A. et al. 1984. Genetically abnormal fibrinogens--strategies for structure elucidation, including fibrinopeptide analysis. *Curr Probl Clin Biochem*. **14**, pp.273-320.
- Henschen, A. et al. 1983. Covalent structure of fibrinogen. *Ann N Y Acad Sci*. **408**, pp.28-43.
- Hethershaw, E.L. et al. 2014. The effect of blood coagulation factor XIII on fibrin clot structure and fibrinolysis. *J Thromb Haemost*. **12**(2), pp.197-205.
- Hirose, S. et al. 1988. Biosynthesis, assembly and secretion of fibrinogen in cultured rat hepatocytes. *Biochemical Journal*. **251**(2), pp.373-377.
- Hogan, K.A. et al. 2000. Recombinant fibrinogen Vlissingen/Frankfurt IV. The deletion of residues 319 and 320 from the gamma chain of firbinogen alters calcium binding, fibrin polymerization, cross-linking, and platelet aggregation. *J Biol Chem*. **275**(23), pp.17778-85.
- Howes, J.M. et al. 2012. Complement C3 is a novel plasma clot component with anti-fibrinolytic properties. *Diab Vasc Dis Res*. **9**(3), pp.216-25.

- Hua, B. et al. 2015. Coexisting congenital dysfibrinogenemia with a novel mutation in fibrinogen  $\gamma$  chain ( $\gamma$ 322 Phe→Ile, Fibrinogen Beijing) and haemophilia B in a family. *Haemophilia*. **21**(6), pp.846-851.
- Huang, S. et al. 1993. The role of amino-terminal disulfide bonds in the structure and assembly of human fibrinogen. *Biochem Biophys Res Commun*. **190**(2), pp.488-95.
- Induruwa, I. et al. 2018. Platelet collagen receptor Glycoprotein VI-dimer recognizes fibrinogen and fibrin through their D-domains, contributing to platelet adhesion and activation during thrombus formation. **16**(2), pp.389-404.
- Ivaskevicius, V. et al. 2010. Identification of eight novel coagulation factor XIII subunit A mutations: implied consequences for structure and function. *Haematologica*. **95**(6), pp.956-962.
- Jain, S. et al. 2011. Acute-phase proteins: As diagnostic tool. *Journal of Pharmacy and Bioallied Sciences*. **3**(1), pp.118-127.
- James, A.H. 2009. Pregnancy-associated thrombosis. *ASH Education Program Book*. **2009**(1), pp.277-285.
- Jerjes-Sanchez, C. 2005. Venous and arterial thrombosis: a continuous spectrum of the same disease? *European Heart Journal*. **26**(1), pp.3-4.
- Johnson, H.M. et al. 2010. Effects of Smoking and Smoking Cessation on Endothelial Function: One-Year Outcomes from a Randomized Clinical Trial. *Journal of the American College of Cardiology*. **55**(18), pp.1988-1995.
- Johnson, W.C., Jr. 1990. Protein secondary structure and circular dichroism: a practical guide. *Proteins*. **7**(3), pp.205-14.
- Jones, C.I. et al. 2008. The antithrombotic effect of dextran-40 in man is due to enhanced fibrinolysis in vivo. *J Vasc Surg*. **48**(3), pp.715-22.
- Jung, S.M. et al. 2008. Collagen-type specificity of glycoprotein VI as a determinant of platelet adhesion. *Platelets*. **19**(1), pp.32-42.
- Kant, J.A. et al. 1985. Evolution and organization of the fibrinogen locus on chromosome 4: gene duplication accompanied by transposition and inversion. *Proc Natl Acad Sci U S A*. **82**(8), pp.2344-8.
- Karimi, M. et al. 2009. Factor XIII Deficiency. *Semin Thromb Hemost*. **35**(4), pp.426-38.
- Kelly, J.M. et al. 2018. Using rotational thromboelastometry clot firmness at 5 minutes (ROTEM® EXTEM A5) to predict massive transfusion and in-hospital mortality in trauma: a retrospective analysis of 1146 patients. *Anaesthesia*. **73**(9), pp.1103-1109.
- Kim, O.V. et al. 2014. Structural basis for the nonlinear mechanics of fibrin networks under compression. *Biomaterials*. **35**(25), pp.6739-6749.
- Kim, O.V. et al. 2013. Fibrin Networks Regulate Protein Transport during Thrombus Development. *PLOS Computational Biology*. **9**(6), pe1003095.
- Kingdon, H.S. and Lundblad, R.L. 2002. An adventure in biotechnology: the development of haemophilia A therapeutics -- from whole-blood transfusion to recombinant DNA to gene therapy. *Biotechnol Appl Biochem*. **35**(Pt 2), pp.141-8.
- Kollman, J.M. et al. 2009. Crystal structure of human fibrinogen. *Biochemistry*. **48**(18), pp.3877-86.

- Konings, J. et al. 2011. Factor XIIa regulates the structure of the fibrin clot independently of thrombin generation through direct interaction with fibrin. *Blood*. **118**(14), pp.3942-51.
- Kononova, O. et al. 2013. Molecular Mechanisms, Thermodynamics, and Dissociation Kinetics of Knob-Hole Interactions in Fibrin. *The Journal of Biological Chemistry*. **288**(31), pp.22681-22692.
- Koopman, J. et al. 1991. A congenitally abnormal fibrinogen (Vlissingen) with a 6-base deletion in the gamma-chain gene, causing defective calcium binding and impaired fibrin polymerization. *J Biol Chem*. **266**(20), pp.13456-61.
- Koopman, J. et al. 1992. Abnormal fibrinogens IJmuiden (B beta Arg14----Cys) and Nijmegen (B beta Arg44----Cys) form disulfide-linked fibrinogen-albumin complexes. *Proceedings of the National Academy of Sciences*. **89**(8), p3478.
- Kostelansky, M.S. et al. 2002. 2.8 A crystal structures of recombinant fibrinogen fragment D with and without two peptide ligands: GHRP binding to the "b" site disrupts its nearby calcium-binding site. *Biochemistry*. **41**(40), pp.12124-32.
- Kostelansky, M.S. et al. 2004a. B beta Glu397 and B beta Asp398 but not B beta Asp432 are required for "B:b" interactions. *Biochemistry*. **43**(9), pp.2465-74.
- Kostelansky, M.S. et al. 2004b. Calcium-binding site beta 2, adjacent to the "b" polymerization site, modulates lateral aggregation of protofibrils during fibrin polymerization. *Biochemistry*. **43**(9), pp.2475-83.
- Kostelansky, M.S. et al. 2007. Probing the gamma2 calcium-binding site: studies with gammaD298,301A fibrinogen reveal changes in the gamma294-301 loop that alter the integrity of the "a" polymerization site. *Biochemistry*. **46**(17), pp.5114-23.
- Krakow, W. et al. 1972. An electron microscopic investigation of the polymerization of bovine fibrin monomer. *Journal of Molecular Biology*. **71**(1), pp.95-103.
- Lacroix, R. et al. 2007. Activation of plasminogen into plasmin at the surface of endothelial microparticles: a mechanism that modulates angiogenic properties of endothelial progenitor cells in vitro. *Blood*. **110**(7), pp.2432-2439.
- Landmesser, U. et al. 2000. Endothelial dysfunction in hypercholesterolemia: mechanisms, pathophysiological importance, and therapeutic interventions. *Semin Thromb Hemost*. **26**(5), pp.529-37.
- Lane, D.A. et al. 1983. Delayed release of an abnormal fibrinopeptide A from fibrinogen Manchester: effect of the A $\alpha$  16 Arg  $\rightarrow$  His substitution upon fibrin monomer polymerization and the immunological crossreactivity of the peptide. *British Journal of Haematology*. **53**(4), pp.587-597.
- Lauricella, A.M. et al. 2006. Influence of homocysteine on fibrin network lysis. *Blood Coagul Fibrinolysis*. **17**(3), pp.181-6.
- Li, W. et al. 2017. Nonuniform Internal Structure of Fibrin Fibers: Protein Density and Bond Density Strongly Decrease with Increasing Diameter. *BioMed Research International*. **2017**, p13.
- Li, W. et al. 2016. Fibrin Fiber Stiffness Is Strongly Affected by Fiber Diameter, but Not by Fibrinogen Glycation. *Biophysical Journal*. **110**(6), pp.1400-1410.

- Lim, B.B. et al. 2008. Molecular basis of fibrin clot elasticity. *Structure*. **16**(3), pp.449-59.
- Litvinov, R.I. et al. 2007. Polymerization of fibrin: Direct observation and quantification of individual B:b knob-hole interactions. *Blood*. **109**(1), pp.130-8.
- Litvinov, R.I. et al. 2018. Regulatory element in fibrin triggers tension-activated transition from catch to slip bonds. *Proceedings of the National Academy of Sciences*. **115**(34), p8575.
- Liu, W. et al. 2010. The mechanical properties of single fibrin fibers. *Journal of thrombosis and haemostasis : JTH*. **8**(5), pp.1030-1036.
- Longstaff, C. and Kolev, K. 2015. Basic mechanisms and regulation of fibrinolysis. *J Thromb Haemost*. **13 Suppl 1**, pp.S98-105.
- Longstaff, C. et al. 2013. Mechanical Stability and Fibrinolytic Resistance of Clots Containing Fibrin, DNA, and Histones. *The Journal of Biological Chemistry*. **288**(10), pp.6946-6956.
- Lorand, L. and Middlebrook, W.R. 1952. The action of thrombin on fibrinogen. *Biochemical Journal*. **52**(2), pp.196-199.
- Lord, S.T. 2011. Molecular mechanisms affecting fibrin structure and stability. *Arteriosclerosis, thrombosis, and vascular biology*. **31**(3), pp.494-499.
- Lord, S.T. et al. 1993. Purification and characterization of recombinant human fibrinogen. *Blood Coagul Fibrinolysis*. **4**(1), pp.55-9.
- Lounes, K.C. et al. 2000. Fibrinogen Ales: a homozygous case of dysfibrinogenemia (gamma-Asp(330)-->Val) characterized by a defective fibrin polymerization site "a". *Blood*. **96**(10), pp.3473-9.
- Ma, T.M. et al. 2017. Structure, Mechanics, and Instability of Fibrin Clot Infected with *Staphylococcus epidermidis*. *Biophysical Journal*. **113**(9), pp.2100-2109.
- Maaroufi, R.M. et al. 1997. Mechanism of thrombin inhibition by antithrombin and heparin cofactor II in the presence of heparin. *Biomaterials*. **18**(3), pp.203-11.
- Machlus, K.R. et al. 2011. Causal relationship between hyperfibrinogenemia, thrombosis, and resistance to thrombolysis in mice. *Blood*. **117**(18), p4953.
- MacKintosh, F.C. et al. 1995. Elasticity of Semiflexible Biopolymer Networks. *Physical Review Letters*. **75**(24), pp.4425-4428.
- Mackman, N. 2009. The role of tissue factor and factor VIIa in hemostasis. *Anesthesia and analgesia*. **108**(5), pp.1447-1452.
- Macrae, F.L. et al. 2018. A fibrin biofilm covers the blood clot and protects from microbial invasion. *J Clin Invest*.
- Magalhaes, A. et al. 2016. LDL-Cholesterol Increases the Transcytosis of Molecules through Endothelial Monolayers. *PLoS ONE*. **11**(10), pe0163988.
- Magatti, D. et al. 2013. Modeling of fibrin gels based on confocal microscopy and light-scattering data. *Biophys J*. **104**(5), pp.1151-9.
- Mammen, E.F. et al. 1969. Congenital dysfibrinogenemia: fibrinogen detroit. *Journal of Clinical Investigation*. **48**(2), pp.235-249.
- Mangin, P.H. et al. 2018. Immobilized fibrinogen activates human platelets through glycoprotein VI. *Haematologica*. **103**(5), pp.898-907.
- Mann, K.G. et al. 1998. The role of the tissue factor pathway in initiation of coagulation. *Blood Coagul Fibrinolysis*. **9 Suppl 1**, pp.S3-7.

- Marguerie, G. et al. 1977. The binding of calcium to bovine fibrinogen. *Biochim Biophys Acta*. **490**(1), pp.94-103.
- Maroney, S.A. and Mast, A.E. 2008. Expression of Tissue Factor Pathway Inhibitor by Endothelial Cells and Platelets. *Transfusion and apheresis science : official journal of the World Apheresis Association : official journal of the European Society for Haemapheresis*. **38**(1), pp.9-14.
- Marshall, B.T. et al. 2003. Direct observation of catch bonds involving cell-adhesion molecules. *Nature*. **423**, p190.
- Mason, T.G. and Weitz, D.A. 1995. Optical Measurements of Frequency-Dependent Linear Viscoelastic Moduli of Complex Fluids. *Physical Review Letters*. **74**(7), pp.1250-1253.
- Mast Alan, E. 2016. Tissue Factor Pathway Inhibitor. *Arteriosclerosis, Thrombosis, and Vascular Biology*. **36**(1), pp.9-14.
- Mathonnet, F. et al. 2002. Fibrinogen Saint-Germain I: a case of the heterozygous Aalpha GLY 12 --> VAL fibrinogen variant. *Blood Coagul Fibrinolysis*. **13**(2), pp.149-53.
- McEver, R.P. and Zhu, C. 2010. Rolling Cell Adhesion. *Annual Review of Cell and Developmental Biology*. **26**(1), pp.363-396.
- Mendis, S. 2017. Global progress in prevention of cardiovascular disease. *Cardiovascular Diagnosis and Therapy*. **7**(Suppl 1), pp.S32-S38.
- Messner, B. and Bernhard, D. 2014. Smoking and cardiovascular disease: mechanisms of endothelial dysfunction and early atherogenesis. *Arterioscler Thromb Vasc Biol*. **34**(3), pp.509-15.
- Meyer, M. et al. 2003a. New molecular defects in the gamma subdomain of fibrinogen D-domain in four cases of (hypo)dysfibrinogenemia: fibrinogen variants Hannover VI, Homburg VII, Stuttgart and Suhl. *Thromb Haemost*. **89**(4), pp.637-46.
- Meyer, M. et al. 2003b. Fibrinogen Magdeburg I: a novel variant of human fibrinogen with an amino acid exchange in the fibrinopeptide A (Aalpha 9, Leu-->Pro). *Thromb Res*. **109**(2-3), pp.145-51.
- Morse, D.C. 1998a. Viscoelasticity of Concentrated Isotropic Solutions of Semiflexible Polymers. 1. Model and Stress Tensor. *Macromolecules*. **31**(20), pp.7030-7043.
- Morse, D.C. 1998b. Viscoelasticity of Concentrated Isotropic Solutions of Semiflexible Polymers. 2. Linear Response. *Macromolecules*. **31**(20), pp.7044-7067.
- Morse, D.C. 1999. Viscoelasticity of Concentrated Isotropic Solutions of Semiflexible Polymers. 3. Nonlinear Rheology. *Macromolecules*. **32**(18), pp.5934-5943.
- Mosesson, M.W. et al. 1987. Studies on the ultrastructure of fibrin lacking fibrinopeptide B (beta-fibrin). *Blood*. **69**(4), pp.1073-81.
- Mujumdar, V.S. et al. 2001. Induction of oxidative stress by homocyst(e)ine impairs endothelial function. *J Cell Biochem*. **82**(3), pp.491-500.
- Mullin, J.L. et al. 2000a. Recombinant Fibrinogen Studies Reveal That Thrombin Specificity Dictates Order of Fibrinopeptide Release. *Journal of Biological Chemistry*. **275**(33), pp.25239-25246.
- Mullin, J.L. et al. 2000b. Decreased lateral aggregation of a variant recombinant fibrinogen provides insight into the polymerization mechanism. *Biochemistry*. **39**(32), pp.9843-9.

- Mutch, N.J. et al. 2010. Polyphosphate modifies the fibrin network and down-regulates fibrinolysis by attenuating binding of tPA and plasminogen to fibrin. *Blood*. **115**(19), p3980.
- Nagy, J.A. et al. 1988. Biosynthesis of factor XIII A and B subunits. *Adv Exp Med Biol*. **231**, pp.29-49.
- Nair, C.H. et al. 1986. Effect of temperature, pH and ionic strength and composition on fibrin network structure and its development. *Thrombosis Research*. **42**(6), pp.809-816.
- Naudin, C. et al. 2017. Factor XII Contact Activation. *Semin Thromb Hemost*. **43**(8), pp.814-826.
- Nelb, G.W. et al. 1976. Rheology of fibrin clots. III. Shear creep and creep recovery of fine ligated and coarse unligated clots. *Biophys Chem*. **5**(3), pp.377-87.
- Nickerson, J.M. and Fuller, G.M. 1981. Modification of fibrinogen chains during synthesis: glycosylation of B beta and gamma chains. *Biochemistry*. **20**(10), pp.2818-21.
- Nieswandt, B. and Watson, S.P. 2003. Platelet-collagen interaction: is GPVI the central receptor? *Blood*. **102**(2), p449.
- Niwa, K. et al. 1993. Fibrinogen Mitaka II: a hereditary dysfibrinogen with defective thrombin binding caused by an A alpha Glu-11 to Gly substitution. *Blood*. **82**(12), pp.3658-63.
- Okumura, N. et al. 1997. Severely impaired polymerization of recombinant fibrinogen gamma-364 Asp --> His, the substitution discovered in a heterozygous individual. *J Biol Chem*. **272**(47), pp.29596-601.
- Paul, B.Z.S. et al. 1999. Molecular Mechanism of Thromboxane A<sub>2</sub>-induced Platelet Aggregation: ESSENTIAL ROLE FOR P2T AC and  $\alpha$ 2ARECEPTORS. *Journal of Biological Chemistry*. **274**(41), pp.29108-29114.
- Pechik, I. et al. 2006. STRUCTURAL BASIS FOR SEQUENTIAL CLEAVAGE OF FIBRINOPEPTIDES UPON FIBRIN ASSEMBLY. *Biochemistry*. **45**(11), pp.3588-3597.
- Perlmann, G.E. and Longworth, L.G. 1948. The specific refractive increment of some purified proteins. *J Am Chem Soc*. **70**(8), pp.2719-24.
- Peyvandi, F. et al. 2011. Role of von Willebrand factor in the haemostasis. *Blood Transfusion*. **9**(Suppl 2), pp.s3-s8.
- Phillippe, H.M. 2017. Overview of venous thromboembolism. *Am J Manag Care*. **23**(20 Suppl), pp.S376-s382.
- Piechocka, I.K. et al. 2010. Structural Hierarchy Governs Fibrin Gel Mechanics. *Biophysical Journal*. **98**(10), pp.2281-2289.
- Piechocka, I.K. et al. 2017. Recombinant fibrinogen reveals the differential roles of alpha- and gamma-chain cross-linking and molecular heterogeneity in fibrin clot strain-stiffening. *J Thromb Haemost*. **15**(5), pp.938-949.
- Podolnikova, N.P. et al. 2014. The Interaction of Integrin  $\alpha$ IIb $\beta$ 3 with Fibrin Occurs through Multiple Binding Sites in the  $\alpha$ IIb  $\beta$ -Propeller Domain. *Journal of Biological Chemistry*. **289**(4), pp.2371-2383.
- Poredos, P. and Jezovnik, M.K. 2017. Endothelial Dysfunction and Venous Thrombosis. *Angiology*. **69**(7), pp.564-567.
- Pratt, K.P. et al. 1997. The primary fibrin polymerization pocket: Three-dimensional structure of a 30-kDa C-terminal  $\gamma$  chain fragment complexed

- with the peptide Gly-Pro-Arg-Pro. *Proceedings of the National Academy of Sciences of the United States of America*. **94**(14), pp.7176-7181.
- Pretorius, E. et al. 2011. Differences in fibrin fiber diameters in healthy individuals and thromboembolic ischemic stroke patients. *Blood Coagul Fibrinolysis*. **22**(8), pp.696-700.
- Previtali, E. et al. 2011. Risk factors for venous and arterial thrombosis. *Blood Transfusion*. **9**(2), pp.120-138.
- Protopopova, A.D. et al. 2015. Visualization of fibrinogen alphaC regions and their arrangement during fibrin network formation by high-resolution AFM. *J Thromb Haemost*. **13**(4), pp.570-9.
- Protopopova, A.D. et al. 2017. Morphometric characterization of fibrinogen's alphaC regions and their role in fibrin self-assembly and molecular organization. *Nanoscale*. **9**(36), pp.13707-13716.
- Puddu, P. et al. 2000. Endothelial dysfunction in hypertension. *Acta Cardiol*. **55**(4), pp.221-32.
- Redman, C.M. and Xia, H. 2001. Fibrinogen biosynthesis. Assembly, intracellular degradation, and association with lipid synthesis and secretion. *Ann N Y Acad Sci*. **936**, pp.480-95.
- Reganon, E. et al. 1984. Gelation of fibrinogen in plasma. A kinetic study by turbidity measurement. *Haemostasis*. **14**(2), pp.170-8.
- Riedel, T. et al. 2011. Fibrinopeptides A and B release in the process of surface fibrin formation. *Blood*. **117**(5), pp.1700-1706.
- Rijken, D.C. and Uitte de Willige, S. 2017. Inhibition of Fibrinolysis by Coagulation Factor XIII. *BioMed Research International*. **2017**, p6.
- Rocco, M. 2008. Fibrin formation on fast forward. *Blood*. **111**(10), p4839.
- Rooney, M.M. et al. 1998. The contribution of the three hypothesized integrin-binding sites in fibrinogen to platelet-mediated clot retraction. *Blood*. **92**(7), pp.2374-81.
- Rosendaal, F.R. 2016. Causes of venous thrombosis. *Thrombosis Journal*. **14**(1), p24.
- Roth, G.A. et al. 2015. Global and regional patterns in cardiovascular mortality from 1990 to 2013. *Circulation*. **132**(17), pp.1667-78.
- Ruggeri, Z.M. et al. 2006. Activation-independent platelet adhesion and aggregation under elevated shear stress. *Blood*. **108**(6), pp.1903-1910.
- Ryan, E.A. et al. 1999a. Influence of a natural and a synthetic inhibitor of factor XIIIa on fibrin clot rheology. *Biophys J*. **77**(5), pp.2827-36.
- Ryan, E.A. et al. 1999b. Structural Origins of Fibrin Clot Rheology. *Biophysical Journal*. **77**(5), pp.2813-2826.
- Sadler, J.E. 1997. Thrombomodulin structure and function. *Thromb Haemost*. **78**(1), pp.392-5.
- Sahni, A. and Francis, C.W. 2000. Vascular endothelial growth factor binds to fibrinogen and fibrin and stimulates endothelial cell proliferation. *Blood*. **96**(12), pp.3772-8.
- Sahu, A. and Lambris, J.D. 2001. Structure and biology of complement protein C3, a connecting link between innate and acquired immunity. *Immunol Rev*. **180**, pp.35-48.
- Sakariassen, K.S. et al. 2015. The impact of blood shear rate on arterial thrombus formation. *Future Science OA*. **1**(4), pFSO30.
- Sakata, Y. and Aoki, N. 1980. Cross-linking of alpha 2-plasmin inhibitor to fibrin by fibrin-stabilizing factor. *J Clin Invest*. **65**(2), pp.290-7.

- Schielen, W.J. et al. 1990. Structural requirements of fibrinogen A alpha-(148-160) for the enhancement of the rate of plasminogen activation by tPA. *Blood Coagul Fibrinolysis*. **1**(4-5), pp.521-4.
- Schindelin, J. et al. 2012. Fiji: an open-source platform for biological-image analysis. *Nature Methods*. **9**, p676.
- Schmitt, C. et al. 2011. Characterization of blood clot viscoelasticity by dynamic ultrasound elastography and modeling of the rheological behavior. *J Biomech*. **44**(4), pp.622-9.
- Seo, J.-W. et al. 2015. Macrophage Differentiation from Monocytes Is Influenced by the Lipid Oxidation Degree of Low Density Lipoprotein. *Mediators of Inflammation*. **2015**, p235797.
- Shen, L. and Lorand, L. 1983. Contribution of fibrin stabilization to clot strength. Supplementation of factor XIII-deficient plasma with the purified zymogen. *The Journal of Clinical Investigation*. **71**(5), pp.1336-1341.
- Shen, L.L. et al. 1977. Role of fibrinopeptide B release: comparison of fibrins produced by thrombin and Ancrod. *Am J Physiol*. **232**(6), pp.H629-33.
- Sherry, S. 1954. THE FIBRINOLYTIC ACTIVITY OF STREPTOKINASE ACTIVATED HUMAN PLASMIN. *Journal of Clinical Investigation*. **33**(7), pp.1054-1063.
- Shimizu, A. et al. 1992. Photoaffinity labeling of the primary fibrin polymerization site: isolation and characterization of a labeled cyanogen bromide fragment corresponding to gamma-chain residues 337-379. *Proceedings of the National Academy of Sciences*. **89**(7), p2888.
- Sinha, A.K. et al. 1983. Inhibition of thromboxane A2 synthesis in human platelets by coagulation factor Xa. *Proc Natl Acad Sci U S A*. **80**(19), pp.6086-90.
- Slater, A. et al. 2018. Does fibrin(ogen) bind to monomeric or dimeric GPVI, or not at all? *Platelets*. pp.1-9.
- Smith, S.A. and Morrissey, J.H. 2008. Polyphosphate enhances fibrin clot structure. *Blood*. **112**(7), p2810.
- Smith, S.A. et al. 2015. How it all starts: Initiation of the clotting cascade. *Critical reviews in biochemistry and molecular biology*. **50**(4), pp.326-336.
- Spraggon, G. et al. 1997. Crystal structures of fragment D from human fibrinogen and its crosslinked counterpart from fibrin. *Nature*. **389**, p455.
- Stapleton, P.A. et al. 2010. Hypercholesterolemia and microvascular dysfunction: interventional strategies. *Journal of Inflammation (London, England)*. **7**, pp.54-54.
- Staton, C.A. et al. 2003. The role of fibrinogen and related fragments in tumour angiogenesis and metastasis. *Expert Opin Biol Ther*. **3**(7), pp.1105-20.
- Steinmann, C. et al. 1994. A new substitution, gamma 358 Ser--&gt;Cys, in fibrinogen Milano VII causes defective fibrin polymerization. *Blood*. **84**(6), p1874.
- Stoll, G. et al. 2008. Molecular mechanisms of thrombus formation in ischemic stroke: novel insights and targets for treatment. *Blood*. **112**(9), p3555.
- Storm, C. et al. 2005. Nonlinear elasticity in biological gels. *Nature*. **435**(7039), pp.191-4.
- Swiech, K. et al. 2017. Production of recombinant coagulation factors: Are humans the best host cells? *Bioengineered*. **8**(5), pp.462-470.

- Szczepaniak, P. et al. 2015. Increased Plasma Clot Permeability and Susceptibility to Lysis Are Associated with Heavy Menstrual Bleeding of Unknown Cause: A Case-Control Study. *PLoS ONE*. **10**(4), pe0125069.
- Tabas, I. 2010. Macrophage death and defective inflammation resolution in atherosclerosis. *Nature reviews. Immunology*. **10**(1), pp.36-46.
- Takebe, M. et al. 1995. Calcium ion-dependent monoclonal antibody against human fibrinogen: preparation, characterization, and application to fibrinogen purification. *Thromb Haemost.* **73**(4), pp.662-7.
- Takeda, Y. 1966. Studies of the metabolism and distribution of fibrinogen in healthy men with autologous 125-I-labeled fibrinogen. *J Clin Invest.* **45**(1), pp.103-11.
- Talman, V. and Ruskoaho, H. 2016. Cardiac fibrosis in myocardial infarction— from repair and remodeling to regeneration. *Cell and Tissue Research.* **365**(3), pp.563-581.
- Tatsumi, K. and Mackman, N. 2015. Tissue Factor and Atherothrombosis. *J Atheroscler Thromb.* **22**(6), pp.543-9.
- Tchaikovski, S.N. and Rosing, J. 2010. Mechanisms of estrogen-induced venous thromboembolism. *Thromb Res.* **126**(1), pp.5-11.
- Tennent, G.A. et al. 2007. Human plasma fibrinogen is synthesized in the liver. *Blood.* **109**(5), p1971.
- Terukina, S. et al. 1989. Fibrinogen Kyoto III: a congenital dysfibrinogen with a gamma aspartic acid-330 to tyrosine substitution manifesting impaired fibrin monomer polymerization. *Blood.* **74**(8), pp.2681-7.
- Tomaiuolo, M. et al. 2017. Regulation of platelet activation and coagulation and its role in vascular injury and arterial thrombosis. *Interventional cardiology clinics.* **6**(1), pp.1-12.
- Townsend, N. et al. 2016. Cardiovascular disease in Europe: epidemiological update 2016. *European Heart Journal.* **37**(42), pp.3232-3245.
- Tremoli, E. et al. 1999. Tissue factor in atherosclerosis. *Atherosclerosis.* **144**(2), pp.273-283.
- Tsurupa, G. et al. 2011. Structure, stability, and interaction of fibrin alphaC-domain polymers. *Biochemistry.* **50**(37), pp.8028-37.
- Ugarova, T.P. et al. 1998. Identification of a Novel Recognition Sequence for Integrin  $\alpha$ M $\beta$ 2 within the  $\gamma$ -chain of Fibrinogen. *Journal of Biological Chemistry.* **273**(35), pp.22519-22527.
- Ulrych, J. et al. 2016. 28 day post-operative persisted hypercoagulability after surgery for benign diseases: a prospective cohort study. *BMC Surgery.* **16**, p16.
- Undas, A. et al. 2009. Fibrinogen Krakow: a novel hypo/dysfibrinogenemia mutation in fibrinogen gamma chain (Asn325Ile) affecting fibrin clot structure and function. *Thromb Haemost.* **101**(5), pp.975-6.
- Van Zandt Hawn, C. and Porter, K.R. 1947. THE FINE STRUCTURE OF CLOTS FORMED FROM PURIFIED BOVINE FIBRINOGEN AND THROMBIN: A STUDY WITH THE ELECTRON MICROSCOPE. *J Exp Med.* **86**(4), pp.285-92.
- van Kempen, Thomas H. et al. 2014. A Constitutive Model for a Maturing Fibrin Network. *Biophysical Journal.* **107**(2), pp.504-513.
- Varadi, A. and Scheraga, H.A. 1986. Localization of segments essential for polymerization and for calcium binding in the .gamma.-chain of human fibrinogen. *Biochemistry.* **25**(3), pp.519-528.

- Wang, Z. et al. 2003. Platelet alpha2beta1 integrin activation: contribution of ligand internalization and the alpha2-cytoplasmic domain. *Blood*. **102**(4), pp.1307-15.
- Weisel, J.W. 1986. The electron microscope band pattern of human fibrin: various stains, lateral order, and carbohydrate localization. *J Ultrastruct Mol Struct Res*. **96**(1-3), pp.176-88.
- Weisel, J.W. 2004a. The mechanical properties of fibrin for basic scientists and clinicians. *Biophys Chem*. **112**(2-3), pp.267-76.
- Weisel, J.W. 2004b. The mechanical properties of fibrin for basic scientists and clinicians. *Biophysical Chemistry*. **112**(2), pp.267-276.
- Weisel, J.W., Dempfle, C.H. . 2012. Fibrinogen Structure and Function. In: Marder, V.J., Aird, W.C., Bennett, J.S., Schulman S., White, G.C II ed. *Hemostasis and Thrombosis Basic Principles and Clinical Practice*. Philadelphia: Lippincott Williams & Wilkins, pp.254-271.
- Weisel, J.W. and Litvinov, R.I. 2013. Mechanisms of fibrin polymerization and clinical implications. *Blood*. **121**(10), pp.1712-1719.
- Weisel, J.W. and Litvinov, R.I. 2017. Fibrin Formation, Structure and Properties. *Sub-cellular biochemistry*. **82**, pp.405-456.
- Weisel, J.W. and Medved, L. 2001. The structure and function of the alpha C domains of fibrinogen. *Ann N Y Acad Sci*. **936**, pp.312-27.
- Weisel, J.W. and Nagaswami, C. 1992. Computer modeling of fibrin polymerization kinetics correlated with electron microscope and turbidity observations: clot structure and assembly are kinetically controlled. *Biophys J*. **63**(1), pp.111-28.
- Wessler, S. 1962. Thrombosis in the presence of vascular stasis. *The American Journal of Medicine*. **33**(5), pp.648-666.
- Wolfenstein-Todel, C. and Mosesson, M.W. 1980. Human plasma fibrinogen heterogeneity: evidence for an extended carboxyl-terminal sequence in a normal gamma chain variant (gamma'). *Proceedings of the National Academy of Sciences of the United States of America*. **77**(9), pp.5069-5073.
- Wolfenstein-Todel, C. and Mosesson, M.W. 1981. Carboxy-terminal amino acid sequence of a human fibrinogen gamma-chain variant (gamma'). *Biochemistry*. **20**(21), pp.6146-9.
- Woulfe, D. et al. 2001. ADP and platelets: the end of the beginning. *Journal of Clinical Investigation*. **107**(12), pp.1503-1505.
- Xing, X. et al. 1998. LDL oxidation by activated monocytes: characterization of the oxidized LDL and requirement for transition metal ions. *Journal of Lipid Research*. **39**(11), pp.2201-2208.
- Yang, X. and Walsh, P.N. 2005. An ordered sequential mechanism for Factor IX and Factor IXa binding to platelet receptors in the assembly of the Factor X-activating complex. *The Biochemical journal*. **390**(Pt 1), pp.157-167.
- Yang, Z. et al. 2000. A model of fibrin formation based on crystal structures of fibrinogen and fibrin fragments complexed with synthetic peptides. *Proc Natl Acad Sci U S A*. **97**(26), pp.14156-61.
- Yee, V.C. et al. 1997. Crystal structure of a 30 kDa C-terminal fragment from the  $\gamma$  chain of human fibrinogen. *Structure*. **5**(1), pp.125-138.
- Yeromonahos, C. et al. 2010. Nanostructure of the Fibrin Clot. *Biophysical Journal*. **99**(7), pp.2018-2027.

- Yonekawa, O. et al. 1992. Localization in the fibrinogen gamma-chain of a new site that is involved in the acceleration of the tissue-type plasminogen activator-catalysed activation of plasminogen. *Biochem J.* **283 ( Pt 1)**, pp.187-91.
- Yu, S. et al. 1984. Fibrinogen precursors. Order of assembly of fibrinogen chains. *Journal of Biological Chemistry.* **259(16)**, pp.10574-10581.
- Zaky, A. 2017. Thromboelastometry Versus Rotational Thromboelastography in Cardiac Surgery. *Seminars in Cardiothoracic and Vascular Anesthesia.* **21(3)**, pp.206-211.
- Zaman, A.G. et al. 2000. The role of plaque rupture and thrombosis in coronary artery disease. *Atherosclerosis.* **149(2)**, pp.251-66.
- Zamarron, C. et al. 1984. Kinetics of the activation of plasminogen by natural and recombinant tissue-type plasminogen activator. *Journal of Biological Chemistry.* **259(4)**, pp.2080-2083.
- Zhang, J.Z. and Redman, C. 1996. Fibrinogen assembly and secretion. Role of intrachain disulfide loops. *J Biol Chem.* **271(47)**, pp.30083-8.
- Zhmurov, A. et al. 2011. Molecular Structural Origins of Clot and Thrombus Mechanical Properties. *Blood.* **118(21)**, p2257.
- Zhmurov, A. et al. 2016. Structural Basis of Interfacial Flexibility in Fibrin Oligomers. *Structure (London, England : 1993).* **24(11)**, pp.1907-1917.

# **Chapter 9 - Appendices**

## 9.1 - The DNA sequence of the pMLP-γA

>pMLP-γA. Primer binding sites highlighted in blue, start and stop codons of fibrinogen in yellow, target codons during mutagenesis highlighted in red.

```
CATCATCAATAATATACCTTATTTTTGGATTGAAGCCAATATGATAATGAGGGGGTGGAGT
TTGTGACGTGGCGCGGGGCGTGGGAACGGGGCGGGTGACGTAGTAGTGTGGCGGAAGTGT
GATGTTGCAAGTGTGGCGGAACACATGTAAGCGACGGATGTGGCAAAAGTGACGTTTTTTG
GTGTGCGCCGGTGTACACAGGAAGTGACAATTTTTCGCGCGGTTTTAGGCGGATGTTGTAG
TAAATTTGGGCGTAACCGAGTAAGATTTGGCCATTTTCGCGGGAAAACCTGAATAAGAGGA
AGTGAAATCTGAATAATTTGTGTTACTCATAGCGCGTAATATTTGTCTAGGGCCCAAGC
TTGTTTGCAAAAGCCTAGGCCTCCAAAAAGCCTCCTCACTACTTCTGGAATAGCTCAGA
GGCCGAGGCGGCCTCGGCCTCTGCATAAATAAAAAAATTAGTCAGCCATGGGGCGGAGA
ATGGGCGGAACCTGGGCGGAGTTAGGGGCGGGATGGGCGGAGTTAGGGGCGGACTATGGT
TGCTGACTAATTGAGATGCATGCTTTGCATACTTCTGCCTGCTGGGGAGCCTGGGGACTT
TCCACACCTGGTTGCTGACTAATTGAGATGCATGCTTTGCATACTTCTGCCTGCTGGGGA
GCCTGGGGACTTTCACACCCCTAAGTACACACATTCACAGCTGGTTCTTTCCGCCTCA
GAAGGGTACCCGGTCTCCTCGTATAGAAACTCGGACCACTCTGAGACGAAGGCTCGCGT
CCAGGCCAGCACGAAGGAGGCTAAGTGGGAGGGTAGCGGTGCTTGTCCACTAGGGGGTCT
CACTCGCTCCAGGGTGTGAAGACACATGTGCGCCTCTTCGGCATCAAGGAAGGTGATTGG
TTTATAGGTGTAGGCCACGTGACCGGGTGTTCCTGAAGGGGGGCTATAAAAGGGGGTGGG
GGCGCGTTCGTCCTCACTCTCTTCCGCATCGCTGTCTGCGAGGGCCAGCTGTTGGGCTCG
CGTTGAGGACAAAACCTCTTCGCGGTCTTTCCAGTACTCTTGATCGGAAACCCGTCGGCC
TCCGAACGTACTCCGCCACCGAGGGACCTGAGCGAGTCCGCATCGACCGGATCGGAAAAC
CTCTCGAGAAAGCGTCTAACCAGTCACAGTCGCAAGGTAGGCTGAGCACCGTGGCGGGC
GGCAGCGGGTGGCGGTGGGGTTGTTTCTGGCGGAGGTGCTGCTGATGATGTAATTAAG
TAGGCCGTCTTGAGACGGCGGATGGTTCGAGCTTGAGGTGTGGCAGGCTTCAGATCTGGCC
ATACACTTGAGTGACAATGACATCCACTTTGCCTTTCTCTCCACAGGTGTCCACTCCAG
GTCCAACCTGATCAGAATTGCGCCGCTCTCGAGTGAATTTGTCGACCGGCCCCAGCTCC
GGGCACCTCAGACATCATGATGTTGGTCTTGCACCCCGGAATTTAATTCTCTACTTCTAT
GCTCTTTTATTTCTCTCTTCAACATGTGTAGCATATGTTGCTACCAGAGACAACCTGCTGC
ATCTTAGATGAAAGATTTCGGTAGTTATTGTCCAACCTACCTGTGGCATTGCAGATTTCCCTG
TCTACTTATCAAACCAAAGTAGACAAGGATCTACAGTCTTTGGAAGACATCTTACATCAA
GTTGAAAACAAAACATCAGAAGTCAAACAGCTGATAAAGCAATCCAACCTCACTTATAAT
CCTGATGAATCATCAAACCAAATATGATAGACGCTGCTACTTTGAAGTCCAGGAAAAATG
TTAGAAGAAATATGAAATATGAAGCATCGATTTTAAACATGACTCAAGTATTCGATAT
TTGCAGGAAATATATAATTCAAATAATCAAAGATTGTTAACCTGAAAGAGAAGGTAGCC
CAGCTTGAAGCACAGTCCAGGAACCTTGCAAAGACACGGTGCAAATCCATGATATCACT
GGGAAAGATTGTCAAGACATTGCCAATAAGGGAGCTAAACAGAGCGGGCTTTACTTTATT
AAACCTCTGAAAGCTAACCAGCAATCTTAGTCTACTGTGAAATCGATGGGTCTGGAAAT
GGATGGACTGTGTTTCAAGAGAGACTTGTATGGCAGTGTAGATTTCAAGAAAAACTGGATT
CAATATAAAGAAGGATTTGGACATCTGTCTCCTACTGGCACAACAGAATTTTGGCTGGGA
AATGAGAAGATTCAATTGATAAGCACACAGTCTGCCATCCCATATGCATTAAGAGTGGAA
CTGGAAGACTGGAATGGCAGAACCACTGACTGCAGACTATGCCATGTTCAAGGTGGGACCT
GAAGCTGACAAGTACCGCCTAACATATGCCTACTTTCGCTGGTGGGGATGCTGGAGATGCC
TTTGATGGCTTTGATTTTGGCGATGATCCTAGTGACAAGTTTTTTCACATCCCATATGGC
ATGCAGTTCAGTACCTGGGACAATGACAATGATAAGTTTGAAGGCAACTGTGCTGAACAG
GATGGATCTGGTGGTGGATGAACAAGTGTACGCTGGCCATCTCAATGGAGTTTATTAC
CAAGGTGGCACTTACTCAAAAAGCATCTACTCCTAATGGTTATGATAATGGCATTATTTGG
GCCACTTGGAAAACCCGGTGGTATTCCATGAAGAAAACCACTATGAAGATAATCCCATTC
AACAGACTCACAATTGAGAAGGACAGCAACACCACCTGGGGGGAGCCAAACAGGCTGGA
GACGTTTAAAGACCGTTTCAAAGAGATTTACTTTTTTAAAGACTTTATCTGAACAGA
GAGATATAATGGGCGGCCGCAATTCTGATCATAATCAGCCATACCACATTTGTAGAGGTT
TTACTTGCTTTAAAAAACCTCCACACCTCCCCCTGAACCTGAAAACATAAAATGAATGCA
ATTGTTGTTGTTAACTTGTATTATTCAGCTTATAATGGTTACAAATAAAGCAATAGCATC
ACAAATTTCAAAAATAAGCATTTTTTTCACTGCATCTAGTTGTGGTTTTGTCCAACTC
```

*pMLP-F1*

*FbgGg-F1*

*FbgGg-F2*

*pMLP-R1*

ATCAATGTATCTTATCATGTCTGGATCCTCTACGCCGGACGCATCGTGGCCGGCATCACC  
GGCGCCACAGGTGCGGTTGCTGGCGCCTATATCGCCGACATCACCGATGGGGAAGATCGG  
GCTCGCCACTTCGGGCTCATGAGCGCTTGTTTCGGCGTGGGTATGGTGGCAGGCCCGTG  
GCCGGGGACTGTTGGGCGCCATCTCCTTGCATGCACCATTCTTGGGGCGCGGTGCTC  
AACGGCCTCAACCTACTACTGGGCTGCTTCTTAATGCAGGAGTCGCATAAGGGAGGGCTC  
TAGACGATGCCCTTGAGAGCCTTCAACCCAGTCAGCTCCTTCCGGTGGGCGCGGGGCATG  
ACTATCGTCGCCGCACTTATGACTGTCTTCTTTATCATGCAACTCGTAGGACAGGTGCCG  
GCAGCGCTCTGGGTCATTTTCGGCGAGGACCGCTTTCGCTGGAGCGCGACGATGATCGGC  
CTGTGCTTGGGATATTCGGAATCTTGCACGCCCTCGCTCAAGCCTTCGTCACTGGTCCC  
GCCACCAACGTTTCGGCGAGAAGCAGGCCATTATCGCCGGCATGGCGGCCGACCGCGTG  
GGCTACGTCCTTGTGGCGTTTCGCGACGCGAGGCTGGATGGCCTTCCCATTATGATTCTT  
CTCGCTTCCGGCGGCATCGGGATGCCCGCTTGCAGGCCATGCTGTCCAGGCAGGTAGAT  
GACGACCATCAGGGACAGCAAAAGGCCAGCAAAAGGCCAGGAACCGTAAAAAGGCCGCT  
TGCTGGCGTTTTTCCATAGGCTCCGCCCCCTGACGAGCATCAAAAAATCGACGCTCAA  
GTCAGAGGTGGCGAAAACCCGACAGGACTATAAAGATACCAGGCGTTTCCCCCTGGAAGCT  
CCCTCGTGCGCTCTCTGTTCCGACCCTGCCGCTTACCGGATACCTGTCCGCTTTCTCC  
CTTCGGGAAGCGTGGCGCTTTCTCATAGCTCACGCTGTAGGTATCTCAGTTCGGTGTAGG  
TCGTTGCTCCAAGCTGGGCTGTGTGCACGAACCCCCGTTAGCCCGACCGCTGCGCCT  
TATCCGGTAACCTATCGTCTTGAGTCCAACCCGGTAAGACACGACTTATCGCCACTGGCAG  
CAGCCACTGGTTAACAGGATTAGCAGAGCGAGGTATGTAGCGGTGCTACAGAGTTCTTGA  
AGTGGTGGCCTAACTACGGCTACACTAGAAGGACAGTATTTGGTATCTGCGCTCTXTGA  
AGCCAGTTACCTTCGGAAGAAAGAGTTGGTAGCTCTTGATCCGGCAAAACAAACCACCGCTG  
GTAGCGGTGGTTTTTTTTGTTTGAAGCAGCAGATTACGCGCAGAAAAAAGGATCTCAAG  
AAGATCCTTTGATCTTTTTCTACGGGGTCTGACGCTCAGTGAACGAAAACCTCACGTTAAG  
GGATTTTGGTATGAGATTATCAAAAAGGATCTTACCTAGATCCTTTTAAATTAATAAT  
GAAGTTTTAAATCAATCTAAAGTATATATGAGTAACTTGGTCTGACAGTTACCAATGCT  
TAATCAGTGAGGCACCTATCTCAGCGATCTGTCTATTTTCGTTTCATCCATAGTTGCCTGAC  
TCCCCGTCGTGTAGATAACTACGATACGGGAGGGCTTACCATCTGGCCCCAGTGTGCAA  
TGATACCGCGAGACCCACGCTCACCGGCTCCAGATTTATCAGCAATAAACCAGCCAGCCG  
GAAGGGCCGAGCGCAGAAGTGGTCCTGCAACTTTATCCGCCTCCATCCAGTCTATTAATT  
GTTGCCGGGAAGCTAGAGTAAGTAGTTCCGCAAGTTAATAGTTTGCGCAACGTTGTTGCCA  
TTGCTGCAGGCATCGTGGTGTACGCTCGTCTGTTGGTATGGCTTCATTCAGCTCCGGTT  
CCCAACGATCAAGGCGAGTTACATGATCCCCATGTTGTGCAAAAAAGCGGTTAGCTCCT  
TCGGTCTCCGATCGTTGTGAGAAGTAAGTTGGCCGAGTGTATCACTCATGGTTATGG  
CAGCACTGCATAATCTCTTACTGTATGCCATCCGTAAGATGCTTTTCTGTGACTGGTG  
AGTACTCAACCAAGTCATTTCTGAGAATAGTGTATGCGGCGACCCGAGTTGCTCTTGCCCGG  
CGTCAACACGGGATAATACCGCGCCACATAGCAGAACTTTAAAAGTGCTCATCATTGGAA  
AACGTTCTTCGGGGCGAAAACCTCTCAAGGATCTTACCCTGTTGAGATCCAGGTCGATGT  
AACCCACTCGTGCACCCAACTGATCTTTCAGCATCTTTTACTTTTACCAGCGTTTCTGGGT  
GAGCAAAAACAGGAAGGCAAAATGCCGCAAAAAAGGGAATAAGGGCGACACGGAATGTT  
GAATACTCATACTCTTCTTTTTCAATATTTATGAAGCATTTATCAGGGTTATTTGTCTCA  
TGAGCGGATACATATTTGAATGTATTTAGAAAAATAAACAAATAGGGGTTCCGCGCACAT  
TTCCCCGAAAAGTGCCACCTGACGTCTAAGAAACCATTATTTATCATGACATTAACCTATA  
AAAATAGGCGTATCACGAGGCCCTTTCTGCTTCAAGA

## 9.2 - Sequence alignments of WT with recombinant variants

### D297N variant

>pMLP+Fbg-γ WT compared to pMLP+Fbg-γ D297N

WT	ATGAGTTGGTCCTTGCACCCCGGAATTTAATTCTCTACTTCTATGCTCTTTTATTCTC	60
D297N	ATGAGTTGGTCCTTGCACCCCGGAATTTAATTCTCTACTTCTATGCTCTTTTATTCTC *****	60
WT	TCTTCAACATGTGTAGCATATGTTGCTACCAGAGACAACCTGCTGCATCTTAGATGAAAGA	120
D297N	TCTTCAACATGTGTAGCATATGTTGCTACCAGAGACAACCTGCTGCATCTTAGATGAAAGA *****	120
WT	TTCGGTAGTTATTGTCCAACCTACCTGTGGCATTGCAGATTTCTGTCTACTTATCAAACC	180
D297N	TTCGGTAGTTATTGTCCAACCTACCTGTGGCATTGCAGATTTCTGTCTACTTATCAAACC *****	180
WT	AAAGTAGACAAGGATCTACAGTCTTTGGAAGACATCTTACATCAAGTTGAAAACAAAACA	240
D297N	AAAGTAGACAAGGATCTACAGTCTTTGGAAGACATCTTACATCAAGTTGAAAACAAAACA *****	240
WT	TCAGAAGTCAAACAGCTGATAAAAAGCAATCCAACCTCACTTATAATCCTGATGAATCATCA	300
D297N	TCAGAAGTCAAACAGCTGATAAAAAGCAATCCAACCTCACTTATAATCCTGATGAATCATCA *****	300
WT	AAACCAAATATGATAGACGCTGCTACTTTGAAGTCCAGGAAAATGTTAGAAGAAATATG	360
D297N	AAACCAAATATGATAGACGCTGCTACTTTGAAGTCCAGGAAAATGTTAGAAGAAATATG *****	360
WT	AAATATGAAGCATCGATTTTAAACACATGACTCAAGTATTTCGATATTTGCAGGAAATATAT	420
D297N	AAATATGAAGCATCGATTTTAAACACATGACTCAAGTATTTCGATATTTGCAGGAAATATAT *****	420
WT	AATTCAAATAATCAAAGATTGTTAACCTGAAAGAGAAGGTAGCCAGCTTGAAGCACAG	480
D297N	AATTCAAATAATCAAAGATTGTTAACCTGAAAGAGAAGGTAGCCAGCTTGAAGCACAG *****	480
WT	TGCCAGGAACCTTGCAAAGACACGGTGCAAATCCATGATATCACTGGGAAAGATTGTCAA	540
D297N	TGCCAGGAACCTTGCAAAGACACGGTGCAAATCCATGATATCACTGGGAAAGATTGTCAA *****	540
WT	GACATTGCCAATAAGGGAGCTAAACAGAGCGGGCTTTACTTTATTAAACCTCTGAAAGCT	600
D297N	GACATTGCCAATAAGGGAGCTAAACAGAGCGGGCTTTACTTTATTAAACCTCTGAAAGCT *****	600
WT	AACCAGCAATTCTTAGTCTACTGTGAAATCGATGGGTCTGGAAATGGATGGACTGTGTTT	660
D297N	AACCAGCAATTCTTAGTCTACTGTGAAATCGATGGGTCTGGAAATGGATGGACTGTGTTT *****	660
WT	CAGAAGAGACTTGATGGCAGTGTAGATTTCAAGAAAACTGGATTCAATATAAAGAAGGA	720
D297N	CAGAAGAGACTTGATGGCAGTGTAGATTTCAAGAAAACTGGATTCAATATAAAGAAGGA *****	720
WT	TTTGACATCTGTCTCCTACTGGCACAACAGAATTTTGGCTGGGAAATGAGAAGATTCAT	780
D297N	TTTGACATCTGTCTCCTACTGGCACAACAGAATTTTGGCTGGGAAATGAGAAGATTCAT *****	780
WT	TTGATAAGCACACAGTCTGCCATCCCATATGCATTAAGAGTGGAACCTGGAAGACTGGAAT	840
D297N	TTGATAAGCACACAGTCTGCCATCCCATATGCATTAAGAGTGGAACCTGGAAGACTGGAAT *****	840
WT	GGCAGAACCAGTACTGCAGACTATGCCATGTTCAAGGTGGGACCTGAAGCTGACAAGTAC	900
D297N	GGCAGAACCAGTACTGCAGACTATGCCATGTTCAAGGTGGGACCTGAAGCTGACAAGTAC *****	900
WT	CGCCTAACATATGCCTACTTCGCTGGTGGGGATGCTGGAGATGCCTTTGATGGCTTTGAT	960
D297N	CGCCTAACATATGCCTACTTCGCTGGTGGGGATGCTGGAGATGCCTTTGATGGCTTTGAT *****	960
WT	TTTGGCAGATGATCCTAGTGACAAGTTTTTTCACATCCCATAAATGGCATGCAGTTCAGTACC	1020
D297N	TTTGGCAGATGATCCTAGTGACAAGTTTTTTCACATCCCATAAATGGCATGCAGTTCAGTACC *****	1020

WT	TGGGACAATGACAATGATAAGTTTGAAGGCAACTGTGCTGAACAGGATGGATCTGGTTGG	1080
D297N	TGGGACAATGACAATGATAAGTTTGAAGGCAACTGTGCTGAACAGGATGGATCTGGTTGG *****	1080
WT	TGGATGAACAAGTGTACGCTGGCCATCTCAATGGAGTTTATTACCAAGGTGGCACTTAC	1140
D297N	TGGATGAACAAGTGTACGCTGGCCATCTCAATGGAGTTTATTACCAAGGTGGCACTTAC *****	1140
WT	TCAAAGCATCTACTCCTAATGGTTATGATAATGGCATTATTTGGGCCACTTGGAAAACC	1200
D297N	TCAAAGCATCTACTCCTAATGGTTATGATAATGGCATTATTTGGGCCACTTGGAAAACC *****	1200
WT	CGGTGGTATTCATGAAGAAAACCCTATGAAGATAATCCATTCAACAGACTCACAATT	1260
D297N	CGGTGGTATTCATGAAGAAAACCCTATGAAGATAATCCATTCAACAGACTCACAATT *****	1260
WT	GGAGAAGGACAGCAACACCACCTGGGGGGAGCCAACAGGCTGGAGACGTTTAA1314	
D297N	GGAGAAGGACAGCAACACCACCTGGGGGGAGCCAACAGGCTGGAGACGTTTAA1314 *****	

### **E323Q variant**

#### **>pMLP+Fbg-γ WT compared to pMLP+Fbg-γ E323Q**

WT	ATGAGTTGGTCCTTGACCCCGGAATTTAATCTCTACTTCTATGCTCTTTTATTCTC	60
E323Q	ATGAGTTGGTCCTTGACCCCGGAATTTAATCTCTACTTCTATGCTCTTTTATTCTC *****	60
WT	TCTTCAACATGTGTAGCATATGTTGCTACCAGAGACAACCTGCTGCATCTTAGATGAAAGA	120
E323Q	TCTTCAACATGTGTAGCATATGTTGCTACCAGAGACAACCTGCTGCATCTTAGATGAAAGA *****	120
WT	TTCGGTAGTTATTGTCCAACCTACCTGTGGCATTGCAGATTTCCTGTCTACTTATCAAACC	180
E323Q	TTCGGTAGTTATTGTCCAACCTACCTGTGGCATTGCAGATTTCCTGTCTACTTATCAAACC *****	180
WT	AAAGTAGACAAGGATCTACAGTCTTTGGAAGACATCTTACATCAAGTTGAAAACAAAACA	240
E323Q	AAAGTAGACAAGGATCTACAGTCTTTGGAAGACATCTTACATCAAGTTGAAAACAAAACA *****	240
WT	TCAGAAGTCAAACAGCTGATAAAAGCAATCCAACCTCACTTATAATCCTGATGAATCATCA	300
E323Q	TCAGAAGTCAAACAGCTGATAAAAGCAATCCAACCTCACTTATAATCCTGATGAATCATCA *****	300
WT	AAACCAAATATGATAGACGCTGCTACTTTGAAGTCCAGGAAAATGTTAGAAGAAATATG	360
E323Q	AAACCAAATATGATAGACGCTGCTACTTTGAAGTCCAGGAAAATGTTAGAAGAAATATG *****	360
WT	AAATATGAAGCATCGATTTTAAACACATGACTCAAGTATTCGATATTTGCAGGAAATATAT	420
E323Q	AAATATGAAGCATCGATTTTAAACACATGACTCAAGTATTCGATATTTGCAGGAAATATAT *****	420
WT	AATTCAAATAATCAAAGATTGTTAACCTGAAAGAGAAGGTAGCCAGCTTGAAGCACAG	480
E323Q	AATTCAAATAATCAAAGATTGTTAACCTGAAAGAGAAGGTAGCCAGCTTGAAGCACAG *****	480
WT	TGCCAGGAACCTTGCAAAGACACGGTGCAAATCCATGATATCACTGGGAAAGATTGTCAA	540
E323Q	TGCCAGGAACCTTGCAAAGACACGGTGCAAATCCATGATATCACTGGGAAAGATTGTCAA *****	540
WT	GACATTGCCAATAAGGGAGCTAAACAGAGCGGGCTTACTTTATTAAACCTCTGAAAGCT	600
E323Q	GACATTGCCAATAAGGGAGCTAAACAGAGCGGGCTTACTTTATTAAACCTCTGAAAGCT *****	600
WT	AACCAGCAATTCTTAGTCTACTGTGAAATCGATGGGTCTGGAAATGGATGGACTGTGTTT	660
E323Q	AACCAGCAATTCTTAGTCTACTGTGAAATCGATGGGTCTGGAAATGGATGGACTGTGTTT *****	660
WT	CAGAAGAGACTTGATGGCAGTGTAGATTTCAAGAAAACTGGATTCAATATAAAGAAGGA	720
E323Q	CAGAAGAGACTTGATGGCAGTGTAGATTTCAAGAAAACTGGATTCAATATAAAGAAGGA *****	720
WT	TTTGGACATCTGTCTCCTACTGGCACAACAGAATTTTGGCTGGGAAATGAGAAGATTTCAT	780
E323Q	TTTGGACATCTGTCTCCTACTGGCACAACAGAATTTTGGCTGGGAAATGAGAAGATTTCAT *****	780

WT	TTGATAAGCACACAGTCTGCCATCCCATATGCATTAAGAGTGGAAGTGAAGACTGGAAT	840
E323Q	TTGATAAGCACACAGTCTGCCATCCCATATGCATTAAGAGTGGAAGTGAAGACTGGAAT *****	840
WT	GGCAGAACCAGTACTGCAGACTATGCCATGTTCAAGGTGGGACCTGAAGCTGACAAGTAC	900
E323Q	GGCAGAACCAGTACTGCAGACTATGCCATGTTCAAGGTGGGACCTGAAGCTGACAAGTAC *****	900
WT	CGCCTAACATATGCCTACTTCGCTGGTGGGGATGCTGGAGATGCCCTTGATGGCTTTGAT	960
E323Q	CGCCTAACATATGCCTACTTCGCTGGTGGGGATGCTGGAGATGCCCTTGATGGCTTTGAT *****	960
WT	TTTGGCGATGATCCTAGTGACAAGTTTTTTCACATCCCATATGGCATGCAGTTCAGTACC	1020
E323Q	TTTGGCGATGATCCTAGTGACAAGTTTTTTCACATCCCATATGGCATGCAGTTCAGTACC *****	1020
WT	TGGGACAATGACAATGATAAGTTTCAAGGCAACTGTGCTGAACAGGATGGATCTGGTTGG	1080
E323Q	TGGGACAATGACAATGATAAGTTTCAAGGCAACTGTGCTGAACAGGATGGATCTGGTTGG *****	1080
WT	TGGATGAACAAGTGTACGCTGGCCATCTCAATGGAGTTTATTACCAAGGTGGCACTTAC	1140
E323Q	TGGATGAACAAGTGTACGCTGGCCATCTCAATGGAGTTTATTACCAAGGTGGCACTTAC *****	1140
WT	TCAAAGCATCTACTCCTAATGGTTATGATAATGGCATTATTTGGGCCACTTGAAAAACC	1200
E323Q	TCAAAGCATCTACTCCTAATGGTTATGATAATGGCATTATTTGGGCCACTTGAAAAACC *****	1200
WT	CGGTGGTATTCATGAAGAAAACCACTATGAAGATAATCCATTCAACAGACTCACAATT	1260
E323Q	CGGTGGTATTCATGAAGAAAACCACTATGAAGATAATCCATTCAACAGACTCACAATT *****	1260
WT	GGAGAAGGACAGCAACACCACCTGGGGGGAGCCAAACAGGCTGGAGACGTTAA1314	
E323Q	GGAGAAGGACAGCAACACCACCTGGGGGGAGCCAAACAGGCTGGAGACGTTAA1314 *****	

## **K356Q variant**

### **>pMLP+Fbg-γ WT compared to pMLP+Fbg-γ K356Q**

WT	ATGAGTTGGTCCTTGCACCCCGGAATTTAATTCCTACTTCTATGCTCTTTATTCTC	60
K356Q	ATGAGTTGGTCCTTGCACCCCGGAATTTAATTCCTACTTCTATGCTCTTTATTCTC *****	60
WT	TCTTCAACATGTGTAGCATATGTTGCTACCAGAGACAACCTGCTGCATCTTAGATGAAAGA	120
K356Q	TCTTCAACATGTGTAGCATATGTTGCTACCAGAGACAACCTGCTGCATCTTAGATGAAAGA *****	120
WT	TTCGGTAGTTATTGTCCAACCTACCTGTGGCATTGCAGATTCCTGTCTACTTATCAAACC	180
K356Q	TTCGGTAGTTATTGTCCAACCTACCTGTGGCATTGCAGATTCCTGTCTACTTATCAAACC *****	180
WT	AAAGTAGACAAGGATCTACAGTCTTTGGAAGACATCTTACATCAAGTTGAAAACAAAACA	240
K356Q	AAAGTAGACAAGGATCTACAGTCTTTGGAAGACATCTTACATCAAGTTGAAAACAAAACA *****	240
WT	TCAGAAGTCAAACAGCTGATAAAAGCAATCCAACCTCACTTATAATCCTGATGAATCATCA	300
K356Q	TCAGAAGTCAAACAGCTGATAAAAGCAATCCAACCTCACTTATAATCCTGATGAATCATCA *****	300
WT	AAACCAAATATGATAGACGCTGCTACTTTGAAGTCCAGGAAAATGTAGAAGAAATATG	360
K356Q	AAACCAAATATGATAGACGCTGCTACTTTGAAGTCCAGGAAAATGTAGAAGAAATATG *****	360
WT	AAATATGAAGCATCGATTTTAAACACATGACTCAAGTATTCGATATTTGCAGGAAATATAT	420
K356Q	AAATATGAAGCATCGATTTTAAACACATGACTCAAGTATTCGATATTTGCAGGAAATATAT *****	420
WT	AATTCAAATAATCAAAGATTGTTAACCTGAAAGAGAAGGTAGCCAGCTTGAAGCACAG	480
K356Q	AATTCAAATAATCAAAGATTGTTAACCTGAAAGAGAAGGTAGCCAGCTTGAAGCACAG *****	480
WT	TGCCAGGAACCTTGCAAAGACACGGTGCAAATCCATGATATCACTGGGAAAGATTGTCAA	540
K356Q	TGCCAGGAACCTTGCAAAGACACGGTGCAAATCCATGATATCACTGGGAAAGATTGTCAA *****	540

WT	GACATTGCCAATAAGGGAGCTAAACAGAGCGGGCTTACTTTATTAAACCTCTGAAAGCT	600
K356Q	GACATTGCCAATAAGGGAGCTAAACAGAGCGGGCTTACTTTATTAAACCTCTGAAAGCT *****	600
WT	AACCAGCAATTCTTAGTCTACTGTGAAATCGATGGGCTGGAAATGGATGGACTGTGTTT	660
K356Q	AACCAGCAATTCTTAGTCTACTGTGAAATCGATGGGCTGGAAATGGATGGACTGTGTTT *****	660
WT	CAGAAGAGACTTGATGGCAGTGTAGATTTCAAGAAAACTGGATTCAATATAAAGAAGGA	720
K356Q	CAGAAGAGACTTGATGGCAGTGTAGATTTCAAGAAAACTGGATTCAATATAAAGAAGGA *****	720
WT	TTTGGACATCTGTCTCCTACTGGCACAACAGAATTTTGGCTGGGAAATGAGAAGATTCAT	780
K356Q	TTTGGACATCTGTCTCCTACTGGCACAACAGAATTTTGGCTGGGAAATGAGAAGATTCAT *****	780
WT	TTGATAAGCACACAGTCTGCCATCCCATATGCATTAAGAGTGGAACTGGAAGACTGGAAT	840
K356Q	TTGATAAGCACACAGTCTGCCATCCCATATGCATTAAGAGTGGAACTGGAAGACTGGAAT *****	840
WT	GGCAGAACCAGTACTGCAGACTATGCCATGTTCAAGGTGGGACCTGAAGCTGACAAGTAC	900
K356Q	GGCAGAACCAGTACTGCAGACTATGCCATGTTCAAGGTGGGACCTGAAGCTGACAAGTAC *****	900
WT	CGCCTAACATATGCCTACTTCGCTGGTGGGGATGCTGGAGATGCCTTTGATGGCTTTGAT	960
K356Q	CGCCTAACATATGCCTACTTCGCTGGTGGGGATGCTGGAGATGCCTTTGATGGCTTTGAT *****	960
WT	TTTGGCGATGATCCTAGTGACAAGTTTTTACATCCCATAATGGCATGCAGTTCAGTACC	1020
K356Q	TTTGGCGATGATCCTAGTGACAAGTTTTTACATCCCATAATGGCATGCAGTTCAGTACC *****	1020
WT	TGGGACAATGACAATGATAAGTTTGAAGGCAACTGTGCTGAACAGGATGGATCTGGTTGG	1080
K356Q	TGGGACAATGACAATGATAAGTTTGAAGGCAACTGTGCTGAACAGGATGGATCTGGTTGG *****	1080
WT	TGGATGAACAAGTGTACGCTGGCCATCTCAATGGAGTTTATTACCAAGGTGGCACTTAC	1140
K356Q	TGGATGAACAAGTGTACGCTGGCCATCTCAATGGAGTTTATTACCAAGGTGGCACTTAC *****	1140
WT	TCAAAGCATCTACTCCTAATGGTTATGATAATGGCATTATTTGGGCCACTTGGAAAACC	1200
K356Q	TCAAAGCATCTACTCCTAATGGTTATGATAATGGCATTATTTGGGCCACTTGGAAAACC *** *****	1200
WT	CGGTGGTATTCATGAAGAAAACCCTATGAAGATAATCCCATTCACAGACTCACAATT	1260
K356Q	CGGTGGTATTCATGAAGAAAACCCTATGAAGATAATCCCATTCACAGACTCACAATT *****	1260
WT	GGAGAAGGACAGCAACACCACCTGGGGGGAGCCAAACAGGCTGGAGACGTTTAA1314	
K356Q	GGAGAAGGACAGCAACACCACCTGGGGGGAGCCAAACAGGCTGGAGACGTTTAA1314 *****	

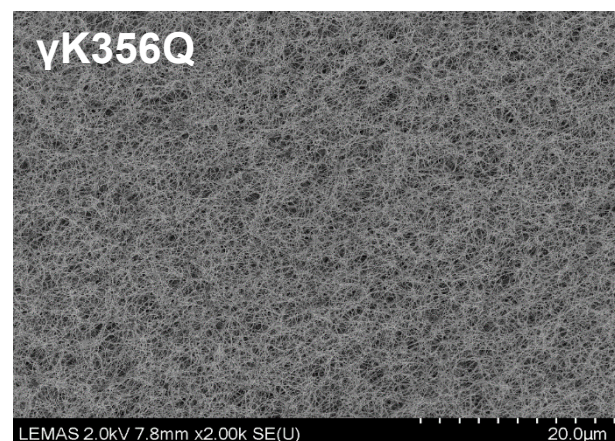
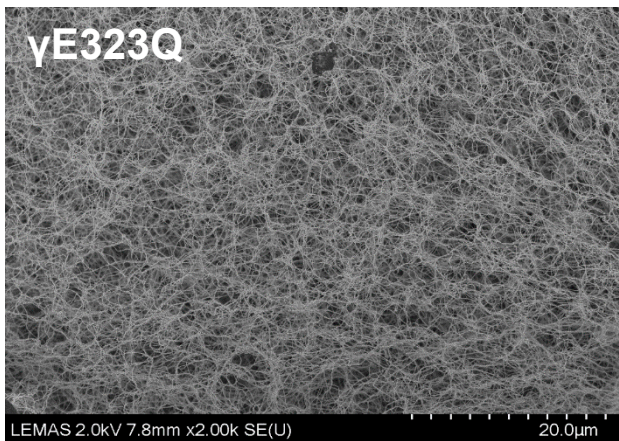
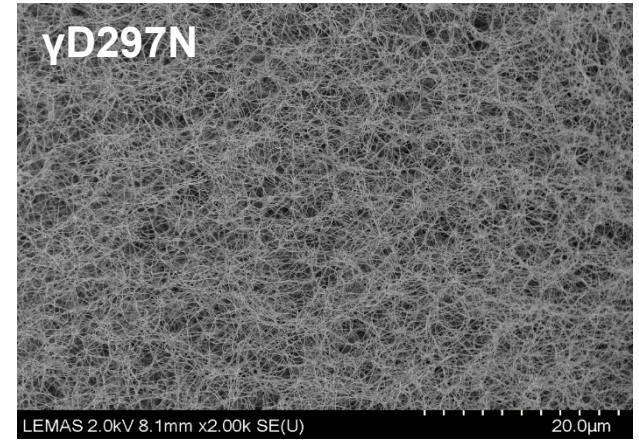
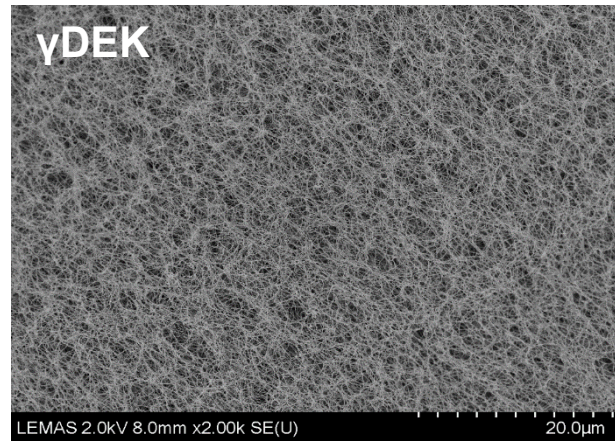
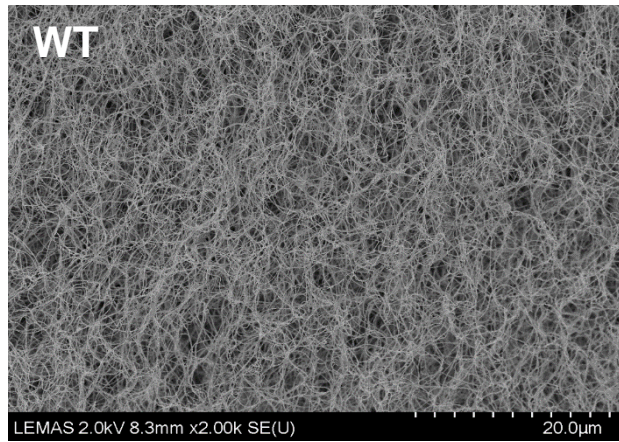
## yDEK (triple mutant) variant

>pMLP+Fbg-γ WT compared to pMLP+Fbg-γ D297N-E323Q-K356Q (γDEK)

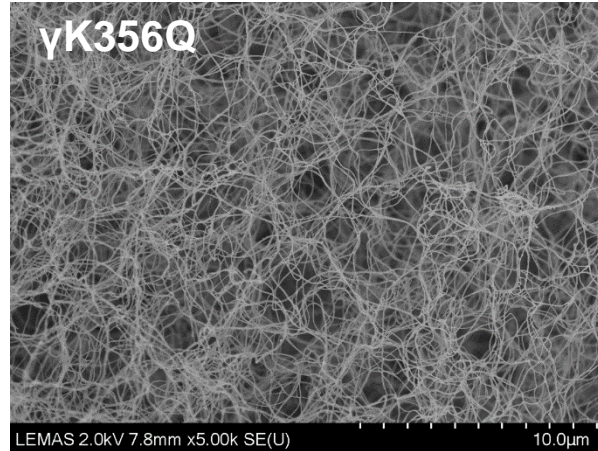
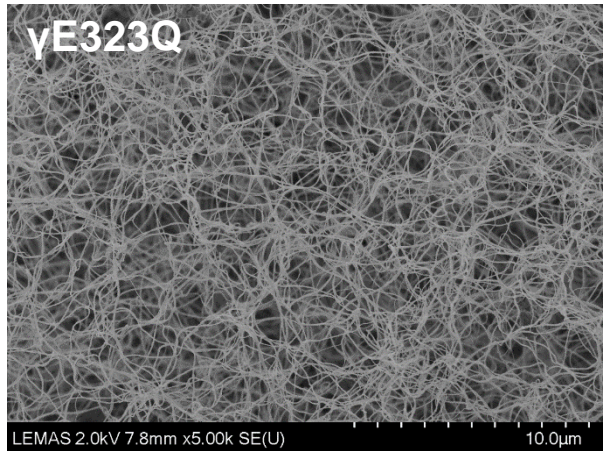
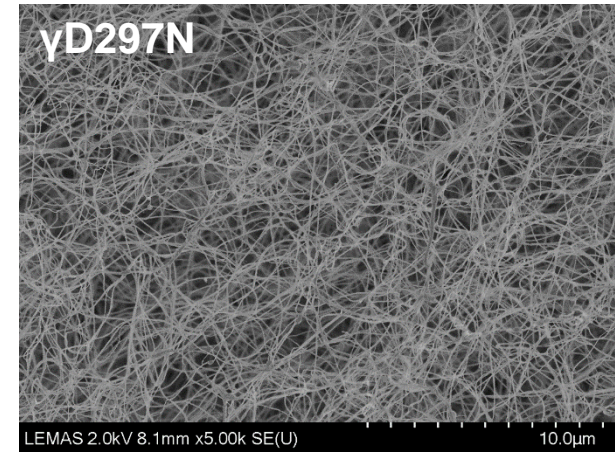
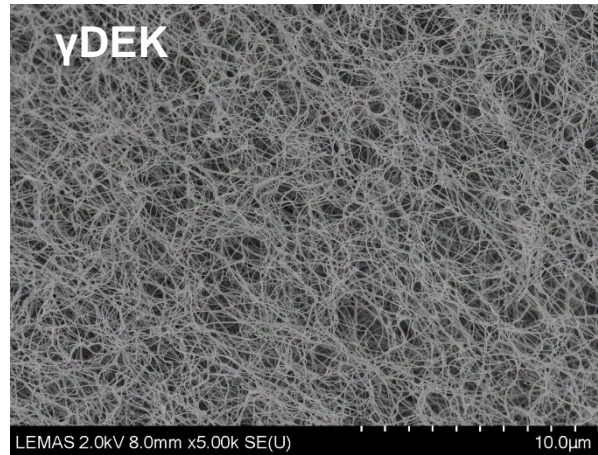
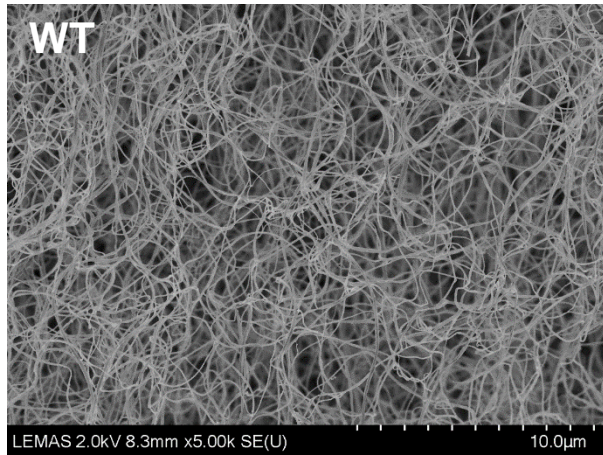
WT	ATGAGTTGGTCCCTTGCACCCCGGAATTTAATTCTCTACTTCTATGCTCTTTTATTTCTC	60
YD297N-E323Q-K356Q	ATGAGTTGGTCCCTTGCACCCCGGAATTTAATTCTCTACTTCTATGCTCTTTTATTTCTC *****	60
WT	TCTTCAACATGTGTAGCATATGTTGCTACCAGAGACAACCTGCTGCATCTTAGATGAAAGA	120
YD297N-E323Q-K356Q	TCTTCAACATGTGTAGCATATGTTGCTACCAGAGACAACCTGCTGCATCTTAGATGAAAGA *****	120
WT	TTCGGTAGTTATTGTCCAACCTACCTGTGGCATTGCAGATTTCCCTGTCTACTTATCAAACC	180
YD297N-E323Q-K356Q	TTCGGTAGTTATTGTCCAACCTACCTGTGGCATTGCAGATTTCCCTGTCTACTTATCAAACC *****	180
WT	AAAGTAGACAAGGATCTACAGTCTTTGGAAGACATCTTACATCAAGTTGAAAACAAAACA	240
YD297N-E323Q-K356Q	AAAGTAGACAAGGATCTACAGTCTTTGGAAGACATCTTACATCAAGTTGAAAACAAAACA *****	240
WT	TCAGAAGTCAAACAGCTGATAAAAAGCAATCCAACCTCACTTATAATCCTGATGAATCATCA	300
YD297N-E323Q-K356Q	TCAGAAGTCAAACAGCTGATAAAAAGCAATCCAACCTCACTTATAATCCTGATGAATCATCA *****	300
WT	AAACCAATATGATAGACGCTGCTACTTTGAAGTCCAGGAAAATGTTAGAAGAAATTATG	360
YD297N-E323Q-K356Q	AAACCAATATGATAGACGCTGCTACTTTGAAGTCCAGGAAAATGTTAGAAGAAATTATG *****	360

WT	AAATATGAAGCATCGATTTTAAACACATGACTCAAGTATTCGATATTTGCAGGAAATATAT	420
YD297N-E323Q-K356Q	AAATATGAAGCATCGATTTTAAACACATGACTCAAGTATTCGATATTTGCAGGAAATATAT *****	420
WT	AATTCAAATAATCAAAGATTGTTAACCTGAAAGAGAAGGTAGCCCAGCTTGAAGCACAG	480
YD297N-E323Q-K356Q	AATTCAAATAATCAAAGATTGTTAACCTGAAAGAGAAGGTAGCCCAGCTTGAAGCACAG *****	480
WT	TGCCAGGAACCTTGCAAAGACACGGTGCAAATCCATGATATCACTGGGAAAGATTGTCAA	540
YD297N-E323Q-K356Q	TGCCAGGAACCTTGCAAAGACACGGTGCAAATCCATGATATCACTGGGAAAGATTGTCAA *****	540
WT	GACATTGCCAATAAGGGAGCTAAACAGAGCGGGCTTTACTTTATTAACCTCTGAAAGCT	600
YD297N-E323Q-K356Q	GACATTGCCAATAAGGGAGCTAAACAGAGCGGGCTTTACTTTATTAACCTCTGAAAGCT *****	600
WT	AACCAGCAATTCCTAGTCTACTGTGAAATCGATGGGCTCGGAAATGGATGGACTGTGTTT	660
YD297N-E323Q-K356Q	AACCAGCAATTCCTAGTCTACTGTGAAATCGATGGGCTCGGAAATGGATGGACTGTGTTT *****	660
WT	CAGAAGAGACTTGATGGCAGTGTAGATTTCAAGAAAACTGGATTCAATATAAAGAAGGA	720
YD297N-E323Q-K356Q	CAGAAGAGACTTGATGGCAGTGTAGATTTCAAGAAAACTGGATTCAATATAAAGAAGGA *****	720
WT	TTTGACATCTGTCTCCTACTGGCACAACAGAATTTTGGCTGGGAAATGAGAAGATTGAT	780
YD297N-E323Q-K356Q	TTTGACATCTGTCTCCTACTGGCACAACAGAATTTTGGCTGGGAAATGAGAAGATTGAT *****	780
WT	TTGATAAGCACACAGTCTGCCATCCCATATGCATTAAGAGTGGAACTGGAAGACTGGAAT	840
YD297N-E323Q-K356Q	TTGATAAGCACACAGTCTGCCATCCCATATGCATTAAGAGTGGAACTGGAAGACTGGAAT *****	840
WT	GGCAGAACCAGTACTGCAGACTATGCCATGTTCAAGGTGGGACCTGAAGCTGACAAGTAC	900
YD297N-E323Q-K356Q	GGCAGAACCAGTACTGCAGACTATGCCATGTTCAAGGTGGGACCTGAAGCTGACAAGTAC *****	900
WT	CGCCTAACATATGCCTACTTCGCTGGTGGGGATGCTGGAGATGCCTTTGATGGCTTTGAT	960
YD297N-E323Q-K356Q	CGCCTAACATATGCCTACTTCGCTGGTGGGGATGCTGGAGATGCCTTTGATGGCTTTGAT *****	960
WT	TTTGGCAGATGATCCTAGTGACAAGTTTTCACATCCCATAAATGGCATGCAGTTCAGTACC	1020
YD297N-E323Q-K356Q	TTTGGCAGATGATCCTAGTGACAAGTTTTCACATCCCATAAATGGCATGCAGTTCAGTACC *****	1020
WT	TGGGACAATGACAATGATAAGTTTCAAGGCAACTGTGCTGAACAGGATGGATCTGGTTGG	1080
YD297N-E323Q-K356Q	TGGGACAATGACAATGATAAGTTTCAAGGCAACTGTGCTGAACAGGATGGATCTGGTTGG *****	1080
WT	TGGATGAACAAGTGTACGCTGGCCATCTCAATGGAGTTTATTACCAAGGTGGCACTTAC	1140
YD297N-E323Q-K356Q	TGGATGAACAAGTGTACGCTGGCCATCTCAATGGAGTTTATTACCAAGGTGGCACTTAC *****	1140
WT	TCAAAGCATCTACTCCTAATGGTTATGATAATGGCATTATTTGGGCCACTTGGAAAACC	1200
YD297N-E323Q-K356Q	TCAAAGCATCTACTCCTAATGGTTATGATAATGGCATTATTTGGGCCACTTGGAAAACC ***	1200
WT	CGGTGGTATTCATGAAGAAAACCACTATGAAGATAATCCATTCAACAGACTCACAATT	1260
YD297N-E323Q-K356Q	CGGTGGTATTCATGAAGAAAACCACTATGAAGATAATCCATTCAACAGACTCACAATT *****	1260
WT	GGAGAAGGACAGCAACACCACCTGGGGGGAGCCAAACAGGCTGGAGACGTTTAA	1314
YD297N-E323Q-K356Q	GGAGAAGGACAGCAACACCACCTGGGGGGAGCCAAACAGGCTGGAGACGTTTAA *****	1314

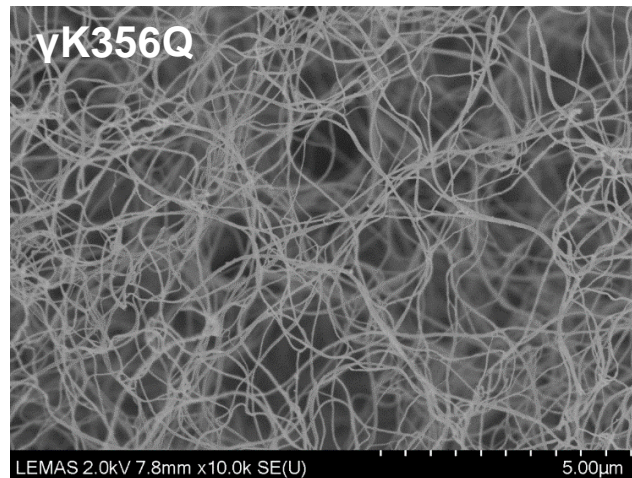
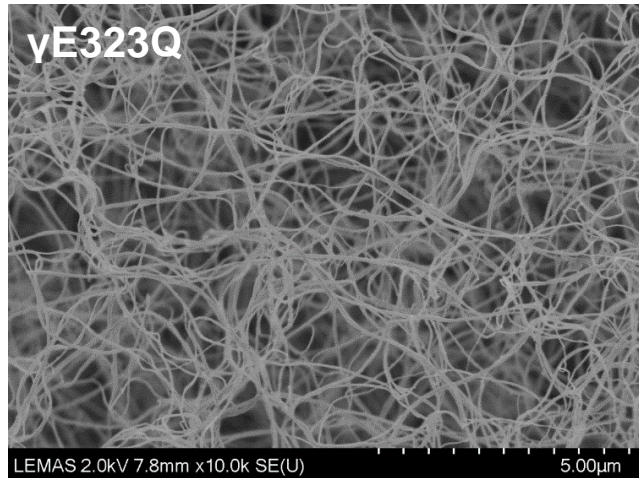
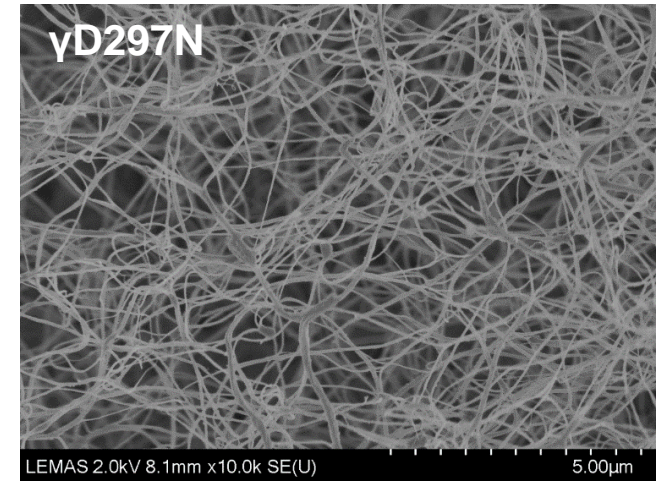
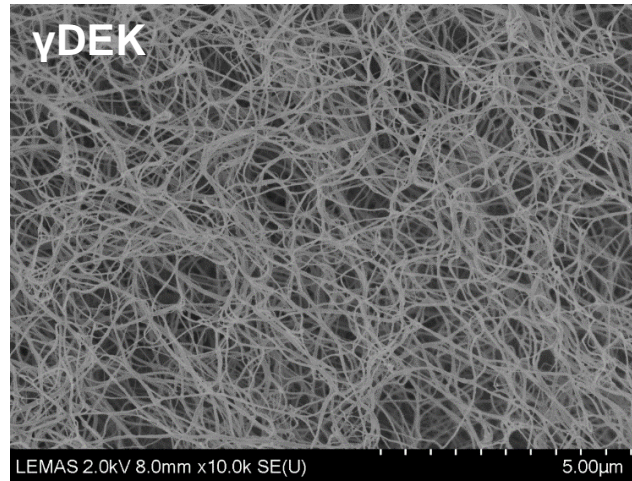
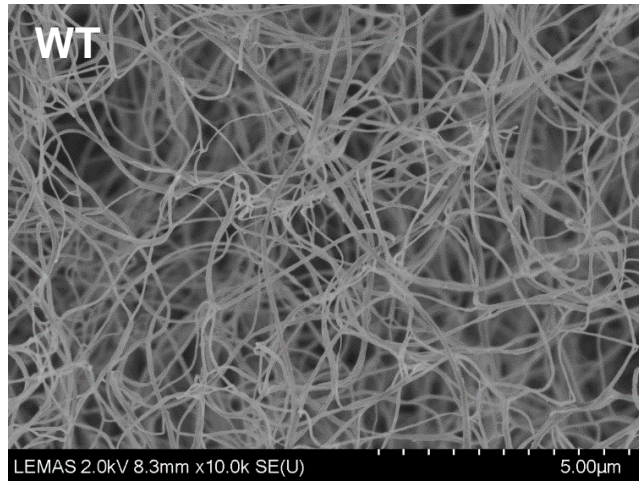
### 9.3 - Representative SEM Images at x2000 magnification



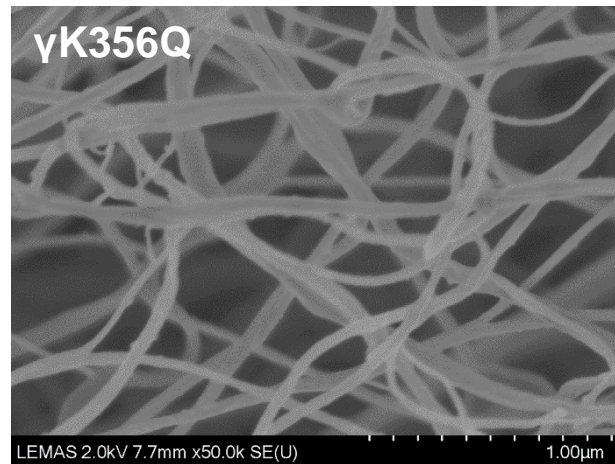
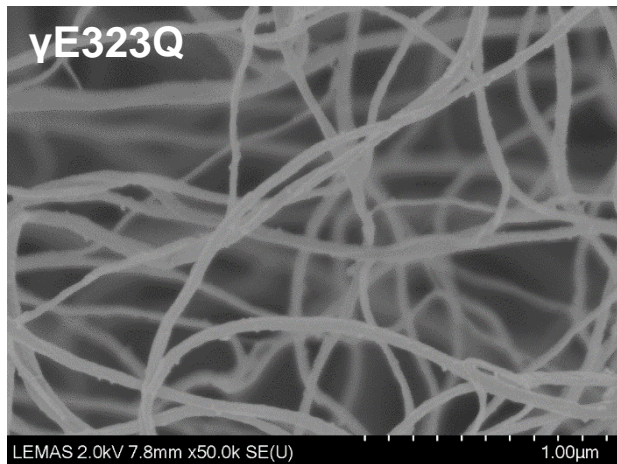
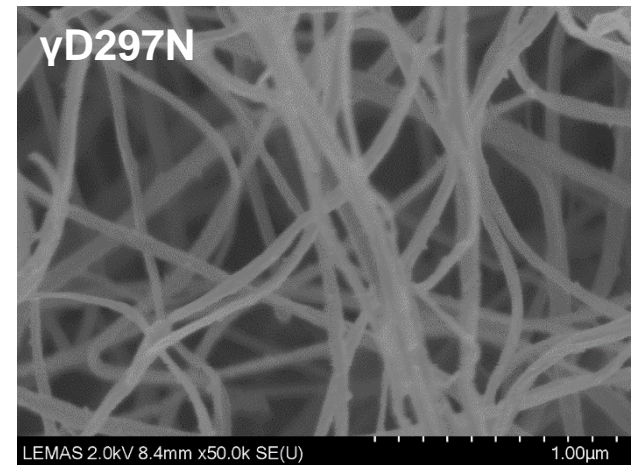
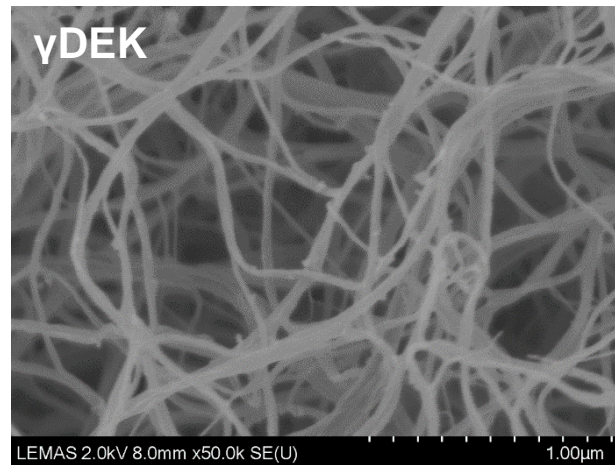
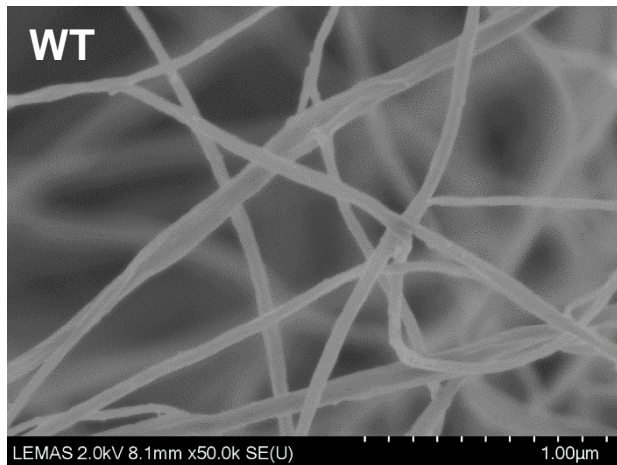
#### 9.4 - Representative SEM images at x5000 magnification



## 9.5 - Representative SEM images at x10000 magnification



## 9.6 - Representative SEM images at x50000 magnification



## 9.7 - Abstracts

XXVIth Congress International Society of Thrombosis and Haemostasis Congress, Berlin, Germany, 2017

### **Extended D-E interaction sites near the classical knob-hole binding site play an important role in fibrin polymerisation and clot formation**

Asquith N.L.<sup>1</sup>, Duval C.<sup>1</sup>, Domingues M.M.<sup>1,2</sup>, McPherson H.R.<sup>1</sup>, Macrae F.L.<sup>1</sup>, Connell S.D.<sup>3</sup>, Barsegov V.<sup>4</sup>, Ariëns R.A.S.<sup>1</sup>

<sup>1</sup> *Thrombosis and Tissue Repair Group; Division of Cardiovascular and Diabetes Research; Leeds Institute of Cardiovascular And Metabolic Medicine; University of Leeds; UK*

<sup>2</sup> *Institute of Molecular Medicine, University of Lisbon, Lisbon, Portugal*

<sup>3</sup> *Molecular and Nanoscale Physics group, School of Physics and Astronomy, University of Leeds, UK*

<sup>4</sup> *Department of Chemistry, University of Massachusetts, Lowell, Massachusetts, USA*

**BACKGROUND:** Molecular simulations indicate the presence of an extended binding interface beyond the traditional knob-hole interactions that occur when thrombin converts fibrinogen to fibrin (Kononova, JBC 2013). Within this extended binding interface,  $\gamma$ Asp297,  $\gamma$ Glu323 and  $\gamma$ Lys356 in the D-region of one fibrin molecule interact with  $\beta$ Lys58,  $\beta$ Asp61 and  $\beta$ His67 in the E-region of another, respectively. The effects of these novel electrostatic interactions on fibrin polymerisation and clot structure are unknown.

**AIMS:** To study the role of the extended knob-hole interface in polymerisation kinetics, clot structure and clot mechanics.

**METHODS:** Recombinant human fibrinogen  $\gamma$ DEK variant ( $\gamma$ D297N/E323Q/K356Q) and wild-type (WT) were produced in CHO cells and purified by affinity chromatography. Clot polymerisation kinetics were studied by turbidity. Clot visco-elastic properties were determined by magnetic tweezers. Confocal microscopy was used to study clot formation, clot structure and clot lysis.

**RESULTS:**  $\gamma$ DEK showed extended lag phase (+30%), slower clotting rate (-45%) and lower maximum OD (-41%) compared to WT. This variant produced a denser clot network (+41%) in hydrated conditions compared to WT, which resulted in slower lysis rates (-37%). Frequency dependent moduli were calculated and  $G'$  (elastic modulus), was similar at 0.1Hz but higher at 1 and 10Hz, compared to WT.  $G''$  (energy loss modulus) was increased at 0.1Hz 1Hz and 10Hz, compared to WT. The loss tangent ( $\tan\delta$ , visco-elasticity) was increased at 0.1Hz and 1Hz but similar at 10Hz.

**CONCLUSIONS:** The abolition of electrostatic interactions responsible for the extended binding interface results in altered polymerisation kinetics (prolonged protofibril formation), clot structure and viscoelastic properties. Our findings support previous molecular simulations and demonstrate that the D-E binding interface extends beyond the classical knob-hole interaction to reinforce fibrin polymerisation.

5<sup>th</sup> British Heart Foundation Fellows Meeting, Cambridge, UK, 2017

**Extended D-E interactions near the classical knob-hole binding site play an important role in fibrin polymerisation and clot stability**

Asquith N.L.<sup>1</sup>, Duval C.<sup>1</sup>, Baker S.<sup>1</sup>, Domingues M.M.<sup>1,2</sup>, McPherson H.R.<sup>1</sup>, Macrae F.L.<sup>1</sup>, Connell S.D.<sup>3</sup>, Barsegov V.<sup>4</sup>, Ariëns R.A.S.<sup>1</sup>

<sup>1</sup> *Thrombosis and Tissue Repair Group; Division of Cardiovascular and Diabetes Research; Leeds Institute of Cardiovascular and Metabolic Medicine; University of Leeds; UK*

<sup>2</sup> *Institute of Molecular Medicine, University of Lisbon, Lisbon, Portugal*

<sup>3</sup> *Molecular and Nanoscale Physics group, School of Physics and Astronomy, University of Leeds, UK*

<sup>4</sup> *Department of Chemistry, University of Massachusetts, Lowell, Massachusetts, USA*

**BACKGROUND:** Molecular simulations indicate a role for extended electrostatic binding beyond the classical knob-hole polymerisation sites generated during fibrinogen to fibrin conversion. The effects of these novel electrostatic interactions on fibrin polymerisation and stability are unknown.

**RESULTS:** Recombinant  $\gamma$ DEK-fibrinogen, created to eliminate extended binding, showed altered polymerisation compared to WT.  $\gamma$ DEK-fibrinogen produced a denser clot with thinner fibres. Frequency dependent moduli were calculated to study clot mechanics, the loss tangent ( $\tan\delta$ ) was increased, indicating a more viscous clot.

**CONCLUSIONS:** Our findings demonstrate that the D-E binding interface extends beyond the classical knob-hole interaction during fibrin polymerisation and reinforces clot stability.

**Extended D-E interactions near the classical knob-hole binding site play an important role in fibrin polymerisation and clot stability**

Asquith N.L.<sup>1</sup>, Duval C.<sup>1</sup>, Baker S.<sup>1</sup>, Domingues M.M.<sup>1,2</sup>, McPherson H.R.<sup>1</sup>, Macrae F.L.<sup>1</sup>, Connell S.D.<sup>3</sup>, Barsegov V.<sup>4</sup>, Ariëns R.A.S.<sup>1</sup>

<sup>1</sup> *Thrombosis and Tissue Repair Group; Division of Cardiovascular and Diabetes Research; Leeds Institute of Cardiovascular and Metabolic Medicine; University of Leeds; UK*

<sup>2</sup> *Institute of Molecular Medicine, University of Lisbon, Lisbon, Portugal*

<sup>3</sup> *Molecular and Nanoscale Physics group, School of Physics and Astronomy, University of Leeds, UK*

<sup>4</sup> *Department of Chemistry, University of Massachusetts, Lowell, Massachusetts, USA*

**BACKGROUND:** Molecular simulations indicate the presence of an extended binding interface beyond the traditional knob-hole interactions that occur when thrombin converts fibrinogen to fibrin (Kononova, JBC 2013). Within this extended binding interface,  $\gamma$ Asp297,  $\gamma$ Glu323 and  $\gamma$ Lys356 in the D-region of one fibrin molecule interact with  $\beta$ Lys58,  $\beta$ Asp61 and  $\beta$ His67 in the E-region of another, respectively. The effects of these novel electrostatic interactions on fibrin polymerisation and clot structure are unknown.

**AIMS:** To study the role of the extended knob-hole interface in polymerisation kinetics, clot structure and clot mechanics.

**METHODS:** Recombinant human fibrinogen  $\gamma$ DEK variant ( $\gamma$ D297N/E323Q/K356Q) and wild-type (WT) were produced in CHO cells and purified by affinity chromatography. Clot polymerisation kinetics were studied by turbidity. Clot visco-elastic properties were determined by magnetic tweezers. Confocal microscopy was used to study clot formation, clot structure and clot lysis. Single  $\gamma$ D297N,  $\gamma$ E323Q and  $\gamma$ K356Q fibrinogen mutants were also produced and characterised.

**RESULTS:**  $\gamma$ DEK showed extended lag phase (+30%), slower clotting rate (-45%) and lower maximum OD (-41%) compared to WT. This variant produced a denser clot network (+41%) in hydrated conditions compared to WT, which resulted in slower lysis rates (-37%). Frequency dependent moduli were calculated and  $G'$  (elastic modulus), was similar at 0.1Hz but higher at 1 and 10Hz, compared to WT.  $G''$  (energy loss modulus) was increased at 0.1Hz 1Hz and 10Hz, compared to WT. The loss tangent ( $\tan\delta$ , visco-elasticity) was increased at 0.1Hz and 1Hz but similar at 10Hz. Preliminary turbidity data for  $\gamma$ D297N  $\gamma$ E323Q and  $\gamma$ K356Q fibrinogen variants show reduced maximum OD similar to  $\gamma$ DEK.

**CONCLUSIONS:** The abolition of electrostatic interactions responsible for the extended binding interface results in altered polymerisation kinetics (prolonged protofibril formation), clot structure and viscoelastic properties. Our findings support previous molecular simulations and demonstrate that the D-E binding interface extends beyond the classical knob-hole interaction to reinforce fibrin polymerisation.

25<sup>th</sup> International Fibrinogen Workshop, Winston Salem, North Carolina, USA, 2018.

**Extended D-E interactions near the classical knob-hole binding site play an important role in fibrin polymerisation and clot stability**

Asquith N.L.<sup>1</sup>, Duval C.<sup>1</sup>, Baker S.<sup>1</sup>, Domingues M.M.<sup>1,2</sup>, McPherson H.R.<sup>1</sup>, Macrae F.L.<sup>1</sup>, Connell S.D.<sup>3</sup>, Barsegov V.<sup>4</sup>, Ariëns R.A.S.<sup>1</sup>

<sup>1</sup> *Thrombosis and Tissue Repair Group; Division of Cardiovascular and Diabetes Research; Leeds Institute of Cardiovascular and Metabolic Medicine; University of Leeds; UK*

<sup>2</sup> *Institute of Molecular Medicine, University of Lisbon, Lisbon, Portugal*

<sup>3</sup> *Molecular and Nanoscale Physics group, School of Physics and Astronomy, University of Leeds, UK*

<sup>4</sup> *Department of Chemistry, University of Massachusetts, Lowell, Massachusetts, USA*

**BACKGROUND:** Previous studies indicate the presence of an extended binding interface beyond the traditional knob-hole interactions that occur when thrombin converts fibrinogen to fibrin (Kononova, JBC 2013):  $\gamma$ Asp297,  $\gamma$ Glu323 and  $\gamma$ Lys356 in the D-region interact with  $\beta$ Lys58,  $\beta$ Asp61 and  $\beta$ His67 in the E-region from another adjacent fibrin monomer.

**AIMS:** To investigate the role of the extended knob-hole interface in polymerisation kinetics, clot structure and mechanics.

**METHODS:** Four recombinant human fibrinogen variants and WT were produced:  $\gamma$ DEK ( $\gamma$ D297N/E323Q/K356Q) with mutations in all  $\gamma$ -chain residues involved in extended knob-hole binding, and variants with single mutations at  $\gamma$ D297N,  $\gamma$ E323Q or  $\gamma$ K356Q.

**RESULTS:** Maximum OD for all variants was reduced compared to WT, whereas lag phase was only extended for  $\gamma$ DEK.  $\gamma$ DEK was more readily deformable (loss tangent,  $\tan\delta$ ), but single mutant variants were unchanged compared to WT. Electron microscopy showed  $\gamma$ DEK forming the densest clots, followed by the single mutants, then WT. Fibers for all variants were thinner than WT, with  $\gamma$ DEK being the thinnest. Variants  $\gamma$ DEK and  $\gamma$ E323Q produced a denser clot network in hydrated conditions, whereas  $\gamma$ D297N and  $\gamma$ K356Q were similar to WT, and all were slower to lyse, except  $\gamma$ D297N. There were no differences in clot size between  $\gamma$ D297N and WT fibrinogen in an in vivo model of murine femoral thrombosis.

**CONCLUSIONS:** The abolition of electrostatic interactions responsible for extended binding results in altered polymerisation kinetics, clot structure and viscoelastic properties. Our findings demonstrate that the D-E binding interface extends beyond the classical knob-hole interaction to reinforce fibrin polymerisation.